Author:
Williams, Gareth

Title:
Development of self-healing carbon fibre reinforced plastic utilising an embedded hollow glass fibre delivery system

University of BRISTOL

Development of Self-Healing Carbon Fibre Reinforced Plastic Utilising an Embedded Hollow Glass Fibre Delivery System

Gareth Williams

Department of Aerospace Engineering
University of Bristol

July 2008

A dissertation submitted to the University of Bristol
In accordance with the requirements of the degree of
Doctor of Philosophy in the Faculty of Engineering

Word Count: 52,696

Abstract

There is a drive for modern engineering structures to exploit the excellent specific properties of advanced fibre reinforced composite materials, particularly in aerospace, where manufacturers are under intense pressure to reduce costs and engineer lighter more efficient aircraft. However it is widely recognised that the susceptibility of these materials to transverse impact damage is restricting the extent to which these benefits can be exploited.

The current methodologies to develop more damage tolerant materials result in reduced in-plane strength and stiffness, which can be counter-productive. Furthermore, they do not eliminate the need to subsequently detect and repair damage. This increases costs for the maintenance and inspection of aircraft.

A new technology is emerging, which draws inspiration from the response of naturally occurring biological structures to damage. This technology is termed self-healing or self-repair. A growing amount of research is focussing on this topic, though as yet, little has been reported to address low velocity impact damage in unidirectional, pre-impregnated carbon fibre technology.

The use of resin bearing hollow glass fibre (HGF) as discrete units embedded at critical interfaces within carbon fibre reinforced plastics (CFRP) is considered. The fundamental principal is that damage induced into the laminate ruptures the HGF, releasing the healing resin, which then infiltrates and repairs the damage once cured. A number of analytical methods have been used to develop a tailored distribution of HGF within the laminate, specific to the impact conditions and specimen dimensions.

Flexural four point bend testing was used to assess the capability of the system to address damage initiated by quasi-static indentation, in conjunction with compression after impact (CAI) to assess the response to damage initiated by low velocity drop weight impact. Both test methods demonstrated that resin bearing HGF is capable of restoring the laminate strength to levels approaching that of the undamaged state. Furthermore, CAI assessment identified that the laminate failure mode was altered

due to the presence of impact damage, after the laminates were healed, the failure mode was returned to that of the undamaged state. Ultrasonic non-destructive evaluation indicated that the impact damage present within the healed laminates did not propagate under compressive loading. In addition, optical microscopy has shown that the delaminations and matrix shear cracks, formed during the impact event, were almost completely infiltrated with healing resin. This repaired the damage such that it was practically indistinguishable from the surrounding laminate.

Keywords: *self-healing, self-repair, FRP, CFRP, compression after impact, flexural strength, compression strength, impact damage, fractography*

Publications

The following publications have been produced as a result of the work contained within this thesis:

Williams, G.J, Trask, R.S. and Bond, I.P. "Bioinspired Self-Healing of Advanced Composite Structures using Hollow Glass Fibres," Journal of the Royal Society Interface, Vol. 4, No. 13, 2007 DOI: 10.1098/rsif.2006.0194

Williams, G., Trask, R. and Bond, I. "A Self-Healing Carbon Fibre Reinforced Polymer for Aerospace Applications," Composites A (2007) Vol.38: 1525-1532

Bond, I., Trask, R., Williams, H.R. and Williams, G "Self-Healing Fibre-reinforced Polymer Composites: an Overview" Self Healing Materials an Alternative Approach to 20 Centuries of Materials Science (2007), Editor Sybrand van der Zwaag

Williams, G., Bond, I. and Trask, R. "Compression After Impact Assessment of Self-Healing CFRP," Composites A (2008) DOI: 10.1016/j.compositesa.2008.05.021

Bond, I.P., Trask, R.S., Williams, G.J. and Williams, H.R. "Self-Healing Functionality in Fibre Reinforced Polymer Composites" MRS Bulletin- special issue on self-cleaning and self-cleaning materials (2008)

Acknowledgements

I would like to thank Dr Ian Bond for his support and guidance throughout my research. Firstly, he gave me the opportunity and responsibility to undertake this project. Secondly, he gave me the trust and independence to control my own direction. Lastly, for his 'grasp of the English language'.

I also owe thanks to Dr Richard Trask and Dr Julie Etches for their continued support and especially for their knowledge and direction in the first steps of this project.

My family have provided motivation when needed, support as required and it has been a big reward for me to know that they are proud of my achievements.

Last, but definitely not least, my wife Nina. For waiting until the end of my PhD to get married, for waiting until the end of my thesis to move to Australia, I am grateful and I am sorry! I appreciate your patience and I know they were both worth the wait. For your support, your motivation and your understanding I will always be grateful.

"Every word is just nonsense, but I understand it all..."

Anna Begins, Counting Crows, 1993

Author's Declaration

I declare that the work in this dissertation was carried out in accordance with the Regulations of the University of Bristol. The work is original, except where indicated by special reference in the text or described in the acknowledgements, and no part of this dissertation has been submitted for any other academic award. Any views expressed in the dissertation are those of the author.

Signed .....

Date 4.1.7.1.08..

CONTENTS

Figures

Tables

1. Introduction

1.1 Research Motivation

The development of advanced fibre reinforced composite materials has presented new opportunities in the design and operation of modern structures and vehicles. The excellent specific properties and the ability to tailor them as required allow for the manufacture of lighter and more efficient structures. The constituent components of advanced FRPs (Fibre Reinforced Polymers) occupy a wide range of geometric scales: polymeric constituents within the matrix (molecular), reinforcing fibres (micro), FRP laminate (milli) and ultimately the structural components for which they are used (macro). This agglomeration of components each with their own purpose within the material provides a unique hierarchical structure. It is this unique hierarchical structure of advanced composite materials that allows the incorporation of additional materials or features which provide multi-functionality to structures which further improves their benefits, desirability and also increases the complexity of this hierarchy. However, a fundamental problem with fibre reinforced polymers (FRP's) is that they have relatively poor through thickness strength properties and so are inherently susceptible to impact damage from foreign bodies during operational use and handling/maintenance. This is of particular relevance to the aerospace industry where immense commercial pressures are exerted on aircraft manufacturers to reduce weight, improve efficiency and reduce the overhead costs of maintenance and inspection. Of particular concern is the occurrence of barely visible impact damage (BVID) which can ultimately lead to a significant reduction in material performance.

Therefore, it is evident that there is a need to develop mechanisms by which this deficiency in composite materials is addressed in order to maximise the efficiency of their use. At present, damage tolerant designs are used which are limited by a 'no crack growth' criterion, although developments have been made that utilise novel reinforcement architectures and matrix chemistries to improve the damage tolerance capabilities. However, if nature is taken as an inspiration then an effective method to address damage would be to seek a method of self-healing. This could be achieved by exploiting the hierarchical structure of fibre reinforced polymers to add functionality in the form of an ability to repair. Furthermore, this functionality would ideally be autonomous, as an external decision based detection/control system would add cost and complexity.

1.2 Research Objectives

The global aim of this research is to develop an autonomous process for self-repair that is suitable for Carbon Fibre Reinforced Plastics (CFRP). The healing process will be targeted at low velocity impact events in order to overcome the limitations arising from the relatively poor through thickness properties of CFRP. The healing process will require no manual intervention and, furthermore, will allow recovery of a laminate's mechanical performance after a damage event.

2. Literature Review

In order to fully understand the challenges posed in developing a self-healing system for CFRP, it is pertinent to investigate the fundamentals of material behaviour, how other approaches have attempted to mitigate the effect of impact damage, the effectiveness of alternative self-healing strategies, and assessment of self-healing performance.

2.1 Fibre Reinforced Polymers (FRP)

2.1.1 Introduction

Advanced aerospace FRP's combine strong, stiff, reinforcing fibres within a robust protective polymer matrix. This results in FRP's with excellent specific properties. Two common methods for the manufacture of FRP's are resin pre-impregnated fibre tape (pre-preg) and fibre resin infusion. Pre-preg systems are commonly used in aerospace structures however they are relatively expensive in terms of raw material and labour costs. Fibre infusion is lower-cost but is restricted by the characteristics of the infused resin, in particular its viscosity. Three materials (glass, aramid and carbon) are commonly used as reinforcing fibres. Each offers their own set of characteristics which determines their suitability for structural applications (Table 2-1). Likewise, a variety of polymer matrices can be used in aerospace FRP's, each offering various attributes (Table 2-2).

Fibre Type	Diameter (μm)	Modulus (GPa)	Fracture Strength (GPa)
Glass (E-Glass)	11	76	2
Aramid (Kevlar™)	15/12	190/130	2/3
Carbon HM/HS	8/8	390/250	2.2/2.7

Table 2-1: ***Properties for Typical Fibres used in Fibre Reinforced Polymers [1]***

Resin Type	Advantages	Disadvantages
Epoxy	Good mechanical properties, processing flexibility, large range of available systems and acceptable cost	Low strain to failure, sensitive to moisture
Cyanate	Tough and moisture resistant	Lack of data and manufacture experience
Bismaleimide	Tough, moisture resistant, ease of handling and high operating temperature	Brittle, long cure cycles required
Polyimide	High operating temperature	Low toughness, difficult handling and manufacture
Polyurethane	High toughness,	Low mechanical properties
Polyester	High operational temperature above cure temp	Expensive, toxic components in manufacture, brittle, flammable sensitive to moisture, aircraft fluids and solvents
Phenolic	Heat and fire resistant	High water content causes blistering during cure
Thermoplastic	Low moisture absorption, unlimited shelf life, reworked with application of heat, low cost manufacture	Poor resistance to organic solvents, problems with thermal degradation

Table 2-2: ***Advantages and Disadvantages for typical Matrix Resin Systems for Fibre Reinforced Polymers [1-2]***

2.1.2 Advances in FRP's: Multifunctionality

The hierarchical nature of FRPs internal structure has stimulated increasing interest in the incorporation of non-structural functionality to create 'smart materials'. For example, Spillman et al [3] attempted to define what constitutes smart materials and structures. The authors begin from the viewpoint they must be considered as systems in which the whole is greater than the sum of the parts. More specifically, it is concluded that a smart structure is a non-biological physical structure having the following attributes:

1. A definite purpose
2. Means and imperative to achieve that purpose
3. A biological pattern of functioning

One development has been the evolution of 'morphing structures' which is a technology that strives to achieve more efficient structures and mechanisms for flight control surfaces and wing structures [4,5]. The aim has been to replace complex and heavy mechanisms with structures that are able to deform through local or internal actuation. This actuation is achieved through the use of embedded materials such as piezoceramics or shape memory alloys [6-11]. This can also be used in addition to novel lay-ups which enable bi-stable or multi-stable structures [12-14].

Forms of active vibration control have been developed to address the large vibrations experienced by modern rotary wing aircraft via the use of actuators such as piezoceramics [15-16] and electro or magneto-rheological fluids [17,18] in order to reduce noise, improve fatigue life and prevent the dynamic performance degradation.

Structural health monitoring (SHM) has evolved as a technique to monitor structures in order to detect and characterise damage formation or to identify when a structure is experiencing high load levels. SHM involves incorporating sensors into structures for the detection of acoustic waves [19-22] emitted from defects/impact events or the distortion of waveguide fibre optics [23,24], to detect, locate and characterise damage within the material.

Although the hierarchical structure of composite materials allows the incorporation of additional functionality to bring added benefits to structural applications, their laminated

nature means that they are susceptible to various forms of out-of-plane damage which are detrimental to the overall performance and which are often difficult to detect.

2.2 Damage to Fibre Reinforced Polymers

2.2.1 Overview

Damage threats to FRP's are classified by Baker et al [25] into the following categories:

- Manufacturing: Voids, delaminations, disbands (in bonded joints), surface damage and miss-drilled holes
- In-Service: Cuts/scratches, abrasion, delaminations, disbands, hole elongation, dents (delaminations and crushed core), edge damage and penetration
- Environmental: Surface oxidation, delamination, disbonds and surface swelling

Environmental damage can be addressed by adequate surface treatment and regular maintenance schedules. Manufacturing damage is more problematic and can be difficult to detect, but is generally addressed by improving manufacturing processes and non destructive testing (NDT) methods are used to screen components for defects. The most critical damage occurs during service due to events such foreign body impact and damage created by operational loads.

Damage formation is a mechanism for the dissipation of energy created by applied loads, within FRP's and can be characterised into four fundamental modes [26-28]:

i. Matrix: *Intraply cracking mode* (matrix cracks), occurs parallel to the fibres due to tension, compression or shear
ii. Delamination: *Interply failure, produced by inter-laminar stresses*
iii. Fibre: *Fibre failure, tensile fibre breakage and compressive fibre buckling*
iv. Penetration: *Impactor completely perforates the impact surface*

In general, fibre failure is found to be the most disruptive to laminates as the majority of the strength and stiffness is provided by the reinforcement. However, Prevorsek et al [26] identified that the majority of damage for aircraft structures is restricted to the matrix, with the exception of severe events such as ballistic penetration. Occurrences of fibre failure are easily detectable as they are caused by penetration of the surface due to a foreign body impact and will often lead to catastrophic failure. Therefore, structures are designed to

withstand impact events during normal operation such that fibre failure does not occur or is minimised. If fibre damage does occur the effects are usually immediately evident or are identified during routine maintenance.

Matrix cracks are the first occurrence of damage within FRP's, although they do not significantly reduce the residual properties of the laminate. However, upon reaching a threshold energy level, matrix cracks develop into delaminations at ply interfaces [28-30] Two types of matrix crack can be considered [31]:

1. Bending cracks: Induced by high tensile bending stresses and are characteristically perpendicular to the ply interface
2. Shear cracks: Induced by high transverse shear stress through the material and are inclined at 45° to the ply interface

Liu et al [32] showed through an analytical model that delaminations formed from shear cracks are unstable and delaminations formed from bending cracks grow in a stable manner that is proportional to the applied load.

Delaminations were found to be the most significant and problematic form of damage, as they are induced by foreign body impacts and can occur within the structure without any indication of their presence. This phenomenon is known as barely visible impact damage (BVID) and can result in a 50-60% decrease in strength [25]. Delaminations can be detected with the use of NDT methods (primarily ultrasonic C-scanning and X-ray). However, these methods are not practical or economically feasible for large structures at high frequency intervals. Therefore, the susceptibility of composite materials to impact damage has resulted in a large number of investigations considering impact events and how laminated materials respond. In particular, low velocity impact is a focus of research as the generation of BVID at low energy impact levels is of particular concern.

2.2.2 Damage Mechanisms in Low Velocity Impact Events

Sjoblom et al [33] and Shivakumar [34] characterise impact events by their velocity: low, high and hyper. Generally, it was found that for aerospace applications only low velocity and high velocity impacts are encountered (hyper velocity is encountered in space). Low velocity impact was found to be of most interest as these impact events are causes of BVID. Abrate [35] characterised low velocity as an impact event during which the entire

structure deforms as waves propagate to the boundary and are reflected back several times. They can be treated as quasi-static, typically in the range of 1-10ms^{-1}. Abrate also characterised high velocity as an impact event where the deformation of the structure is localised in a small zone surrounding the contact area during the duration of contact and dominated by stress wave propagation [33-35].

Only matrix cracking and delaminations occur during low velocity impact events, therefore they can also be classified by the damage incurred [36,37]. For thick, stiff laminates, low velocity impacts initiate damage due to high, localised contract stresses. Damage then progresses from the top surface down in a 'pine tree' pattern. For thin, flexible laminates low velocity impacts produce bending, which generates high tensile stresses in the lowest ply. This causes matrix cracks to develop in the lowest ply, which are deflected at the interface to form a delamination. The delamination is then deflected by matrix cracks in the layer above and the process repeats itself to form an inverted 'pine tree' pattern [28,30,38].

Delaminations occur where two dissimilar ply directions separate at their interface due to the bending stiffness mismatch between them [39], although Takeda et al [40] revealed that delaminations do not always run precisely along the interface but can run marginally to either side. The delamination forms a 'peanut-shaped' region at ply interfaces with the major axis orientated in the fibre direction of the lower ply of that interface. Furthermore, the larger the difference in fibre orientation of the two plies at the interface, the larger the delamination area, i.e. 0/90 being the worst case. Matrix delaminations are a significant form of damage and can reduce the load bearing capability of a laminate by up to 50% [41]. Impact induced delaminations can buckle under compressive load and subsequently spread, further decreasing the load carrying capacity of the structure. This buckling occurs in three modes of instability [28]:

1. Global instability: Where the whole structure buckles, typically occurs with short delaminations
2. Local instability: Where a section of the delaminated structure buckles, typically occurs with long delaminations
3. Local-global instability: Both a delaminated section and the entire structure buckles in a mixed mode combination, occurs at intermediate lengths.

These instabilities contribute to poor post-impact performance of composite materials by causing large reductions in compressive strength. However, compression after impact testing is extremely difficult to undertake as a sufficiently large gauge section must be provided to accommodate the damage whilst being small enough to prevent global buckling. This results in the need for complex anti-buckling guides that support the specimen to prevent global buckling but provide the freedom for local instability [42].

Resistance to low velocity impact and the subsequent effects on the load bearing capability of a composite material is dependant on its ability to store energy elastically within the fibres. This is characterised by fibres that have large areas under their stress/strain curves [43].

The most common types of fibre used in advanced fibre reinforced polymer composite materials are glass, carbon and aramid. Carbon is widely used in the aerospace industry as it has the highest strength and stiffness [1], however it also has the lowest strain to failure [43]. This low allowable strain produces susceptibility to impact damage and prevents full utilisation of the material's excellent mechanical properties. Glass fibres have lower strength and stiffness but have a larger strain to failure. The mechanical performance of aramid lies between that of carbon and glass. General trends in fibre technology are driving fibre diameters down in order to increase their strain to failure and thereby increasing the energy absorbing capacity of the fibres [43].

Epoxy resins are the most commonly used matrix resins for aerospace materials. These thermoset resins are excellent adhesives with high chemical and corrosion resistance as well as good mechanical and thermal properties. However, they are brittle resulting in poor resistance to crack propagation and impact damage due to their low toughness. Different methods and modifications have been applied to increase their toughness without a significant reduction in their mechanical properties. Chikhi et al [45] commented on early studies using glass beads, alumina tri-hydrate, or silica. However, alternative techniques involve the addition of a suitable elastomer such as liquid amine terminated copolymers of butadiene (ATBN) and more recently the use of thermoplastics (polyphenyl oxide, PPO) and interpenetrating polymer networks (IPN). In particular, thermoplastic additions are preferred by the aerospace industry for toughening resin systems as they are not

susceptible to degradation from aggressive chemicals, such as hydraulic fluid, with which contact is not entirely avoidable.

Strain rate can also be an issue for composite materials as glass fibres have been proven to show a degree of strain-rate dependant behaviour as modulus and tensile strain increase with strain rate. However, a number of workers have found that carbon fibre composites are strain rate insensitive particularly in fibre-dominated modes [28,30,35,43]. For matrix-dominated modes of failure, brittle thermosets such as epoxy resins are not found to exhibit significant strain rate dependant behaviour, unlike the latest generation of tougher thermoplastic-based systems such as PEEK. Richardson and Wisheart's review paper [28] concluded that for low velocity impact testing, fibre strain rate effects can be ignored. This becomes relevant when attempting to use static or quasi-static testing to model a dynamic impact event.

2.3 Addressing Damage to Polymer Composite Materials

The increase in use of FRP's for structural components has stimulated a drive to address their susceptibility to impact damage. As a result, a wealth of research has been undertaken into techniques that address the damage events that composite materials are expected to encounter in an operational environment. The core efforts have focused along two pathways and consider measures that can be taken before and after a damage event:

1. Damage Tolerance (before): Improving the response of FRP's to damage thereby reducing the detrimental effects of a damage event
2. Repair (after): Improving techniques to detect damage and enable efficient repairs

2.3.1 Damage Tolerance

To account for the challenges posed by the anisotropy of composite materials the current design philosophy is one of damage tolerance. This accounts for all sources of damage, whether arising during manufacture or inflicted during normal service operations or as a result of environmental degradation. It is defined by Chen et al [46] as the ability of a structure to tolerate a reasonable level of damage or defects that might be encountered during manufacture or while in service, without jeopardising aircraft safety. Baker et al [25] adds that provision must be made for both the location and initial size of the defect

and to its likely size after a representative period of service (i.e. between inspection intervals). Essentially, a composite structure should be designed for provision to receive a given level of damage and to perform at the desired level until such time as it can be detected and corrective action can be taken whether that is to repair or replace the part. Furthermore, the growth of that damage must either be accounted for [25] or restricted (no growth condition) [47] during normal service conditions without preventing the structure from performing to its designed specification.

Therefore, damage tolerance can be further subdivided into three constituent parts:

1. Design for damage tolerance: *Structural components are sized and stressed such that they can receive a given level of damage and still achieve the desired level of performance.*
2. Damage resistance: *The material's ability to tolerate a given level of damage by limiting/preventing propagation during expected loading conditions.*
3. Impact resistance: *The material's ability to minimise the level of damage sustained due to foreign body impact damage.*

It is evident that all three constituents to damage tolerance are inherently entwined as, for example, it is not possible to address impact resistance without also affecting the damage resistance of a material. The consequences of designing for damage tolerance are that the full advantages of the excellent specific properties of composite materials are not achieved. Furthermore, conservative design approaches mean that the undamaged material is often over designed for normal operational service. This is reflected in the typical design allowable strain for CFRP of between 0.3-0.4% [48] whereas its strain to failure can reach values of up to 2.4% [49].

The majority of damage tolerance work considers impact events. This is considered in two major areas: impact damage/response, and damage resistance/tolerance. However, very little work has been conducted which considers both these areas simultaneously. This is surprising as in order to design for damage tolerance it must be beneficial to acquire an accurate understanding of the damage event [50]. Elder et al [51] conducted an extensive review of tools that have been developed with the aim of predicting the formation of impact damage due to low velocity impact events. The conclusions drawn highlight the difficulties faced by current techniques and the need for further developments in order to

achieve accurate delamination predictions to meet the demands of aircraft engineers. Until such tools exist, composite structures will continue to be over designed.

Prevorsek et al [26] identified that the majority of damage to composite structures is restricted to the matrix and fibre damage is negligible. Consequently fracture toughness and crack propagation resistance in modes I (opening) and II (shearing) are typically used to assess the suitability of a matrix material for a damage tolerant design.

Improvements in creating damage tolerant composite materials have been made by focusing on four main parameters:

1. Stacking sequence
2. Reinforcing fibre architecture
3. Strain to failure of CFRP
4. Alterations to matrix material.

The stacking sequence of a composite laminate can be seen to have a large effect on the damage tolerance of a composite material [52,55]. Therefore, laminate parameters are defined in order to guide designers in order to achieve the most suitable stacking sequence.

- Balanced: Angle plies must be balanced in order to avoid undesirable stiffness coupling effects
- Symmetric: Required to prevent bend-twist coupling
- Limit on contiguous plies: No more than four plies of the same orientation should be contiguous to avoid severe matrix cracking which increases the risk of delamination

Further measures can also be taken such as a limit to the fibre direction mismatch between adjacent plies to ≤45° [52] and ensuring non load-bearing plies located on the outer surface of the structure. Generally, it is observed that matrix-dominated stacking sequences ('soft' laminates) or high in-plane shear concepts that contain a high proportion of off-axis plies are more damage tolerant than fibre dominated stacking sequences ('hard' laminates) that have a high proportion of load-bearing plies [53,54].

Additional research has looked into methods of optimising the laminate lay-ups. Todoroki et al [56] developed an optimisation technique which uses a genetic algorithm and repair technique to produce an optimised lay-up which meets the three design guidelines outlined above. Tanimoto [55] considered naturally occurring fibre reinforcement architecture to develop a biomimetic laminate of 78° angle difference between successive plies as opposed to conventional 45° or 90°. These optimised lay-ups showed potential improvements to laminate design, though consideration for manufacturing implications were not considered.

The architecture of reinforcing fibres within a laminate has a significant effect on damage tolerance by suppressing the initiation and propagation of delaminations at weak ply interfaces [54]. The fibrous nature of reinforcing material used for FRPs creates the possibility of non-planar reinforcement, using fabrication methods originally developed for the textile industry [57] (Figure 2-1).

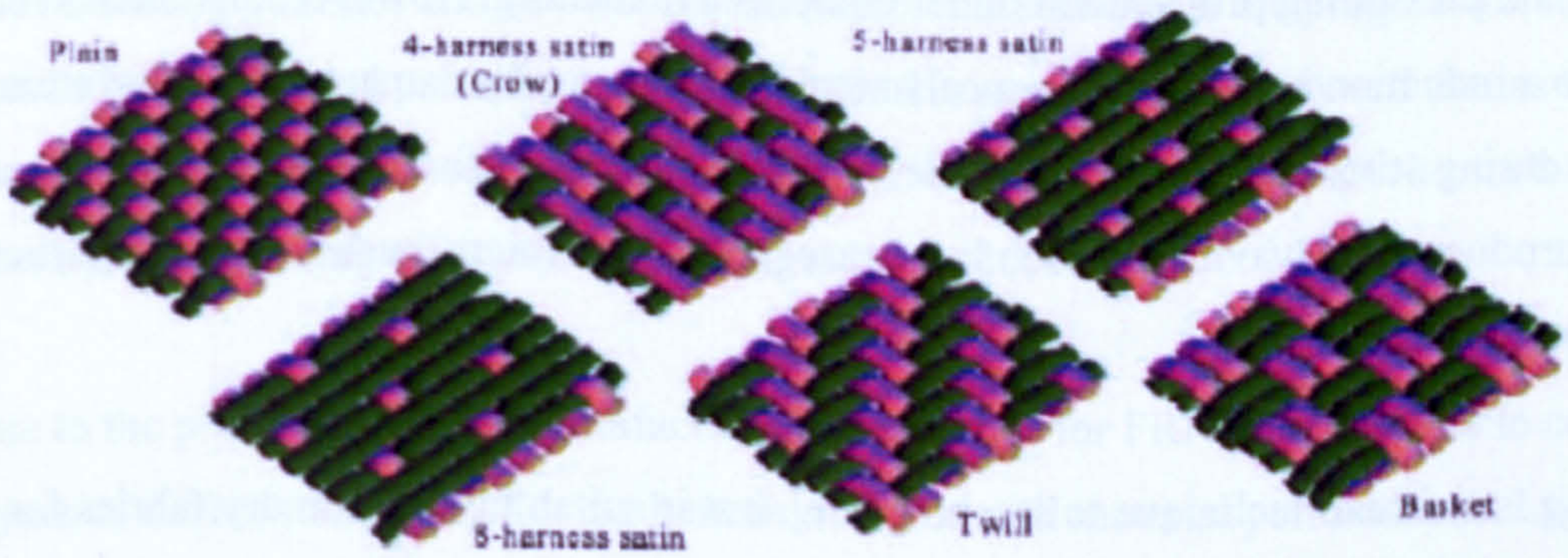

Figure 2-1: ***Three Dimensional Reinforcing Fibre Architecture [58]***

These techniques weave reinforcing fibres into complex reinforcement architectures which impede the propagation of shear cracks and delaminations. Also, due to their more compliant nature, a larger proportion of impact energy is absorbed through structural response rather than the formation of damage. However, the provision of strength and stiffness in two directions and the undulations in the woven fibre means that fabric FRPs cannot achieve the levels of performance typically found in unidirectional tape FRPs [1]. Some of the detrimental effects of using woven fabric can be overcome through the use of non-crimp fabrics (NCF) where unidirectional fibre tows are held together by a binding stitch, usually of a different material (polyester or glass) to the reinforcing fibre. Again, a

degree of fibre crimping and waviness can develop which leads to a reduction in mechanical performance.

The addition of reinforcing fibre in the 3rd dimension further extends the use of fabric technology to improve the material's damage tolerance. The incorporation of through thickness fibre reinforcement improves delamination resistance, however, it does create potential for other failure modes that are not of concern in unidirectional laminates. Furthermore, any improvements achieved using this technique is inherently dependant on factors such as weave pitch and tow size.

An additional technique developed to good effect in FRPs is stitching [57,59]. This involves driving highly flexible material such as aramid or glass fibre, in a complex stitching pattern into the laminate to bind the reinforcing plies prior to curing. This greatly improves the impact resistance and damage tolerance of laminates made from unidirectional pre-impregnated tape by inhibiting delamination formation during an impact event and preventing propagation under compressive loading. However, this method can lead to a reduction in the in-plane mechanical performance by damaging the reinforcing fibres during stitching. Furthermore, the stitches can act as initiation sites for damage and can introduce fibre waviness which has consequences for micro-buckling and in particular compressive failure.

Tufting is a similar technique to stitching [60], but is suitable for use in dry fabrics for RTM manufacture. It has a simplified manufacturing process but also poses the same problems as stitching.

Another interesting proposal is the insertion of through thickness reinforcement (Z-pins) in the form of high stiffness, high strength materials such as titanium alloy, steel or fibrous carbon composite into uncured pre-preg tape [60,61]. The diameters used range from 0.2-1.0mm and are inserted using ultrasonic assistance. Mauritz et al [62] have recently conducted an extensive review of this topic and their paper should be consulted for a detailed overview. In general, the benefits of this technique were found to be improved delamination resistance, damage tolerance through thickness stiffness and joint strength. However, Z-pinning was found to have detrimental effects on in-plane mechanical properties such as elastic modulus, strength and fatigue life. Although it was concluded

that in general the improvements in inter-laminar properties out-weigh the reductions in in-plane properties. The author identified the need for further research into reducing the diameter of the Z-pins as inter-laminar properties could be improved and the detrimental effects to in-plane properties could be minimised. Furthermore, non-axial loading and in-service environmental conditions should also be explored in order to demonstrate maturity of the technology.

Improvements in damage tolerance have also been achieved with the inclusion of a secondary material at key locations in the stacking sequence [54]. The additional material can take the form of discrete toughened layers, toughened particles on the ply surface [63,64] or hybridisation with other composite or metallic materials.

The first use of inter-layered toughening found that although the layer acted as a suppressant against initial impact damage, the low strength and stiffness of the added layer resulted in the need for additional plies to maintain design performance [65]. Along with poor handling qualities and hot-wet performance, this stimulated the progression to distributed toughened particles at ply interfaces. However, it was observed that as the particle size was decreased, they began to disperse throughout the composite such that the interlayer toughening effect would no-longer be produced [63].

Due to the planar nature and manufacturing approaches for FRPs it is possible to combine layers of different materials for the benefit of the overall material performance. Layers of two types of FRP can be combined in order to draw on the specific benefits of each laminate. For example, CFRP laminates can by hybridised with GFRP or aramid fibre laminates in order to improve damage tolerance. More specifically, using outer plies of aramid FRPs improves the impact resistance of a CFRP laminate but the planar mechanical properties of the laminate are reduced [66].

The hybridisation of FRPs with metallic materials has produced materials that combine the durability and machinability of metals with the excellent specific properties, fatigue and fracture characteristics of composites. Products such as GLARE® (glass fibre/aluminium), ARALL® (aramid fibre/aluminium) and CALL® (carbon fibre/aluminium) have all found commercial applications in the aerospace industry. They also provide a number of energy

absorbing characteristics such as ductile tearing and plastic deformation that are not usually present in FRPs.

The properties of the matrix within an FRP have an overriding influence in the impact resistance and damage tolerance. Suppliers of matrix resins and pre-impregnated tape materials have developed increasingly tough resin systems [1]. Some commercially available pre-impregnated tape materials contain toughened inter-layers of thermoplastic particulates located on the surface of plies (Hexcel M21, Toray F3900). Although these materials have been shown to improve damage tolerance they create a larger scatter in performance and poor distribution of the particles can lead to limited improvements in strength.

A variety of modifications to epoxy resin systems have been explored [67] with the introduction of an elastomer phase [68], thermoplastic particles [69-71], hard particles [72], glass micro-beads [73] and hollow glass micro-spheres [74]. The literature has shown that the use of hard particles, micro-beads and more recently glass micro-spheres shows improved damage tolerance by increasing the fracture energy and providing crack pinning effects. The addition of an elastomer-phase to a brittle epoxy matrix was found to lead to important toughening mechanisms: localised shear yielding and improved energy dissipation through plastic yielding.

Although these technologies offer potential toughening mechanisms, the majority have been demonstrated for bulk polymers and therefore the potential detrimental effects of their inclusion within FRPs have not been investigated fully. Moreover, the introduction of an elastomer phase has been shown to decrease the modulus, and increase water absorption with an accompanying loss of properties at elevated temperatures. The addition of thermoplastic particles addresses the issues created by the use of elastomer particles. However the toughening mechanisms are not as well understood and are the focus of continued research.

Morri et al [75] used a modified flexible epoxy to form a hybrid with a conventional epoxy system. The aim was to improve the damping and impact resistance characteristics for GFRP. It was found that if the modified resin was located at the impacted surface, the energy absorption increased exponentially with the increasing fraction of flexible resin.

This was attributed to the recoverable deformation in the flexible resin. However, the mechanical performance of the hybrid matrix laminate in comparison to a conventional matrix laminate was not determined.

Xian and Choy [76] considered replacing the commonly used epoxy resin with a bismaleimide (BMI) resin modified with the incorporation of thermoplastic particles in order to address the problematic brittleness of epoxy resin systems. The result was a high toughness, high temperature resin with ease of processing. It was concluded that the use of the modified BMI resin improved the toughness and fibre/matrix adhesion thereby enhancing the static and fatigue fracture performance. It was also found that the modified BMI laminate achieved a higher fatigue life and damage tolerance than the epoxy laminate and so would be more suitable to a wider range of applications.

Improving damage tolerance of FRPs does not eliminate the formation of damage. Instead, it raises the threshold energy levels required for damage initiation and propagation. Therefore, if the materials are struck by a foreign body with sufficient energy, damage will be formed. If sufficient load is then applied, the damage will propagate. Therefore, the need to repair or replace damaged structural components continues to exist and will be necessary for the foreseeable future.

2.3.2 Methods of Composite Repair

When damage to a composite material is detected, and its impact on the residual performance of the material has been assessed, it must be determined whether the part must be repaired or replaced. The three main categories of composite repair are:

1. Major damage repair: *Significant damage that reduces the load-carrying performance of the material must be repaired immediately, although more adequate permanent repairs must eventually replace these temporary measures. The temporary repair may consist of a bolted metal patch or bonded composite repairs.*
2. Minor damage repair: *Small damage that still allows the material to sustain ultimate load must be repaired within a certain period. Until a permanent repair takes place, the damage site must be addressed to prevent damage propagation, water ingress and disruption to the airflow.*

3. Negligible damage repair: *Cosmetic damage may only require measures to restore the surface of the component.*

The repair technique can be characterised by the method used to attach the repair to the structure, the joint. Two methods exist:

1. Mechanically fastened [77]: *Repair patches are attached to the aircraft structure with the use of mechanical fasteners such as bolts or rivets*
2. Bonded [78]: *Repair patches are attached to the aircraft structure with the use of polymeric adhesives*

Repairs are made using either method or a combination of the both [79].The main advantages of each method of composite repair are outlined by Baker et al [80].

2.3.2.1 Bolted

The use of bolted repairs is primarily for medium to high load applications. The main benefits of mechanical joints are that they are insensitive to surface preparation and generally have a simplified manufacturing process. The overriding problem for use with composite structures is that the preparation process can be damaging to composite components and the final joint creates considerable stress concentrations. Care must be taken if the repair patch is metallic and the composite structure is carbon/epoxy as galvanic corrosion can become an issue. Thus, titanium is often used, or aluminium with an appropriate coating for corrosion protection. The repair must also produce adequate electrical bonding to account for lightning strike protection.

A very simple repair configuration would consist of removal of the damaged material and a metal patch bolted across the damaged region. A number of problems are encountered when utilising bolted repairs on composite structures:

- Drilling: This can cause extensive damage to the composite by causing splitting and delaminations. These effects can be limited by using high speed, low feed drill rates and by supporting the back face.
- Stress concentrations: Adequate spacing between holes must be ensured to limit the stress concentrations present in the structure. Furthermore, adequate spacing must be ensured between the holes and both the damaged region and the repair patch edge for similar reasons.

- Clamping forces: Due to poor through thickness performance in composite materials, any clamping forces exerted by the bolts must be spread over a sufficiently large area.

Bolted joints are almost exclusively used in military operational repairs due to their simplicity and high load performance [81].

2.3.2.2 Bonded

Bonded repairs are typically used in the low to medium stress range. They comprise of a chemically bonded repair patch over the damage site, and have the advantage that no additional stress concentrations are imparted into the structure. The performance of a bonded repair is directly dependent on the selection of an adhesive and its corresponding properties. Careful design of bonded repairs is required to ensure that stress distributions are tolerable and that shear stresses are within the limits sustainable by the adhesive.

Bonded metal patch repairs can be applied with the use of a single scarf joint, which produces a nearly uniform stress distribution in the adhesive and low peel stresses. It has the benefit that unlimited thicknesses can be repaired and smooth external surfaces can be produced. The disadvantages of such a repair are that such a joint is not easily created in the field and that a significant amount of material is removed to achieve the large scarf taper ratios required (18:1-20:1).

Bonded composite repairs generally consist of an external patch, a composite insert and an internal sealing plate all held together with a carefully selected adhesive. The edges of the external patch are often tapered to reduce peel stresses and shear stress concentrations. This also provides a large load transfer region, which increases the load that the adhesive can sustain. Problems arise because of the eccentric load path after application of the patch, resulting in severe bending, peeling stresses in the adhesive and ultimately a reduction in the stability of the repaired component. Some of these issues can be addressed by using a staggered joint. This staggers the layers in the external patch (especially in the regions overlapping the repaired structure) in order to create several load transfer zones as opposed to the small transfer zones in the simple tapered configuration. This has the benefit of reducing peel stresses and stress concentrations in the adhesive.

The Australian Airforce (RAAF) were the pioneers of bonded composite repairs to metallic structures, and a large amount of research and development has been led by Baker [82-84]. Some examples of military and civil aircraft repairs can also be found in other work [85,86]. Primarily, boron/epoxy or graphite/epoxy composite materials were used to patch or reinforce a defective or degraded metallic structure. Composite materials provide a stiff alternative load path and so can be used effectively to repair 'live' cracks. In contrast, standard mechanically fastened metallic patches provide a relatively compliant alternative load path and so cannot be effectively used to repair cracks [86]. The benefits of composite materials for repair and patching of metallic structures are:

1. High stiffness and strength which minimises required patch thickness
2. Highly resistant to damage by cyclic loads
3. High formability for complex shapes

The material of choice for RAAF is boron/epoxy for these further reasons:

4. Low electrical conductivity which facilitates eddy current NDI for health monitoring and eliminates galvanic corrosion
5. Higher coefficient of thermal expansion than CFRP which reduces residual tensile stresses in repaired components.

The use of composite materials as opposed to metallic materials for repairs means that no material is required to be removed from the damaged area, slow crack growth is maintained even on exit from the patch, no corrosion problems occur due to the sealed interface and the ability to detect crack growth under the patch. Finally, the use of composite materials presents the opportunity to incorporate sensors or smart materials into the repair patches.

2.3.2.3 Novel Approaches to Improve Standard Repairs

Advances in smart material applications for composite patches have been developed primarily to monitor the health of the patch and the adhesion between bond and structure. Chui et al [87], and Koh et al [88,89] considered the development of a 'perceptive repair' that would provide information regarding the in-service performance of the repair and associated structure. The aim would be to identify any in-service problems and allow preventative measures to be taken before failure of the repair or repaired structure occurs. The authors proposed the use of piezoelectric or piezoceramic patches that could use impedance to determine the presence of damage and a transfer function technique used to

determine the effect of the disbond between the patch and structure. Although reservations are made for the integrity of the piezoelectrics in the vicinity of high stresses, so the authors suggest that PVDF (Polyvinylidene Fluoride) may be more suitable for the application. Further work by Koh et al considers the use of surface mounted piezoelectric transducers to generate lamb waves [90] and an array of surface mounted lead zirconate titanate and polyvinylidene fluoride sensors [91] in order to detect of disbond under a repair patch.

The embedment of optical fibres into the composite repair patch has also been considered to monitor the strain field variations and determine the health of the repair [92]. The embedding of optical fibres is a promising technology within advanced composite materials and is considered in more detail in Chapter 4, section 3.1.

Wang [93] considered the incorporation of shape memory alloy (SMA) wires into a composite patch in order to produce an active closure stress in the repair process. The SMA (Ti-Ni) wires are capable of recovering their trained shape due to their transformation from martensite to austenite when heated above their transition temperature. When embedded within the composite repair patch they are expected to be able to produce extra bridging stress or active crack closure stress to increase the efficiency of the repair, to increase the fatigue threshold and delay crack growth. Disbonding between the SMA wires and matrix material was found to be a limiting factor on the amount of pre-strain that may be applied to the SMA wires. The volume fraction of SMA, matrix modulus and patch thickness were limiting factors for the achievable active closure stress.

Resin injection is a repair method considered by a number of authors [94-96] to repair delaminations around fastener holes and due to low velocity impact respectively. Liquid resin was infiltrated into the damaged region by attaching the structure to a vacuum pump. Once the resin had infiltrated the damage, pressure was exerted to force the resin into cracks and delaminations. A resin system was specifically developed for the application by meeting the following requirements:

1. Ability to adequately restore inter-laminar strength, fracture toughness and fatigue crack growth resistance of the re-bonded surface.
2. Cure temperature compatible with heat resistance of the structure to be repaired

3. Full cure achieved without the release of volatiles as they would produce voids in the repair.

Additional investigations were reported by Tzetzis et al considering the surface morphology [97] and general performance of resin infused single scarf repairs [98]. It was found that the repair was improved by surface preparation using abrasive techniques and particularly benefited from the removal of the weak boundary layer created from the residual fluorine species deposited from the pre-preg peel ply.

Any form of repairs to composite structures inevitably relies on the ability to detect the occurrence of damage and to adequately assess the region in order to propose an adequate repair solution. The emergence of a new technology is receiving an increasing amount of global interest as a means of autonomously repairing damage to composite materials that is difficult to detect. This technology derives inspiration from biological systems of repair and has coined the term self-healing or self-repairing.

2.3.3 Self-Healing Concept

Current approaches seek to address damage by improving the damage tolerance to minimise its effects, preventing cracks from propagating and by repairing or replacing structures that have experienced an intolerable level of damage. However, improvements in damage tolerance can come with a penalty in terms of mechanical performance, increased weight or increased material costs. Furthermore, improving damage tolerance does not eliminate damage in the structure, it merely seeks to raise the energy threshold for damage initiation and propagation.

Repairing or replacing components is costly in terms of time and financial resources. It also relies on the ability to detect damage which can be problematic for low energy impact damage such as BVID. Furthermore, aircraft components can be over designed and overweight in order to allow for bolted repairs. This effect can be minimised with the use of adhesives to create bonded repairs, however, this can be problematic in a commercial environment for certification purposes and also purely in terms of perception that an adequate and reliable repair has been completed.

Therefore, the concept of self-healing has been developed as an alternative approach and is receiving an increasing amount of interest worldwide as a method of autonomously repairing damage to structural materials and in particular advanced FRP's. An autonomous self-healing approach would theoretically remove the need to detect damage and the need to perform temporary repairs to damaged structures. This concept is a biomimetic approach that derives inspiration from both Mammalian and Plantae tissue repair and regeneration. Although biological systems of repair have a level of complexity that is currently unattainable for engineering structures, the basic principles have served as inspiration for research into self-healing for structural applications and will continue to provide systems to which engineers will aspire.

A review of self-healing must begin with a brief study of mammalian and plantae systems before approaches in engineered structural materials are considered in detail.

2.3.3.1 Biological Self-Repair

The response of organisms to damage in nature is characterised by sealing penetrative damage, restoring/diverting functionality to or from the afflicted region, complex tissue regeneration and eliminating effects such as infection due to the presence of foreign bodies. All of these are autonomous processes that react to an external stimulus with the clever use of biochemical systems within the organisms. They combine to heal damage and ultimately prolong the life of the organism. Parallels can already be made with functional structures and materials used in engineering.

The human method of tissue repair is a good example of a mammalian healing process and represents the ideal functions sought for an engineered structure [99] as living tissue has the remarkable ability to heal itself in response to damage [100]. The healing process (hemostasis) is complex but in essence sees coagulation of blood to form a fibrous patch over the damaged area. Small cells called platelets then combine to repair the tissue damage that was sustained. The process revolves around the biochemical reactions of a series of active enzymes and their inactive precursors known as clotting factors which essentially form an enzyme "cascade" of reactions involving clotting factors, a concept proposed by Macfarlane [101] and Davie and Ratnoff [102]. One of the most notable features of the haemostatic system is that despite the rapid response to injury, system

malfunction is extremely rare [103]. This is ensured by the rapid removal of activated enzymes in the fibrinolysis process, due to the production of plasmin and the action of endothelial cells [101]. Endothelial cells initiate a series of reactions that break down fibrin, such that any fibrin produced in a region of injury and carried away by blood flow is broken down in undamaged areas of the circulation so as not to form clots in undamaged blood vessels [103].

Mammalian healing systems are complex and deal with a wide variety of different materials and structures. Healing systems in plants are often more simplistic and tailored for more rigid structures. Therefore, they may provide a more realistic prospect for approaches that may be used or adapted for engineering structures and materials.

In plant systems e.g. trees, it is internal scabbing or the formation of internal impervious boundary walls that develop over time to protect the inner bark from further damage [104]. This defence mechanism (compartmentalisation) uniquely sacrifices the wounded bark but ensures that fluid diffusion and infectious micro-organisms never extend beyond the wound site [105]. This is applied to some degree at several layers in a tree including the bark, the xylem and phloem vascular tissue and even to some extent within the heartwood deep in the trunk. It is a two-part process in the upper layers:

1. Short term: A chemical boundary is activated to protect against pathogens present at the time of injury
2. Long term: Formation of a barrier zone gives continued protection from pathogens [106,107].

Shigo [106] argues that compartmentalisation allows trees to survive to a great age, despite injuries, providing that sufficient material for "normal function" remains outside the isolated regions of damage. "Normal function" includes structural considerations, since the boundaries are structurally weak and represent a loss of load carrying material; it takes further conventional growth to restore structural performance. There is debate whether this approach can be really be termed self-healing [106,107]. The xylem vascular conduits are themselves compartmentalised and there is no provision for sealing breached vessels although redundancy allows the complete loss of injured vessels [108]. Nevertheless, it has shown to be an evolutionarily successful way of managing injury.

A number of workers have considered the use of naturally occurring elastic proteins for use in structural applications [109,110]. Such examples include 'rubber like proteins' such as resilin and elastin, collagen, spider silks and mussel byssal fibres [109]. Elastic proteins are classified as structural proteins that under appropriate conditions exhibit reversible elasticity and/or stretchiness. All elastic proteins are found to represent good designs however they are not always exceptional in their mechanical properties. In particular, collagen has unmatched capacity for storage of elastic-strain energy and spider silks have unmatched toughness. Distal byssus fibres are an intriguing hybrid combining features of spider silk and tendon collagen in the same material. They consist of two distinct regions:

- Distal portion: Typical fibre reinforced composite in which oriented collagen-containing fibrils are dispersed in a soft proteinaceous matrix. Contains collagenous proteins preCol D (hard segments) and preCol NG (intermediate segments) in the thread.
- Proximial portion: Densely packed fibrous bundles held together by intermolecular covalent and non-covalent cross-links. Contains collagenous proteins preCol P (soft segments) and preCol NG in the thread.

When dried or plasticised by solvents these fibres were found to achieve greater strength with little compromise in extensibility. Byssal fibres also exhibit a degree of self-healing [110]. When fibres have undergone cyclic tensile testing under certain solvent treatments, they have been observed to completely recover their initial Young's Modulus within 3 cycles (60mins). Although the understanding is not currently mature enough for adaptation to structural applications it presents interesting possibilities for healing of damaged reinforcing fibres.

2.3.3.2 Cementitious Composite Materials

The earliest work on self-healing materials was used to address damage formed in cementitious composites for civil engineering applications. Dry et al [111-115] detailed several approaches for the deliverance of crack healing adhesives and permeability improving chemicals. Two active systems were proposed:

1. Wax coated porous fibres which required temperature to melt the coating and release the stored monomer (Figure 2-2)
2. Porous fibres continually refilled with a vacuum pump (Figure 2-3)

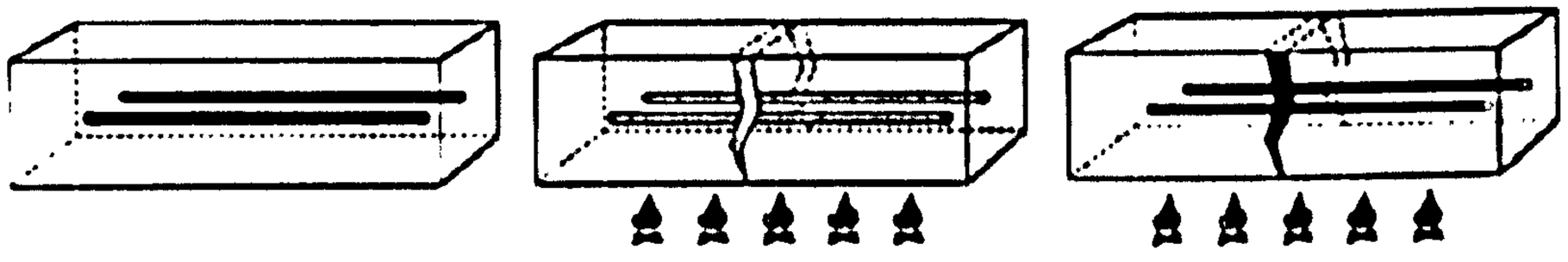

Figure 2-2: ***Active System for Self-Heal within Cementitious Composites [18]***

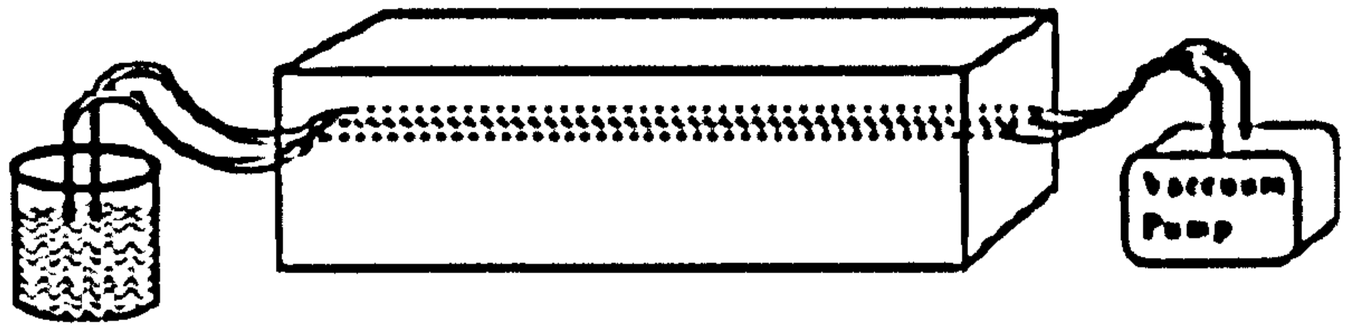

Figure 2-3: ***Method for Refilling Self-Heal Adhesive [18]***

Results showed that the active systems of delivering the monomer from an internal source produced improved compressive strength and less permeability than conventional surface applications.

A passive method was also considered by incorporating adhesive filled hollow glass pipettes. This method was shown to fill gaps and cracks within the material with a solid matrix, restored strength and structural flexibility. It was also used for a successful demonstration in large scale concrete bridge decks to drying shrinkage cracks and shear cracks. It was found that the fibres allowed the control of the crack location as they acted as damage initiators.

Additional work conducted by Dry [113] identified the possibility of using the hollow fibres as light carrying medium in order to assess the volume of healing resin remaining in the fibres. However this does assume that the repair resin remains uncured within the fibres, which may not be the case for some resin systems that rely on polymerisation. Work conducted by Dry lead to the submission and acceptance of a US patent covering a broad perspective of self-healing for structural applications [116].

Li V.C. et al [117] used a passive approach similar to previous authors and recognised the need to restrict the crack width in order to ensure that:

1. The capillary action of the small crack surfaces exceeds that produced by the fibre and facilitates the release of the resin into the crack surfaces
2. To limit the amount of repair resin required to heal the surfaces thereby keeping the glass pipette dimensions to a minimum.

Initial testing demonstrated the potential success of the method and also identified the need to address viable large scale manufacturing techniques and also refinement of the resin system.

Although the initial exploits into self-healing materials originated in cementitious materials, the methods used are not directly applicable to FRP's because of differences in the material microstructure, manufacturing and operational use. Furthermore the motivation behind the need for self-healing functionality is also based on different requirements such as altering material permeability and sealing damage with less emphasis on recovering mechanical performance. However, some of the conclusions drawn from the work have relevance and should be considered in the development of any self-healing system.

2.3.3.3 Self-healing in Bulk Polymers: Compartmentalised Approach

A significant body of research has considered self-healing approaches for bulk polymers. For some, demonstration of a self-healing concept is first conducted in bulk polymers before progression into fibre reinforced polymers. The possibilities for self-healing in bulk polymers are somewhat simplified by the absence of reinforcing fibres.

Dry undertook a rudimentary study into the application of self-healing functionality to polymers [118]. Here it was noted that micro-cracks present within a polymer matrix acted as sites for environmental degradation (water ingress) and as sites for the further nucleation of micro-cracks. Conclusions drawn from the work were that the adhesive (two part crosslinking epoxy and single part cyanoacrylate):

- Migrated along and healed the cracks
- Impeded crack propagation
- Prevented cracks from reopening and instead forced new ones to form
- Restored impact strength and the ability to deflect while carrying a load

Approximately 8-12 months was the time allocated for the healing events, which is not a realistic time frame for the healing of damage in composite materials.

A group at the University of Illinois have contributed a substantial amount of work to the field of self-healing in bulk polymeric materials. The method employed has focused on the distribution of a microencapsulated healing agent, Dicyclopentadiene, (DCPD) and a catalytic chemical trigger Grubb's catalyst (bis(tricyclohexylphosphine) benylidine ruthenium (IV) dichloride) within the host epoxy matrix [119-132]. Propagating cracks rupture the microcapsules, releasing the liquid healing agent via capillary action which infiltrates the crack plane and polymerises upon contact with the exposed catalyst (Figure 2-4). The microcapsule shells were formed from urea-formaldehyde in a process that simultaneously encapsulated the DCPD repair agent [120]. Therefore, it was a critical requirement that the healing agent was compatible with an encapsulation process. This is a potential limitation in the selection of a healing agent and may limit the further applicability of this method.

An extension of this work has investigated alternative healing systems based on a Polydimethylsiloxane where the catalyst is encapsulated and the healing agent is phase separated in a vinyl-ester resin matrix. This offered the benefits of simplifying manufacture, reducing cost and maintaining the stability of the system in humid or wet environments [121].

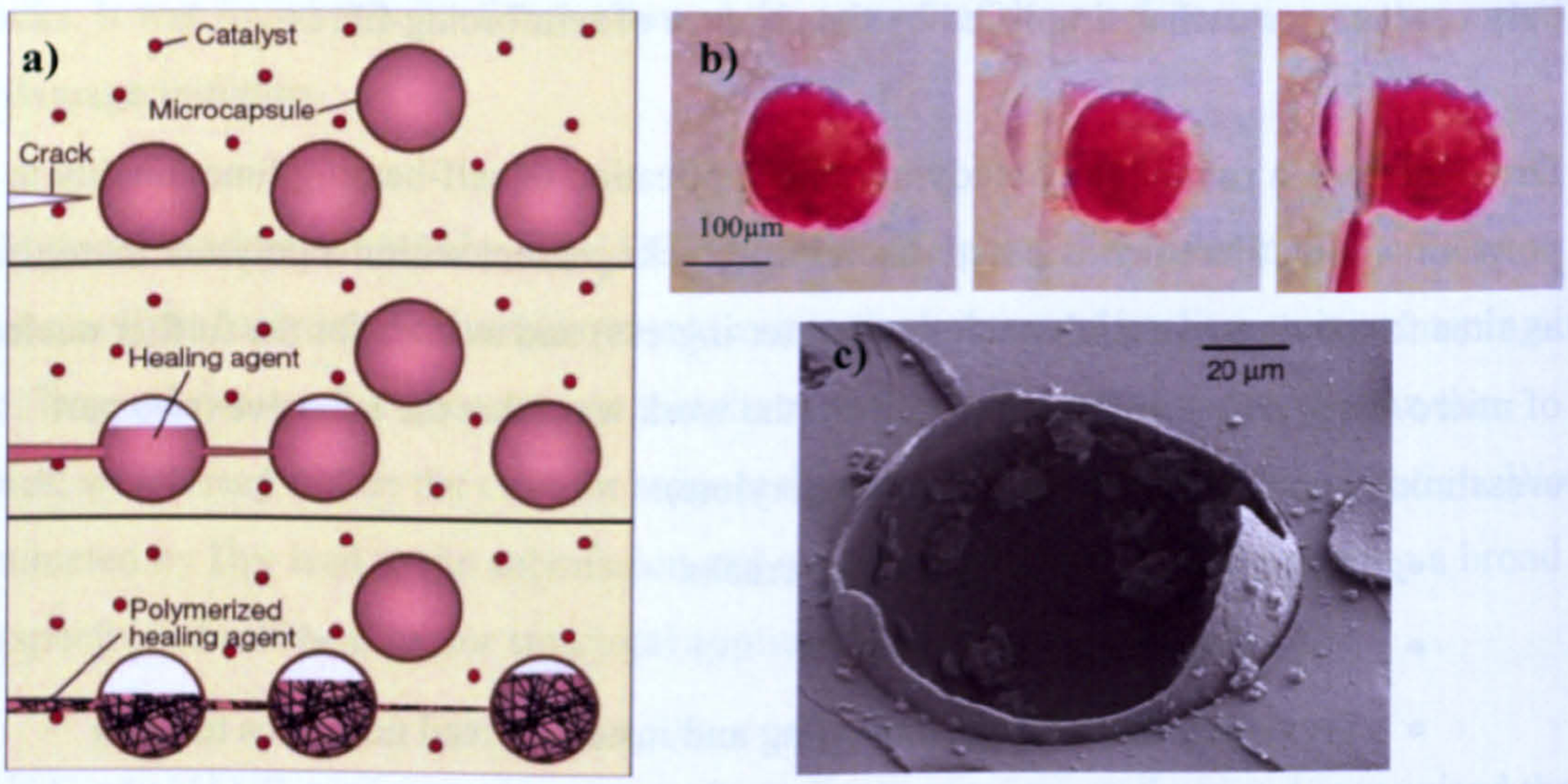

Figure 2-4: ***a) Schematic of the Autonomic Healing Process b)Rupture of a Microcapsule using Red Dye for Visualisation c) Ruptured Microcapsule using Scanning Electron Microscope*** **[119]**

A number of authors have considered optimisation of the ring opening metathesis polymerisation (ROMP) reaction [122-124] and the choice of catalyst [125]. Polymerisation of DCPD with Grubb's catalyst can occur within 5 minutes in ideal conditions as the system undergoes ROMP. Grubb's catalyst is classified as a 'living' catalyst and so it remains active after polymerisation. DCPD was selected as a suitable system to meet the diverse requirements for a self healing system: long shelf-life, low monomer viscosity, low monomer volatility, rapid polymerisation at ambient conditions and low shrinkage upon polymerisation. Furthermore, DCPD was found to be suitable for microencapsulation. However, the low viscosity and low molecular weight of DCPD led to rapid diffusion from the damaged surface before polymerisation could occur. If this issue is combined with the high cost of Grubb's catalyst, the suitability of this system for large scale industrial application is questionable.

The use of DCPD/Grubbs as an effective self-healing system in bulk polymers has been assessed using tapered cantilever beam (TDCB) testing in order to assess the mechanical performance of the system under static and fatigue loading. A sharp 'pre-crack' was initiated at the centre of specimens which was then propagated, crack closed, healed and re-tested to assess healing efficiency. Three different configurations were considered which represented different levels of autonomy:

1. Manually injected DCPD and Grubb's catalyst: Not autonomous
2. Manually injected DCPD and in-situ Grubb's catalyst: Partially autonomous
3. In-situ DCPD and Grubb's catalyst: Autonomous

This enabled assessment of the effect of microcapsule and catalyst dispersal within the matrix and the exploration of their contributions to both the mechanical performance of the material and the efficiency of the healing. The efficiency of the healing was found to decrease as the autonomy of the system increased: 100%, 60%, 40% respectively. However, the propagation of a single crack through a polymeric material is not truly representative of real damage modes that would be expected if the material was to be used in structural applications and could lead to a further reduction in healing efficiency. It was found that improvements could be made by altering both catalyst and microcapsule size and distribution, which was also found to have beneficial effects on the host material [126,

127]. The application of heat was also found to increase the efficiency of the healing by increasing the rate of polymerisation and the degree of cure of the healing agent.

The inclusion of microcapsules and particulate catalyst within the neat epoxy acted as a toughening mechanism which produced 'hackle markings', 'tails' and subsurface micro-cracks, characteristic of fluid filled microcapsules and not seen with solid particle fillers [127]. It was also noted that good adhesion was required between the microcapsules and epoxy matrix in order for them to rupture and to contribute towards any subsequent toughening. Laminates containing microcapsules with poor adhesion behaved like voids of similar concentration.

It was found that Grubb's catalyst was susceptible to deactivation upon exposure to air and the DETA curing agent used in the epoxy matrix [126]. In order to achieve higher healing efficiencies it was found that smaller catalyst particles at higher concentrations were required which increased the risk of deactivation [125,126]. Thus, a technique to wax-coat the catalyst particles in order to prevent deactivation was developed. This coating was dissolved by the DCPD during the healing process [128].

Cyclic loading of TDCB samples [129-132] has shown that extended fatigue life results have been achieved for manual injection and in-situ placement of the healing agent. In this case, healing was achieved by two mechanisms:

1. Viscous flow of healing agent to retard crack growth
2. Short term adhesion of crack faces and long term crack closure.

In particular it was found that the fatigue life could be extended by thirty times for neat epoxy with embedded microcapsules. At low load levels it was found that the chemical kinetics of the healing dominated and prevented further crack growth. Faster chemical kinetics were achieved by wax coated catalyst or more readily soluble catalyst morphologies. In most cases rest periods in the load history were required to facilitate the healing process.

The micro-encapsulation approach has shown promise in terms of addressing damage to polymeric materials and particularly under cyclic loading conditions. However, it is restricted by the need for polymerisation to take place before the volatile monomer diffuses

from the crack plane. Furthermore, the healing efficiencies are significantly reduced as the level of autonomy is increased. The healing system was unable to be incorporated into a polymer at sufficient volumes to provide an efficient heal without significantly impacting the materials mechanical properties.

2.3.3.4 Self-Healing in Bulk Polymers: Molecular Approach

Taking a molecular approach, Chen et al [133] have developed a transparent organic, polymeric material that has the ability to mend itself under the application of heat and pressure. The material is a highly cross-linked polymer with mechanical properties 'equalling those of commercial epoxy resins'. The monomer has a weak bond which breaks when the material is loaded to failure or heated above its glass transition temperature. However, this bond is thermally reversible and so reforms when cooled. Samples were mechanically tested using a compact tension specimen, which consisted of extending a sharp pre-crack until structural failure occurred. The two pieces were then clamped together with the crack surfaces in contact and heated at between 120°C to 150°C in a nitrogen atmosphere for 2 hours. Visually, the two surfaces were repaired although small surface defects were observed due to the misalignment of the cracked surfaces. Healing efficiencies of around 50% were achieved with potentially limitless heal-ability, which offers some advantages compared to the compartmental alternatives mentioned above. However, the applicability of this technique to real structural applications may be restricted due to the need for fractured surfaces to be perfectly re-aligned and the reliance on heating/cooling cycles to facilitate healing.

Plaisted et al [134-136] have considered embedding wire (50-100μm diameter) within a similar polymer system [134] to produce in-situ heating required for healing. Tests showed that the wires could heat the polymer uniformly to 80°C to achieve a heal time of 24 hours. Taking this idea forward, the inclusion of wires for the purpose of heating the laminate would cause significant disruption to a FRP laminate. Furthermore, the system is not autonomous requiring a method of detecting any damage before application of heat. No assessment was made regarding the mechanical properties or integrity of the material during the heating cycle which could have implications for real structures.

Work by Hayes et al [137,138] considered a method of self-repair by dissolving a linear thermoplastic polymer into a thermosetting epoxy resin matrix. The solubility parameters were matched such that the healing agent remained uniformly dissolved within the matrix, without phase separation. The healing agent remained attached to the three dimensional epoxy matrix via hydrogen bonding but became mobile after the temperature was raised above 130°C, at which point the mobile polymer was able to bridge any cracks formed within the matrix. Charpy impact testing was used to assess the repair efficiency which was reported to achieve up to 75% depending on the percentage weight contribution of healing agent. However, it was identified that the pure matrix resin system also exhibited a degree of self-healing under application of heat, despite undergoing a post-cure. The authors also reported a visual reduction in impact induced delamination and micro-cracking when the system was employed in a glass fibre reinforced laminate. However, no mechanical assessment of this healing was conducted. The reliance of this system on the application of heat again removes the possibility of autonomy and introduces resilience upon damage detection, which is likely to be problematic.

2.3.3.5 Self-healing Polymer Composites

Motuku et all [139] conducted studies on self-repairing approaches in response to impact induced damage. A range of hollow fibres were embedded within an FRP in addition to the reinforcing fibres. Micro-capillary borosilicate glass and glass Pasteur pipets alongside copper and aluminium tubing were assessed for their viability as storage vessels for repair chemicals. Though the hollow fibre diameters used were relatively large compared to the reinforcing fibres and nothing was reported with regards to the implications this had on the host laminate. It was concluded that borosilicate glass was the most promising as it fractured easily and allowed the release of the resin. The presence of the hollow glass pipettes was shown not to influence the impact response of the laminate.

Bleay et al [140] developed this concept further by considering two derivations of this method for the self-healing (Figure 2-5):

- One part resin system contained in hollow glass fibres
- Two part resin system with resin contained in one fibre direction and hardener contained in another fibre direction

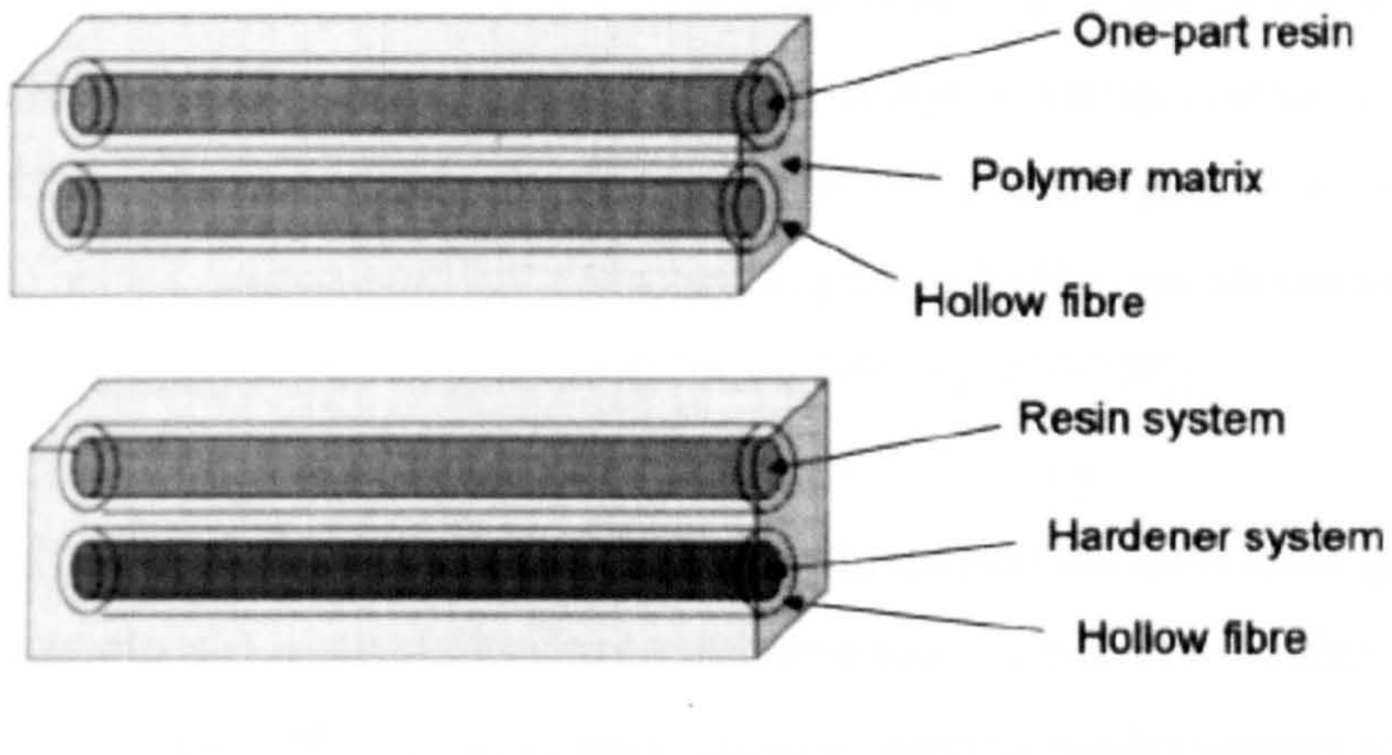

Figure 2-5: ***Two Approaches for Self-Healing Composites*** **[140]**

The hollow glass fibres used were commercially supplied Owens-Corning 'Hollex' S2-glass with an outer diameter of 15μm and an internal diameter of 5μm. It was estimated that with a fibre volume fraction of 0.65, a repair resin volume fraction of around 0.072 could be theoretically achieved. The hollow fibres were impregnated with HTM40U epoxy resin to form an entirely hollow glass UD prepreg, which was then used to manufacture 24ply $[(0,90)_{12}]_S$ and $[(\pm45,0,90)_6]_S$ glass hollow fibre composite panels for testing. Several systems were selected for assessment as the healing resin: one part isoacrylates and cyanoacrylates were selected over a range of cure times and viscosities (viscosities not specified), also two epoxy two-part resin systems were selected; MY750 and LY5120.

Only the low viscosity LY5120, successfully infiltrated into the fibres after it was diluted with acetone to form a 40%vol. solution and heated to 60°C. A 1% weight gain was measured after the infiltration of the two-part epoxy resin. Problems were encountered in the release of the resin system after impact damage and so heat and a vacuum were applied, to improve the situation. In addition to the repair system, an X-ray opaque dye penetrant was successfully infiltrated into the hollow fibres to visually demonstrate the HGF fracture upon impact. This also identified the ability to deliver a self-repair agent to damaged regions within the composite, although minimal strength recovery was achieved. It was also concluded that the use of larger diameter glass fibres could improve resin release and increase the volume of repair resin available.

Pang and Bond [141,142] undertook initial studies on self-healing laminates at the University of Bristol utilising the bespoke fibre manufacturing facility developed by

Hucker et al [143-146]. Their approach utilised drawn hollow glass fibres of 60μm external and 40 μm internal diameter respectively, embedded within a 913 epoxy resin film to form hollow glass fibre prepreg. An 18 ply 0°/90° hybrid solid/hollow glass epoxy laminate was manufactured utilising a hand layup process with stacking sequence

$$\{[90°/0°]_{(solid)},[90°/0°/90°/0°]_{(hollow)},[90°/0°/90°]_{(solid)}\}_S.$$

The healing resin selected was an epoxy, MY750 Ciba-Geigy, modified with 30%wt acetone to reduce the resin viscosity in order to facilitate the infiltration into the 0° hollow fibres. The corresponding hardener was infiltrated into the 90° hollow fibres. A UV fluorescent dye was also infiltrated into the 0° hollow fibres, mixed with the epoxy resin, to act as a damage visualisation medium upon damage initiation. Samples were damaged using quasi-static indentation at 3mm/min up to a maximum load of 1200N, which was equated to a 0.6J impact event. Samples were then tested in flexural four point bending to assess the recovery of mechanical properties after a healing event.

The damage event caused a reduction in strength of 12% and after healing, samples achieved 89% of the undamaged strength after 1.5hrs cure time and 97% of the undamaged strength after 24hrs. However, the need to dilute the repair resin to achieve infiltration suggests that the resin system is not suitable for the purpose of self-healing. Furthermore, the inclusion of discrete HGF plies would probably not be acceptable for realistic composite structure designs.

Trask and Bond [147] extended this work, again utilising HGF as storage vessels within GFRP laminates. The resin selected was a Cycom 823 epoxy which required the input of temperature to initiate cure (2 hours at 100°C). This resin selection was based on the target application of a satellite in low earth orbit with a view to effect repair of damage within one orbit (~90 mins) and exposure to ±100°C. Up to 87% flexural strength recovery was achieved when tested in four point bending after quasi-static indentation as the damage initiator. An initial reduction of 16% was observed due to the substitution of HGF plies for conventional glass plies. Furthermore, the use of UV dye mixed with the healing resin allowed visual observation of the damage infiltration which verified that the resin was released upon HGF fracture.

Kessler et al [148,149] extended the work on microencapsulation to explore the suitability of the DCPD/Grubb's system in woven E-glass/epoxy [148] and carbon fibre/epoxy [149] laminates. The best results were reported for plain weave CFRP where three levels of autonomy were tested, again resulting in decreasing healing efficiency as the level of autonomy was increased:

1. Premixed DCPD + catalyst injected: 99% heal efficiency
2. Injected DCPD, catalyst in situ: 73% heal efficiency
3. In-situ DCPD and catalyst: 38% heal efficiency

The effectiveness of the heal was found to be reliant upon the bond strength between the healing agent and fibre reinforcement as all failed samples exhibited interfacial de-bonding. Furthermore, it was noted that fibre bridging, which is a critical parameter for the inherent toughness of the material, would not be applicable to the healed material unless the crack path deviated from the virgin path. However this was not witnessed in the work conducted [148,149]

Three main problems were identified when using microencapsulated DCPD and Grubb's catalyst within FRP's:

1. The mean microcapsule diameter is relatively large (mean diameter 166μm Figure 2-6) when compared to the reinforcing fibre diameter. This resulted in an increase in ply thickness (60%) and consequently lower toughness.
2. Fracture was found to be primarily interfacial between fibre and matrix. Microcapsules were only fractured when the crack path deviated into the matrix.
3. Catalyst particles were found to form clusters which reduced the occurrence of in-situ polymerisation

The first point can be addressed by reducing microcapsule size, however the volume of resin stored is already relatively low and therefore limits the size of the damage that could be addressed. The slow rates of in-situ polymerisation also present challenges for structural applications as it may be necessary to recover mechanical properties and/or prevent damage propagation in several minutes, whereas the authors found that the maximum healing efficiency was reached in ten hours.

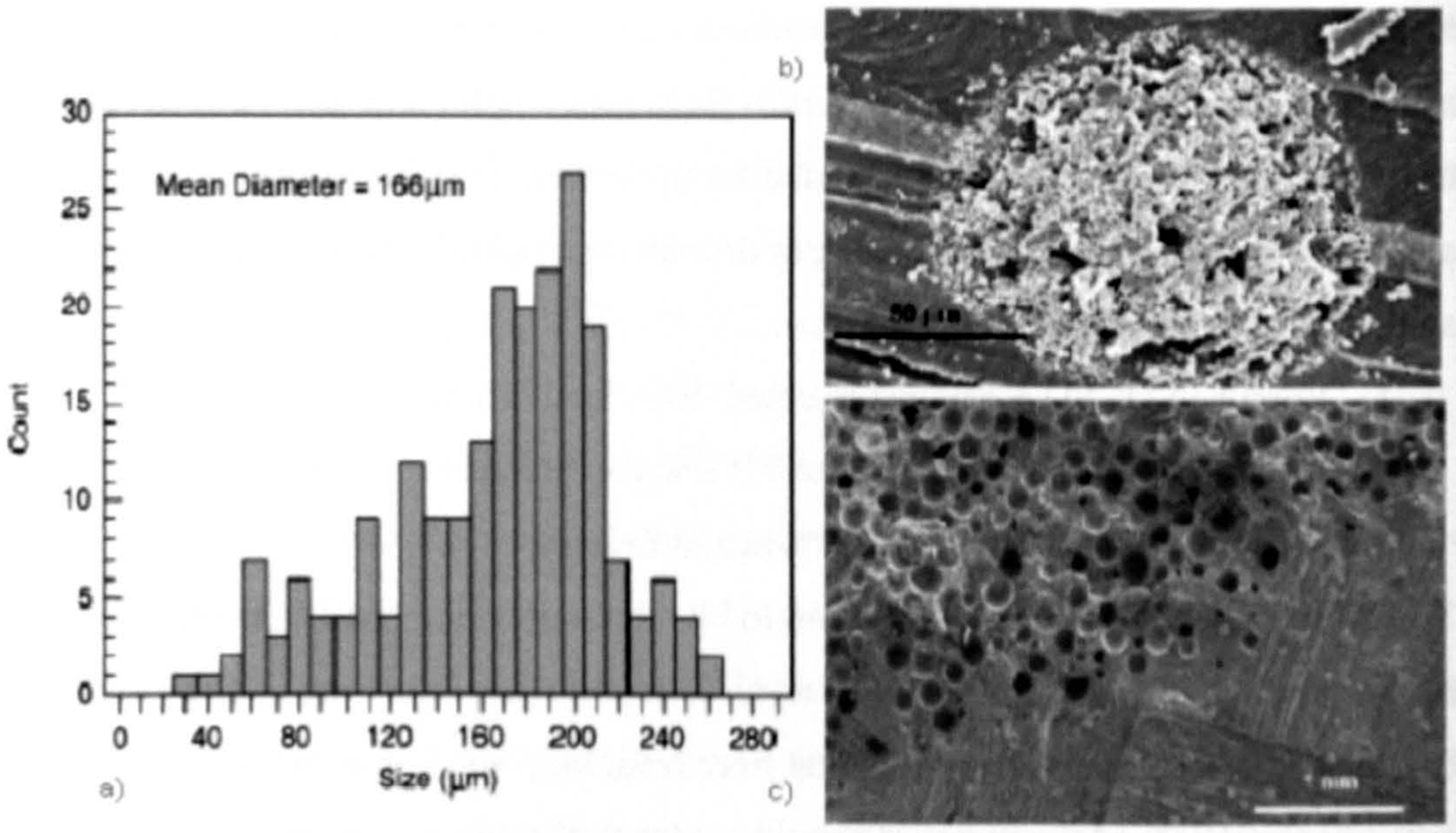

Figure 2-6: ***a)Size Distribution of Microcapsules b)Clustering of Catalyst (SEM) c)Fracture Surface showing Ruptured Microcapsules to Left***

Zako et al [150] considered an approach that comprised of an ambient temperature cure epoxy matrix, reinforced with unidirectional glass fibres and particles of thermosetting epoxy distributed throughout the matrix as the healing medium (max size 50µm). The epoxy particles were activated by the application of heat (120°C), which caused them to melt and infiltrate cracks before solidifying to heal the damage. Problems were encountered in the suitable application of heat to the damaged area without warping the matrix. Furthermore, this method relies inherently on the detection of damage in order to supply the required heat which removes the possibility of an autonomous approach.

Yin and colleagues [151,152] have microencapsulated an epoxy resin system and dispersed a soluble latent hardener in the epoxy matrix during manufacture. The host laminate was a woven E-glass/epoxy which was tested under DCB loading. The healing resin system required exposure to 130°C for one hour to initiate cure and average healing efficiencies of 68% were reported. The approach taken for mechanical assessment was similar to that taken by previous authors that have reported self-healing using microcapsules [119-132]. Therefore, as DCB testing involves the propagation of a single crack plane it is not truly representative of impact induced damage.

2.3.3.6 Self-Healing at the Nanoscale

Verberg et al [153] and Alexeev et al [154,155] have considered the modelling of a theoretical method for self-repair in which a microcapsule is driven along a heterogenous, adhesive substrate surface by the surrounding fluidic flow. When the particle encounters damage, its motion is halted which stimulates the release of stored nano-particles into the substrate in order to repair the underlying surface and allow the particle to continue its motion. This relies upon the phenomenon that a damaged substrate interrupts the flow of the microcapsule, and the release of repair nano-particles is dictated by Brownian dynamics. The workers report a model that examines the motion of the released nano-particles into the surrounding fluid with the aim of repairing the substrate, thereby allowing the particle to become mobile once again. Although this work presents an interesting concept for self repair within microchannels and microfluidic devices, there has yet to be a practical demonstration. Furthermore, this concept would be restricted to the repair of membranes and substrates in such devices and would not be suitable within fibre reinforced polymer composites

Lee JY et al [156] have conducted research which considers the possibility of using nanoparticles to mend cracks within a polymer matrix composite. The concept is based on the localisation of nanoparticles at nanoscale cracks to form 'patches' and effectively heal the damaged region. Computer modelling has been used to demonstrate the principle and also micromechanic simulations were utilised to evaluate the effectiveness of the healing process, which suggested that damaged composites could be restored to between 75%-100% of their original properties. The nanoparticles are dispersed within a polymer layer, which are used to repair a brittle surface layer in materials typically used for applications in optical communications, display technologies and biomedical engineering. However, the viability of this technology for use in structural composite materials is limited as the target damage is on a much smaller scale.

2.4 Observations and Conclusions

This extensive review of the open literature has illustrated the need for provisions to be made for FRPs in order to account for their susceptibility to foreign body impact damage. The detrimental effects caused by impact induced damage (delaminations and shear

cracks) have been highlighted. More significantly, the difficulties in detecting this damage, characterised as BVID, and the subsequent effect this has on the design allowables for aircraft structures have been highlighted.

The occurrence of foreign body impact damage has been categorised as 'in-service' due to operational hazards such as hailstones, runway debris and tool drop during maintenance tasks. In general, the most problematic classification of impact damage occurs at low velocity, creating damage that is primarily confined to the matrix in the form of matrix micro-cracks, shear cracks and delaminations. This BVID damage has been shown to cause a 50-60% reduction in strength without being outwardly visible.

The constant need to improve damage tolerance will continue in the form of improvements in commercially available resins systems. This may involve the migration from epoxy based systems or increasing the use of particle toughening. The use of novel fibre reinforcement architecture has also shown benefits and these materials have their uses in specific applications. However, for many structural components, unidirectional pre-impregnated tape manufacturing technology will continue to be preferred due to the excellent in plane mechanical performance that can be achieved. Improvements in damage tolerance will not prevent damage from initiating or propagating and therefore the need to repair or replace a component will still be necessary for the foreseeable future.

Comprehensive repair methods exist to address a wide range of damage events in composite materials, and they have been used successfully for both civil and military applications. Repairs to composite structures take the form of either bolted or bonded patches to transfer load across the damaged area and therefore maintain the structural performance of the material. However, the quality and lifetime of repairs reduces significantly depending on where the repairs are undertaken, a closely controlled environment being the preferred option. Repairs to composite materials will continue to be an essential maintenance option when structures are damaged such that they can not achieve their design performance. However repairs to mitigate 'wear and tear' may be replaceable if methods can be found to autonomously self-repair damaged laminates in-situ to a sufficient level either to completely mitigate the damage or to prevent damage propagation until a suitable permanent repair can be made.

Self-healing offers scope to address low velocity impact induced damage and has been shown to recover mechanical properties in bulk polymers and FRPs. In particular, the use of microcapsules and hollow glass fibres as delivery systems for a liquid resin to tackle matrix cracks and delaminations has been shown to give promising results for bulk polymers and GFRP respectively. However, neither technique has been optimised to address CFRP, the most commonly used fibre reinforcement for aerospace structures. The use of an autonomous self-healing system for aerospace FRPs would remove the need to identify the occurrence of low velocity impact damage that would characteristically form BVID. It would provide a system to recover or sustain the required mechanical performance of a damaged structure until such time as it was deemed necessary to perform a repair or replacement of the damaged component. Furthermore, for occurrences of small damage formation, self-healing may remove the need for repair completely and may also have a positive effect on design of composite structures and maintenance schedules which would lead to more efficient structures that are cheaper to maintain.

3. Direction of Research

It is evident that the susceptibility of composite materials to impact damage is preventing the complete weight saving potential of the material properties from being utilised. For the aerospace industry in particular, minimising weight is of prime importance in terms of maximising the performance and cost effectiveness of air vehicles which are invariably tied to both manufacturing and operational costs. Furthermore, minimising the detrimental effects of impact damage would have implications on maintenance schedules which would further contribute to in service cost reductions. A comprehensive review has identified the possibility for manipulation of the hierarchical nature of composite materials to facilitate multi-functionality and in particular self-healing in order to address these issues.

The most successful approaches that have been employed to date for fibre reinforced plastics (FRP) utilise the embedment of either microcapsules or hollow glass fibres (HGF) within the laminate as a storage vessel for a liquid resin system. In particular, HGF have proved successful for creating a self-healing system in unidirectional glass fibre laminates (GFRP). This is primarily due to the similarity in aspect between the HGF and reinforcing fibres which allow the laminate to facilitate embedded HGF with minimal disruption to the laminate architecture. However, carbon fibre reinforced plastics (CFRP) are the most promising composite materials for aerospace applications and currently no self-healing strategy has been successfully employed to address impact damage in CFRP. Adopting the same HGF strategy as for self-healing GFRP would not be acceptable in CFRP as it involves substituting substantially stronger and stiffer reinforcing fibres for 'self-healing' HGF plies and would effectively create a hybrid carbon/glass laminate. This would cause unacceptable reductions in the CFRP laminate mechanical properties and so would not be a reasonable approach. Therefore, a new strategy was required in order to deploy HGF as a delivery system for self-healing in CFRP.

It was envisaged that in order to minimise disruption to the host laminate, there would be a requirement to drive towards smaller OD HGF which could be directly embedded into the CFRP laminate without too much difficulty. The HGF would only act as storage vessels for the resin system and would not be expected to contribute any structural reinforcement to the material. The HGF could be embedded at 'critical'

interfaces more susceptible to damage and sufficiently spaced to provide an adequate supply of healing resin whilst minimising any disruption to the laminate.

The incorporation of HGF with diameters below 100μm was expected to have a tolerable effect on the mechanical performance of the CFRP laminate. However, this effect would require assessment in order to optimise the design. The integration of HGF within CFRP can be improved by:

1. Minimising OD: *Reducing the OD of the HGF will reduce the disruption to the laminate architecture*
2. Common direction interface: *Placing HGF between two CFRP plies of the same fibre orientation improves integration by increasing tessellation between HGF and CF*
3. Minimising number of HGF: *Decreasing the overall amount of HGF embedded within the laminate will reduce any detrimental effects caused by substituting load bearing CF with HGF*
4. Minimising density of HGF: *Increasing the spacing between HGF improves the tessellation of CF and HGF*

The purpose of integrating HGF is to supply damage within CFRP with a volume of resin sufficient to heal any damage present and ultimately recover mechanical properties. The supply of resin can be improved by:

1. Maximising OD: *Increasing OD increases the storage volume*
2. Maximising hollowness: *Increasing hollowness increases storage volume and reduces the amount of HGF required per unit volume of healing resin*
3. Non-common interface: *Damage, such as delaminations, do not occur between plies of same fibre orientation, therefore ensure HGF are located near to damage by placing at interfaces of dissimilar ply directions.*
4. Maximising number of HGF: *Increases total resin volume stored within the laminate thereby increasing the damage size that can be healed*
5. Maximising density of HGF: *Increases concentration of resin for a given volume of laminate thereby increasing resin available locally to each damage site*

From the above it can be seen that the main drivers for integrating HGF and healing damage are conflicting and so must be optimised in order to provide a complete solution.

The type of mechanical testing was chosen to reflect that laminates are more sensitive to inclusions when tested in compression. However, initial testing was conducted using flexural four point bend testing for three reasons:

1. The upper surface of test samples experience pure compression
2. The tests have been used previously and successfully to assess self-healing with HGF
3. The tests have small sample sizes and minimal sample preparation is required.

However, the small sample sizes involved with flexural testing meant that low velocity drop weight impact was not a viable method of creating damage, and thus had to be substituted by quasi-static indentation. The validity of this is explored in Chapter 6.

Compression After Impact testing was proposed to further assess the performance of the laminates and in order to optimise the delivery mechanism for a self-healing system suitable for CFRP laminates. This was chosen for the following reasons:

1. Provides a more stringent assessment of laminate performance
2. Allows low velocity drop weight impact which is more representative of real damage events
3. Facilitates larger sample sizes and damage areas which provide a more definitive assessment of the self-healing laminate performance.

3.1 Overall Project Aim

3.1.1 Statement:

To develop and optimise an efficient HGF delivery system to facilitate a Self-Healing function in a representative Carbon Fibre Reinforced Plastic, ensuring minimal disruption to the laminate's innate mechanical performance.

3.1.2 Specific Objectives:

1. Select a suitable healing resin system for use in self healing
    a. To determine the requirements for an optimised healing resin system
    b. Identify suitability of existing resin systems
    c. Select suitable resin for testing stages
2. Design and optimise a HGF delivery mechanism for imparting a self healing function to a laminate
    a. Address requirements to maximise supply of resin volume
    b. Address requirements to minimise effect on mechanical properties
3. Optimise manufacturing process(es) for production of self-healing laminates
    a. Manufacture of HGF
    b. Integration of HGF into CFRP laminate
    c. Healing resin infiltration
4. Assess self-healing functionality of laminates
    a. Flexural testing to provide initial insight into laminate disruption and strength recovery after healing
    b. Compression After Impact testing to provide a more stringent assessment of laminate disruption and measure of healing efficacy

In order to meet these objectives an experimental work plan was created (Figure 3-1). The activity has been broken down into three sections which also form the basis of the subsequent chapters in this report:

1. <u>Preliminary Self-Healing System Design</u> (*Chapter 4*): *This section considers initial selections that must be made and that are fundamental to the project:*
    *a. **HGF Dimensions:** Outer Diameter (OD), Hollowness (K^2)*

b. ***Resin System**: Possible solutions and final selection*

2. **<u>Self-Healing Laminate Design</u> (*Chapter 5, Section 1 in Chapters 6, 7, 8*)**: *This section uses two tools to generate and theoretically assess laminate configurations.*
    a. ***Configuration**: Detailed assessments made to determine the performance of different HGF distributions in terms of pitch spacing, volume fractions, healing resin and expected reduction to in-plane properties (modulus used as indicator).*
    b. ***Volumetric Assessment**: Considers the damage volume created by a specific level of damage and verifies that the configuration can supply a sufficient volume of resin.*
3. **<u>Test and Manufacture</u> (Chapters 6, 7, 8)**: *This section considers the practical stages used to assess laminate performance.*
    a. **Manufacture**: *HGF, Lamination and Resin Infiltration*
    b. **Mechanical Assessment**: *Flexural and Compression After Impact Analysis*
    c. **Post Mechanical Assessment Analysis**: *Ultrasonic Assessment* and *Optical Microscopy*

Within the testing section, it was decided that there were three primary assessment criteria for the laminate performance with a self-healing network. This was to fully determine the effects of embedded HGF and the most effective system to employ:

1. **Undamaged**: *Assessed the disruption to the laminate caused by the presence of HGF by monitoring the initial reduction in mechanical properties. This was essential as the recovery due to healing would be irrelevant if the initial reduction in undamaged properties was not tolerable.*
2. **Damaged**: *Assessed the reduction in laminate mechanical properties due to the presence of damage. This also determined if there were any improvements in damage tolerance resulting from the embedded HGF or if they acted as nucleation sites for damage.*
3. **Healed**: *Assessed the recovery of mechanical properties after damage due to healing. This determined the effectiveness of the healing system and justified the development of self-healing composite materials for structural applications.*

The testing process was also categorised into three stages as seen in Figure 3-2:

1. **Stage 1.** *(Chapter 6)*

   Laminates were configured (self-healing laminate design) for damage inflicted by quasi-static indentation. Two configurations were selected for mechanical assessment using flexural four point bend testing.

2. **Stage 2.** *(Chapter 7)*

   Laminate configurations from Stage 1 were checked against low velocity drop weight impact testing using Configuration and Volumetric Assessment. Laminates were then mechanically assessed using compression after impact assessment to determine their suitability after low velocity impact under compressive loading.

3. **Stage 3.** *(Chapter 8)*

   The results from Stage 1 and Stage 2 were considered and an optimised design proposed, suitable for compression after impact assessment. Laminates were then mechanically assessed to verify the optimised configuration.

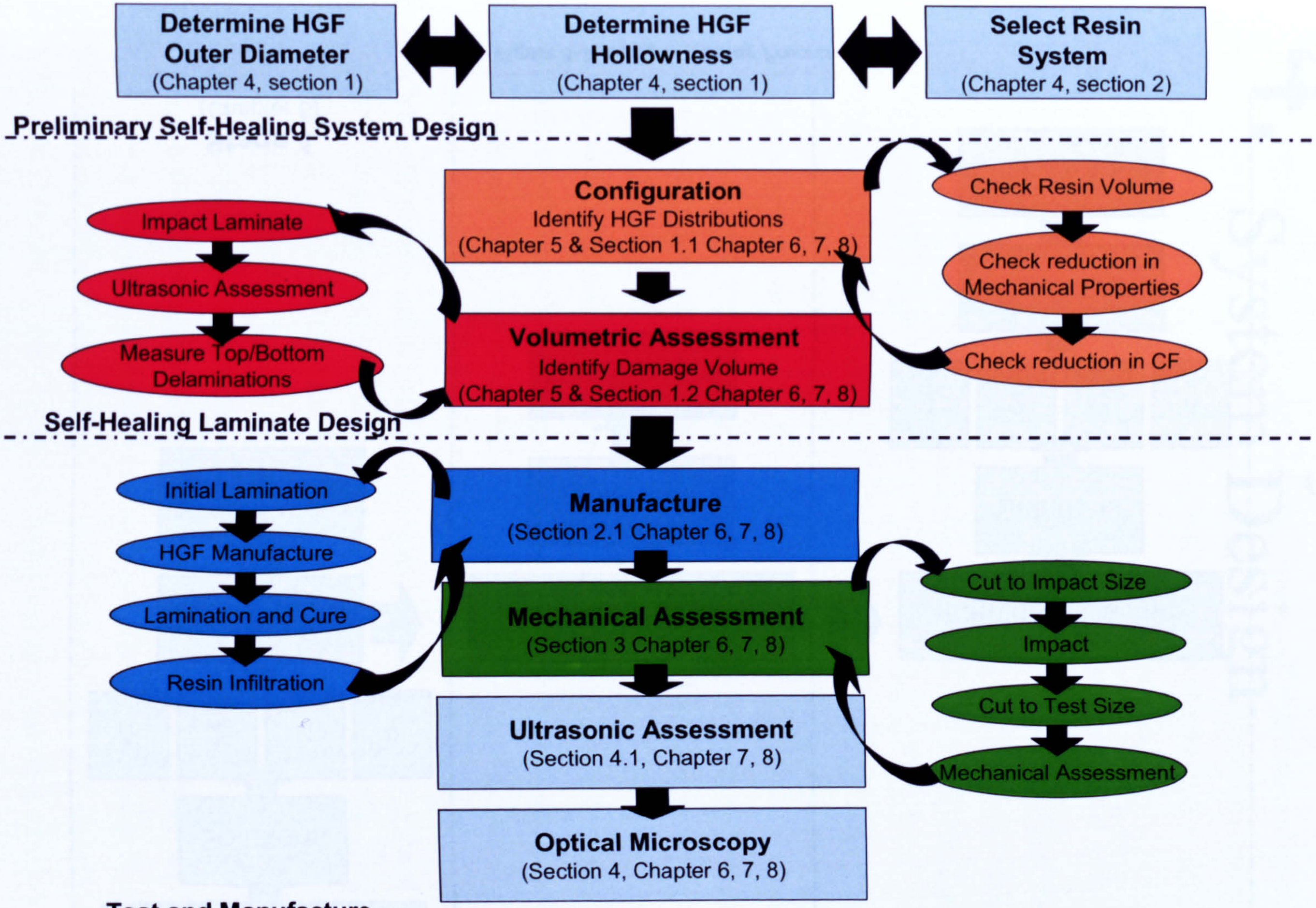

Figure 3-1: ***Global Workflow***

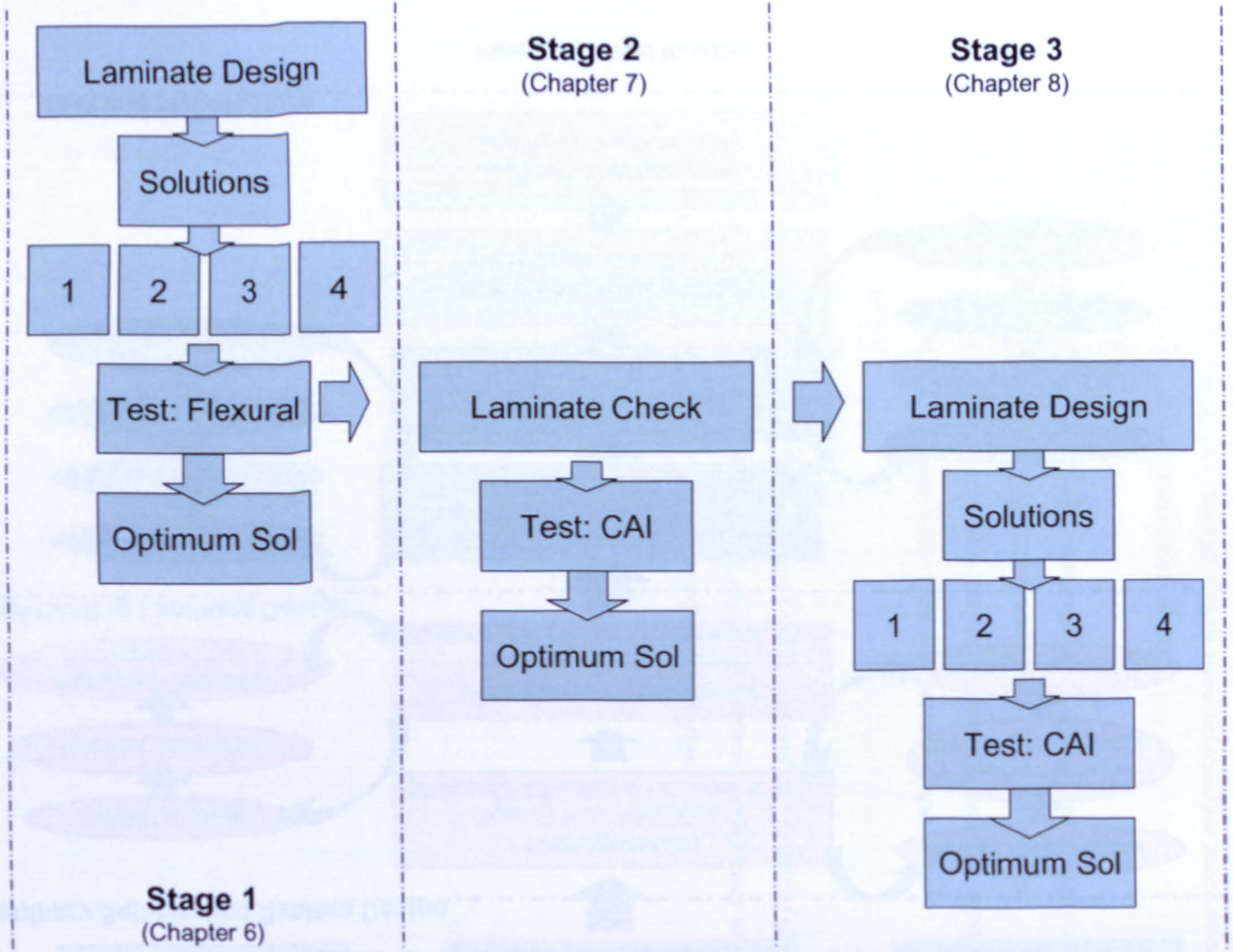

Figure 3-2: ***Design - Testing Process***

4. Preliminary Self-Healing System Design

In order to develop an efficient and effective self healing delivery system utilising resin filled hollow glass fibres, there are two main components that must be specified. These are the precise HGF geometry and the healing resin system. It is useful first to explore the background of these components in order to better understand the implications of their selection.

4.1 Hollow Glass Fibre

Hollow glass fibres (HGF) used for composite reinforcement have been found to offer improved performance in comparison to solid fibres in terms of increased specific flexural rigidity, improved post-impact performance, reduced transmission of thermal and acoustic energy and variable dielectric properties. The structural performance of HGF is reviewed in order to assess the potential utilisation of HGF as a containment vessel for a healing agent.

4.1.1 Background

Siefert [157] briefly considered the viability of hollow glass manufacture at commercial production rates. Initial difficulties were overcome to allow 100 filament strands to be produced from molten glass. This technique also permitted a range of diameters between 10-17.5μm to be produced at a range of hollowness fractions ($K^2=\pi R_{ID}^2/\pi R_{OD}^2$) limited to a maximum of 0.49 due to the individual fibre crushing during handling. The proposed use of these hollow fibre laminates was to produce thicker but equal mass laminates with improved rigidity, with an application for deep-sea diving vessels.

Early studies concentrated on the characterisation of hollow glass fibres and their composites. Burgman [158] concluded that on an equal weight per unit length and equal packing basis, hollow fibre laminates have a considerably larger flexural rigidity than solid and furthermore, this difference was maximised for hollow fibre laminates with the thinnest walls (highest hollowness). Proposed uses were for deep-sea vessels, radomes and filtration media. Therefore, there is a considerable amount of literature considering the use of hollow fibres for their thermal, electrical and filtration

purposes but these will not be considered herein, the focus being hollow fibres for structural applications.

Work by ESA [159] considered hollow fibres with a range of outer diameters and different wall thickness (S) to outer diameter ratios (D) ($^{S}/_{D}$). In particular, this work identified the potential for tuning the $^{S}/_{D}$ ratio in order to match the strain of the surrounding resin and produce hollow fibre composites suitable for different uses. For example it was concluded that $^{1}/_{8}$ (hollowness K^2=0.56) would be suitable for high strength laminates, $^{1}/_{12}$ (K^2=0.7) would be suitable for low density, stiff laminates and $^{1}/_{15}$ (K^2=0.75) would be suitable for laminates used as core materials in sandwich constructions. Therefore, intuitively an increase in the $^{S}/_{D}$ ratio increases the second moment of area of the fibres, reduces their strength and reduces the mass of the resulting laminate. It was also concluded that in order to meet the requirement to minimise the outer diameter and yet provide adequate mechanical properties, the range of fibre diameters deemed to be suitable were 50-100μm for E-glass. It should be noted that the absolute values from these conclusions can be altered by changing the glass composition which was not considered in this work.

Watson et al [160] considered a theoretical analysis of the flexural rigidity and strength of hollow fibre laminates compared to solid. The work concluded that hollow fibre composites are more rigid and can withstand higher bending moments. It was found that at high hollowness fractions, interstitial resin adds significant mass to the material, although this was still outweighed by the potential gain in rigidity and strength. For a hollowness of 50%, an increase of 300% in rigidity, 100% increase in bending moment before failure and only a 23% increase in mass was demonstrated when compared to solid fibre laminates. Furthermore Finite Element Analysis determined that the ability of hollow fibres to deform elliptically significantly reduced tangential and radial stress by 17% and 69% respectively for a hollowness of 0.64.

Boniface et al [161] compared the mechanical properties of solid fibre, hollow fibre and hybrid S2 glass laminates. It was found that the hollow glass fibres produced a 23% reduction in laminate density compared to the solid fibre. However, it was expected that this could be improved as optical micrographs suggested that there was a large variability in the fibre construction and some appeared solid. The presence of

hollow fibres in the laminates resulted in a reduction in absolute values for mechanical properties with the exception of compressive failure strain. However, when normalised, the relative density meant that the hollow fibre laminate properties compared more favourably, particularly in compression. The hollow fibre laminates also showed improved compression after impact performance which was attributed to the ability of the fibres to crush and absorb impact energy.

Bleay et al [162] considered the use of hollow glass, S2 glass and Nicalon fibre laminates. With hollow fibre/Nicalon hybrid laminates it was possible to retain the high modulus of Nicalon fibres with the hollow glass fibres providing improved tensile strength, compressive strength and damage tolerance. This was conducted primarily to address the unsuitability of carbon fibre in applications where microwave transmissivity is required.

HGF have been used primarily to maximise structural stability whilst minimising mass. Furthermore, they have been used in structural applications where carbon fibre was unsuitable due to issues such as microwave transmissivity in radomes, for example. However, it has been seen that manipulation of the $^{s}/_{D}$ ratio allows HGF to be specifically tailored for high strength or stiffness. It was also observed that resistance to impact damage can be improved by the ability of HGF to collapse and absorb impact energy. As a result, they are an ideal medium to integrate into a structural material.

A bespoke fibre making facility has been developed for manufacture of HGF as a result of a previous project between BAE Systems, DERA and the University of Bristol [143-146]. This facility allows manufacture of HGF by drawing down a hollow glass pre-form through a furnace operating at the softening temperature of the glass before collecting the resulting filament on a cylindrical drum to produce continuous fibre (Figure 4-1). The dimensions of the manufactured HGF are dependant on the interaction between furnace temperature, fibre draw rate and preform feed rate. A laser measurement device is positioned directly below the furnace outlet in order to determine the outer diameter of the HGF. However this device gives no indication of the hollowness fraction. Control of the translational

motion of the collecting drum allows HGF to be uniformly distributed transversely at the specified pitch spacing.

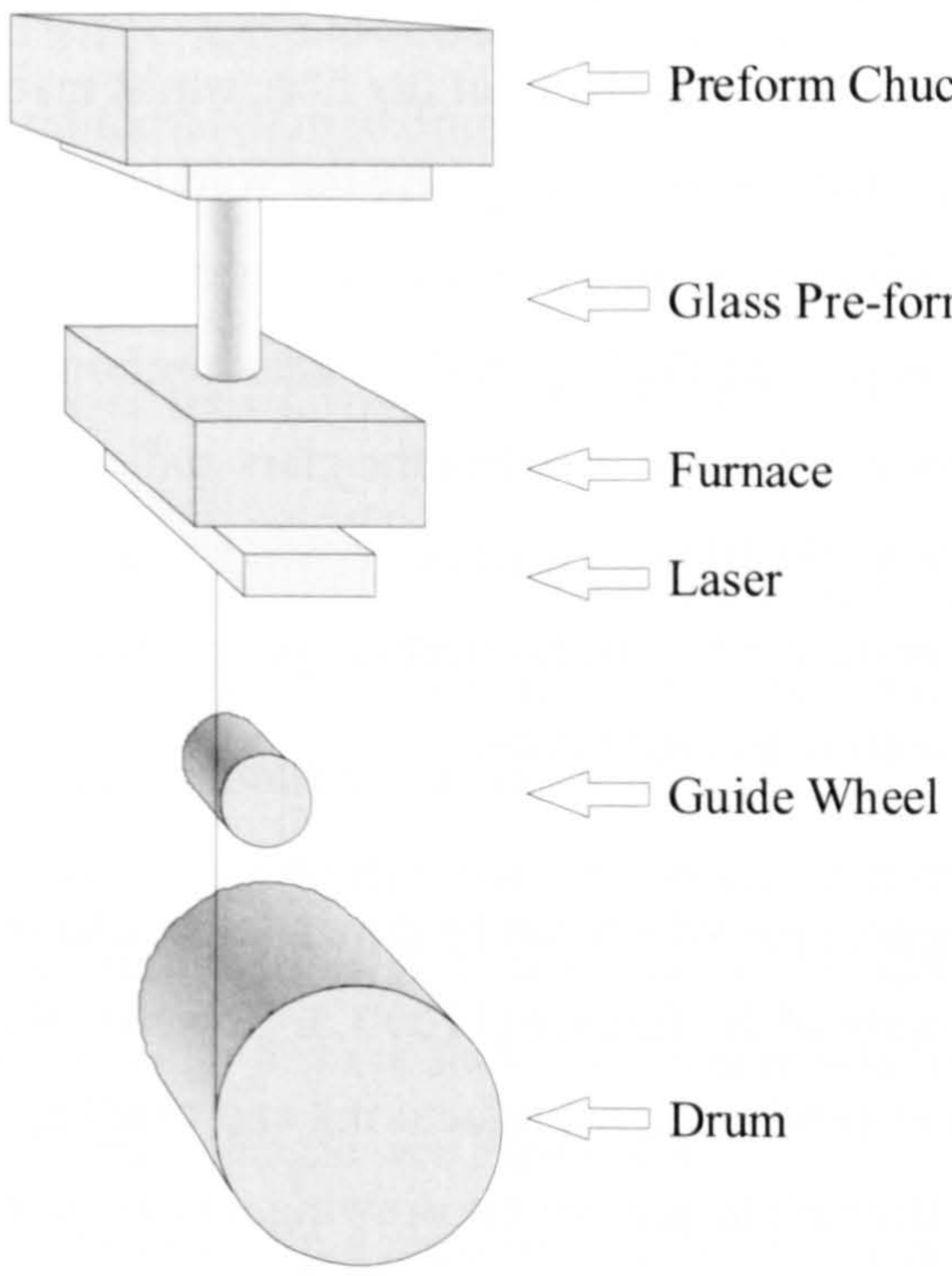

Figure 4-1*: Schematic Diagram of Bespoke HGF making Facility*

Hucker et al [143-146] used this facility to investigate the potential of using HGF laminates for improving or tailoring the mechanical performance of HGF laminates compared to solid equivalent. The authors explored the effects of varying the furnace temperature on the fibre hollowness and the interaction between glass viscosity and surface tension effects for DURAN (Schott) borosilicate HGF. It was concluded that for a given temperature and draw rate there was a single condition where the fibre hollowness was at a maximum and the external diameter a minimum [143]. It was also found that the resulting tensile strength of the HGF was inherently dependant on the manufacturing parameters. It was suggested that the outside surface of the HGF experienced compressive residual stresses and the internal surface experienced tensile residual stresses due to thermal gradients created as the drawn fibre cooled [144]. In general, it was concluded that improved specific compressive strength could be achieved, compared to an equivalent solid laminate, by decreasing OD and maximising K^2 (Hollowness) [145,147].

4.1.2 Manufacture

The manufacture of HGF can be problematic due to the unique behaviour of glass as an amorphous solid. The process of drawing HGF seeks to balance the competing forces involved with reducing the diameter of the fibre whilst maintaining the hollowness. Equilibrium must be achieved where the volume of glass entering the furnace (feed rate) is equivalent to the volume leaving the furnace (draw rate). The basic concept relies upon passing the large hollow glass preform into the furnace which at its hottest point is sufficient to soften the glass and cause the diameter to rapidly reduce. This allows the fibre to be drawn down into a filament, maintaining some degree of hollowness, and by careful control specific fibre dimensions can be achieved by altering the draw and feed rates.

The choice of glass composition which can be drawn into a filament is only restricted by the temperature capacity of the furnace (1100°C). However, the drawn filament must be robust enough to survive the manufacturing and handling processes and must possess enough innate strength to survive the drawing process without fracture. To meet these prerequisites, a robust, high temperature alkaline earth aluminosilicate glass composition was selected, 8252 (Schott). The softening point begins at 935°C thus the furnace was set to 970°C to ensure that an adequate working viscosity at the necking point was achieved. The properties of the 8252 glass can be seen in comparison to the glass used in previous work [143-146] in Figure 4-2 below.

Property	DURAN	8252	Units
Transformation Temp (Tg)	525	720	°C
Annealing Point	560	725	°C
Softening Point	825	935	°C
Working Point		1240	°C
Modulus of Elasticity (E)	64	81	GPa
Poisson's ratio	0.2	0.24	
Density @ 25°C	2.23	2.63	gcm^{-3}

Figure 4-2: ***Glass 8252 Properties of Interest***

$$Annealing\ Point = 10^{13}\ Poise$$

$$Softening\ Point = 10^{7.6}\ Poise$$

$$Working\ Point = 10^{4}\ Poise$$

The specifics of the manufacturing process are outlined below:

1. Furnace set to 970°C and allowed to reach stability.
2. Hollow glass preform (OD=18.3mm, ID=15.5mm) was thoroughly cleaned with acetone to remove residual contaminants that may be entrained during manufacture.
3. Preform was placed into the chuck clamp before aligning with the centreline of the furnace opening.
4. The furnace has an adjustable Nickel iris to maintain temperature stability within the furnace (Figure 4-3). The iris is enclosed around the HGF preform such that a 2-3mm circumferential gap is present.
5. Transverse position of preform relative to furnace centreline is adjusted throughout manufacture using X-Y motor drives to maintain alignment.
6. Preform is lowered into furnace such that ~50mm was below the hot-zone (around 2/3 of furnace length, see Figure 4-4).
7. Preform begins to neck (rapid reduction in OD) in the hot-zone and the preform mass below this point initiates fibre drawing.
8. After exiting the furnace, the filament passes through a laser measuring device before passing a guide wheel.
9. Several meters of HGF are initially pulled manually and removed until external diameter is sufficiently reduced to facilitate wrapping around take-up drum.
10. Draw rate and pitch rate control are engaged and set to 60ms^{-1} and 100μm/rev respectively
11. When external diameter reaches 130μm, preform feed rate control is engaged and set to 110 giving a feed rate of around 29.4μms^{-1}.
12. Draw rate is periodically increased in increments of 10 to allow the external diameter to reach equilibrium. This process ceasing once the external diameter reaches 70μm.
13. Pitch rate control is then set to the desired pitch increment for manufacture.
14. Fine adjustments to draw rate are required throughout manufacture to maintain external diameter at desired value.

15. To cease production, draw rate is reduced to zero and the filament is cut and attached to the drum. All other controls are returned to zero and the preform is reversed from the furnace until the filament tail can be cut and the iris closed.

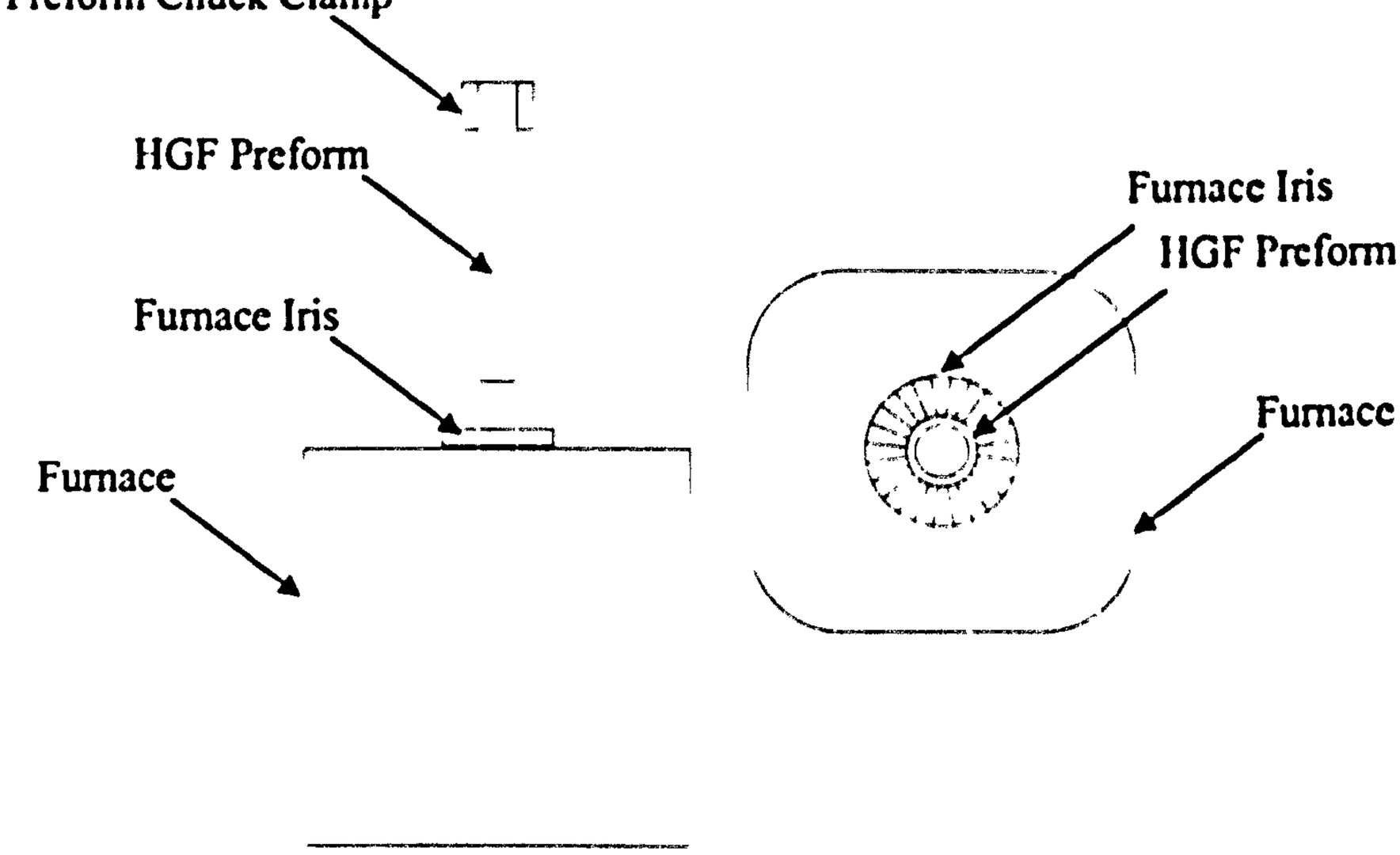

Figure 4-3: ***Diagram of Preform Feed through Furnace Iris***

The manufacture of HGF is a delicate process and any adjustments made during manufacture are small and incremental, so the glass can reach equilibrium. Maintaining a precise gap between the iris and the glass preform was essential as if too large the HGF would be embrittled and would fracture during manufacture. Also, the draw rate was increased very slowly to avoid any detrimental effects on the hollowness fraction of the fibre.

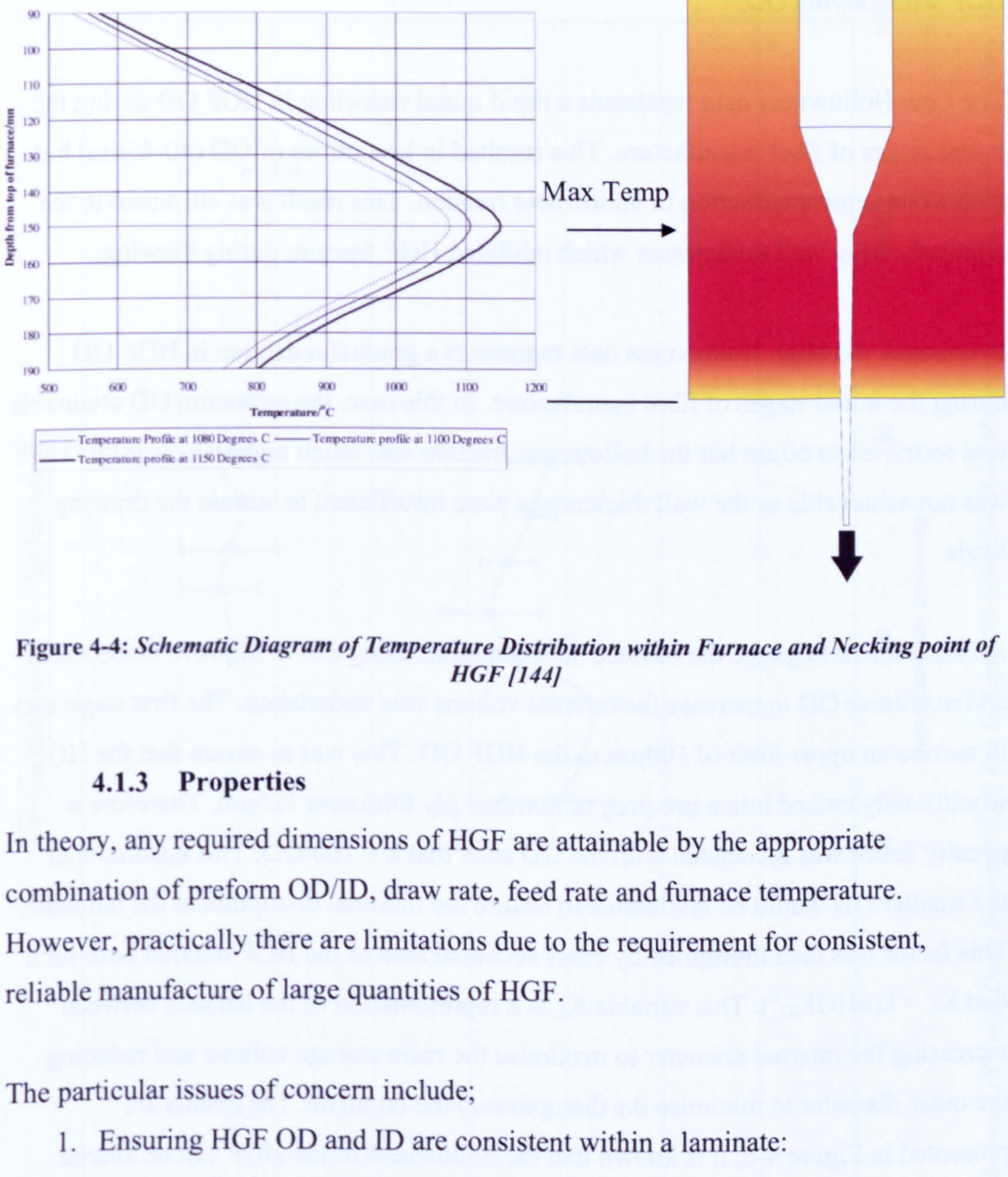

Figure 4-4: ***Schematic Diagram of Temperature Distribution within Furnace and Necking point of HGF [144]***

4.1.3 Properties

In theory, any required dimensions of HGF are attainable by the appropriate combination of preform OD/ID, draw rate, feed rate and furnace temperature. However, practically there are limitations due to the requirement for consistent, reliable manufacture of large quantities of HGF.

The particular issues of concern include;

1. Ensuring HGF OD and ID are consistent within a laminate:
    a. reducing scatter in results from coupon testing
    b. consistent internal volume
2. Ensuring HGF OD and ID are consistent between laminates.
3. HGF fracture during manufacture resulted in significant time and materials wastage.

Another significant issue was the rate at which manufacturing parameters were adjusted to decrease HGF OD upon commencement of the drawing process. This is illustrated in Figure 4-5 which shows the results of two manufacturing runs creating HGF with varying OD.

The Low Hollowness data represents a rapid initial reduction in HGF OD during the initial stages of fibre manufacture. This resulted in low values of OD (40-45μm) but with a consequent reduction in hollowness fraction. This result was attributed to the relatively large wall thicknesses which inhibited HGF fracture during drawing.

In contrast, the High Hollowness data represents a gradual reduction in HGF OD during the initial stages of fibre manufacture. In this case, the minimum OD attainable was restricted to 60μm but the hollowness fraction was much higher. Lower OD HGF was not achievable as the wall thicknesses were insufficient to sustain the drawing loads.

An assessment to gauge the balance between minimising OD to improve embedment and maximise OD to increase the internal volume was undertaken. The first stage was to ascribe an upper limit of 100μm to the HGF OD. This was to ensure that the HGF would easily embed into a pre-preg of nominal ply thickness 125μm. Therefore a penalty factor was associated with the OD such that k = 100-OD. This ensured that the smaller OD would be favourable to ensure the minimal disruption to the laminate. This factor was then multiplied by cross sectional area of the HGF internal bore such that $K_L = k(\pi HGF_{ID}^2)$. This variable K_L is a representation of the balance between increasing the internal diameter to maximise the resin storage volume and reducing the outer diameter to minimise the disruption to the laminate. The results are presented in Figure 4-6, it is known that the hollowness of the HGF can be altered during the manufacturing process; therefore the results for two HGF hollowness are presented. The results identify that the optimum OD lies in the range 60-70μm.

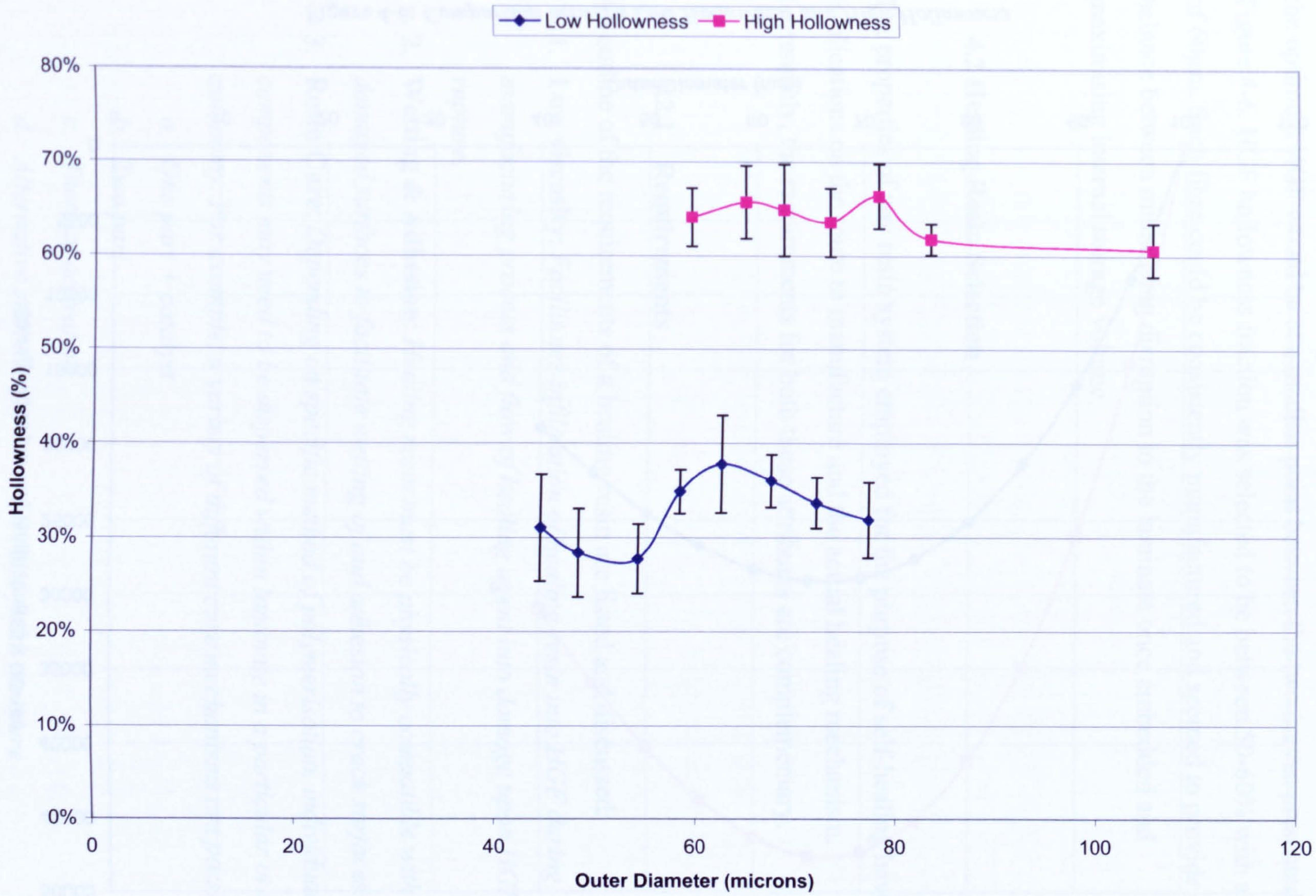

Figure 4-5: ***Variation of HGF Hollowness (K^2) with Outer Diameter (OD) due to Rapid OD reduction (Low Hollowness) and Gradual OD Reduction (High Hollowness)***

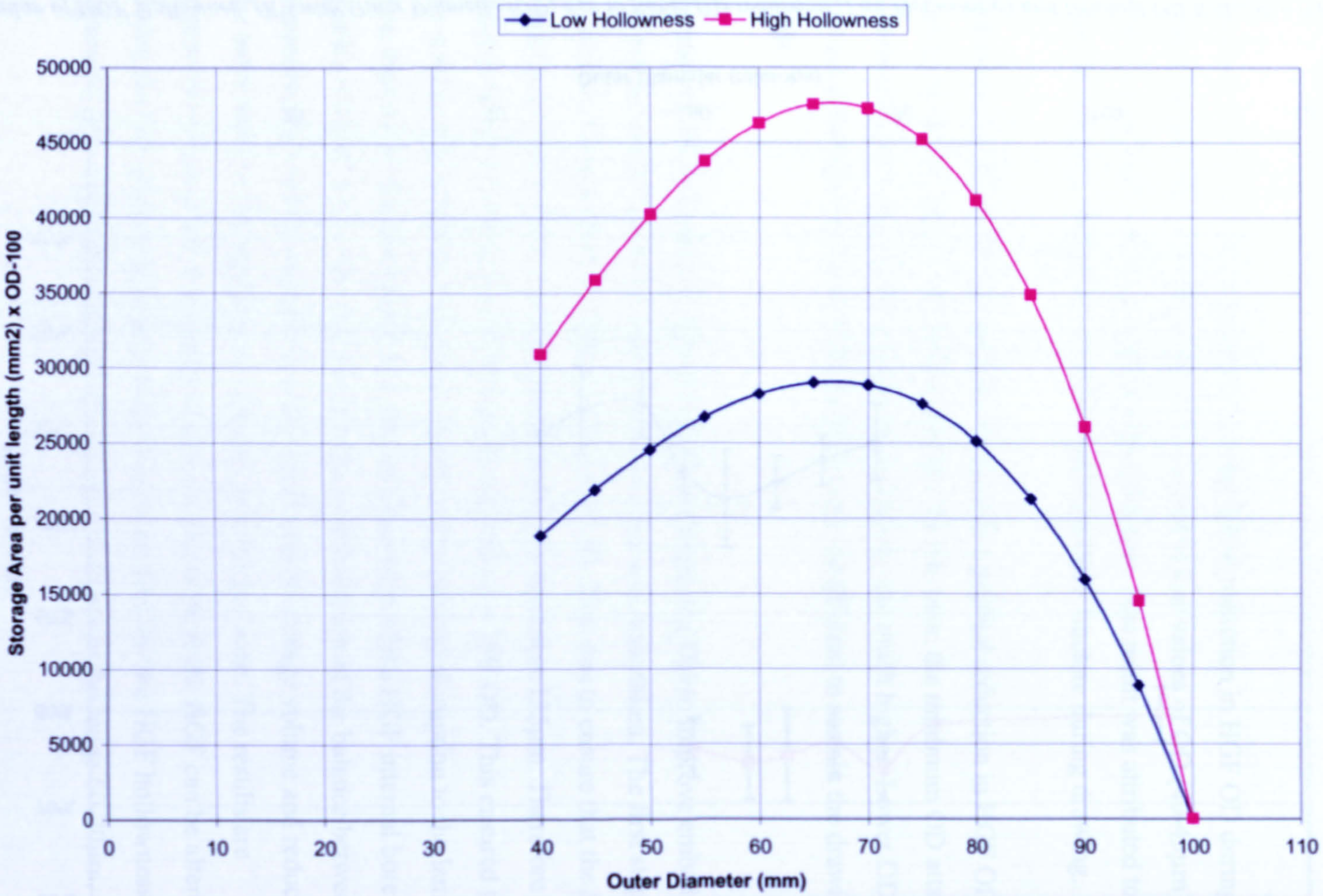

Figure 4-6: ***Comparison between Low Hollowness and High Hollowness***

4.1.4 Fibre Geometry Selection

To ensure consistent results in testing, specific values for OD and K^2 (hollowness) were defined. With reference to the data presented in section 4.1.3, it was decided that the optimum HGF would be at a median point between the two curves presented in Figure 4-6. HGF hollowness fraction was selected to be between 50-60% with an OD of 60μm. Such fibre could be consistently manufactured and seemed to provide a balance between minimising disruption to the laminate once embedded and maximising internal storage volume.

4.2 Healing Resin Selection

The properties of any resin system employed for the purpose of self-healing have implications on the route to manufacture and the actual healing mechanism. Fortunately, the requirements for both these attributes are complementary.

4.2.1 Requirements

An outline of the requirements of a healing resin are listed and discussed:

1. **Low viscosity**: *Facilitates infiltration of healing resin into HGF during manufacturing process and flow of healing agent into damage upon HGF rupture.*
2. **Wetting & Adhesion**: *Healing resin must be physically compatible with damaged surfaces to facilitate wetting of and adhesion to crack surfaces.*
3. **Resin Cure**: *Depending on specific method of polymerisation, individual components may need to be dispersed within laminate in a particular order for autonomy. For example, a variety of different cure mechanisms are possible;*
    a. *One part + catalyst*
    b. *Two part*
    c. *Thermal activation*
    d. *Alternative stimulus for cure: UV, EM field, moisture*
4. **Speed of cure**: *Dependent on resin formulation, but viscosity must remain sufficiently low to allow resin infusion into damage before rapid cure*

5. **Mechanical Properties:** *Must be sufficiently robust to prevent the healed damage from propagating further and pristine properties are restored.*

4.2.2 Possible Candidate Systems

A number of resin types meet various aspects of the requirements identified above. In order to select the most suitable system, each will be assessed for the following criteria:

1. **Long term Stability**

   The resin system is required to remain inactive in a containment vessel until released into a damage zone. It will then be expected to cure effectively and to achieve the desired mechanical performance. Three criteria which need to be met can be identified:

   a. **Environmental resistance**

      Resistance to environmental factors such as water ingress

   b. **Storage Life**

      The duration that an uncured system can survive in storage

   c. **Volatiles content**

      Release of volatiles during cure which could lead to voids in a healed region

2. **Structural Efficiency**

   The mechanical performance of a cured healing resin system should be optimised or at worst be similar to that of the FRP matrix material.

3. **Other Practical Requirements**

   a. Resin Viscosity

      The viscosity should be as low as possible at ambient temperature to facilitate both the infiltration of resin into the hollow glass fibre and, upon fracture, its release into the damage site

b. Stoichiometric/cure stimulus

Sensitivity to non-stoichiometric mixing if the system is multi-part, or if an external stimulus is required (e.g. UV), this must be available upon damage initiation.

It was necessary to identify candidate resin families and to assess their relative suitability as a candidate for a self-healing system. An outline of the features of resin systems considered as FRP matrix reinforcement can be seen in Table 2-2, Chapter 2. From this, epoxy and cyanate ester systems were considered as the most suitable candidate resin types, primarily due to good mechanical performance, compatibility with the host laminate, availability and relatively low cost. In addition, silicone was also considered as it is commonly used to as a crack filler although its mechanical performance is relatively low. The performance of the three candidate resin types is considered in Table 4-1.

Performance Indicators		Priority	Potential Healing Agent		
			Epoxy	Cyanate Ester	Silicone
Long term Stability (uncured)	**Environmental resistance**	High	Poor-average	Good	Good
	Storage Life	Unknown	Unknown	Unknown	Unknown
	Volatiles content	High	Low-medium	Low	Low
Structural Efficiency	**Mechanical Performance**	High	Good	Good	Poor-average
Practical Requirements	**Resin Viscosity**	High	Low-medium	Low-medium	Low-high
	Stoichiometric/Stimulation	Medium	Heat, hardener, catalyst, UV	Heat, hardener, catalyst, UV	Heat, hardener, catalyst, UV

Table 4-1: ***Comparison of Resin Types as Candidates for a Self-Healing Resin System***

The requirements for a self-healing resin system are unlikely to be met by systems that are commercially available. This is because the specific requirements in this case are novel, and most existing resin system formulations are targeted at specific applications. Overall it was considered that the epoxy systems were likely to best meet most of the criteria. Epoxy systems are widely used and therefore provide a wide range of 'off the shelf' systems from which to select a candidate system. These incorporate a range of viscosities and curing methods which generally achieve good mechanical performance and with low volatiles content. Furthermore, the FRP materials that were being considered as host laminates comprised of epoxy matrices. Therefore, to ensure physical and chemical compatibility between healing resin and matrix, an epoxy system was deemed to be the most suitable candidate for further consideration.

A critical requirement for this study was deemed to be the viscosity of the healing system; viscous systems would be problematic to infiltrate into HGF and more significantly would inhibit the resin flow into damaged regions. Resin Transfer Moulding epoxy systems offer a promising solution as the viscosity requirements are similar. The addition of heat into RTM systems allows a reduction in viscosity to facilitate infiltration into fabric cloths. Thus it was decided that a similar approach could be used to temporarily reduce the viscosity of the system in order to achieve the immediate requirements for self-healing.

Previous work by Pang et al [141,142] used Ampreg 20 (SPS Systems) with the addition of acetone as a diluent to reduce viscosity, while work by Trask et al [147] used Cycom 823 (Cytec), a system developed for RTM, which was primarily selected for its very low out-gassing performance in a simulated space environment. These systems were considered as previous work had successfully demonstrated their suitability as self-healing resin systems.

It was recognised that a system that may be suitable for testing and validation of the self-healing delivery system would not necessarily provide an efficient, autonomous, self-healing agent. However, the purpose of this work is to provide an optimised delivery system to facilitate self-healing in CFRP and not an optimised resin system.

With this in mind, four epoxy candidates were compared (Table 4-2).

1. **EP30** (Masterbond): *Low viscosity, transparent adhesive, sealant, coating and potting epoxy. Exceptionally low shrinkage*
2. **Cycom 823** (Cytec): *Low viscosity one or two part epoxy resin system primarily used in Resin Transfer Moulding*
3. **Ampreg 20** (SP Systems): *Low viscosity, two part epoxy laminating system*
4. ***SP106*** (SP Systems): *Simple low viscosity, two part epoxy system for joining, coating, laminating and filling.*

Performance Indicators		Material	Epoxy System		
		EP30	Cycom 823	Ampreg 20	SP106
Long term Stability	Environmental resistance	Medium	Medium	Medium	Medium
	Storage life (months @RT)	Unknown	6	24	12
	Volatiles content	Unknown	Unknown	Unknown	Unknown
Structural Efficiency	Mechanical Performance	Unknown	Good	Good	Unknown
Practical Issues	Viscosity @ RT	400-500	250	865	862
	Viscosity @ Temp	Unknown	20 @125	573 @30	545 @30
	Activation Method	2 part	2 part	2 part	2 part
	Cure time @RT	18-24hrs	4-5days	5 hrs	14.5 hrs
	Cure time @Temp °C	2-3hrs @93	1 hr @125	2.5hrs	11 hrs

Table 4-2: ***Comparison of Four Candidate Epoxy Resin Systems for Selection as Self-Healing Agent***

4.2.3 Resin System Selection

The system chosen was Cycom 823 (Appendix A_1) for the following reasons:

- Commonality with the host matrix system
- Good mechanical performance
- Low viscosity, especially at elevated temperature
- Reasonably rapid cure (at elevated temperature)

It was recognised that this system was not optimised for the purposes of self-healing and therefore would not be suitable for an industrial application of this technology. However, the properties of this system, in particular the ability to reduce its viscosity with temperature, enabled manipulation of the system to mimic the properties required from a bespoke self-healing resin system. The Cycom 823 was used in its premixed form (1 part) to eliminate sensitivity to stoichiometric mixing to ensure that optimum cure was achieved for the purposes of this study. Additionally, temperature was used to accelerate the cure of the system to provide a more realistic time frame of a self-healing cycle (≈1-2 hours).

4.3 Integrating HGF into Polymer Composites

A primary driver in the development of an effective self-healing system, utilising filled HGF for healing agent delivery, is that their presence does not unduly affect the mechanical performance of the laminate. As this study describes, for the first time, integration of HGF at a defined distribution as opposed to entire layers [141,142,147] no guidance exists as to how to ensure they are efficiently embedded. The incorporation of optical fibres (OF) into composite laminates for sensing etc. have been studied extensively [163]. The geometric form of OF and the need to improve their integration into polymer composites is comparable to that required herein for the HGF. A brief overview of published work in this field is considered below.

4.3.1 Embedding Optical Fibre in Polymer Composites

Optical fibres (OF) are glass (or polymer) fibres with a non-uniform variation of refractive index perpendicular to their axis [163]. They typically consist of a central silica core surrounded by an annular silica cladding of 125μm external diameter, and a further polymer coating, which can increase the diameter up to 250μm [164], although some development on small-diameter optical fibres has been conducted [165-169]. The

application of optical fibres within composite materials has the potential to provide an integrated structural health monitoring system as part of a 'smart structure' [164]. However, the relatively large diameters of optical fibres are an order of magnitude larger than typical reinforcing fibres (8-15μm) in a composite material [170]. Therefore, extensive research efforts have been conducted to determine the effects that the embedment of such fibres have on a composite material.

Case and Carman [171] conducted an in depth study into the effect of embedding optical fibres at different orientations to the reinforcing plies. The authors recognised that embedded OF generated local undulations in the reinforcing fibre which increased the local concentration of matrix resin. An analytical model was formulated to predict the dimensions of the lenticular region created by the undulation and the effect that this would have on the laminate strength. Extensive parametric studies were conducted considering the effects of OF diameter on compression strength in a unidirectional composite. The results showed that increasing OF diameter decreased the compression strength. Furthermore, it was observed that if OF orientation deviated by more than 10° from that of the reinforcing fibres, it was found to reduce the compression strength by around 50%. In addition, it was concluded that an OF orientation of 30° is as disruptive to the composite as if it were at 90° to the reinforcing fibres. This has particular implications for the need to ensure a good alignment between the reinforcing fibres and the OF. However, as the fibre diameter is reduced, the sensitivity of compression strength to OF alignment is reduced. More specifically, it was shown that a 100μm OF fibre could be misaligned with reinforcing fibre by up to 20° before a reduction in strength was realised.

The presence of a 'resin rich' region was also considered by Shivakumar and Emmanwori [172] who used micrographic images to assess the effect of fibre orientation on the area and disturbance angle of these regions in unidirectional carbon/epoxy laminates. They concluded that for 145μm diameter OF oriented at 30°, 45°, 60° and 90°, the disturbance angle and resin area variation were assumed constant at around ten times the cross-sectional area of the OF for a 16 ply laminate.

Laka and Bayo undertook an extensive study of OF embedment in composite structures [173]. They observed that OF can be placed accurately with respect to the neutral axis and will not deviate from their position during the cure process as the viscosity of the resin

decreases. They also observed that large diameter OF (>125μm) caused bending of adjacent plies, which could be eliminated if OF were embedded between two 0° plies (i.e. in parallel).

Skontrop considered two configurations of OF (125μm diameter) [174]. The first was a parallel configuration where two OF (spaced 1mm apart) were aligned with the surrounding reinforcement. The second configuration was a single OF looped around at a constant curvature to produce two fibres in parallel, aligned with the reinforcing fibres at 8mm spacing. The resulting laminates were inspected using optical microscopy. Conclusions drawn from the work suggested that closely spaced optical fibres (1mm) embedded in parallel with the reinforcing fibre did not cause significant changes to the composite microstructure. However, OF not aligned with the reinforcement produced distortion and generated resin rich areas. Skontorp concluded that there were no significant adverse affects due to the fibres in static tension and compression for the OF configurations considered. Further to this, it was determined that the OF did not initiate or directly cause fibre-dominated failures in the composite. However, it was found that OF did affect the damage evolution by creating sites of preferred matrix cracking. Finally, it was concluded that embedded OF did not significantly affect fatigue life.

Lee et al [175] considered the effects of OF orientation and concentration in glass fibre laminates. It was found that the inclusion of one or three OF at 6mm spacing in either cross ply (0°/90°) or unidirectional (UD) laminates had no significant effect on static tensile stiffness and strength. This was reinforced by the findings of Jensen et al [176,177] who considered the effects of embedding 250μm OF within a carbon fibre/bismaleimide laminate. Specimens were tested under uni-axial tensile and compressive loading to investigate the effects of OF orientation with respect to the reinforcing fibre and loading direction. The conclusions drawn were that uni-axial tensile strength and stiffness were reduced by less than 10%. Compressive strength and stiffness were found to be more sensitive, and were significantly reduced by 70% and 20% respectively. It was observed that OF embedded perpendicular to both the reinforcing fibre and loading direction caused the largest reduction in strength and stiffness under both tensile and compressive loads. However, the compressive strength reductions were limited to 15% by placing the OF parallel with the reinforcing fibre. This study highlighted the sensitivity of compressive strength to the presence, and in particular, the orientation of OF. The tensile and

compressive strength results from Jensen et al [176,177] were supported by those from Shivakumar and Emmanwori [172], who found a maximum reduction of 10% and 40% respectively.

Surgeon and Wevers [178,179] conducted studies into the effect of placing 140μm diameter OF on certain interfaces within a carbon/epoxy laminate $[0,\pm45,90]_S$. Four types of testing were conducted: tensile, three point bend, four point bend and fatigue. It was observed that tensile testing exhibited only minimal degradation when OF were located near the load bearing 0° plies. A similar effect was observed for 3 and 4 point bend tests, where degradation in strength of up to 51% was observed with OF embedded in the outer 0°/45° interface. It was concluded that this testing highlighted the increased sensitivity of compressive loading to embedded OF. Further testing identified a substantial degradation in tensile fatigue properties, leading to an extensive stiffness degradation and ultimately, premature failure of the specimens. The most sensitive interfaces were found to be the 0°/45° (load bearing fibres) and -45°/90° (prone to delamination). Therefore, it was concluded that the optimum interface for embedding OF is either 45°/-45° or 90°/90°, of which the latter is recommended. The authors identified that the inclusion of OF perpendicular to the load direction is the worst case scenario.

Takeda et al [168,169] considered a fibre Bragg grating (FBG) sensor array with OF diameter of 52μm. Visual observation of the embedded fibre at the 0°/90° interface identified an absence of resin rich regions surrounding the fibre. Furthermore, due to its smaller diameter, the OF was confined within one 0° ply. It was again stated that the absence of resin rich regions around the embedded OF would mean that the mechanical performance of the laminate would be unaffected by the presence of the fibres. However, no data was provided to support this statement.

Jeon et al [180] considered the influence of embedded OF on the formation of damage due to low velocity impact and subsequent buckling behaviour. It was concluded that the presence of OF had no influence on the shape of the impact damage. However, it was observed that the delamination area, for a given impact energy, was increased for OF orientated at 45° to adjacent reinforcing fibre which was attributed to the formation of resin rich regions. Lastly, it was shown that the delamination buckling resistance of the damaged laminates could be improved due to the OF imposing waviness into the fracture surface.

This was expected to increase the fracture surface area, increasing the energy required to propagate a crack.

4.3.2 Discussion

Large diameter (>125μm) optical fibres cause disruption to a composite material by distorting host laminate plies. This effect is minimised by reducing OF diameter and by embedding them in a direction aligned with the surrounding reinforcing fibres. As the OF becomes increasingly misaligned with the local reinforcing fibres, a lenticular resin rich region is formed which has a direct influence on the static mechanical properties. The alignment of the OF with the local reinforcement is critical but becomes less so as the OF diameter is reduced. A 100μm OF can be misaligned by around 20° without a marked reduction in strength, and this allowable angle increases with further reduction in OF diameter.

The tensile strength of FRPs is not significantly degraded by the inclusion of OF, regardless of fibre diameters, fibre spacing, and fibre orientations. Carman et al [171] suggest that the tensile strength is dominated by the strain to failure of reinforcing fibres. For OF embedded parallel to the reinforcing fibre, no local anomaly is produced that would induce a strain concentration within the reinforcing fibre. For OF embedded off-axis to the reinforcing fibre, a local undulation is formed. However, the resulting stress induced is not sufficient to significantly reduce the tensile properties of the laminate.

The compressive strength is most sensitive to OF whilst stiffness is affected but by a lesser amount. The optimum location of OF is parallel with the reinforcing fibres and load direction. OF orientated transverse to the reinforcing fibre cause local deformation in the load bearing fibres which degrades their performance.

The effect on fatigue performance of a composite material with embedded optical fibres is inconclusive as only a limited amount of work has been conducted and the results are variable. Carman and Sendeckyj [163] have conducted an extensive review of the mechanics of embedded optical sensors and they have proposed a variety of conclusions. Overall a significant degradation in cycles to failure and fatigue strength can be expected due to the inclusion of OF, although further research is required.

4.4 Summary

The variables in HGF geometry have been fixed at the most suitable values for the purpose of mechanical assessment of self-healing CFRP. Section 1 outlines that the OD will be fixed at 60μm which determines the hollowness will be between 50% and 60% (dependent on fluctuations in ambient temperature, atmospheric conditions and variability in manufacturing settings).

It was recognised in section 2 that existing resin systems do not meet all requirements outlined for a self-healing system. Therefore, a system was selected that would best suit the purpose of this work, that is to demonstrate the suitability of HGF as a delivery system for self-healing CFRP. Cycom 823 (Cyctec engineered materials) was selected in a pre-mixed form (resin + hardener) for its excellent mechanical properties, compatibility with the laminate host matrix, quick cure time and variation in viscosity with temperature.

Section 3 has explored the incorporation of optical fibre (OF) within FRPs as the similarity in dimension between HGF and OF provides some commonality. The conclusions drawn were:

- The incorporation of OF results in two primary disruptions to the laminate microstructure
  - Generation of resin rich regions around OF due to the dimensional mismatch with the reinforcing fibre
  - Waviness in the reinforcing fibre due to orientation mismatch and hence generation of local lenticular resin rich regions
- The disruption to the laminate is dependant on the misalignment angle between OF and reinforcing fibre. The 0°/±45° interface was proposed as being the most sensitive to OF embedment.
- The disruptive effects of OF embedment can be minimised by
  - Reducing the OF outer diameter (<100μm)
  - Embedding OF between reinforcing plies of the same orientation, aligned in the OF direction.

- Laminates with embedded OF are most sensitive to compressive and fatigue loading. Embedded OF appeared to have very little effect on the tensile properties of the laminates considered.

The literature on optical fibres suggest that mechanical assessment of any laminates incorporating large diameter fibres should include compressive loading to determine any detrimental effects. Furthermore, the design of self-healing laminates with large diameter HGF will be made with reference to the conclusions drawn above.

5. Self-Healing Laminate Design

Providing a solution to enable self-healing functionality in a CFRP laminate posed two conflicting requirements:

1. Maximise the healing capability
2. Minimise the disruption to the laminate

The inclusion of HGF within a CFRP laminate is likely to have a detrimental effect on mechanical performance as a result of hybridisation. Conversely, it is essential that an effective storage capacity for any healing agent is provided. If this is not achieved, the benefits of providing self-healing would have been negated by the reduction in the baseline mechanical properties of the laminate. This chapter considers the design methodology taken in order to manage these conflicting requirements (as referred to in chapter 3 Figure 3-2) and devise an optimised configuration.

5.1 HGF Integration

The embedment of HGF within CFRP and the optimisation of a self-healing system were influenced by two variables:

1. **Location:** *Ply interfaces at which the HGF should be placed*
2. **Distribution:** *The spacing between adjacent HGF*

These variables have a direct impact on the structural performance of the laminate and the ability to provide a self-healing function.

5.1.1 Location

The ply interfaces at which HGF should be located were determined by three factors:

1. **Embedment:** *To minimise disruption to the laminate, HGF must be aligned with the fibre direction of at least one adjacent reinforcing ply*
2. **Damage Exposure:** *To maximise occurrence of HGF rupture and access of resin to damaged zone, HGF must be located at interfaces that experience delaminations and shear cracks*
3. **Resin volume:** *To maximise volume of resin supplied by each HGF upon rupture, length of HGF must be maximised within the laminate*

To satisfy 1 and 2, every interface within a quasi-isotropic laminate potentially provides a suitable location, although due to the typical 'pine tree' damage distribution there is an increased occurrence of damage towards the back face. Also, any interfaces with adjacent plies having the same fibre orientation will not be suitable as they are unlikely to experience delamination.

To satisfy 3, HGF were located adjacent to 0° plies (Chapter 4, Section 3.1). This is because for optimum performance in mechanical testing, the 0° fibre direction will be orientated with the primary loading direction which is generally the maximum sample dimension. Therefore, to ensure the maximum healing resin volume is available when a HGF is ruptured, it is desirable to select the 0° direction (Figure 5-1a). The maximum fibre length is clearly a function of specimen aspect ratio (length vs. width) and stacking sequence. In general, for impact damage susceptible laminates, the 45° ply orientation will usually provide the maximum length of HGF for low aspect ratio samples (Figure 5-1c) and the 0° ply orientation will usually provide the maximum length of HGF for high aspect ratio samples (Figure 5-1a). However orientation of the HGF at 45° would have created a difficult manufacturing process, thus the 0° direction was the preferred choice for all aspect ratios.

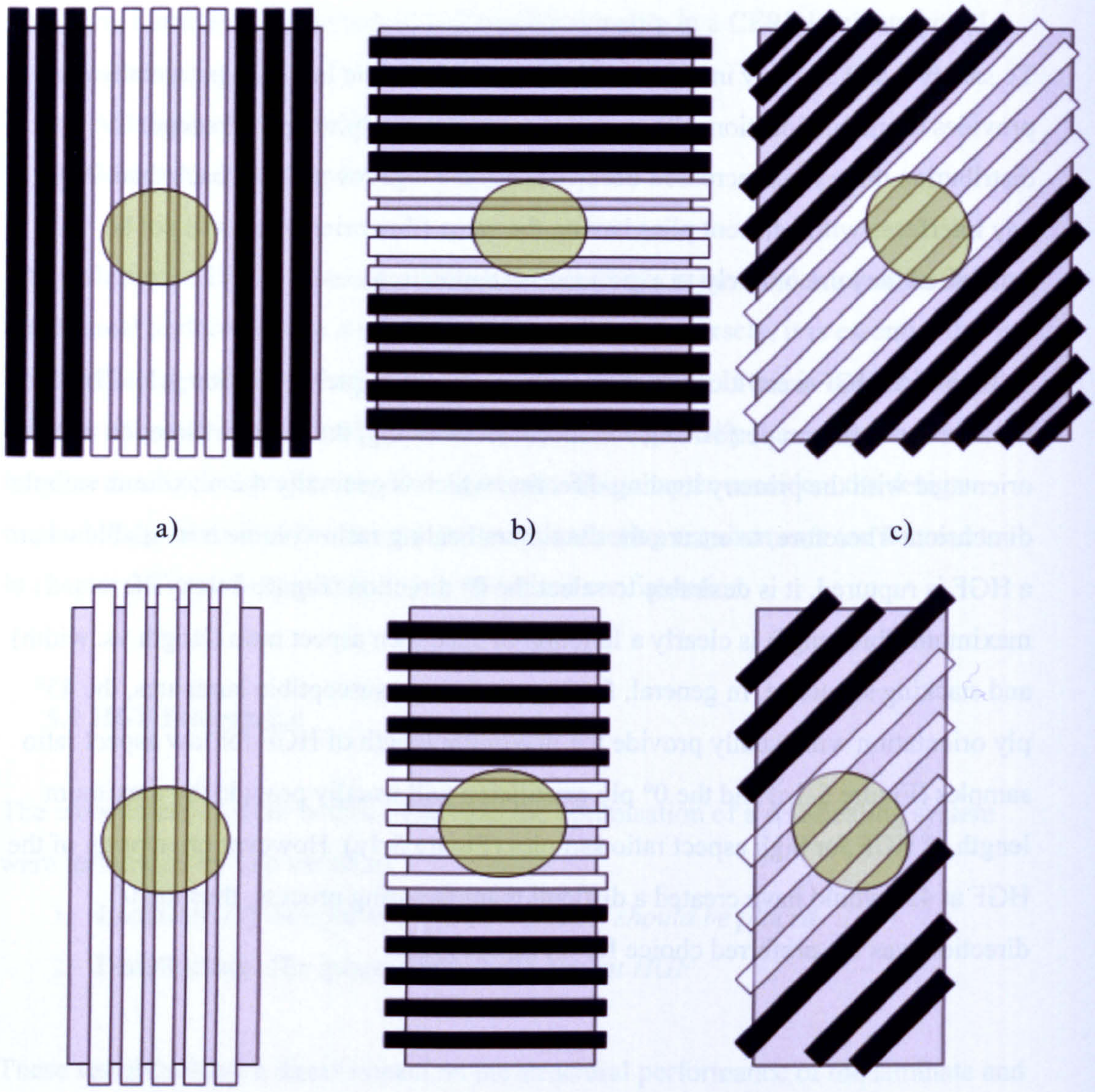

Figure 5-1: ***a) 0° b) 90° c) 45° HGF in Low Aspect Ratio (top) and High Aspect Ratio Samples (bottom)***

In a 16 ply quasi-isotropic laminate, 6 possible locations (see below) were identified for the location of HGF (centreline not considered as two unidirectional plies are unlikely to suffer delamination under low velocity impact):

$$(-45°/90°/45°/\underline{X_5}/0°/\underline{X_1}/-45°/90°/45°/\underline{X_3}/0°/0°/\underline{X_4}/45°/90°/-45°/\underline{X_2}/0°/\underline{X_6}/45°/90°/-45°)$$

x_n = locations identified for placement of HGF

It is important to note that in real structural applications the 0° fibre direction will not provide ideal locations for HGF placement as these plies provide the primary load bearing capability of the structure, and therefore should not be disrupted by the

inclusion of HGF. However, for this study they were deemed to be the most suitable location for the reasons outlined previously, and as a result the data contained herein can be assumed to be a 'worst case scenario'. Furthermore, in a larger structure that does not have the dimensional constraints seen here for coupon testing, a more suitable interface could be selected in order to minimise the overall detrimental effects on the laminate's mechanical performance.

5.1.2 Distribution

The bespoke HGF manufacturing facility permits precise fibre pitch control during the drawing process and thus determines the spacing between HGF within the laminate. The HGF outer diameter was selected as a suitable spacing increment with an additional 10μm added to account for variability in manufacturing process. This allowed the following distributions to be defined (Figure 5-2):

1. 70μm: *Adjacent HGF*
2. 140μm: *One HGF diameter spacing between fibres*
3. 210μm: *Two HGF diameter spacing between fibres*

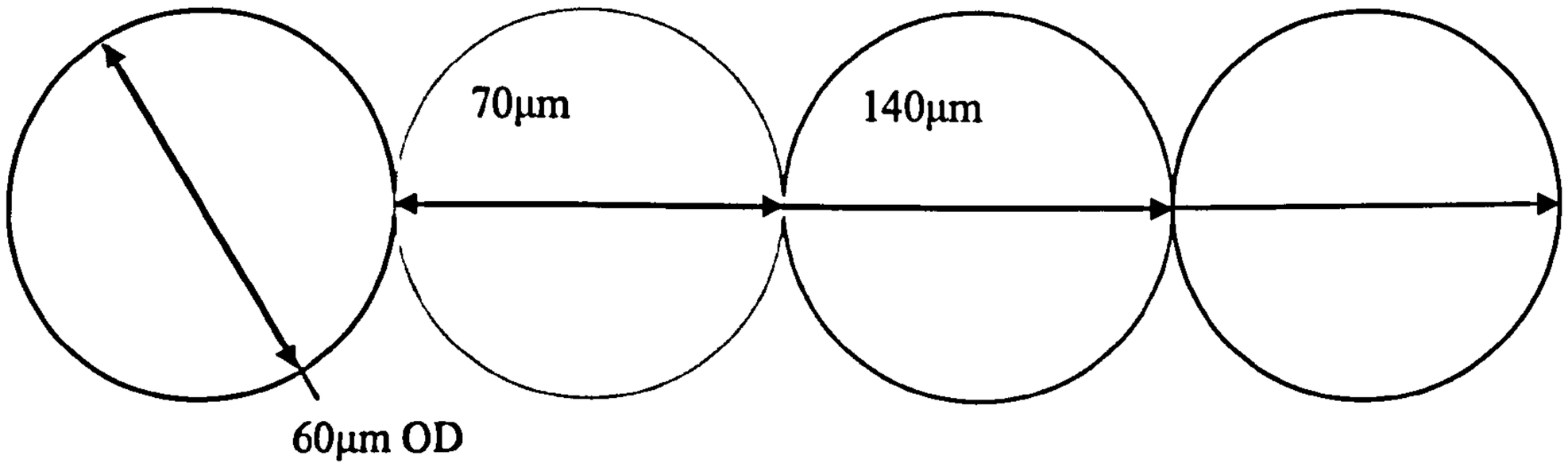

Figure 5-2: ***Schematic of HGF Distribution at 70μm, 140μm and 210μm Respectively***

It was expected that a lower HGF spacing was likely to result in a less effective embedment and therefore, would result in greater disruption to the laminate, a less orderly packing of the carbon fibres and increasing resin rich regions. Conversely, a higher HGF spacing would provide an increased storage volume for healing resin and effectively improve the healing potential of the laminates. Therefore, the focus of this research was to explore the consequences of different HGF distributions and locations to determine an optimised solution for self-healing CFRP.

5.2 Self-Healing System Assessment

The precise design of a self-healing system is of paramount importance to balance the competing drivers required for minimising disruption and maximising healing. To create a successful system two assessment tools were developed. These enabled better understanding and characterisation of the candidate designs as outlined in Chapter 3, Figure 3-2 and Figure 3-3. This also enabled the results of mechanical testing (Chapter 6,7,8) to be better explained with reference to the parameters explored within these tools.

5.2.1 Configuration Tool

The *Configuration Tool* addresses the disruption caused by HGF embedment and calculates the resulting fibre volume fractions (V_F) and resin storage volume (V_R). An assessment of possible configurations of HGF spacing within carbon fibre reinforced laminates was used to determine the volume fraction (V_F) of each constituent. This avoided experimental techniques such as matrix burn-off and chemical digestion as these are often difficult and problematic, with inconsistent results.

The tool is based upon simple geometric equations used to characterise the laminate. It permits estimations to be made which address the likely disruption caused by HGF embedment and calculates the resulting fibre volume fractions of each constituent (V_F) and the healing resin storage volume. This enables assessment of possible configurations of HGF spacing within any carbon fibre reinforced laminate which will lead to more effective laminate designs and remove the need to manufacture multiple iterations of laminate design variations.

The tool considers the number of interfaces at which HGF are located and the displacement between two HGF on each interface. The data extracted from this tool is presented in Section 1 of the experimental chapters 6, 7 and 8. This data provided the basis of the laminate designs that were considered for mechanical assessment.

This assessment requires several simplifying assumptions:

1. HGF were ideally spaced at either 70, 140 or 210μm (centre to centre, P_{HGF}) *see Figure **5-3**a)*
2. HGF outer diameter was consistently 60μm and carbon fibre diameter was 7μm
3. Laminate specimens were of fixed dimensions
4. HGF clumping was not present
5. Carbon fibre V_F for the plain laminate was 64%
6. HGF displaced carbon fibre and matrix resin in the ratio 16:9 (V_{FCF}=64%, V_{FR}=36%) *see Figure **5-3**b)*
7. HGF do not contribute to the strength or stiffness of the laminate
8. HGF only displace carbon fibre in the 0°, no other ply direction is affected
9. The ratio of areas for the laminate constituents is representative of the volume fraction per unit length. Therefore A_{CFL} is proportional to V_{FCF} where A_{CFL} represents the total cross sectional area of carbon fibre and V_{FCF} represents the volume fraction of carbon fibre for the laminate.

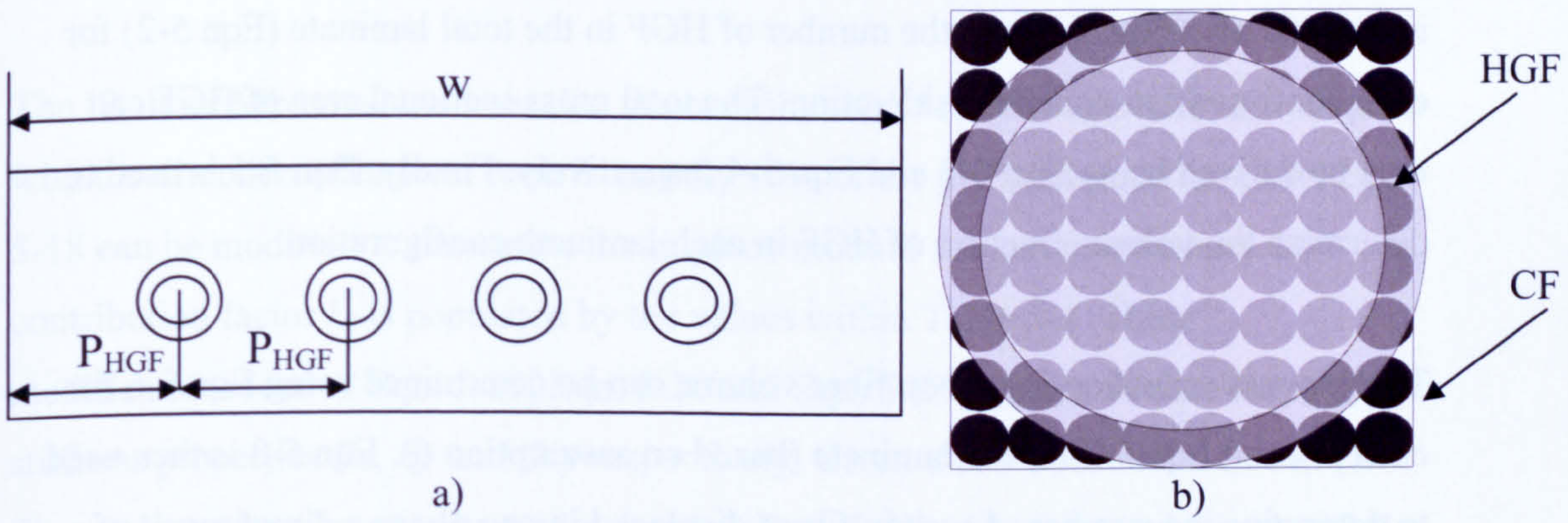

Figure 5-3: ***a) Illustration of Idealised HGF Spacing and b) Displacement of Carbon Fibre/Matrix Resin by HGF***

A number of inputs are required by the configuration tool:

1. Laminate dimensions:
   a. w_L = Width (mm)
   b. l_L = Length (mm)
   c. t_L = Thickness (mm)

d. t_P = Ply thickness (mm)

e. N_P = Number of plies in laminate

2. HGF dimensions:

a. OD_{HGF} = Outer diameter (mm)

b. ID_{HGF} = Inner diameter (mm)

c. K^2 = Hollowness (%) = $\pi(ID_{HGF})^2 / \pi(OD_{HGF})^2$

3. S_{HGF} = HGF spacing (mm)

4. N_I = Number of HGF interfaces

From these inputs and based on assumption 8, the disruption to the overall laminate can be estimated. It was noted that in practice, the HGF may replace more resin than carbon fibre as it is more mobile during the cure cycle resulting in improved V_F and stiffness.

The first stage calculates the number of carbon fibres displaced by HGF for different spacing and numbers of interfaces. This requires a calculation of the number of HGF in a single ply (Eqn 5-1) and the number of HGF in the total laminate (Eqn 5-2) for each configuration under consideration. The total cross sectional area of HGF can then be derived using Eqn 5-3 and Eqn 5-4 respectively. Finally, Eqn 5-5 is used to determine the volume fraction of HGF in each laminate configuration.

The pro-rata reduction in carbon fibre volume can be determined using Eqn 5-6 for each ply and Eqn 5-7 for the laminate (based on assumption 6). Eqn 5-8 is then used to determine the number of carbon fibres displaced in one ply as a direct result of embedded HGF.

The total number of carbon fibres present in the unmodified laminate for the entire laminate and per ply is calculated using Eqn. 5-8 and Eqn. 5-9 respectively. The number of HGF remaining within a modified ply is calculated using Eqn .5-10 and for the laminate using Eqn. 5-11. These are then converted into a percentage reduction in carbon fibre volume for the laminate using Eqn. 5-13 and the residual volume fraction of carbon fibre for the laminate with embedded HGF is derived using Eqn. 5-14 and the volume fraction of HGF is calculated using Eqn. 5-15.

The potential storage volume for healing resin within the laminate is determined by considering the hollowness of the HGF (Eqn. 5-16) and converted to a volume fraction (Eqn. 5-17).

The data manipulation thus far allows a full characterisation of the laminate for all variations of HGF spacing and number of interfaces on which they are deployed. The most significant information is the overall percentage reduction in carbon fibre volume fraction in the 0° ply direction and the overall reduction in carbon fibre volume fraction for the laminate. The potential storage volume and volume fraction for the healing resin are also essential to quantify the healing potential.

In addition, it was recognised that using a simple analysis based on the 'Rule of Mixtures' for composite materials [181], a qualitative assessment could be made to compare the relative reduction in mechanical properties for the modified laminates. It was acknowledged that the stiffness values derived would not be precise. However, this was used for qualitative assessment between laminate configurations to determine the relative effects of HGF distribution.

The 'Rule of Mixtures' assumes that the contribution of fibres in directions unaligned with the direction of interest contribute only 10% of the ply stiffness. Therefore, Eqn. 5-18 can be modified to determine the in-plane modulli for laminates where the contribution factor k_0 is populated by the values within Table 5-1. These modifications lead to Eqn. 5-19, Eqn. 5-20 and Eqn. 5-21 which calculate the in-plane stiffness properties *Ex*, *Ey* and *Gxy* respectively. Given that the reduction in carbon fibre volume fraction per ply can be derived (Eqn. 5-22) and integrated into the 'Rule of Mixtures', the reduced in-plane stiffness for the HGF modified laminate can be obtained (Eqn. 5-23, 5-24 and 5-25). Although the absolute values of the estimated in-plane stiffness are not expected to be precise in predicting the experimental values, they can be compared to the corresponding value for the unmodified laminate (Eqn.'s 5-19, 5-20, 5-21). Therefore, a percentage reduction in in-plane performance is generated for Ex, Ey and Gxy (Eqn. 5-26, 5-27 and 5-28 respectively).

Stiffness	Ply Contribution Factor (k_0)			Stiffness in Fibre Direction
	0°	±45°	90°	
E_X	1.0	0.1	0.1	E_1
E_Y	0.1	0.1	1.0	E_1
G_{XY}	0.1	0.55	0.1	$E_1/(1+v)$

Table 5-1: ***Tabulation of Factors for 10% Rule of Mixtures***

$$N_{HGF1} = \frac{w_L - \frac{P_{HGF}}{1000}}{P_{HGF}} \qquad \textbf{Eqn 5-1}$$

N_{HGF1} = *Number of HGF within one interface*

w_L = *Width of laminate (mm)*

P_{HGF} = *Pitch spacing between HGF (μm)*

$$N_{HGF} = N_I \times N_{HGF1} \qquad \textbf{Eqn 5-2}$$

N_{HGF} = *Number of HGF within laminate*

N_I = *Number of interfaces containing HGF*

$$A_{HGF1} = \pi\left(\frac{HGF_{OD}}{2}\right)^2 \times N_{HGF1} \qquad \textbf{Eqn 5-3}$$

A_{HGF1} = *Total HGF area in one interface (ignoring hollowness)* (mm^2)

HGF_{OD} = *HGF outer diameter (mm)*

$$A_{HGF} = \pi\left(\frac{HGF_{OD}}{2}\right)^2 \times N_{HGF1} \times N_I \qquad \textbf{Eqn 5-4}$$

A_{HGF} = *Total HGF area in laminate (ignoring hollowness)* (mm^2)

$$V_{FHGF} = \frac{A_{HGF}}{w_L \times t_L} \qquad \textbf{Eqn 5-5}$$

V_{FHGF} = *Volume fraction of HGF for laminate*

$$A_{CFX1} = V_{F(CF)} \times A_{HGF1} \quad \textbf{Eqn 5-6}$$

$$A_{CFX} = V_{F(CF)} \times A_{HGF} \quad \textbf{Eqn 5-7}$$

A_{CFX} = *Total area of displaced CF* (mm^2)

$V_{F(CF)}$ = *Volume fraction of carbon fibre* = 0.64

A_{CFX1} = *Total area of displaced CF in one ply* (mm^2)

$$N_{CFX1} = \frac{A_{CFX}}{A_{CF}} = \frac{A_{CFX}}{\pi\left(\frac{CF_{OD}}{2}\right)^2} \quad \textbf{Eqn 5-8}$$

N_{CFX1} = *Number of carbon fibre displaced by HGF in one ply*

A_{CF} = *Area of a single carbon fibre* (mm^2)

CF_{OD} = *Carbon fibre outer diameter (mm)*

$$N_{CF1} = \frac{w_L \times t_P \times V_{FCF}}{A_{CF}} \quad \textbf{Eqn 5-9}$$

N_{CF1} = *Number of carbon fibre in one ply*

t_p = *Thickness of one ply (mm)*

$$N_{CFL1} = N_{CF1} - N_{CFX1} \quad \textbf{Eqn 5-10}$$

N_{CFL1} = *Number of carbon fibre in one ply with embedded HGF*

$$N_{CFL} = (N_{CF1} \times N_P) - (N_{CFL1} \times N_I) \quad \textbf{Eqn 5-11}$$

N_P = *Number of plies*

N_{CFL} = *Number of carbon fibre present in modified laminate with embedded HGF*

$$L_{CFT} = \sum L_{CF} = \sum \frac{N_{CFL1}}{N_{CF1}} \quad \textbf{Eqn 5-12}$$

L_{CFT} = *Total percentage reduction of carbon carbon fibre for 0° plies (%)*

L_{CF} = *Percentage reduction of carbon fibre in individual 0° plies (%)*

$$L_{CF} = 1 - \left(\frac{N_{CFL}}{16 \times N_{CFL1}} \right)$$ **Eqn 5-13**

L_{CF} = Percentage reduction in carbon fibre for modified laminate with embedded HGF (%)

$$V_{FCFL} = \frac{(N_{CFL} \times A_{CF})}{w_L \times t_L}$$ **Eqn 5-14**

V_{FCFL} = Carbon fibre volume fraction in modified laminate with embedded HGF

$$V_{FHGF} = \frac{A_{HGF}}{w_L \times t_L}$$ **Eqn 5-15**

V_{FHGF} = HGF volume fraction

$$V_R = \pi \left(\frac{HGF_{ID}}{2} \right)^2 \times N_{HGF1} \times L_L \times N_1$$ **Eqn 5-16**

V_R = Total storage volume for laminate with embedded HGF (mm^3)

L_L = Length of laminate (mm)

$$V_{FR} = \frac{\left(\frac{V_R}{L_L} \right)}{t_L \times w_L}$$ **Eqn 5-17**

V_{FR} = Volume fraction of healing resin for laminate with embedded HGF

$$E_X = \left[k_0 \times E_1 \times \frac{t_0}{t_T} \right] + \left[k_{45} \times E_1 \times \frac{t_0}{t_T} \right] + \left[k_{90} \times E_1 \times \frac{t_0}{t_T} \right]$$ **Eqn 5-18**

k_0 = ply contribution factor:

For E_X: k_o =1 k_{45} =0.1 k_{90} =0.1

For E_Y: k_o =0.1 k_{45} =0.1 k_{90} =1

For G_{XY}: k_o =0.1 k_{45} =0.55 k_{90} =0.1. Also E_1 ->E_1

E_1 = Stiffness in fibre direction (Nmm^{-2})

t_0, t_{45}, t_{90} = total thickness of 0°, 45°, 90° plies (mm)

$$E_X = \left(\left[1 \times \frac{N_0}{N_P} \right] + \left[0.1 \times \frac{N_{45}}{N_P} \right] + \left[0.1 \times \frac{N_{90}}{N_P} \right] \right) \times E_1 \qquad \textbf{Eqn 5-19}$$

E_X = Elastic modulus in x direction (Nmm^{-2})

N_0, N_{45}, N_{90} = Number of plies in 0°, 45°, 90° direction

N_P = Total number of plies in laminate

E_{XP} = Elastic modulus of unidirectional ply in fibre direction (Nmm^{-2})

$$E_Y = \left(\left[0.1 \times \frac{N_0}{N_P} \right] + \left[0.1 \times \frac{N_{45}}{N_P} \right] + \left[1 \times \frac{N_{90}}{N_P} \right] \right) \times E_1 \qquad \textbf{Eqn 5-20}$$

E_Y = Elastic modulus in Y direction (Nmm^{-2})

E_{YP} = Elastic modulus of unidirectional ply in fibre direction (Nmm^{-2})

$$G_{XY} = \left(\left[0.1 \times \frac{N_0}{N_P} \right] + \left[0.55 \times \frac{N_{45}}{N_P} \right] + \left[0.1 \times \frac{N_{90}}{N_P} \right] \right) \times \left(\frac{E_1}{2 \times \{1 + V_{XYP}\}} \right) \qquad \textbf{Eqn 5-21}$$

G_{XY} = Shear modulus in XY plane (Nmm^{-2})

E_{XP} = Elastic modulus of unidirectional ply in fibre direction (Nmm^{-2})

$$P_{OX} = \frac{N_{CFL1} \times N_1}{N_{CF1} \times 4} \qquad \textbf{Eqn 5-22}$$

P_{OX} = Percentage reduction of CF in 0° fibre direction for laminate (%)

$$E_{XL} = \left(\left[1 \times \{1 - P_{OX}\} \times \frac{N_0}{N_P} \right] + \left[0.1 \times \frac{N_{45}}{N_P} \right] + \left[0.1 \times \frac{N_{90}}{N_P} \right] \right) \times E_{XP} \qquad \textbf{Eqn 5-23}$$

E_{XL} = Elastic modulus in x direction for modified laminate (Nmm^{-2})

$$E_{YL} = \left(\left[0.1 \times \{1 - P_{OX}\} \times \frac{N_0}{N_P} \right] + \left[0.1 \times \frac{N_{45}}{N_P} \right] + \left[1 \times \frac{N_{90}}{N_P} \right] \right) \times E_{XP} \qquad \textbf{Eqn 5-24}$$

E_{YL} = Elastic modulus in y direction for modified laminate (Nmm^{-2})

$$G_{XYL} = \left(\left[0.1 \times \{1 - P_{OX}\} \times \frac{N_0}{N_P} \right] + \left[0.55 \times \frac{N_{45}}{N_P} \right] + \left[0.1 \times \frac{N_{90}}{N_P} \right] \right) \times \left(\frac{E_{XP}}{2 \times \{1 + V_{XYP}\}} \right)$$

Eqn 5-25

G_{XYL} = Shear modulus in xy plane for modified laminate (Nmm^{-2})

$$P_{EX} = \left(\frac{E_{XL}}{E_X} \right) \times 100$$ **Eqn 5-26**

$$P_{EY} = \left(\frac{E_{YL}}{E_Y} \right) \times 100$$ **Eqn 5-27**

$$P_{GXY} = \left(\frac{G_{XYL}}{G_{XY}} \right) \times 100$$ **Eqn 5-28**

P_{EX} = Modified laminate stiffness as percentage of baseline in X direction (%)

P_{EY} = Modified laminate stiffness as percentage of baseline in Y direction (%)

P_{GXY} = Modified laminate stiffness as percentage of baseline in XY plane (%)

The configuration tool provides useful estimates to enable qualitative assessment and comparison between different laminate configurations during the initial design stage. This has allowed consideration of a range of HGF spacings and numbers of interfaces without the need for repeated manufacture and testing. Therefore, a somewhat 'optimised' delivery system could be proposed for consideration against the criteria outlined in the *Volumetric Assessment* tool.

5.2.2 Volumetric Assessment Tool

The *Volumetric Assessment Tool* estimates the volume of damage resulting from a low velocity impact and compares this to the potential resin storage volume (calculated in the *Configuration Tool*) to assess the overall healing potential of the laminate.

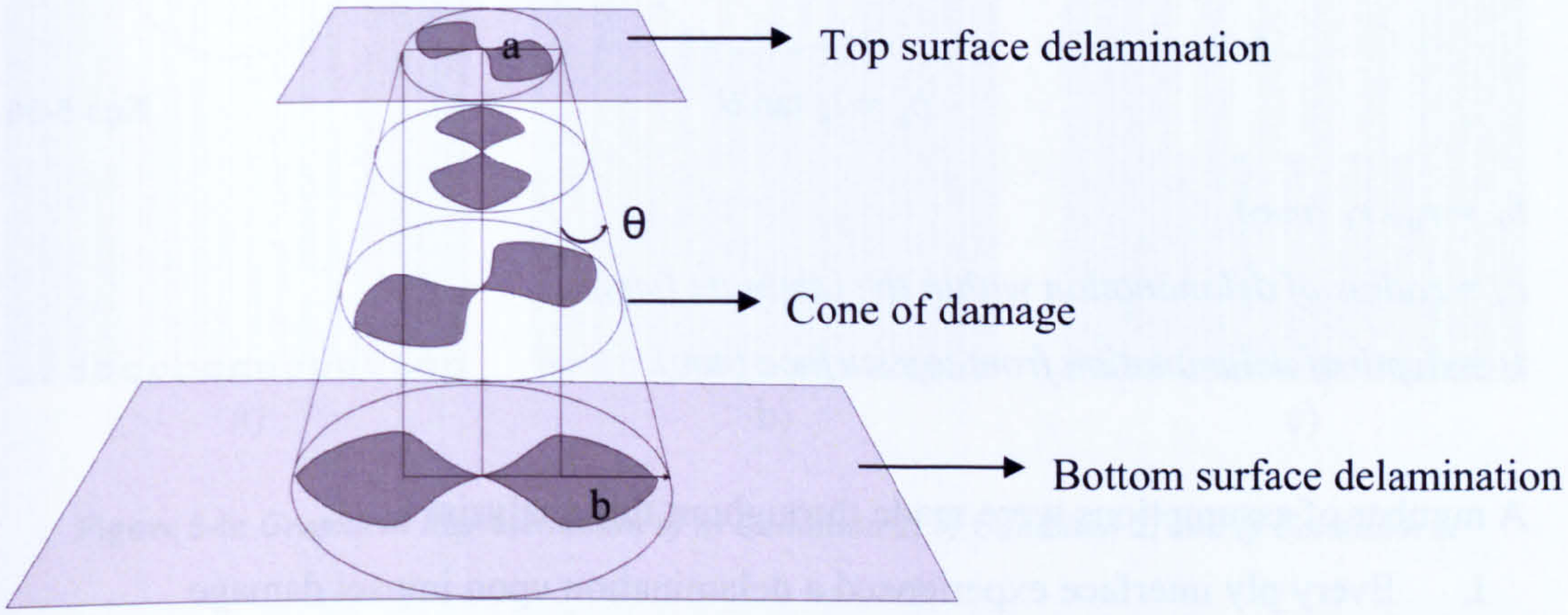

Figure 5-4: ***Schematic Diagram of Internal Damage and Projected Cone of Damage within which all Damage is Assumed to be Contained***

An approximate assessment of damage volume created by specific low velocity impact events was developed using trigonometry and simplifying assumptions. The use of ultrasonic C-scanning allowed the uppermost and lowermost delaminations to be measured in plan form view to determine the approximate cone of projected damage through the thickness of the laminate, Figure 5-4.

The diameter of the delamination in the lowermost ply (d_b) was measured and scribed to form a circle within which all the damage was contained. This was repeated for the uppermost delamination (d_t). Connection of these two circles by projections through the thickness of the laminate creates a 'cone' within which it could be assumed that all delaminations within the laminate would be contained (see Figure 5-4).

This 'cone' of damage was used to estimate the size of delaminations on each ply interface through the stack. The angle θ subtended by the cone to an orthogonal axis

passing directly through the laminate (Figure 5-4) was determined using trigonometry from the following relationships.

$$\theta = \tan^{-1}\frac{b}{t} \qquad \text{Eqn 5-29}$$

$b = r_b - r_t$ *(mm)*

t = *laminate thickness (mm)*

$$b_n = t_n \tan\theta \qquad \text{Eqn 5-30}$$

$b_n = r_n - r_t$ *(mm)*

r_n = *radius of delamination within the laminate (mm)*

t_n = *depth of delamination from top surface (mm)*

A number of assumptions were made throughout this analysis:

i. Every ply interface experienced a delamination upon impact damage
ii. Each delamination was assumed to form a characteristic 'peanut' shape and to fill 50% of the area of a circle scribed by the delaminations maximum dimension (d_n)
iii. Each delamination resulted in a ply separation of 40μm
iv. HGF were ideally spaced at the specified pitch spacing
v. HGF clumping was not present

Three estimates of the resin volume released from HGF during a damage event were derived to provide bounds within which the actual value may lie. These estimates comprised two variables: the number of HGF ruptured and the length of HGF emptied of resin after rupture.

- Condition 1: All HGF intercepted by the maximum delamination dimension are ruptured and completely emptied of resin, Figure 5-5a.
- Condition 2: All HGF intercepted by the maximum delamination dimension are ruptured but only the length of HGF within the 'cone' of damage is emptied of resin, Figure 5-5b.
- Condition 3: As Condition 1 except 50% of HGF are fractured and 50% of their length is emptied of resin, Figure 5-5c

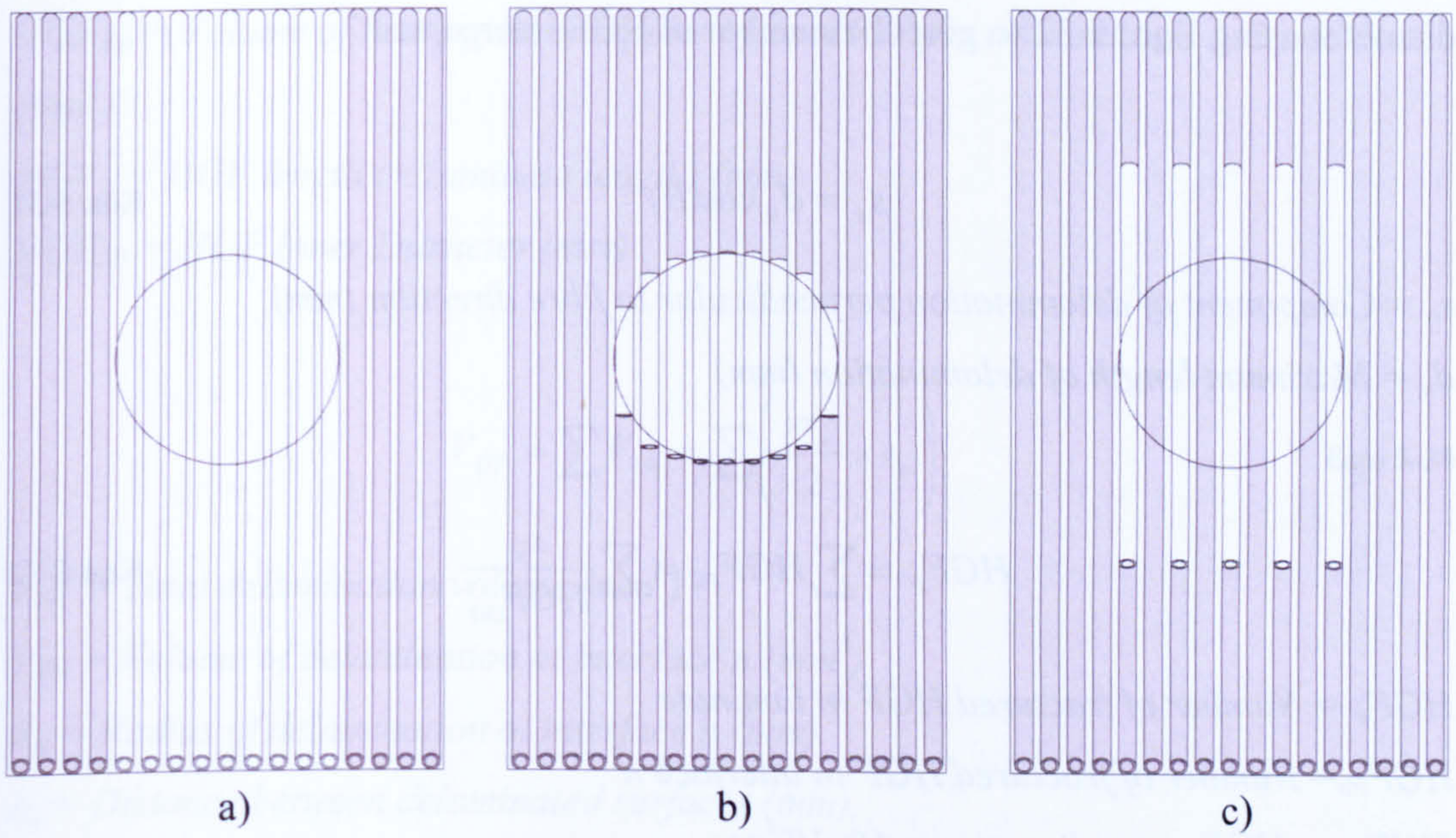

Figure 5-5: ***Graphical Representation of a) Condition 1, b) Condition 2, and c) Condition 3.***

Condition 1 describes the most optimistic situation whilst Condition 2 the most pessimistic. In practice, the real situation is likely to fall somewhere between Conditions 1 and 3.

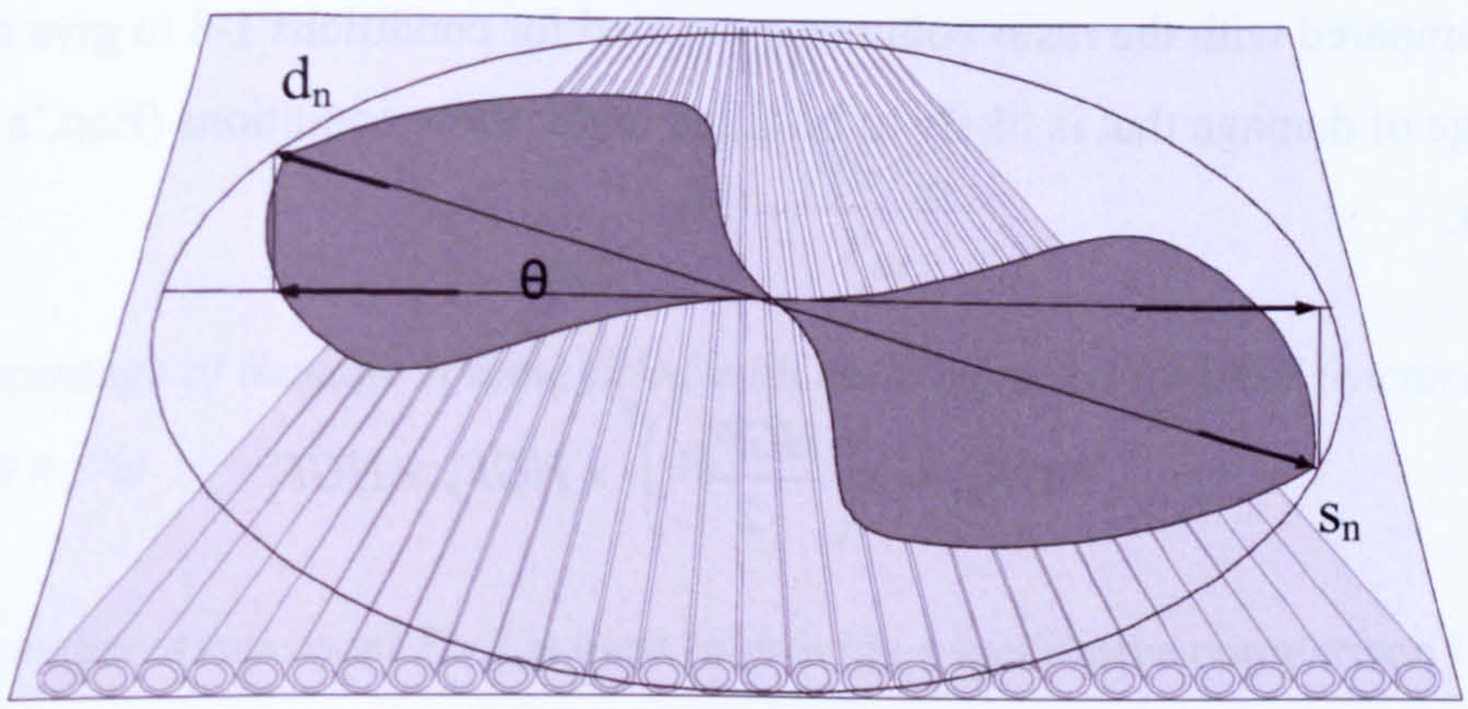

Figure 5-6: ***Schematic Diagram Showing Regions of Overlap between HGF and Delamination Damage***

The number of HGF intercepted by a delamination is obtained by resolving the maximum length of the delamination to an axis perpendicular to the HGF direction as

in Eqn. 5-31 (Figure 5-6). This length (s_n) can then be divided by the HGF outer diameter using Eqn. 5-32 to give the number of HGF intercepted.

$$s_n = d_n \cos(\theta) \qquad \textbf{Eqn 5-31}$$

s_n = Component of delamination perpendicular to fibre direction (mm)

d_n = Maximum length of delamination (mm)

$$HGF_F = \sum HGF_{Fn} = \sum \frac{S_n}{HGF_{OD}} \qquad \textbf{Eqn 5-32}$$

HGF_F = Number of fractured HGF in laminate

HGF_{Fn}= Number of fractured HGF in interface n

HGF_{OD}= HGF outer diamater = $60x10^{-3}$mm

With the number of HGF intercepted by each delamination, it was possible to apply the assumptions outlined above for the three conditions of healing resin release into the damage. Eqn.'s 5-33,. 5-34 and 5-35 are used to determine the volume of healing resin released at each HGF interface for conditions 1, 2 and 3 respectively. The estimated volume of damage within the laminate is calculated using Eqn. 5-36 which can be compared with the resin volumes estimated for conditions 1-3 to give a percentage of damage that is likely to be filled under these conditions (Eqn.'s 5-37, 5-38, 5-39).

$$HGF_{R1} = \pi\left(\frac{HGF_{ID}}{2}\right)^2 \times HGF_F \times HGF_L \qquad \textbf{Eqn 5-33}$$

$$HGF_{R2} = \pi\left(\frac{HGF_{ID}}{2}\right)^2 \times HGF_F \times d_n \qquad \textbf{Eqn 5-34}$$

$$HGF_{R3} = \pi\left(\frac{HGF_{ID}}{2}\right)^2 \times \frac{HGF_F}{2} \times \frac{HGF_L}{2} \qquad \textbf{Eqn 5-35}$$

HGF_F = *No. fractured HGF*

HGF_{Rn} = *Volume of healing resin supplied from HGF for n=condition 1, 2 and 3* (mm^3)

HGF_L = *HGF length (= laminate length) (mm)*

HGF_{ID} = *HGF Inner Diameter (mm)*

$$V_{DT} = \sum V_{Dn} = \sum \left(\frac{\pi r_n^2}{2} \times t_p \right) \quad \textbf{Eqn 5-36}$$

V_{DT} = *Total delamination volume* (mm^3)

V_{Dn} = *Volume of delamination at interface n* (mm^3)

R_n = *Radius of delamination at interface n (mm)*

t_D = *Distance between delaminated surfaces (mm)*

$$V_1 = \frac{HGF_{R1}}{V_{DT}} \quad \textbf{Eqn 5-37}$$

$$V_2 = \frac{HGF_{R2}}{V_{DT}} \quad \textbf{Eqn 5-38}$$

$$V_3 = \frac{HGF_{R3}}{V_{DT}} \quad \textbf{Eqn 5-39}$$

V_n = *Percentage of damage volume filled with resin supplied by HGF fracture condition n (%)*

The *Volumetric Assessment Tool* is used to provide a qualitative comparison between laminate designs by assessing the relative merits of each configuration with regards to how much of the damage volume they are likely to fill with healing resin. It was expected that matching the volume of healing resin to the volume of damage would provide a reasonable indication of the attainable recovery in mechanical performance of the damaged laminates due to healing. This assessment takes into account the HGF spacing and the number of interfaces at which they are located. Furthermore, the front and back face delamination lengths are determined directly from ultrasonic 'time of

flight' imaging at the same impact energy used for subsequent mechanical testing. Although the absolute damage volume and resin volumes calculated are not expected to be an precise, they provide an excellent basis for a comparative study during the design phase (Section 1) of the mechanical assessment Chapters 6, 7 and 8.

5.3 Summary

The *Configuration* and *Volumetric Assessment Tools* provide an initial verification to determine which laminate configurations are worth pursuing in mechanical testing. The results from the use of these tools are presented in the opening sections of each of Chapter 6, 7 and 8. They allow all variations in HGF spacing and number of interfaces to be considered without the need for mechanical testing. They facilitate the assessment of laminate performance in terms of the expected reduction in mechanical properties due to the presence of HGF and the expected recovery in mechanical properties due to the release of healing resin into the damage.

The most significant data generated by the *Configuration Tool* will be presented in tabulated form as can be seen in Table 5-2.

The most significant data generated by the *Volumetric Assessment Tool* will be presented in tabulated form as can be seen in Table 5-3.

HGf Spacing (μm)	No. Interfaces	CF reduction in 0° (%)	Global CF reduction (%)	New V_{CF} (%)	Reduction in Stiffness (%)			Resin Vol (mm^3)	Resin V_{FR} (%)
					E_x	E_y	E_{xy}		
S_{HGF}	N_I	L_{CF0}	L_{CF}	V_{FCFL}	P_{EX}	P_{EY}	P_{GXY}	V_R	V_{FR}

Table 5-2: ***Example of Configuration Tool Data Presented in Experimental Chapters***

HGF Spacing (μm)	No of Interfaces	HGF V_F	HGF Fracture (F) / Damage Fill (V) (%)					
			F_1	V_1	F_2	V_2	F_3	V_3
S_{HGF}	N_I	V_{FHGF}	$\frac{HGF_F}{N_{HGF}}$	V_1	$\frac{HGF_F}{N_{HGF}}$	V_2	$\frac{HGF_F}{2N_{HGF}}$	V_3

Table 5-3*: Example of Volumetric Assessment Tool Data Presented in Experimental Chapters*

6. Self-Healing under Flexure

This chapter considers an initial study to assess the performance of CFRP laminates with embedded HGF. Flexural four point bend testing was used previously to good effect to demonstrate self-healing capability in unidirectional GFRP laminates (Pang et al [141,142] and Trask et al [147]). This study adopts the same approach as this form of testing offers the following:

1. Provides a simple and quick mechanical assessment of laminate performance
2. Suitable for thin laminates and small coupon sizes thereby reducing specimen preparation time
3. Relatively insensitive to edge and surface finish of coupons
4. Use of Linear Variable Differential Transformer (LVDT) avoids need for strain gauges

The flexural strength of specimens in a variety of conditions was assessed:

1. ***Undamaged***. *Assesses any disruption caused by embedded HGF on the flexural strength of the undamaged state.*
2. ***Damaged***. *Assesses interaction between HGF and impact damage to determine whether there is increased damaged tolerance due to the presence of HGF. Furthermore, gauges the effect of damage on flexural strength and provides a point of reference for any recovery after healing.*
3. ***Damaged and Healed***. *Assesses healing efficiency by determining the recovery in flexural strength from the damaged state.*

Four point bend testing was conducted in accordance with the ASTM standard D6272-02 [182]. The benefits of this test method are that the sample region between the loading rollers experiences a constant bending moment and zero shear force (see Figure 6-1). This means that the specimen is subject to pure bending during loading resulting in the upper surface being in compression and the lower surface in tension, according to Eqn 6-1.

$$\sigma = \pm \frac{My}{I} \text{ (MPa)} \qquad \textbf{Eqn 6-1}$$

The flexural strength under this loading condition is given by:

$$S = \left(\frac{PL}{bd^2}\right)\left[1 + \left(\frac{4.7D^2}{L^2}\right) - \left(\frac{7.04Dd}{L^2}\right)\right] \text{ (MPa)} \qquad \textbf{Eqn 6-2}$$

S = stress in outer fibre throughout load span (MPa)

P= load at given point on load deflection curve (N)

L= support span (mm)

b= width of beam (mm)

d= depth of beam (mm)

D= midspan deflection (mm)

The maximum strain at the outer fibres, which occurs at mid-span, is given by:

$$r = \frac{4.7Dd}{L^2} \qquad \textbf{Eqn 6-3}$$

The Tangent Modulus of Elasticity is given by:

$$E_B = \frac{0.21L^3m}{bd^3} \text{ (MPa)} \qquad \textbf{Eqn 6-4}$$

Free Body Diagram

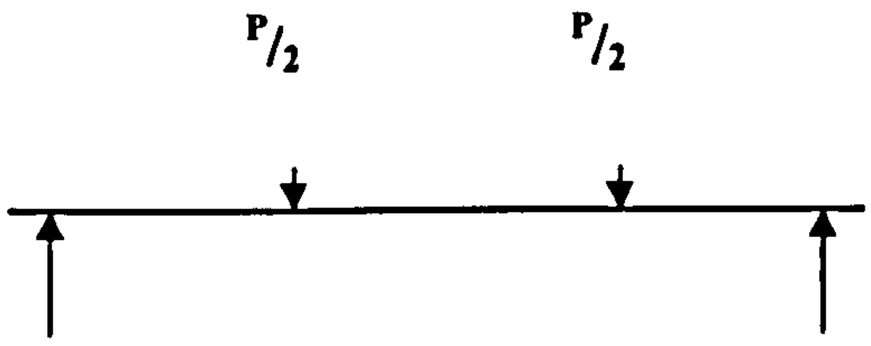

Shear Force

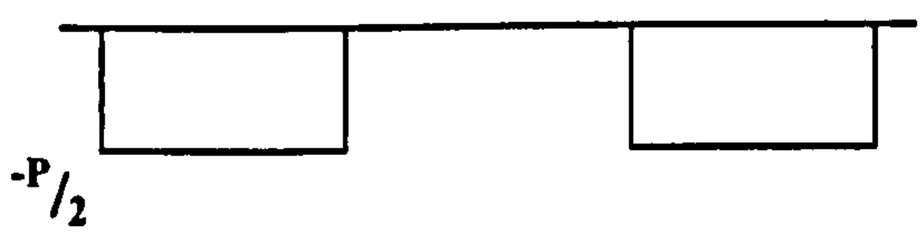

Bending Moment

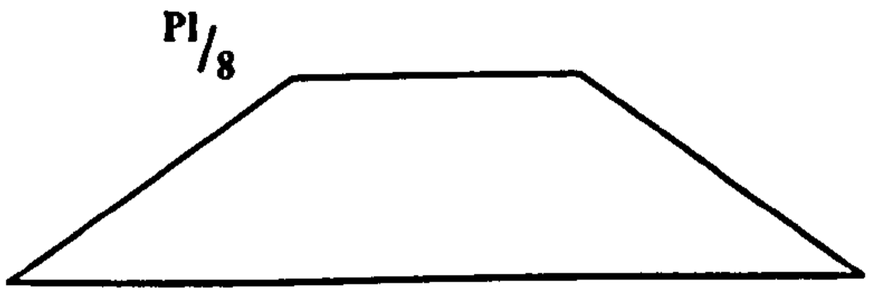

Figure 6-1: ***Free Body Diagram, Shear Force and Bending Moment Plots for Four Point Bend***

6.1 Specimen Design

The CFRP material used was unidirectional T300 carbon fibres pre-impregnated with 914 epoxy resin (Hexcel composites). This system is a high temperature aerospace grade carbon fibre composite for primary aircraft structures. The cure schedule recommended by the suppliers was 1 hour at 175°C at 700kN/m^2 (7 bar) pressure followed by a post-cure dwell at 190°C. The lay-up chosen was $(-45°, 90°, 45°, 0°)_{2S}$ to give a typical quasi-isotropic configuration. The outer wrap of 45° plies provided protection for the load bearing 0° plies which is usual practise for structures that are exposed to impact threats.

6.1.1 HGF Configuration

Two HGF spacings, 70μm and 210μm, were considered. These were selected as it was recognised that the 70μm configuration would provide a large resin volume and the 210μm configuration would provide minimal disruption to the laminate. Details of the *Volumetric Assessment* tool reported in this section can be found in Chapter 5, section 2.1, the results of which are presented in Table 6-1

It can be seen from Table 6-1 that increasing the number of interfaces at which the HGF are located will significantly increase the healing resin volume available within the laminates. However, it can also be seen that a significant reduction in E_X is expected and this is indicative of the reduction in mechanical performance of the laminates as this is largely dictated by the amount of 0° carbon fibre. This reduction is seen most prominently in the 70μm spacing, with a maximum reduction of 35% for HGF at 6 interfaces compared to only a 10% reduction for 210μm spacing. However, the overall reduction in carbon fibre volume fraction for the laminates is not significantly different from the baseline value of 64% for plain CFRP.

HGF Spacing (μm)	No. Interfaces	CF reduction in 0° (%)	Global CF reduction (%)	Resultant V_{CF} (%)	Stiffness (%)			Healing Resin Vol (mm^3)	Healing Resin V_{FR} (%)
					E_x	E_y	E_{xy}		
70	2	13	3	62	90	99	99	80.5	1.61
	3	19	5	61	85	99	99	120.8	2.42
	4	26	6	60	80	98	98	161.0	3.22
	5	32	8	59	75	98	98	201.3	4.03
	6	39	11	58	65	97	97	241.5	4.30
210	2	4	1	63	97	100	100	26.7	0.53
	3	6	2	63	95	100	100	40.0	0.80
	4	9	2	63	93	99	99	53.3	1.07
	5	11	3	62	92	99	99	66.6	1.33
	6	13	3	62	90	99	99	80.0	1.60

Table 6-1: ***Prediction of Laminate Properties for Specimens used in Flexural Testing***

The configuration selected located HGF at two 0°/-45° interfaces above and below the centreline to maintain symmetry:

$$(-45°/90°/45°/0°/\underline{\mathbf{X_1}}/-45°/90°/45°/0°/0°/45°/90°/-45°/\underline{\mathbf{X_2}}/0°/45°/90°/-45°)$$

The two interface configuration was selected for the following reasons:

1. Minimise overall reduction in mechanical properties (70µm=10%, 200µm=3% see
2. Table 6-1) whilst assessing the effect of fibre spacing
3. Provide sufficient healing resin volume to match the estimated damage volume (Est. damage vol. = 22.8mm^3 (Table 6-2), resin volume for 70µm spacing = 80.5mm^3, resin volume for 210µm spacing = 26.7mm^3)
4. Simplify the specimen manufacturing process

6.1.2 Volumetric Assessment

Images were created using an ultrasonic time of flight technique (Described in detail in Chapter 7, section 4.1) in order to assess the damage inflicted by quasi-static indentation (Described in detail in section 2.3). Figure 6-2 shows an example of these images and the associated delamination diameters measured. It can been seen that for a 2000N indentation force the upper delamination exhibited a diameter of 7mm and the lower delamination exhibited a diameter of 13mm.

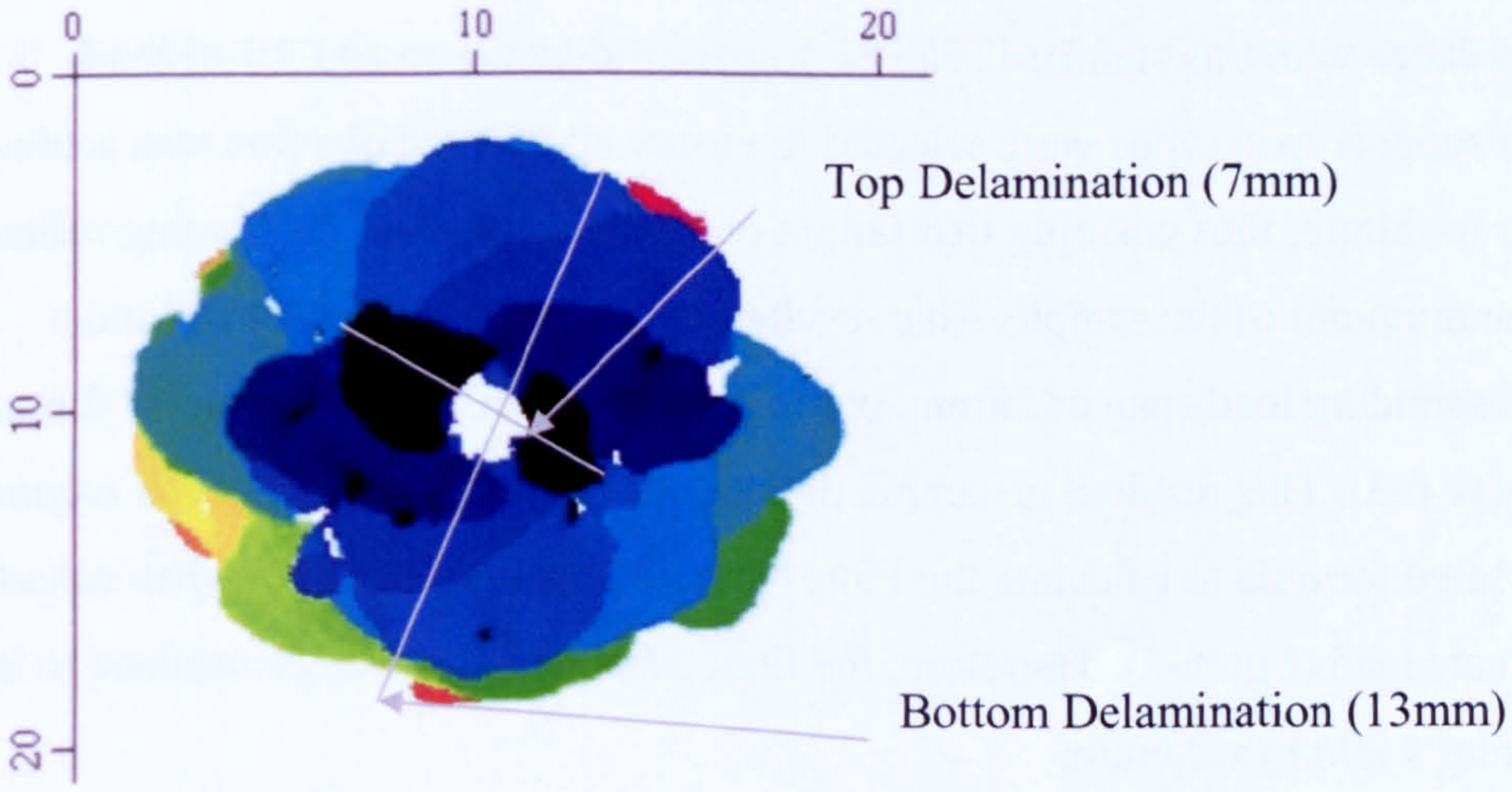

Figure 6-2: ***Ultrasonic Time of Flight Image of Quasi-Static Impact*** **Damage** ***(2000N)***

HGF Spacing (μm)	No of Interfaces	V_{FHGF} (%)	HGF fracture (F_n) / Damage Fill (V_n) (%)					
			F_1	V_1	F_2	V_2	F_3	V_3
70	2	3	44	154	44	17	22	39
210	2	1	43	51	43	6	22	13

Table 6-2: ***Volumetric Assessment Data after Quasi-Static Impact Damage for Conditions 1-3 and Total Damage Volume 22.799mm³***

Details of the *Volumetric Assessment* tool reported in this section can be found in Chapter 5, section 2.2, the results of which are presented in Table 6-2. It can be seen from Table 6-2 that there was a consistent percentage of HGF fracture for the damage inflicted for both HGF spacings (F_{1-3}) It can also be seen that the 70μm HGF spacing was estimated to provide enough healing resin to infiltrate more than 100% of the damage in Condition 1 (outlined in Chapter 5.2.2). Although various assumptions are made in this analysis, it provides a good indication that this configuration should result in significant healing. It was expected that the 210μm HGF spacing would not be so effective. However it should be less disruptive to the laminate performance and thus may provide a more balanced solution.

6.2 Mechanical Assessment

Flexural testing was conducted in accordance with the ASTM standard D6272-02 [182]. Sample dimensions were determined by the nature of the composite material, in accordance with this standard. The 32:1 span-to-depth ratio and 3:1 of load span/support span ratios were selected to ensure adequate deflection was achieved prior to failure, thus ensuring that failure occurred away from the loading rollers and at the midpoint of the sample. This resulted in a support span of 84mm and a corresponding load span of 28mm, based on a 16 ply laminate thickness ≈2.6mm (Figure 6-3). This resulted in sample deflections in excess of 10% which required a corrected formula to calculate the Fibre Stress or Flexural Strength when calculated at ultimate load (Eqn 6-2). Therefore, the final specimen size was determined to be 100mm x 20mm x 2.6mm.

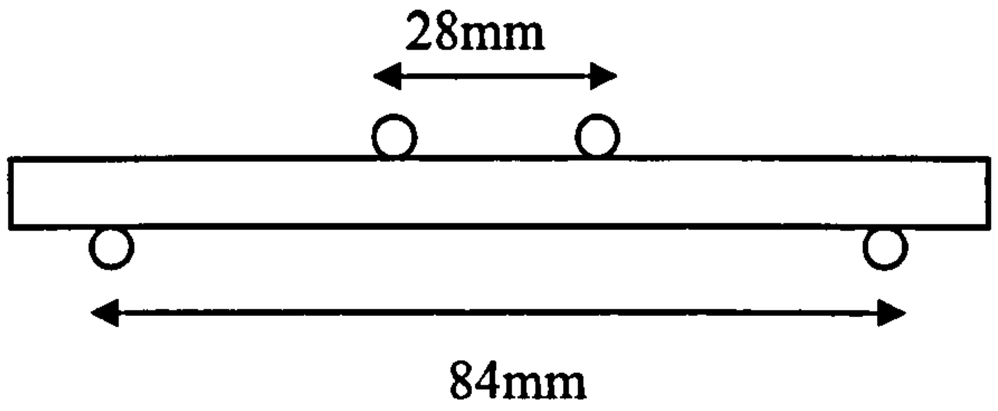

Figure 6-3: ***Load Span (top) and Support Span (bottom) Dimensions***

6.2.1 Laminate Manufacture

Two laminate configurations were proposed for mechanical assessment, as described above in Section 6.1.1. These were 70μm HGF spacing placed at two 0°/-45° interfaces and 210μm HGF spacing placed at two 0°/-45° interfaces. The placement of HGF at the same interface within the laminate meant that commonality was maintained between the two configurations during the manufacturing.

It was proposed in Chapter 3, Figure 3.1 Global Workflow, that the manufacturing process could be sub-divided into four distinct stages:

6.2.1.1 Initial Lamination

A sixteen ply quasi-isotropic lay-up $(-45°/90°/45°/0°)_{2S}$ was selected for the test laminates. The sample dimensions were 100mm x 20mm x 2.6 mm, which resulted in a panel dimension of 230mm x 160mm to provide 10 replicates per laminate with sufficient excess material for losses during the cutting process, as shown in Figure 6-4.

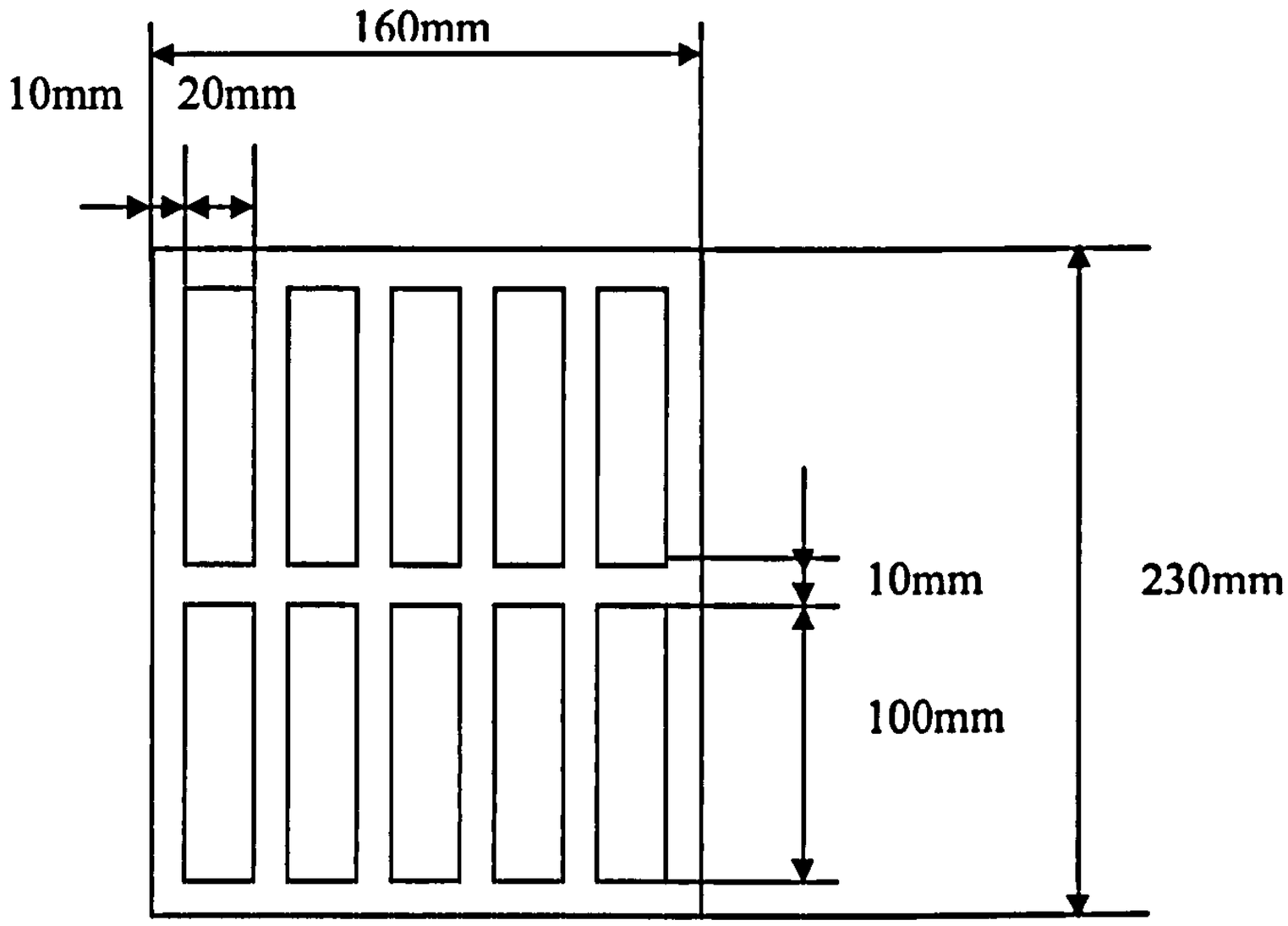

Figure 6-4: ***Schematic Diagram of the Laminate Plates from which Flexural Samples were Cut***

T300/914 carbon fibre/epoxy resin pre-preg tape was removed from storage at -18°C and given adequate time to defrost before being cut to the required ply size.

HGF of the required pitch spacing was to be wound directly onto uncured CFRP plies prior to lamination by locating them directly on the winding drum during the HGF manufacturing process (Figure 6-5). This had two beneficial outcomes:

1. The tension created in the HGF during the manufacturing process was expected to improve HGF embedment
2. Improved manufacturing efficiency minimised unnecessary handling of HGF and simplified its integration into the lamination process

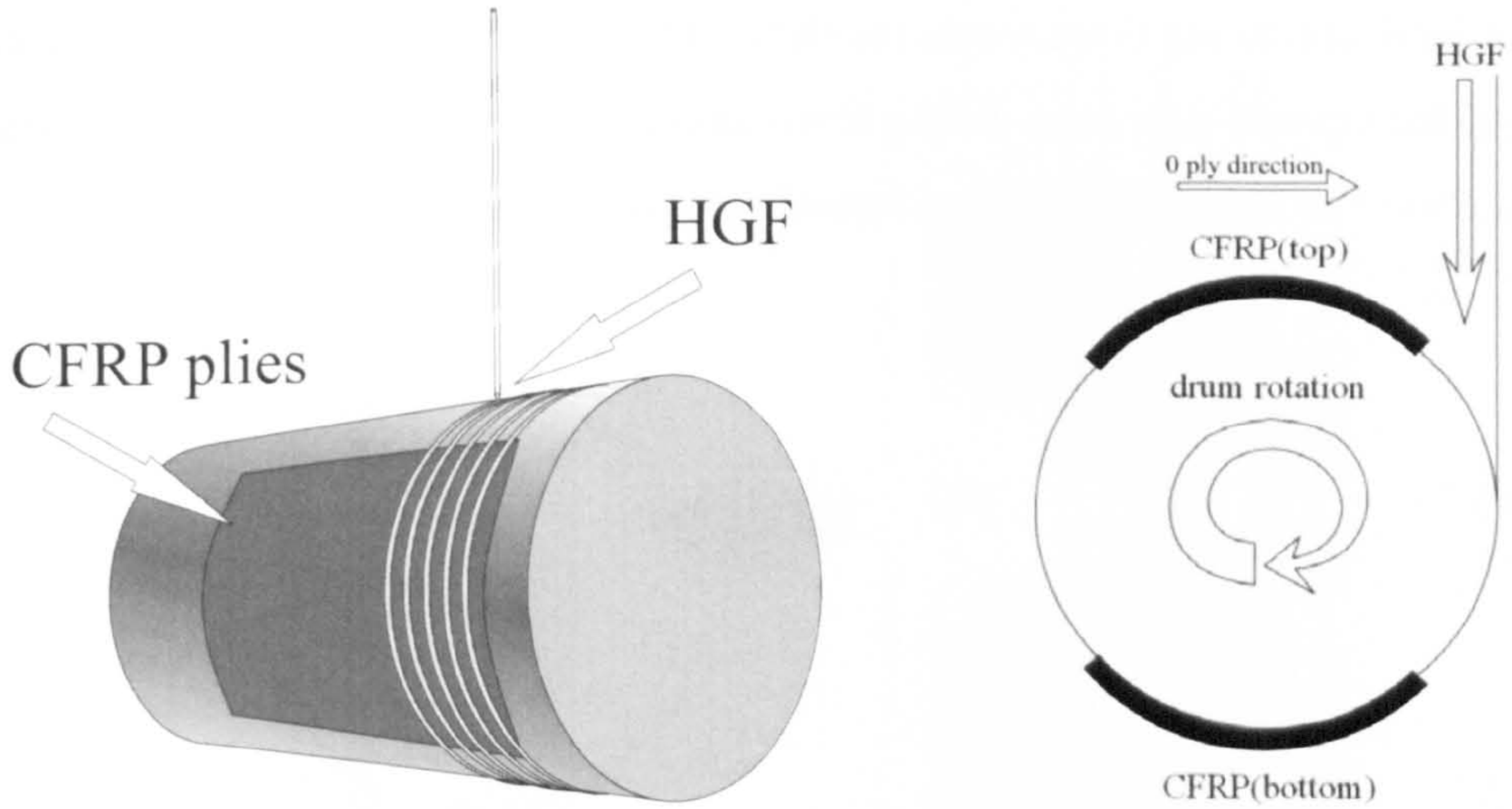

Figure 6-5: ***Schematic of CFRP Sub-Laminates Located on Drum during Manufacture***

To facilitate easier incorporation of the HGF, the 16 ply stacking sequence was divided into three sub-laminates consisting of 3 or 4 plies, as follows:

(-45°/90°/45°/0°/**HGF**/-45°/90°/45°/0°/0°/45°/90°/-45°/**HGF**/0°/45°/90°/-45°)

1. *(45°/90°/-45°/0°/**HGF**)$_{\text{Front Face}}$
2. (-45°/90°/45°/0°/0°/45°/90°/-45°)$_{\text{Middle}}$
3. (-45°/90°/45°/0°/**HGF**)$_{\text{Back Face}}$

***±45 ply directions reversed**

This limited the thickness of the laminate located on the winding drum, during HGF addition, to a maximum of 4 plies and allowed this sub-laminate to conform to the winding drum curvature. It also minimised any wastage to 4 plies of CFRP material should the HGF drawing process be disrupted.

To improve embedment, it was essential that the HGF was wound directly onto the surface of 0° CFRP plies. To facilitate this, the top sub-laminate required the ±45 ply directions to be reversed during lay-up, prior to HGF manufacture. Therefore, after HGF manufacture and during final lamination, the laminate sub-laminate was rotated such that the HGF, which was facing upwards during manufacture, was placed onto

the top of laminate facing downwards (as shown in Figure 6-6). It can be seen that the rotation of the top sub-laminates during final lamination returns the ±45 plies to their correct orientation to form the required quasi-isotropic lay-up.

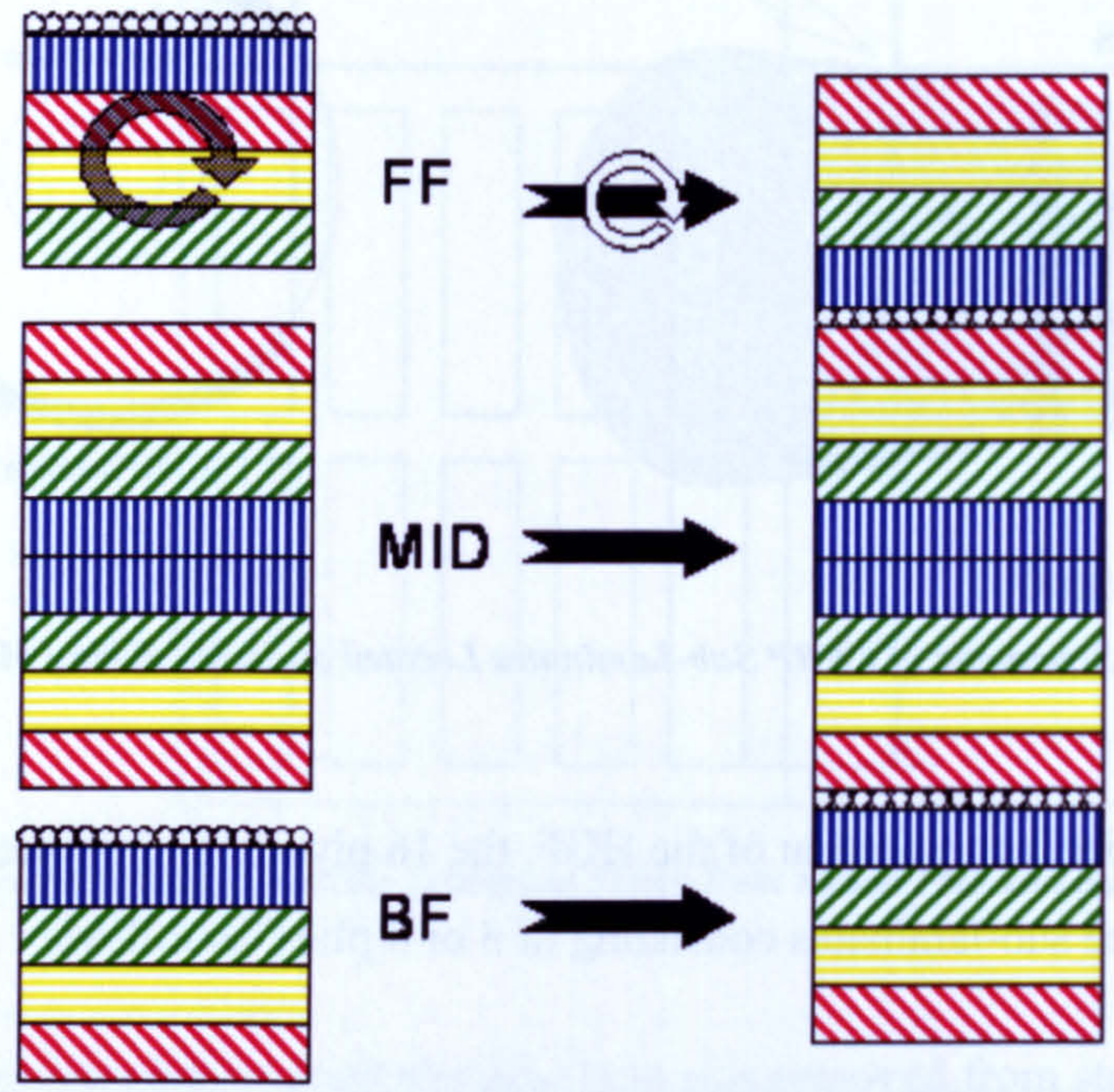

Figure 6-6: ***Construction of Self-Healing Laminate with HGF Embedded at Two Interfaces Highlighting Rotation of Top Sub-Laminate during Final Lamination***

The sub-laminates designated top and bottom were located onto the drum with small squares of double sided tape to hold them in place. They were aligned such that during manufacture, the drawn HGF would be laid into the laminate in the same direction (Figure 6-7). Also their relative position was arranged with sufficient space between them (≈200mm) in order to allow for an adequate length of HGF to extend from the laminate periphery. This length of HGF (approx. 100 mm per laminate) is required to facilitate the resin infiltration process and is considered in detail in Section 6.2.1.4.

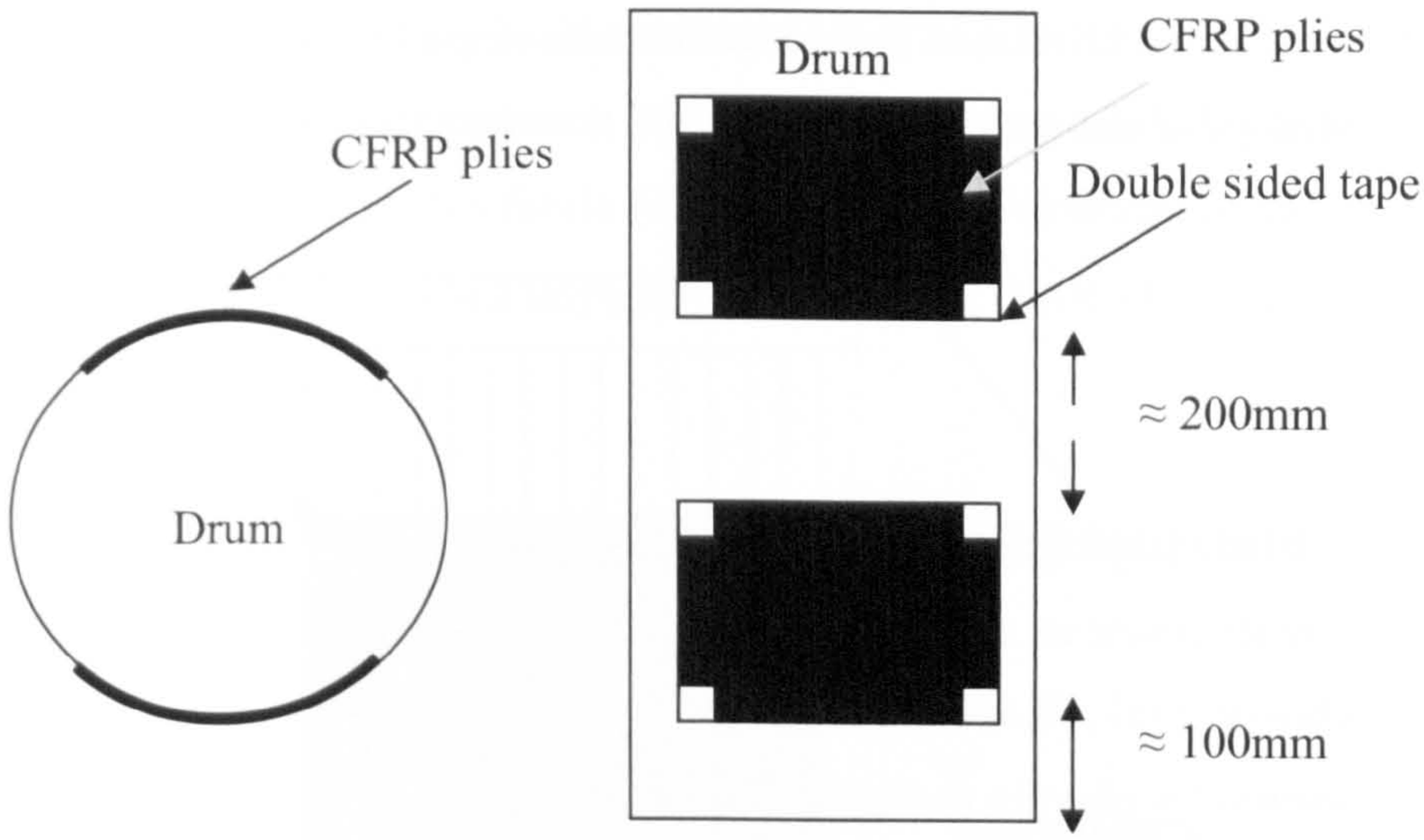

Figure 6-7: ***Placement of CFRP Plies onto Drum during Manufacture***

Once the sub-laminates were prepared and correctly aligned on the drum, the HGF manufacturing process is commenced in accordance with the process outlines in Chapter 4.1.4. However, in addition the HGF is drawn directly onto the laminate sub-laminates located on the drum.

6.2.1.2 HGF Manufacture

This HGF manufacturing process is described in detail in Chapter 4, section 1.2. The only difference in this case is the addition of CFRP plies directly onto the winding drum prior to fibre drawing. The fibre drawing facility settings for the manufacture of the two configurations are given in Table 6-3.

Configuration		OD	Feed Rate	Draw Rate	Pitch Rate
70µm	Setting	58	110	180	70
	Reading		29.4 μms^{-1}	1.26 ms^{-1}	-0.8 µm/rev
210µm	Setting	58	110	180	200
	Reading		29.4 μms^{-1}	1.26 ms^{-1}	-2.31 µm/rev

Table 6-3: ***HGF Manufacturing Settings for 70µm and 210µm Configurations***

Once the respective 4 ply sub-laminate panels were covered with HGF, they were removed from the drum surface using a sharp blade, leaving approximately 100mm of exposed HGF ends at the edge of each panel. Prior to cutting the HGF masking tape

was applied and the blade passed through the centre of the tape (Figure 6-8). This resulted in the HGF tails being attached to a strip of masking tape which improved handling and also ensured that HGF did not entangle during the lamination process.

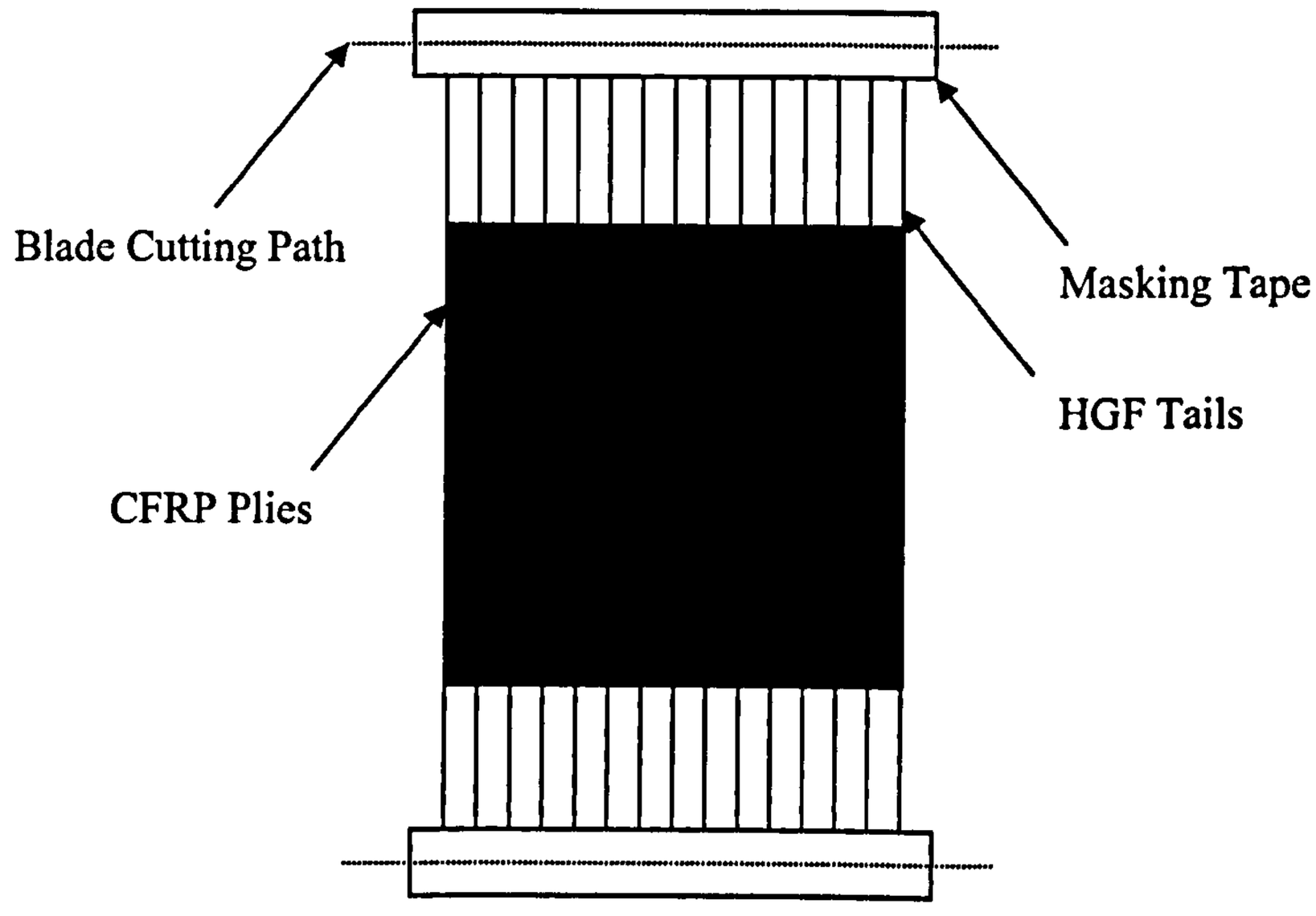

Figure 6-8: ***Removal of CFRP Plies from Drum after HGF Manufacture***

6.2.1.3 Lamination and Cure

After HGF application, all ply sub-laminates were combined (Figure 6-6) using standard hand lay-up techniques and vacuum bagged in preparation for the autoclave. Additional measures were taken during the pre-autoclave 'bagging process' (Figure 6-9) to provide adequate protection to the HGF as outlined below. The autoclave cure process was conducted in accordance with manufacturer's specifications (1 hour @175°C, then post-cured 4 hours @190°C all at pressure of 0.7 MPa/7 bar [1]).

6.2.1.4 Resin Infiltration of HGF

In order to facilitate resin infiltration into the HGF, it was ensured that a length of approximately 100mm of bare HGF 'tails' extended beyond the outer periphery of the laminate. These 'tails' were protected during the autoclave process to prevent HGF fracture and to prevent the matrix resin from infiltrating the internal bore of the HGF.

Laminates containing HGF were carefully handled during subsequent processing and specifically, the HGF tails were handled with extreme care. The HGF ends were sealed with vacuum bag sealant tape and each layer of HGF was surrounded with a wrap of PTFE release film and breather fabric (see Figure 6-10). Furthermore, the entire laminate was covered with at least three layers of breather fabric to further protect the HGF (Figure 6-9e).

The PTFE provides a two fold function. Firstly, separation of the HGF plies to prevent entanglement of fibre. This ensures that each HGF ply can be manipulated individually and minimises HGF contact (and fracture risk). Secondly, is to provide shielding from the excess matrix resin. This reduces the chances of resin infiltration into the exposed HGF and ensures that these fibres remain exposed and unattached.

The breather fabric also provides a cushioning layer to prevent crushing of the HGF during the high pressure cure schedule and minimised any bending of the unsupported fibre extending beyond the periphery of the laminate.

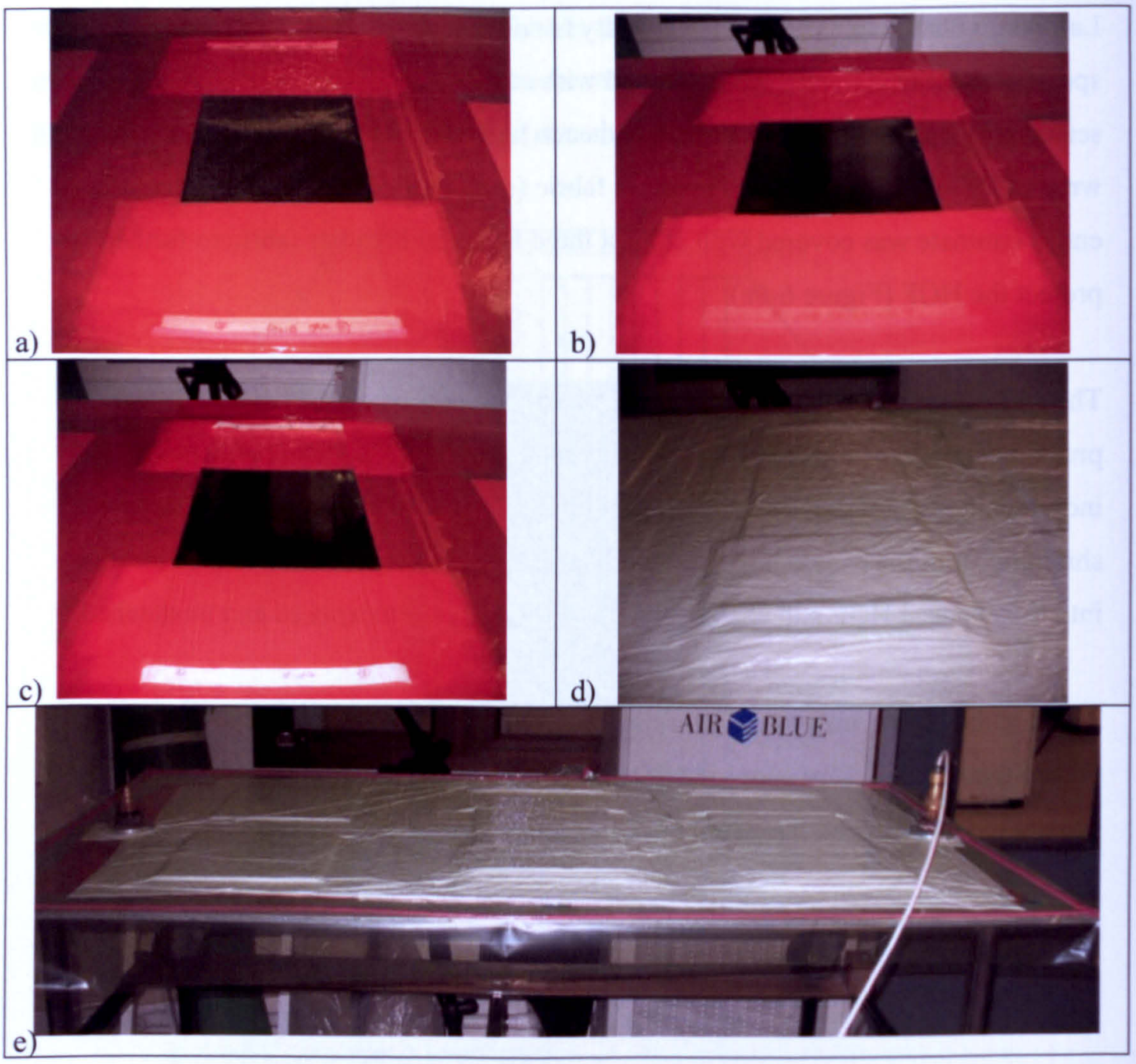

Figure 6-9: ***Final Lamination by Placing Sub-Laminates a) Bottom b) Middle and c) Top onto Tool Plate followed by d) Overlay of Breather Fabric and e)Multiple Laminates Located within one Vacuum Bag***

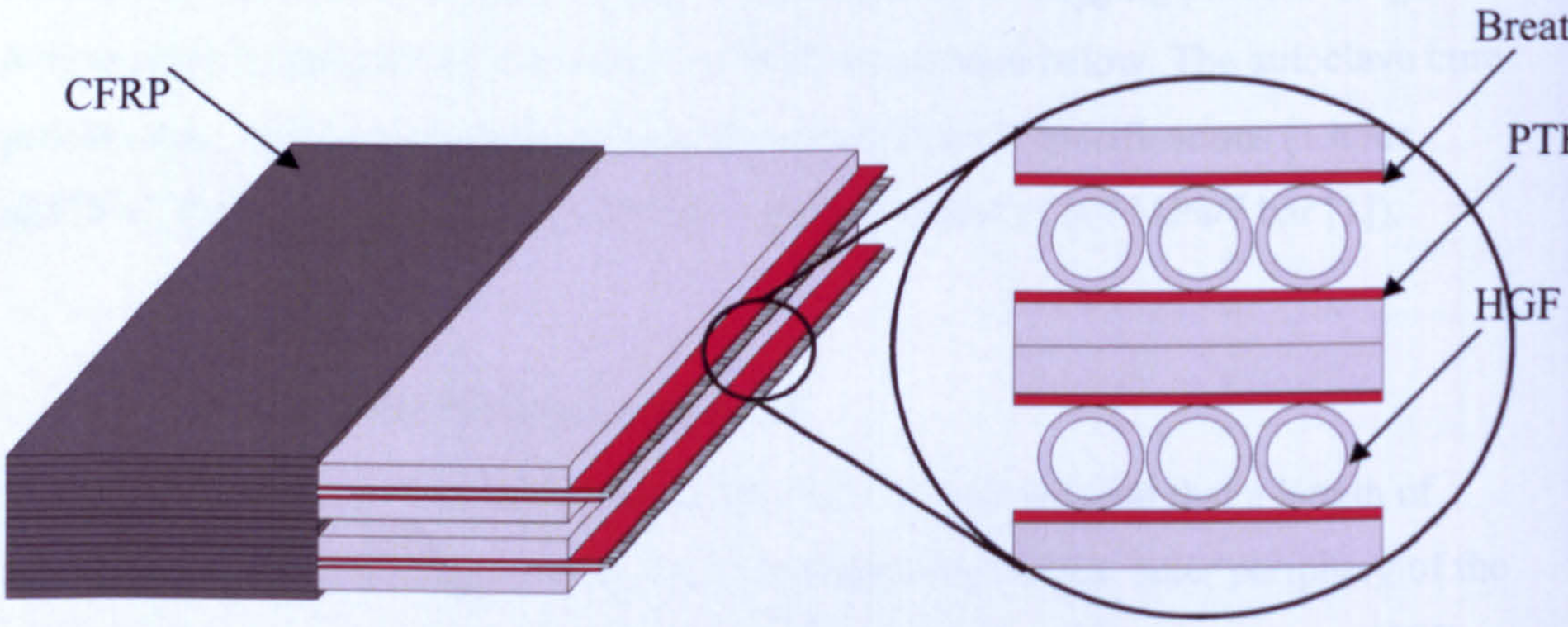

Figure 6-10: ***Schematic Diagram showing the Arrangement of PTFE and Breather Fabric to Protect 'Bare' HGF Tails***

Once the cure schedule was completed and the laminates cooled, they were removed from the autoclave and then from the vacuum bag. The sealed ends of the bare HGF were removed using sharp scissors to expose the hollow ends (Figure 6-11). The breather fabric and PTFE film were then cut at one end of the laminate to expose the bare HGF, Figure 6-12. These HGF 'tails' were placed in a bath of healing resin (Cycom 823) heated to 30°C to reduce viscosity and the other exposed end was enveloped between two additional layers of breather fabric and sealed into a vacuum bag (Figure 6-13). A vacuum was then applied for two hours until the healing resin had fully infiltrated the entire length of the HGF and was visibly wetting the breather fabric within the vacuum bag.

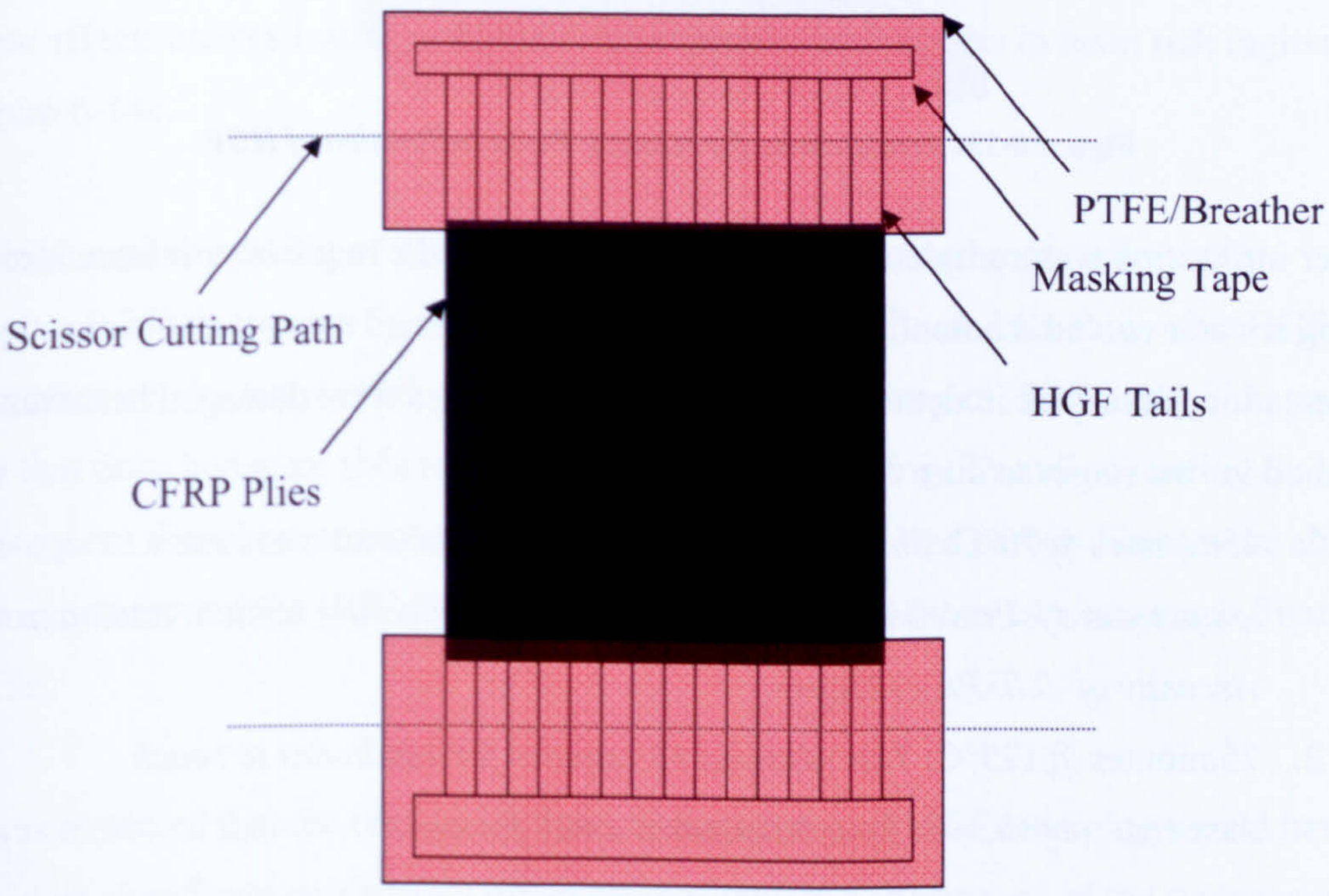

Figure 6-11: ***Removal of Protective PTFE, Breather Fabric and Sealed HGF Ends***

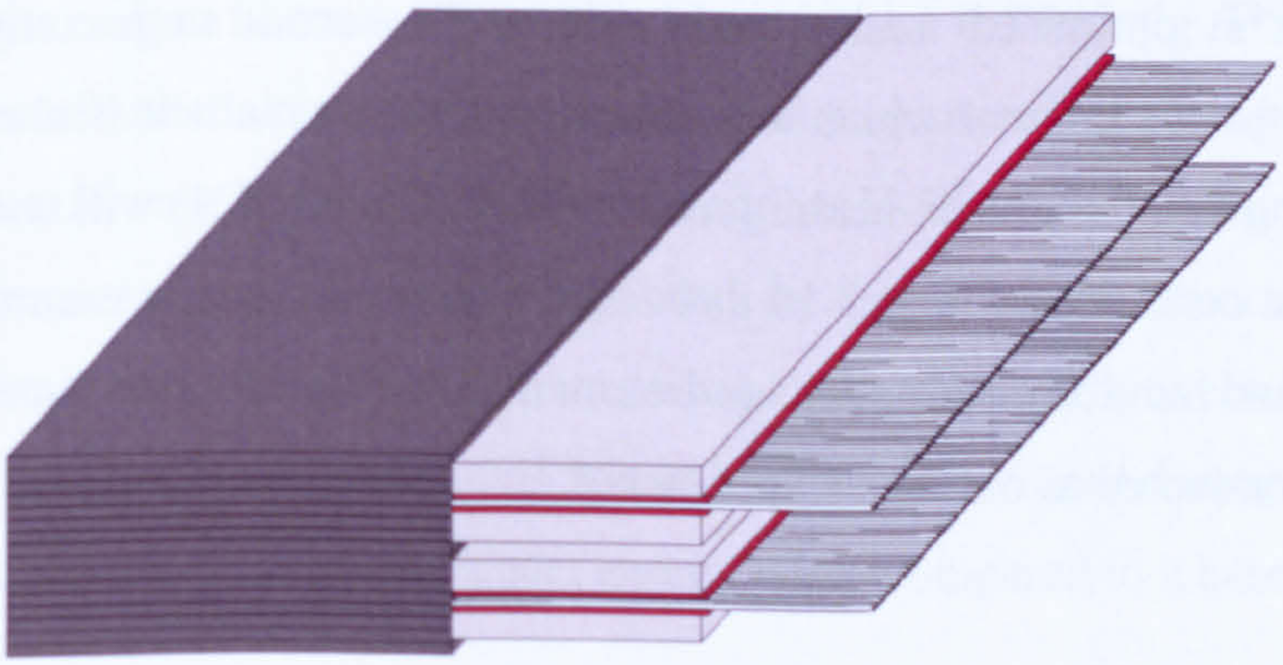

Figure 6-12: ***Removal of PTFE/Breather to Expose HGF Tails***

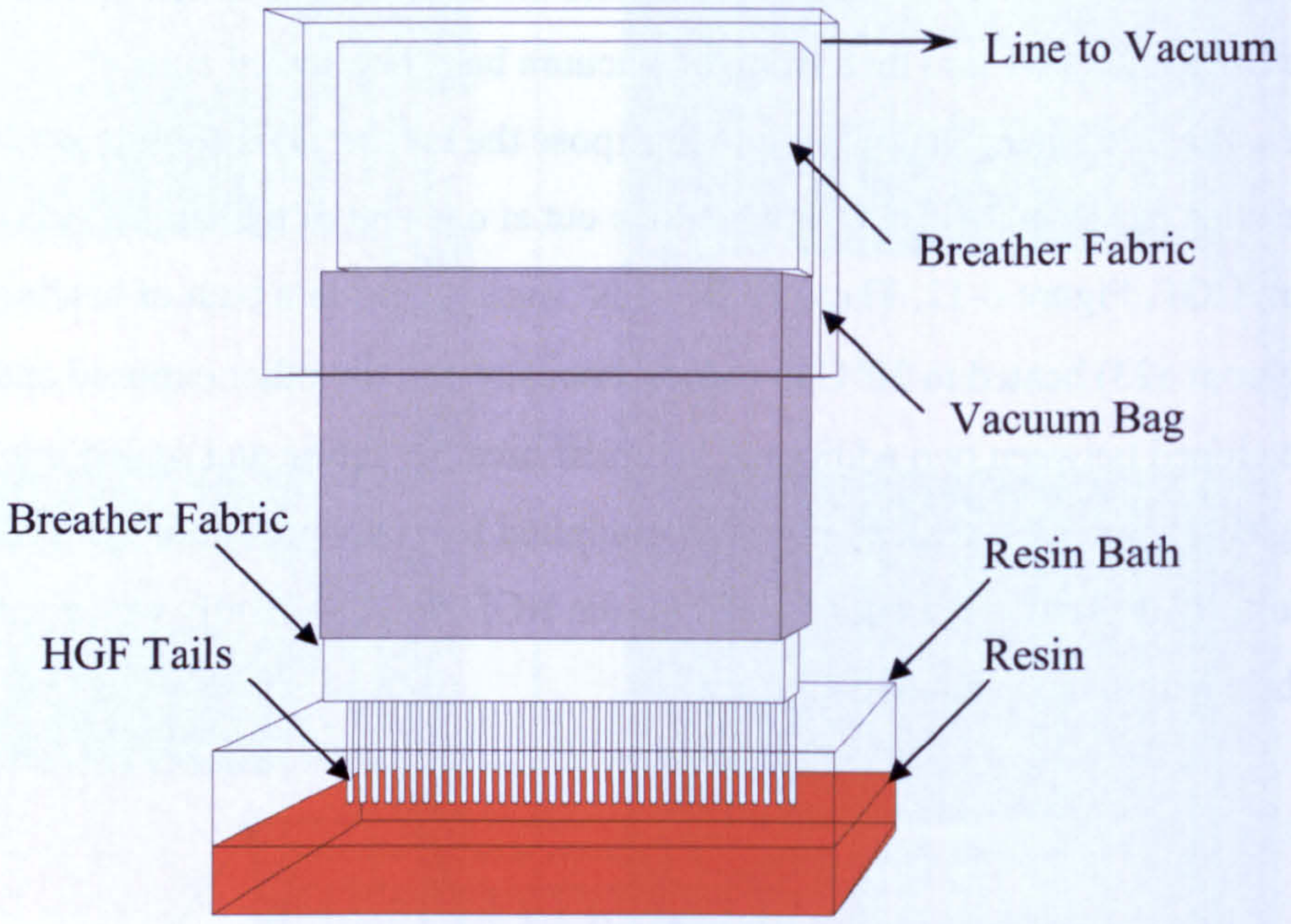

Figure 6-13: ***Arrangement for Healing Resin Infiltration of HGF***

After infiltration was completed, the laminate was cut to the required specimen size using a water cooled diamond saw and then damage imparted using quasi-static indentation (described in detail in 6.2.3). After the samples were damaged heat was applied in two stages to cure the healing resin:

1. 45minutes @70°C: *This allowed 15 minutes for laminates to reach temperature followed by a 30 minutes dwell with healing resin at minimum viscosity of 0.03Pa.s (25cps)*
2. 75minutes @125°C: *This allowed 15 minutes for laminates to reach temperature followed by a 60 minutes dwell for cure*

The initial stage was an attempt to use temperature to mimic the low viscosity required from an 'optimised' healing resin system. The second stage completed the cure cycle within 60 minutes which was considered to be a realistic healing period. It is worth noting that the chosen healing resin system (Cycom 823) will undergo cure under ambient conditions within 7-10 days. After cure specimens were stored in a temperature and humidity controlled environment (19.6°C, 52%) until mechanical testing was conducted as outline in Section 6.3.

6.2.2 Laminate Microstructure

The microstructure of the as-manufactured laminates can be seen in Figure 6-14 and Figure 6-15, which show the distribution of HGF embedded at 70μm and 210μm respectively.

At 70μm spacing, the HGF are tightly packed (Figure 6-14b) as expected. However, some inconsistencies in HGF spacing have occurred during panel manufacture. These are attributed to variability in pitch rate control during the HGF manufacturing process, and also due to the low 'tackiness' of the 914 resin pre-preg allowing HGF to detach and re-attach at random. This often resulted in overlapping fibre which was not overcome during the laminate consolidation in the autoclave. The combination of these effects creates instances of HGF 'clumping' which results in resin rich regions Figure 6-14c.

At higher pitch spacing of 200μm, HGF can be seen to embed more effectively (Figure 6-15). It appears that during the removal of CFRP sub-laminates after HGF manufacture, the matrix resin was able to retain the majority of HGF in position and any that detached were able to reattach without overlapping. Therefore, during the subsequent autoclave consolidation both the matrix resin and carbon fibres were able to migrate around the HGF facilitating excellent embedment as can be seen in Figure 6-15c.

It was expected that the creation of resin rich regions and HGF clumping would have the most significant detrimental effect on mechanical performance of the undamaged laminates. In addition, HGF clumping caused limited distortion (Figure 6-14c) in ply thickness as the carbon fibres were not able to reorganise sufficiently. This could potentially contribute to degradation in mechanical properties by causing waviness in the primary reinforcing fibres. It was considered that HGF clumping may actually increase the impact energy absorption capability by increasing the exposure of HGF to crushing forces and increasing the transmission of such loads between HGF at local clusters of fibre. As a consequence this would improve the overall damage tolerance of the HGF laminates for a given impact energy when compared to a baseline plain CFRP.

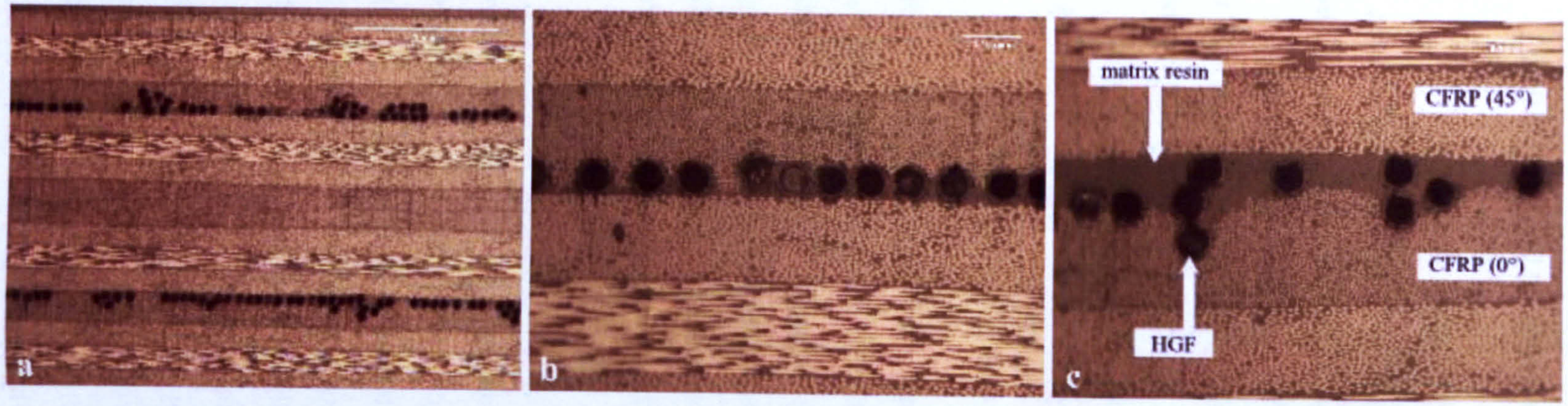

Figure 6-14: ***a) Embedded HGF Spaced at 70μm showing b) Ideally Nestled Side by Side and c) Fibre Clumping and Resin Rich Regions***

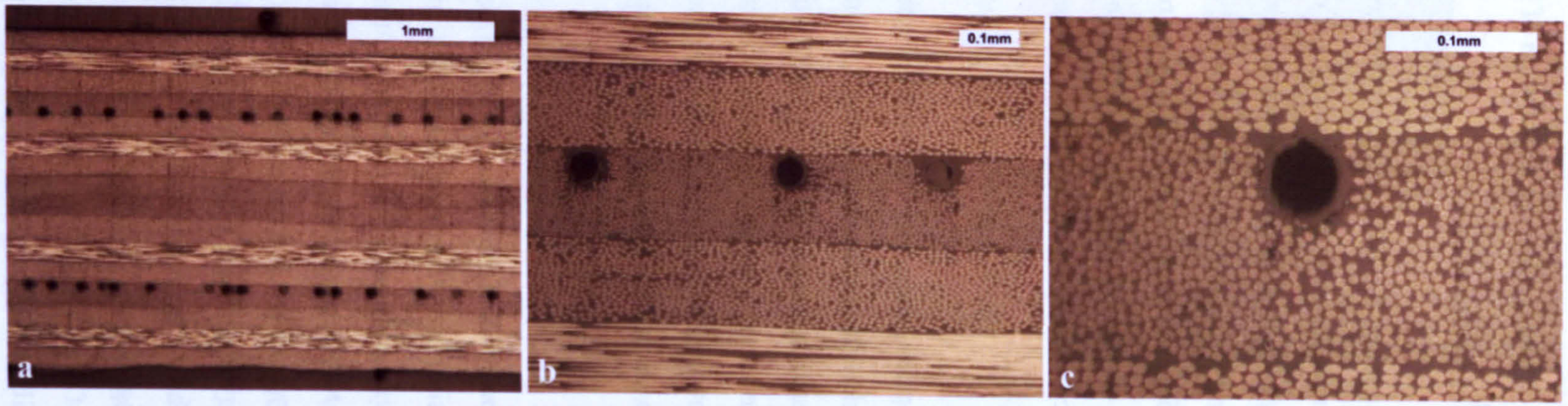

Figure 6-15: ***a) Embedded HGF Spaced at 210μm showing b) Ideally Spaced at 3 HGF Diameters and c) Perfect Embedment***

Individual specimen measurement revealed a small increase in the thickness of the samples that contained HGF when compared to those laminates without, Table 6-4 . However, the flexural strength analysis (Section 6.3) fully accounts for this variation between samples.

		Width (mm)		Thickness (mm)	
210μm	Undamaged	19.95		2.64	
	Damaged	20.42		2.58	
	Healed	20.22		2.59	
70μm	Undamaged	19.86		2.62	
	Damaged	19.75		2.61	
	Healed	19.76	S.D	2.60	S.D
HGF	**Average**	**19.99**	**0.27**	**2.61**	**0.02**
Plain	Undamaged	20.32		2.57	
	Damaged	19.66		2.62	
Baseline	**Average**	**19.99**	**0.47**	**2.60**	**0.04**

Table 6-4: ***Sample Dimensions for Flexural Analysis***

6.2.3 Quasi-Static Indentation

The ASTM D 6272-02 [182] standard for flexural assessment makes no reference to measuring the effects of damage, however the method was deemed suitable as a comparative study for assessing small amounts of damage on mechanical properties. The sample size required for flexural testing excluded the feasibility of drop weight impact as the specimen dimensions were inappropriate. However, the insensitivity of CFRP to strain rate effects, as concluded in Chapter 2 [28,30,35,43], suggested the use of quasi-static indentation as an equivalent alternative

Consideration was given to the ASTM D6264-98 [183] standard for quasi-static indentation. However the chosen specimen dimensions dictated that the support conditions and impactor diameter would need to be modified to ensure the damage was contained within the sample dimensions. It was recognised that the damage created may not be entirely representative of low velocity impact damage expected during operation of real aircraft structures. In particular, this method of damage imparts a more penetrative force into the material at low strain rates and with the boundary conditions required.

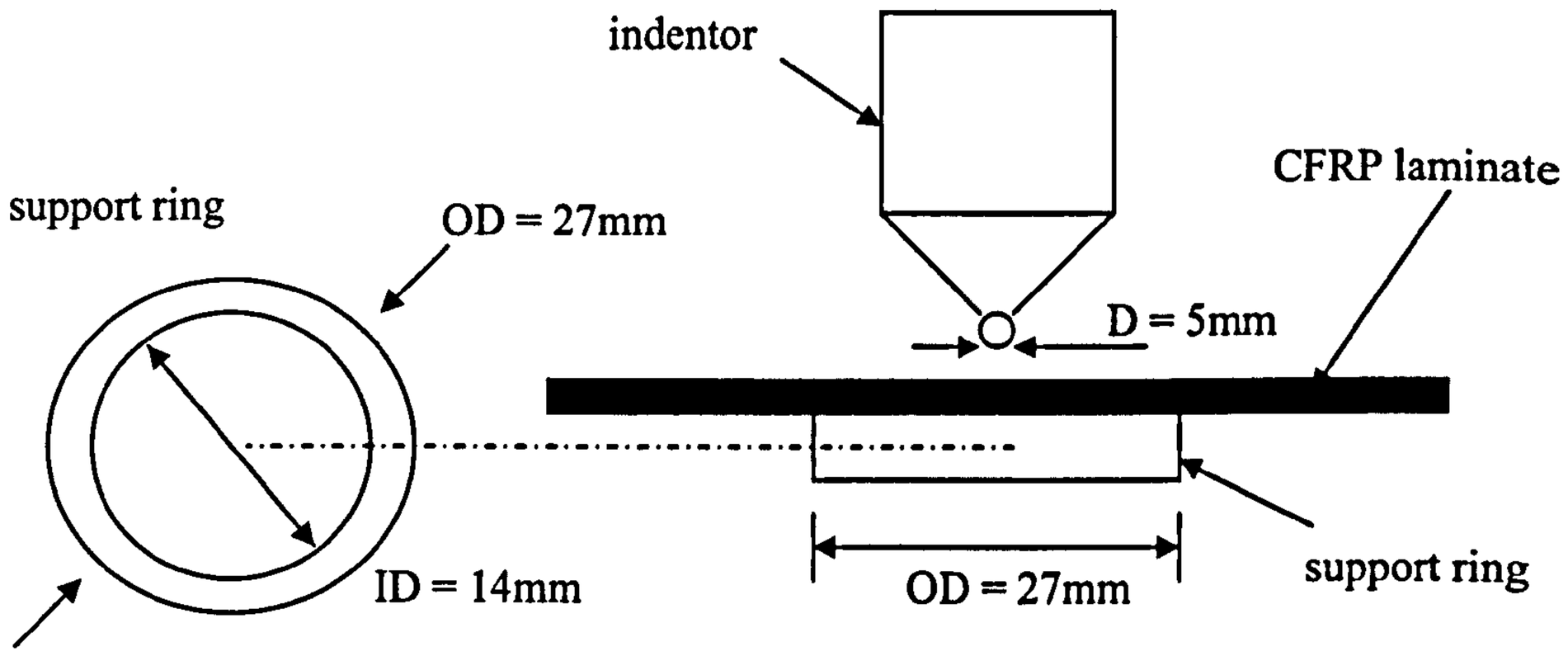

Figure 6-16: ***Schematic Diagram Illustrating Support Ring and Impactor for Quasi-Static Impact***

Pseudo-impact damage was imparted to each specimen using a 5mm diameter hemi-spherical tup mounted on a Hounsfield H20K-W (20kN load cell) electromechanical test machine under load control. The sample was supported by a steel ring of 27mm outer diameter and 14mm inner diameter (Figure 6-16). The indentations were stopped at a peak load of either 1700N or 2000N. A typical load - displacement curve (Figure 6-17) shows two yield points are evident at ~1400N, and ~1700N respectively, with a peak load at 2000N upon which the tup began to penetrate the laminate causing significant back face damage. Up to this load level the damage was contained within the laminate and could be likened to with the following attributes:

- The indent surface exhibited a minor residual indentation (≈0.3mm)
- The back face experienced minimal distortion due to delamination and limited fibre break out.
- The shear crack/delamination distribution within the laminate formed a characteristic 'pine tree' distribution as would be expected from a drop weight impact event.

The peak indentation loads of 1700N and 2000N were identified as the most suitable conditions at which to assess the performance of the self-healing laminates as they provided a sufficient reduction in mechanical properties to demonstrate recovery via healing, sufficient through-thickness loading to initiate HGF rupture, and a level of damage typically found in BVID.

A typical damage distribution resulting from quasi-static indentation to peak loads of 1700N and 2000N can be found in Figure 6-17a) and b) respectively. The most notable difference between them is the reduced separation of delaminations (displacement between delaminated plies) at the higher load level. The increase in delamination area, measured by ultrasonic assessment, was minimal (less than $1mm^2$) i.e. how far the delaminations propagated as the load increased from 1700N to 2000N. This was attributed to the boundary conditions of the specimen during the indentation process effectively 'pinning' the delaminations once they reached a diameter of 14mm (support ring) and preventing further propagation. The additional energy was instead being directed towards driving the delaminated plies further apart as opposed to extending them.

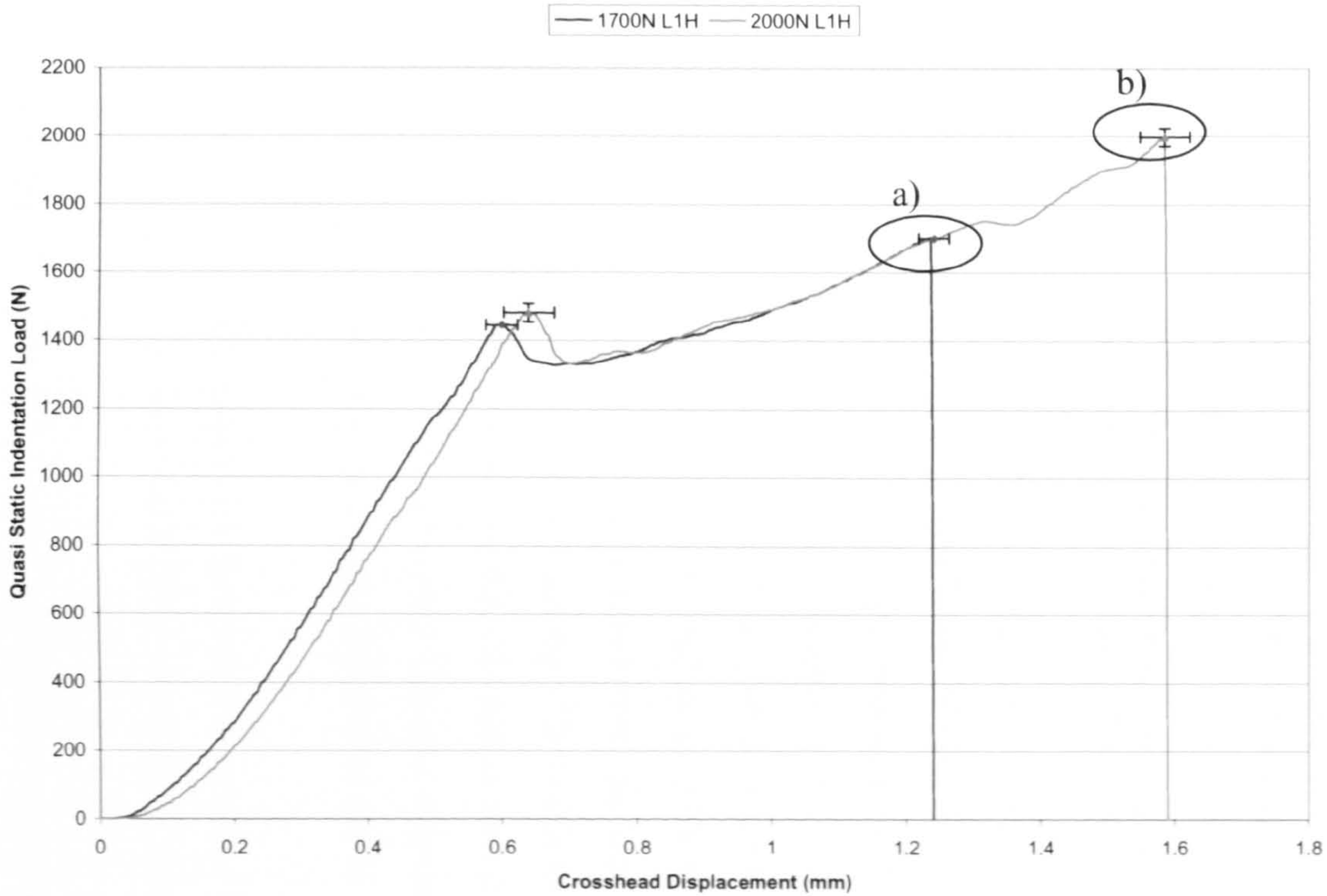

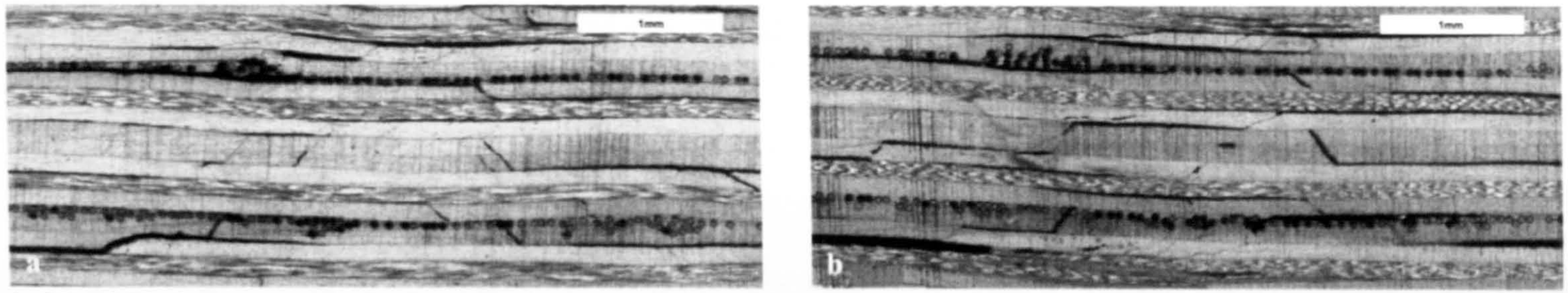

Figure 6-17: ***Typical Load-Displacement curves for Quasi-Static Indentation of CFRP and Corresponding Cross Sectional Damage for Indent Force a) 1700N b) 2000N***

6.3 Results: Flexural Strength

Mechanical testing was conducted using a Roell Amsler HCT25 electromechanical test machine with a 25kN load cell. An Instron 8800 controller was used for data acquisition and Wavemaker Editor software used to generate a constant ramp displacement of 4.4mm/min until ultimate failure of the samples occurs at which point a significant reduction in sustained load was observed and the specimen was unloaded. The specimen deflection was measured at mid-span using a linear-motion potentiometer (conductive plastic) model S13FLP50A from Sakae Tsushin Kogyo Co Ltd. with a mechanical stroke of 50mm. This measurement was typically made within the mid-range of the potentiometer's mechanical stroke so as to ensure that values remained within the device's linear region.

A summary of results from four point bend flexural testing can be seen in Table 6-5 and a graphical representation can be seen in Figure 6-18. Comparisons are made between the performance of undamaged, damaged and healed specimens for the two HGF pitch spacings alongside a baseline plain CFRP laminate with no embedded HGF.

Analysis of the flexural test data (Table 6-5, Figure 6-18) shows that the HGF spaced at 70μm resulted in the largest reduction in undamaged strength (8%). This can be attributed to the significant disruption to the fibre architecture observed in Figure 6-14. However, after a quasi-static impact at 2000N peak load, this configuration exhibited a significant amount of additional damage tolerance when compared to the 210μm HGF spacing and plain baseline laminates. For the 2000N indentation the 70μm configuration achieved a 7% higher flexural strength compared to the baseline plain laminate. This apparent increase in damage tolerance can be attributed to energy absorbed by the crushing of HGF and is supported by the more widely spaced 210μm results which demonstrated values similar to that of the plain baseline laminate. It appears that the initial reduction in strength due to the presence of a significant volume of HGF is offset by an increased damage tolerance. The large volume fraction of HGF in this configuration also provided a larger volume of healing agent as demonstrated by the healed samples achieving 97% of the undamaged strength which

is a recovery of 14%, as shown in Figure 6-18. When compared to the baseline laminate, the 70μm configuration achieved 89% of the undamaged strength which was a recovery of 13%.

The 210μm HGF spacing specimens exhibited a much smaller reduction in undamaged strength (2%) attributable to the reduced disruption to the host laminate (Figure 6-15). These specimens also behaved similarly to the plain baseline laminate when damaged, presumably due to the limited amount of HGF available for crushing. Interestingly, healed samples still achieved 82% of their undamaged strength which was a recovery of 12%. When compared to the baseline laminate, the 210μm configuration achieved 80% of the undamaged strength which was a recovery of 11%. These values were achieved despite the significantly lower volume of healing resin available.

Specimen Type		Undamaged (CV %)	Damaged (CV %)		Healed (CV %)	
			@1700N	@2000N	@1700N	@2000N
Plain CFRP	Strength (MPa)	583.3 (2.3)	538.6 (10.3)	405.0 (16.2)	-	-
	% of undamaged baseline	*100%*	*92%*	*69%*	-	-
HGF spaced @210μm	Strength (MPa)	568.8 (3.3)	490.1 (6.5)	401.0 (13.2)	523.4 (3.6)	466.6 (4.7)
	% of undamaged baseline	*98%*	*84%*	*69%*	*90%*	*80%*
HGF spaced @70μm	Strength (MPa)	534.9 (2.4)	527.3 (1.5)	443.7 (10.7)	529.0 (3.2)	519.6 (5.5)
	% of undamaged baseline	*92%*	*90%*	*76%*	*91%*	*89%*

Table 6-5: ***Summary of Mean Flexural Strength for Baseline Plain, L_{210} and L_{70} Laminates in Undamaged, Damaged and Healed Conditions (Undamaged= 10 samples, Damaged=5 samples@1700N, 5 samples@2000N)***

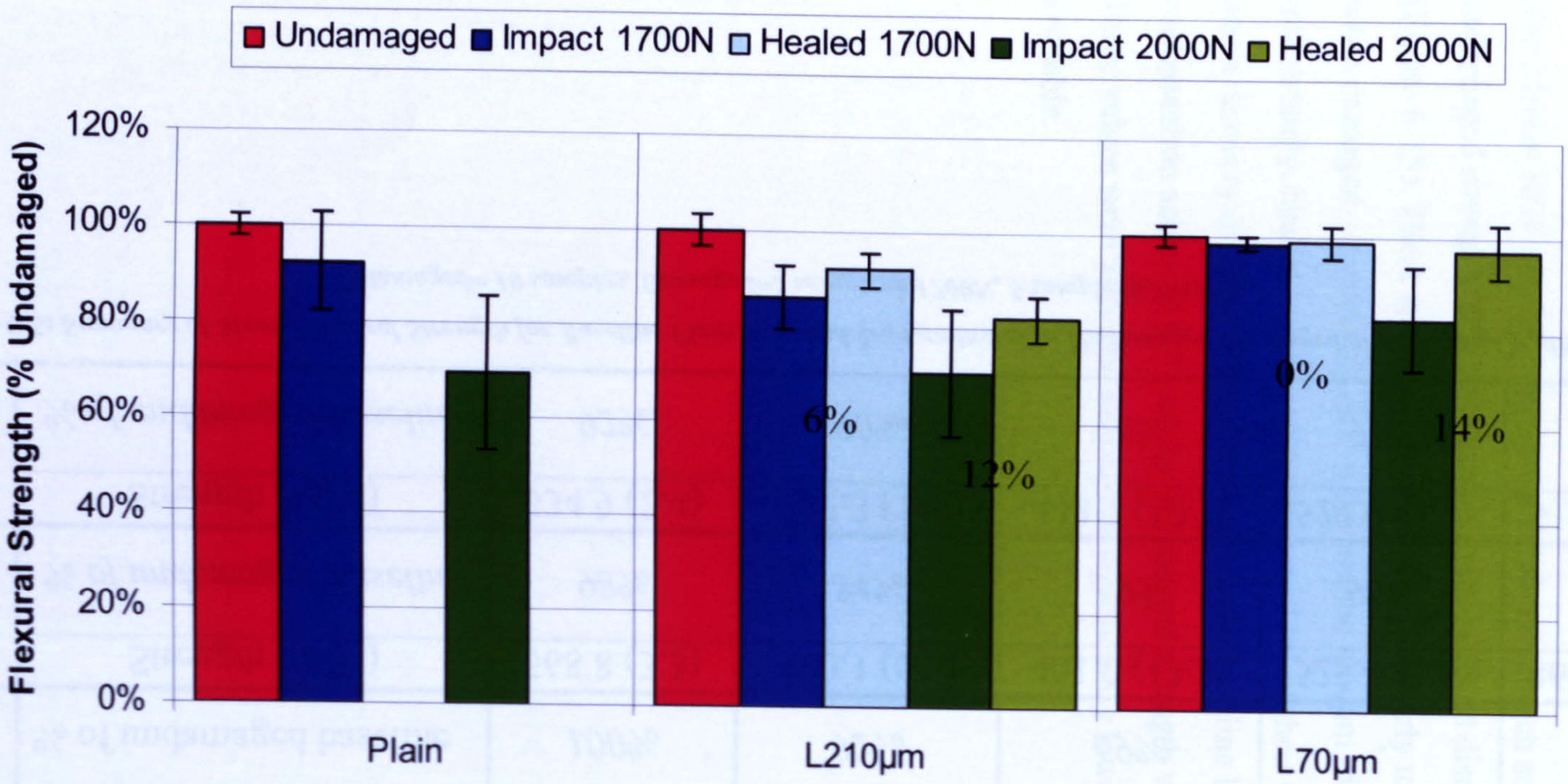

Figure 6-18: ***Summary of Results for Flexural Strength Relative to Undamaged***

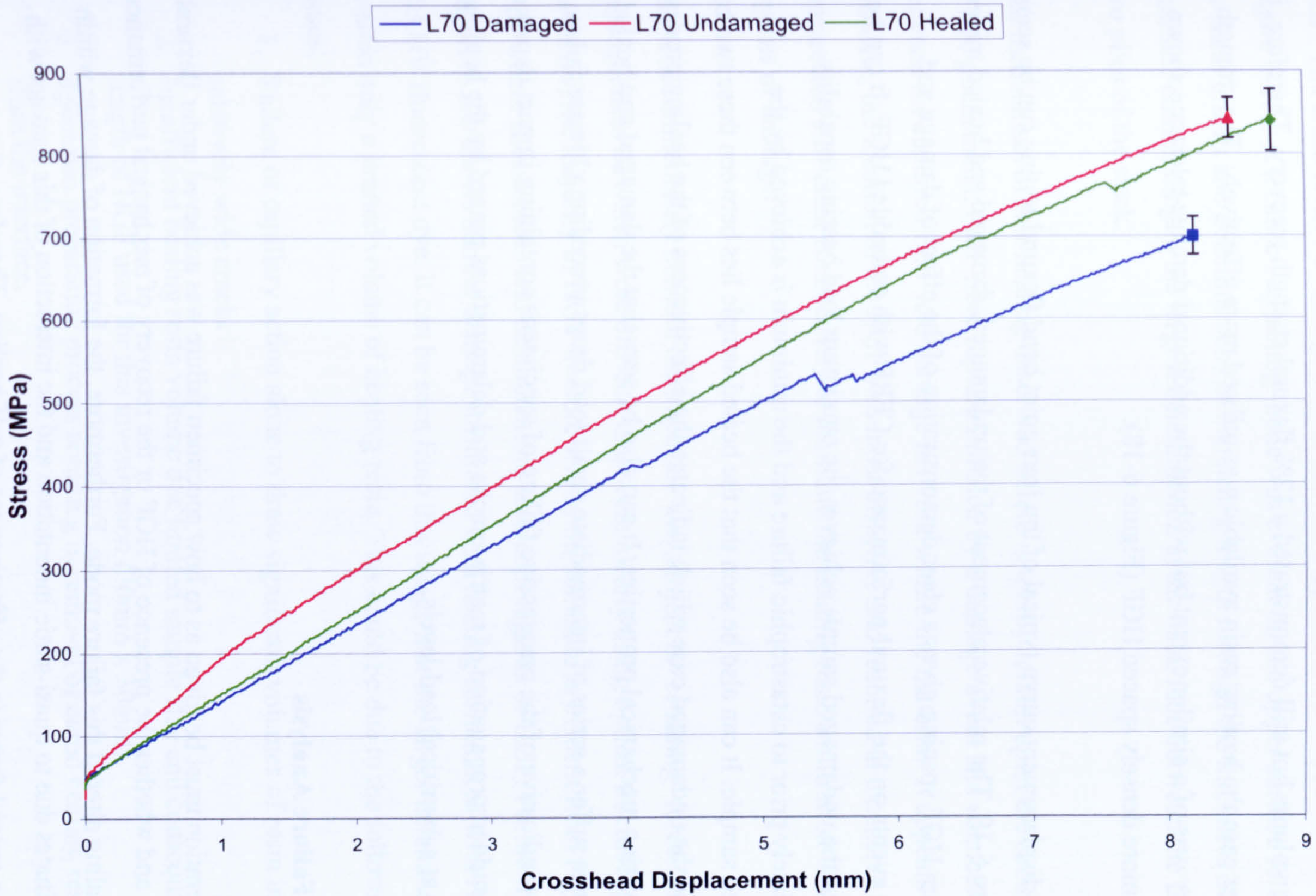

Figure 6-19: ***Typical Load Displacement Curves for Flexural Testing***

When Table 6-2 is considered, it can be seen that the 70μm HGF spacing was predicted to provide 154% volume of healing resin compared to the estimated damage volume which resulted in a 14% flexural strength recovery. The 210μm HGF spacing was predicted to provide only 51% healing resin volume compared to the expected damage volume but still demonstrated a 12% flexural strength recovery. Therefore, in the latter case the healing resin available was utilised more effectively. The strength recovery was of a similar extent but without the additional damage tolerance shown for the more densely spaced HGF (Figure 6-18).

A load-displacement curve typical of the four point bend flexural testing can be seen in Figure 6-19. The relative placement of the undamaged, damaged and healed traces for 70μm HGF spacing gives a clear demonstration of the effect of damage and healing events on the flexural performance for CFRP with embedded HGF. It can be seen that the undamaged sample achieves the maximum load bearing capability immediately prior to catastrophic failure and the minimum is achieved by the damaged sample. It can also be seen that the healed sample lies between these two but nearer to the undamaged case which indicates the effectiveness of the healing process in recovering mechanical properties. It can also be seen that the damaged and healed specimens suffer a series of intermediate small load drops preceding ultimate failure which is indicative of the progressive failure of specimens containing impact damage via the sudden propagation of matrix cracks and delaminations pinned by the healing process at sub-critical load levels.

6.4 Failure Analysis

Consideration must be given as to how specimen failure was achieved under flexural loading and whether the presence of HGF or the recovery of mechanical performance after healing altered this failure mode. Furthermore, the formation of damage within the laminates due to quasi-static indentation and the interaction of this damage with HGF is a crucial factor in the effectiveness of self-healing. Therefore, these are considered herein.

6.4.1 Fractography of Damaged and Healed specimens

Fractographic analysis of specimens after quasi-static indentation (no flexural loading) indicated the mode of damage development and the interaction with the HGF. The cross sectional damage distribution was typical of a BVID event as seen in Figure 6-20a. A localised 'crushing' zone was evident on the upper surface followed by shear cracks and delaminations of increasing length through the thickness of the laminate culminating in the largest delamination at the back face between the final two plies of the stack.

The mechanism of self-healing described herein is totally reliant upon the occurrence of two phenomena; HGF fibre rupture initiated by a damage event and connectivity between the ruptured HGF and damage network within the material. It appears that in this case, the location of the HGF was most effective and resulted in extensive fibre rupture and sufficient connectivity to facilitate the healing resin infiltration into regions of damage.

The HGF immediately beneath the impactor was subject to 'crushing' forces, the consequences of which were difficult to discern clearly using optical microscopy. However, the majority of HGF fracture within the laminate is evident from Figure 6-21 where shear cracks and delaminations intercept regions of HGF. Furthermore, Figure 6-20b shows similar damage infiltrated with healing resin mixed with Ardrox 983 UV fluorescent dye. It can be seen from this image that the larger delaminations contain only a limited volume of healing resin. This could be due to the following issues:

1. Failure of capillary action alone to draw significant volumes of resin into the relatively wide cracks
2. Insufficient healing resin volume due limited sample size and consequently length of HGF used for this investigation (30mm x 30mm).
3. Specimen preparation process resulting in removal of cured healing resin from the interface.

The sample used for UV visualisation (Figure 6-20) was a coupon of 60mm x 60mm x 2.6mm with HGF spaced at 70μm. Four quasi-static indentations were imparted into the centre of each quartile of the panel. Each impact site had a length of

approximately 30mm HGF within a 30mm x 30mm area. In comparison, the dimensions for a flexural test specimen were 100mm x 20mm x 2.6mm, therefore, a substantial increase in HGF length would be present in such a test specimen for supplying healing resin to a damage site.

The panel shown in Figure 6-22 had the HGF within approximately half of the specimen width infiltrated with healing resin mixed with UV dye penetrant (bottom half), and the other half was left empty (top half). After quasi-static indentation, ultrasonic assessment was able to distinguish between the two halves of the laminate by detecting empty HGF (dark blue). It can be seen that a region of HGF running through the impact centres is detected (dark blue), implying that this region of HGF was evacuated of healing resin due to HGF fracture under the impact zone.

As a result it may be that delaminations wider than 30μm are too wide to facilitate complete healing resin infiltration. However, these observations remain inconclusive.

Intra-ply shear cracks are seen to link multiple delaminations in Figure 6-20, Figure 6-21 and Figure 6-23. The presence of these shear cracks is essential for effective self-healing as they provide connectivity between different damage sites in the laminate and facilitate healing at multiple interfaces. Shear cracks can also be seen to have initiated HGF fracture in preference to reinforcing fibre fracture (Figure 6-21). However, the thickness of shear cracks (10μm) is generally smaller than delaminations (30μm) and so they would be expected to generate a larger capillary action (inversely proportional to the radius of the opening between two surfaces).

Delaminations were observed to propagate along interfaces between plies of dissimilar fibre orientation It can be seen that this initiated HGF fracture via two mechanisms. In Figure 6-23c), clusters of HGF and the accompanying resin rich regions have caused a delamination to deviate from its path, causing fibre rupture and release of healing resin. In Figure 6-23d) HGF are ruptured as a delamination propagates along a ply interface suggesting that a HGF's susceptibility to fracture is similar to the matrix as no obvious crack deviation is evident.

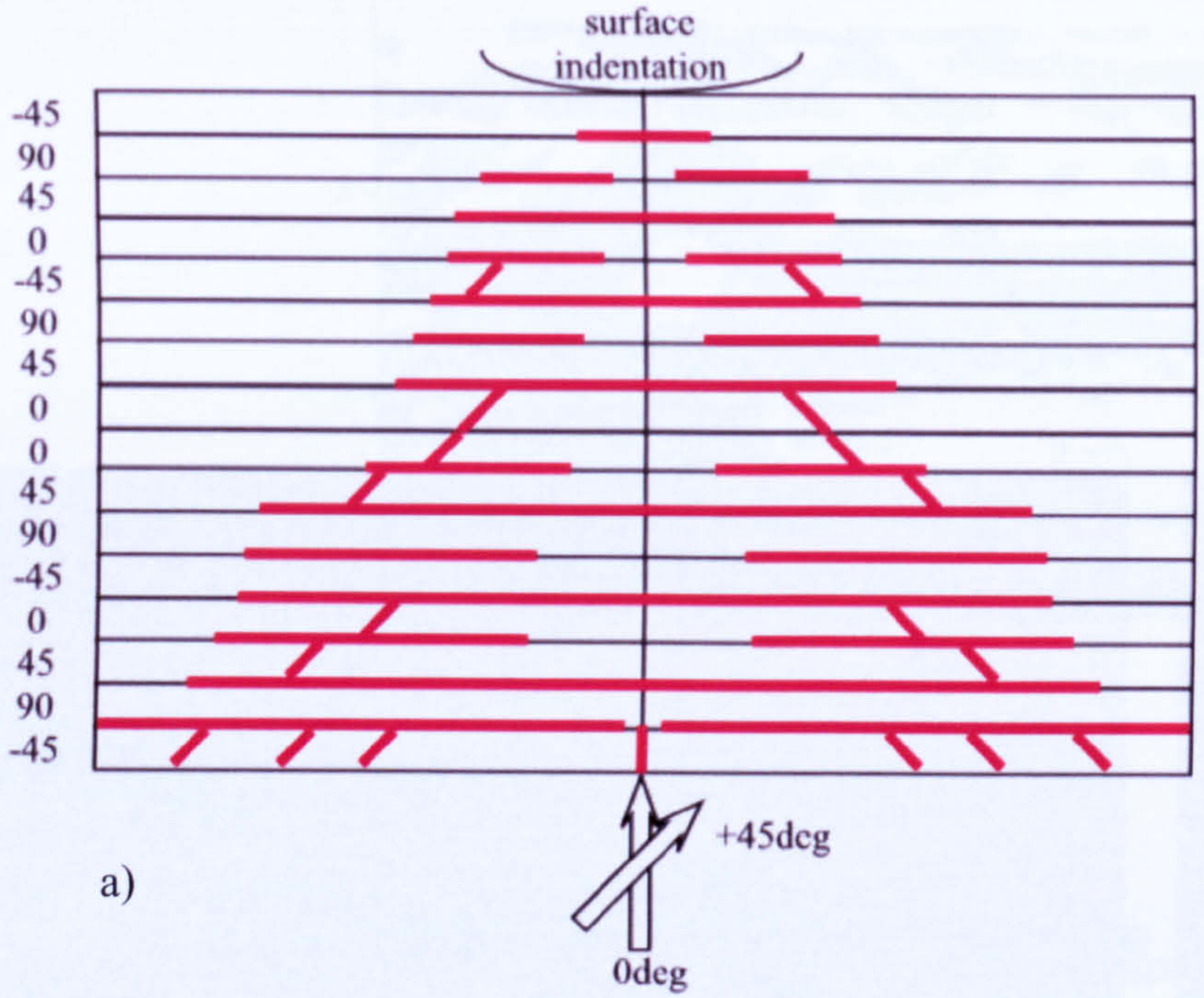

a)

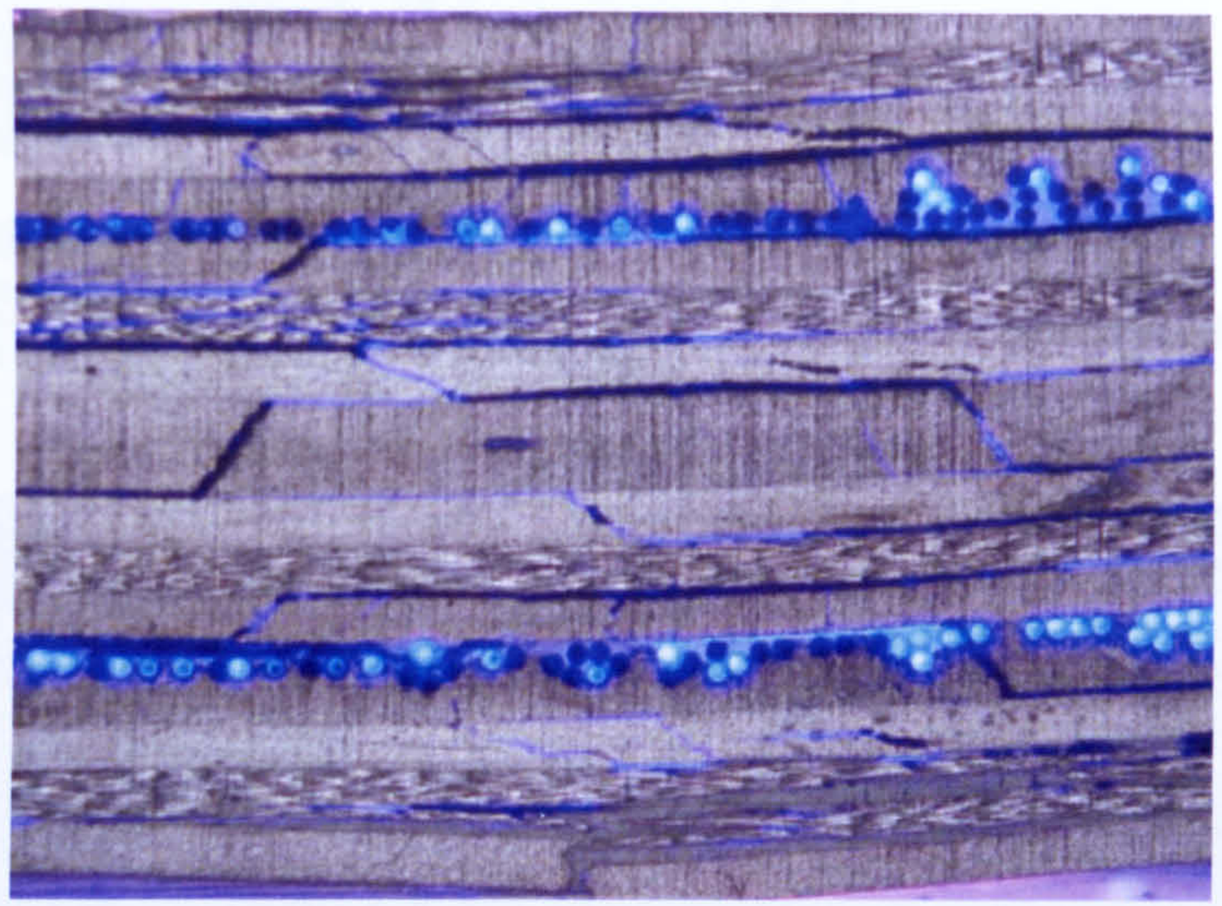

b)

Figure 6-20: ***Typical Damage Distribution after Quasi-Static Indentation Represented by a) Schematic Diagram and b) Optical Micrograph Highlighted with UV-dye Added to Healing Resin***

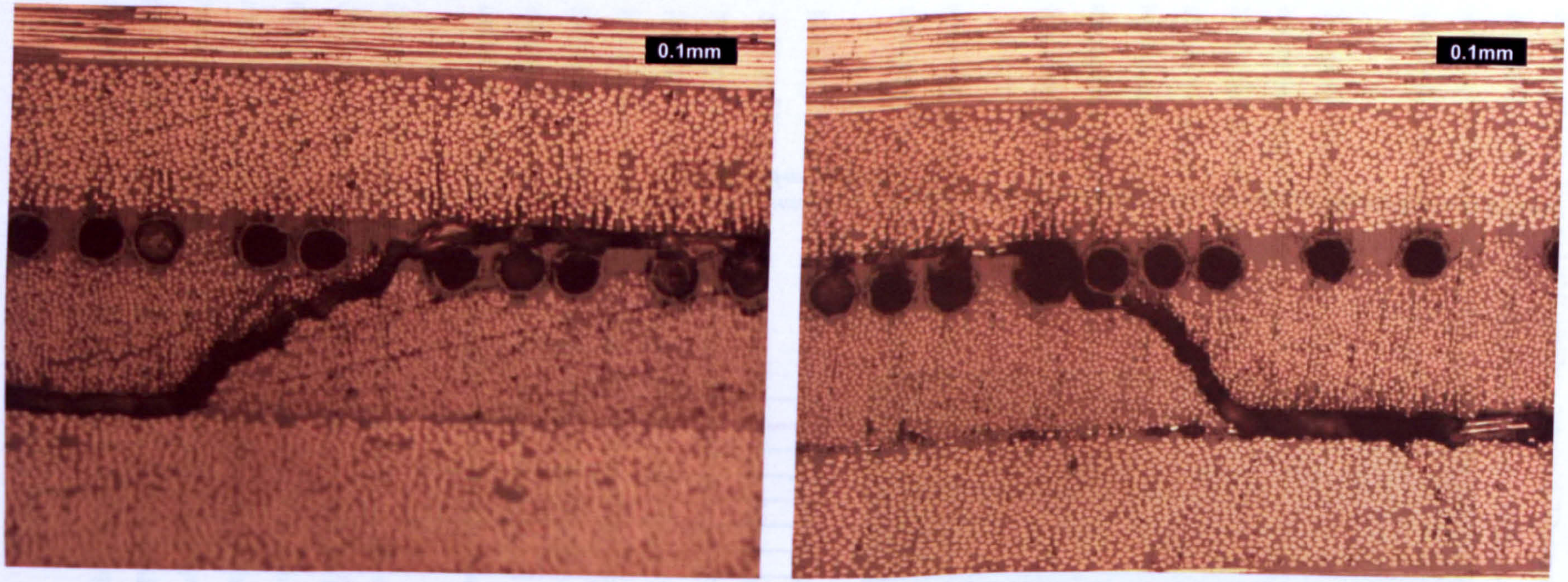

Figure 6-21: ***Optical Micrographs of Shear Cracks and Delaminations Fracturing HGF***

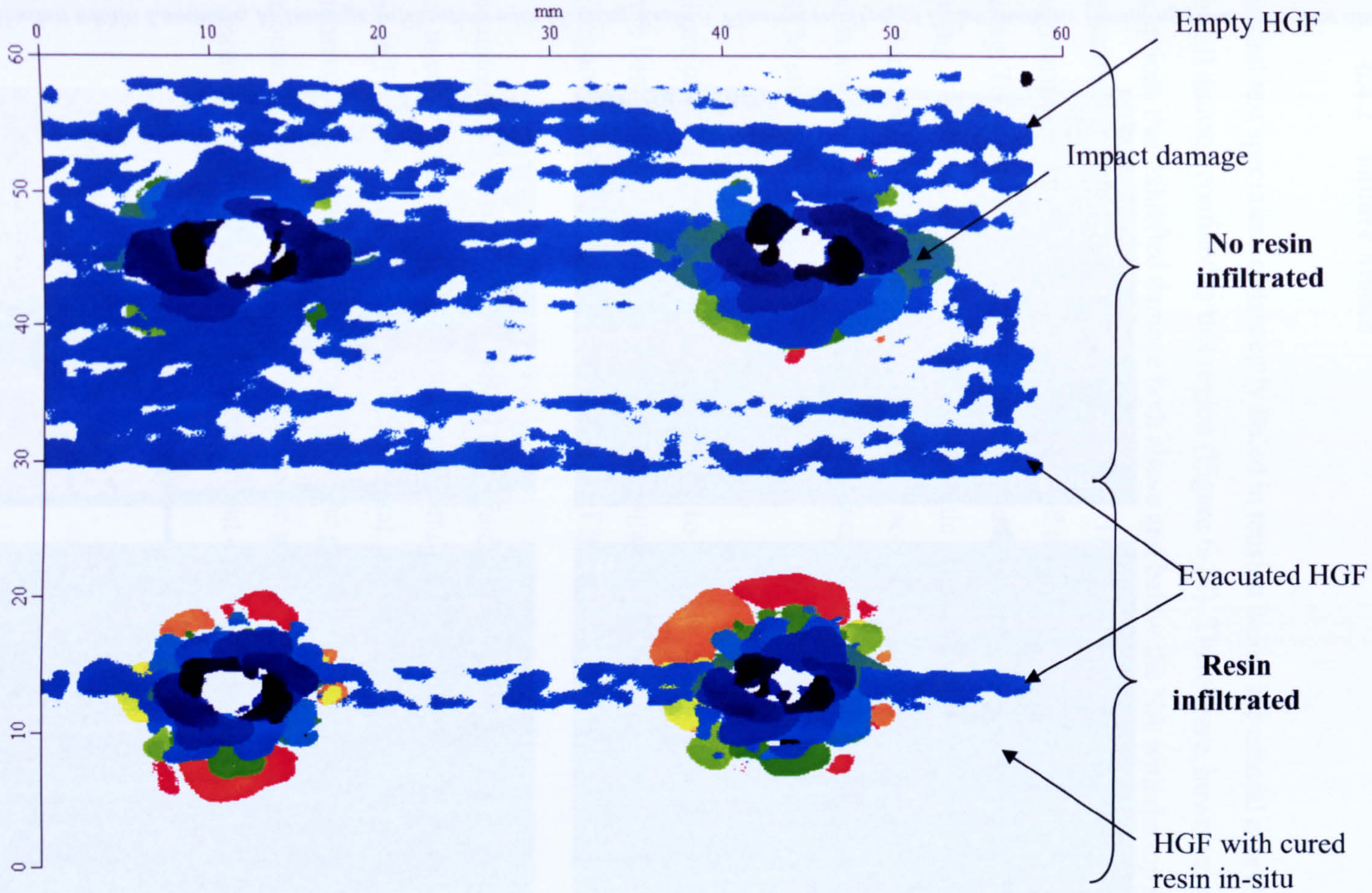

Figure 6-22: ***Ultrasonic Time of Flight Scan of Four Indentation Sites for UV Visualisation***

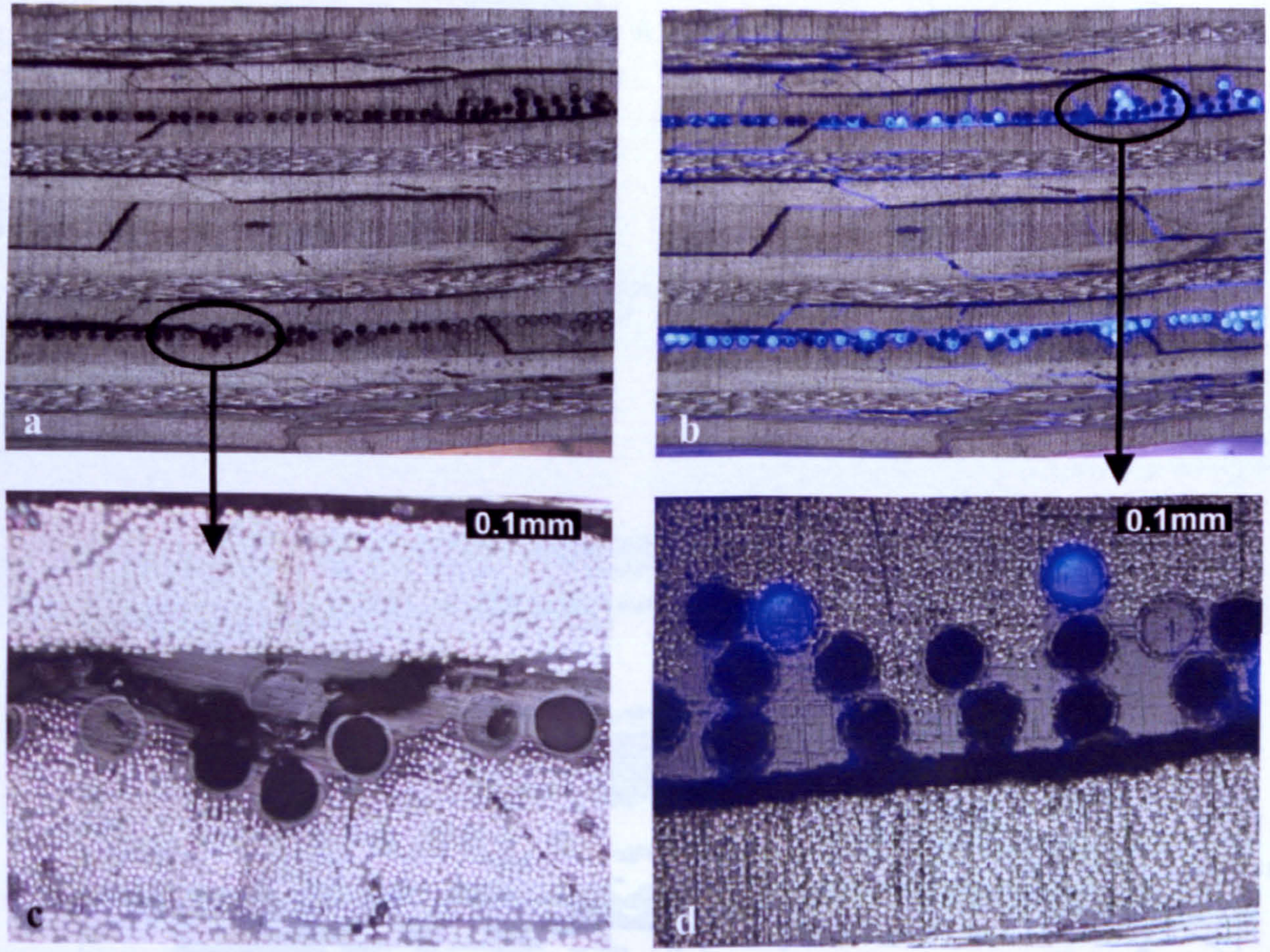

Figure 6-23: ***a) Damage Distribution within Laminate, b) Damage Infiltration with Healing Resin + Fluorescent Dye, c) Delaminations Deviating from Interface and d) Propagating along Interface Initiating HGF Fracture***

6.4.2 Failure Modes

Flexural test specimens consistently failed in tension below the neutral axis (NA) and with all damage confined to this region (Figure 6-24). There were, however, some exceptions that exhibited damage both above and below the NA with the top surface appearing to be more damaged (Figure 6-25). This variation was attributed to irregularities in the specimen manufacture and test fixture misalignment during testing. This suggested that the compressive and tensile strength under flexural loading were sufficiently close that these subtle variations could result in an alteration in failure mode. On all occasions, failure did not occur adjacent to the roller contact points and therefore the failure mechanisms were deemed valid in accordance with the ASTM standard.

Failure of specimens which had been subject to damage was initiated by fibre fracture at the back face in conjunction with the propagation of impact induced delaminations throughout the laminate thickness, as seen in Figure 6-24.

Undamaged specimens were observed to initiate failure by fibre fracture at the back face in conjunction with the propagation of bending induced delaminations that can be seen in Figure 6-26 and Figure 6-27. In general, the final damage state was more extensive at the back face in comparison to the pre-damaged specimens. This was attributed to the higher failure load (and hence greater stored elastic energy) exhibited by undamaged samples leading to a more rapid dissipation of energy.

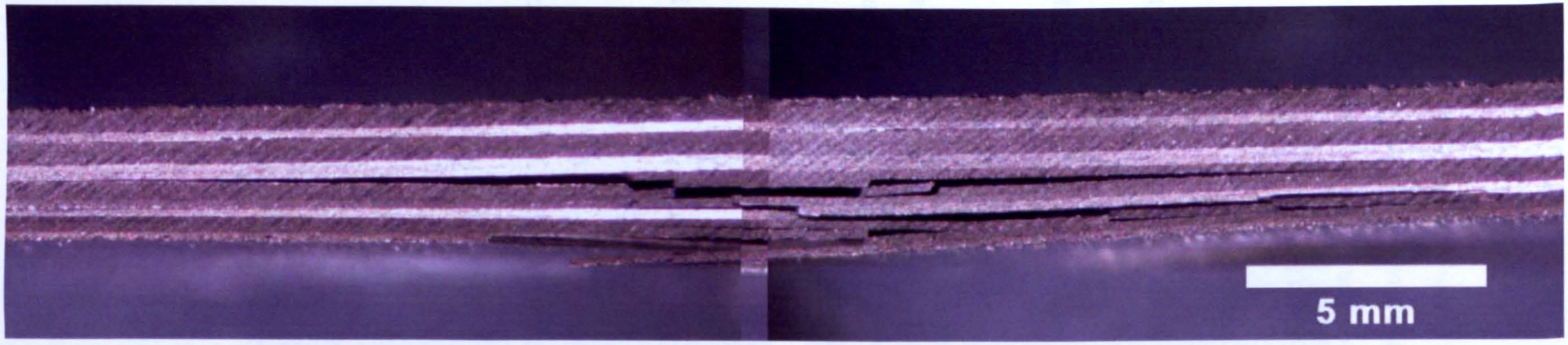

Figure 6-24: ***Optical Micrograph of Flexural Sample Failed below NA (L_{210} Damaged)***

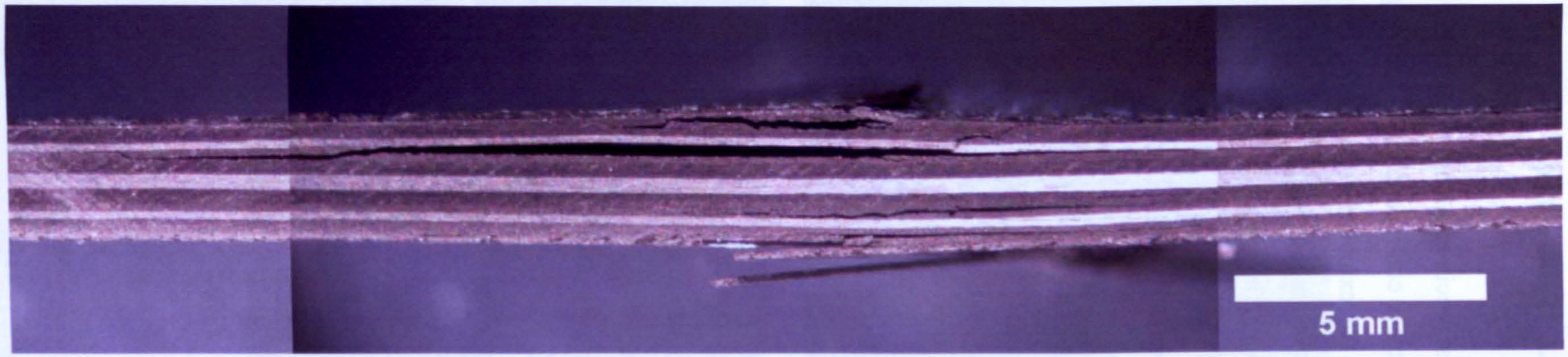

Figure 6-25: ***Optical Micrograph of Flexural Sample Failed above NA (Plain Damaged)***

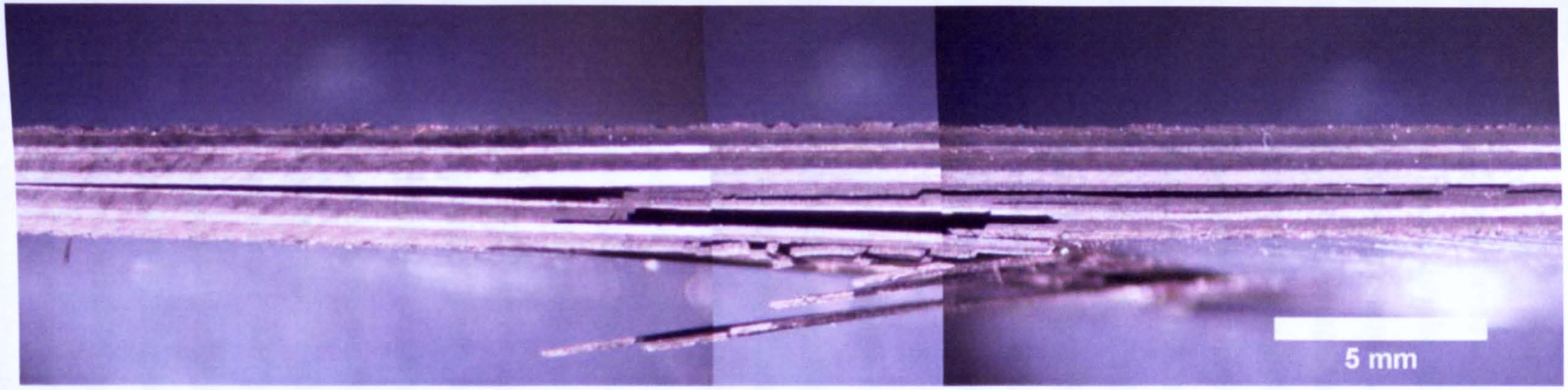

Figure 6-26: ***Optical Micrograph of Flexural Sample Failed below NA (L_{210} Undamaged)***

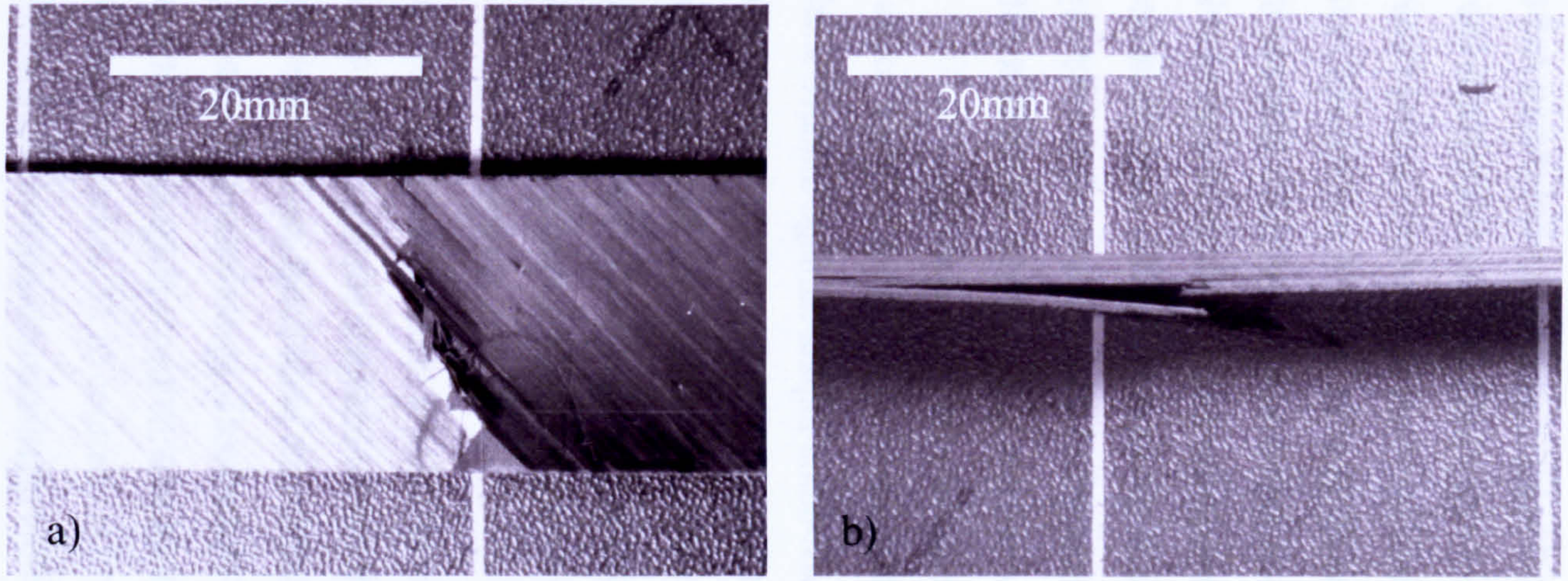

Figure 6-27: ***Optical Macrograph of Failed Flexural Sample a) Back Face and b) Side Views (Plain Undamaged)***

6.5 Discussion

6.5.1 Overview

Both HGF spacings investigated (70μm and 210μm) showed similar trends, experiencing an initial reduction in flexural strength in the undamaged state compared to an unmodified plain baseline. This can be attributed to three effects; disruption of the reinforcing fibre architecture, generation of resin rich regions (crack nucleation/propagation sites) and displacement of reinforcing fibres with non structural HGF (localised reduction in carbon fibre volume fraction). Damage events were seen to cause a reduction in strength due to the generation of shear cracks and delaminations which then propagated under load leading to premature failure. Finally, a strength recovery was experienced after fracture of resin filled HGF where this healing agent was able to infiltrate damage sites and mitigate some detrimental effects of the damage.

The quasi-static impact damage induced shear cracks and delaminations into the laminate which was analogous to BVID from an equivalent drop weight impact event. However, due to the small size indentor and support conditions for the specimens, a more concentrated load occurred in the central section where the sample was unable to deflect and so the applied force induced penetration beyond a load of 2000N.

It was seen that the intermediate yield point at 1700N had a varied effect on the flexural strength for the laminate configurations: 1% reduction for the L_{70} configuration, 8% reduction for the plain configuration and 14% reduction for the L_{210} configuration (Figure 6-18). This effect suggests that the L_{70} configuration exhibits a degree of damage tolerance at this load and the L_{210} configuration behaves worse than that of the baseline laminate.

The 2000N quasi-static indent load caused a more significant effect on the flexural strength: 17% reduction for L_{70}, 31% reduction for baseline and 30% reduction for L_{210} configurations. This again identified the inherent damage tolerance of the L_{70} configuration. Also a degree of damage tolerance is exhibited for the L_{210} configuration at this load in comparison to the baseline laminate especially considering the relative reduction in flexural strength from those achieved after the 1700N QS impact load level.

An increase to 2000N caused a reduction in flexural strength of 25% for the baseline and only 18% reduction for the L_{210}.

These peculiarities observed across the different configurations in response to different QS impact loads suggests that the HGF clumping present in the L_{70} configuration may have increased the damage tolerance of the laminates, particularly at low impact loads. Therefore some impact energy was absorbed/dissipated through HGF fracture at lower energies and the transmission of this load was improved by the occurrence of HGF clumping. At higher loading levels, the absorption of indentation force by HGF becomes saturated at which point the load continues to damage the laminate. In general it appears that HGF clumping may reduce the impact load required for HGF fracture whether this is due to improved transmission of the load through HGF to HGF contact or due to the reduction in carbon fibre volume fraction immediately surrounding the HGF (resin rich regions) reducing the protection offered by the reinforcing fibre.

The maximum flexural strength recovery was for the L_{70} configuration which achieved 97% of its undamaged state: a recovery of 14% after a 2000N quasi-static impact. The L_{210} configuration also exhibited flexural strength recovery achieving 82% of its undamaged state after a 2000N QS impact which was a recovery of 12%. Therefore it can be suggested that the initial reduction in undamaged strength of the laminates due to the presence of HGF can be tolerated when consideration is given to the strength recovery due to self-healing and the damage tolerance exhibited by the laminates with HGF.

The incorporation of HGF within a CFRP laminate has been shown to produce minimal degradation in flexural strength and ply disruption. At fibre spacings of over three HGF diameters (210μm) very good embedment of the HGF was achieved. This is particularly notable as some authors [178, 179, 180] reported that the most sensitive interface to embedded objects as the 0°/±45° interface (Chapter 4, section 3). In contrast, at low fibre spacings (70μm) a small degradation (8%) in flexural strength was experienced. This was compounded by manufacturing issues and the low tack of the pre-preg system which combined to create HGF clumping.

Although the 210μm HGF spacing configuration produced an absolute flexural strength recovery of 12% (similar to the 14% recovery produced by the 70μm configuration), the

relative performance of the laminates after healing compared to the undamaged strength is the most useful indication from the perspective of structural design. This is because laminates using embedded HGF will commonly be assessed using a measure of performance before and after impact damage. Therefore, if the objective is to recover after impact damage as close to 100% of the laminate performance beforehand any increase in damage tolerance should also be considered as significant.

Intra-ply shear cracks and delaminations during an impact event cause HGF fracture and the release of healing resin into the interconnected damage sites. The presence of uniformly distributed HGF at a ply interface does not appear to cause obvious crack path deviation, suggesting that they do not act as sites of weakness under these loading conditions. However, small clusters of HGF combined with accompanying resin rich regions do appear to cause significant disruption resulting in crack path deviation.

It is not yet clear under precisely what conditions the healing resin will infiltrate damage. It is evident that a small displacement between damaged surfaces provides increased capillary action, however it is not conclusive whether damaged surfaces separated by more than 30μm are conducive to resin infiltration. It is also not evident whether the damage must be fully infiltrated by the resin for healing to be effective. It may be sufficient for the resin to simply blunt the crack tip to prevent further damage propagation under load.

It is worth noting that this demonstration of healing under flexural loading after impact has used a far from optimised healing resin system. The use of a premixed resin/hardener and raised temperature, were chosen to eliminate the problems of stoichiometric mix sensitivity and resin viscosity on damage infiltration.

6.5.2 Wider Significance

The results reported in this chapter have shown that for these damage conditions, loading conditions and sample sizes the placement of the HGF has performed well, producing almost 100% healing and minimal disruption to the laminate microstructure. This has extended previous work reported by Pang et al [141,142] and Trask et al [147] who also considered the use of HGF for self-healing in FRP's. It has been shown that HGF can be integrated as discrete units instead of continuous plies in order to minimise the disruption

to the host laminate and maintain its mechanical performance. This has significance as the material used as the host laminate was CFRP as opposed to GFRP reported in previous work [141,142,147]. This material is more widely used for structural applications due to its higher specific strength and stiffness, therefore it was essential to demonstrate that HGF could be integrated without significant degradation to these properties.

The work reported in this chapter has demonstrated similar healing efficiencies to those reported by Pang et al [141,142] and Trask et al [147] using a HGF based approach and also Kessler et al [148,149] and Yin et al [151,152] using a microcapsule based approach. However the microcapsule based approaches were restricted to woven glass laminates due to the need to incorporate the microcapsules into the matrix resin used during RTM manufacture. The use of embedded HGF is suitable for both RTM and pre-preg based systems, though the integration of unidirectional HGF into woven laminates has not yet been considered. In addition the microcapsule based systems have not been shown to address impact induced damage that is a damage mechanism of particular concern for composite materials. This reinforces the benefits of using a HGF system for self-healing of impact induced damage as they can provide sufficient volume of storage for healing resin. Microcapsules are unable to provide a total storage volume suitable to address impact damage without causing unacceptable disruption to the host laminate. Moreover, the volume supplied per unit fracture is significantly greater for HGF than for microcapsules. This reduces the reliance on damage intercepting a sufficient number of storage units and initiating fracture in order to provide healing.

The combination of quasi-static indentation and flexural four point bend testing were recognised as a somewhat contrived situation for developing a self-healing composite material. Therefore, it was decided that following this study, compression after impact should be used for subsequent investigations along with low velocity drop weight impact (Stage 2 and Stage 3). It was expected that the 210μm HGF spacing configuration would be unable to provide sufficient healing capability for the anticipated increase in specimen/damage size. Therefore two additional configurations were considered:

1. 140μm@2 interfaces: Intermediate HGF spacing to provide increased resin volume whilst maintaining adequate HGF embedment
2. 210μm@4 interfaces: High HGF spacing maintains HGF embedment and the increased number of interfaces provides an increased resin volume

7. Compression After Impact Assessment: Effect of HGF Content

Compression after impact (CAI) provides a rigorous assessment of material performance following a low velocity impact damage event. The material compressive strength is extremely sensitive to internal damage and is expected to provide a critical assessment of self-healing efficiency. The larger specimen size typically necessary for this test method enables drop weight impact to be used as the damage initiator. CAI represents an industry standard used for assessing the affects of low velocity impact damage typically found in an operational environment. Therefore, it was necessary to review the open literature to better understand the options available for CAI testing.

Although CAI is a key methodology to assess the damage tolerance of composite materials, this form of testing is very complex as it must provide boundary conditions for the given specimen which prevent global buckling and allow assessment of the local instabilities produced by the impact induced damage. A range of test methods have been described and used in the literature (Table 7-1).

CAI method	Specimen Dimensions (mm) (thickness x length x width)	Specimen lay-up
NASA: [184]	6.35 x 254-317 x 178	(45,0,-45,90)
Boeing: [185]	4-5 x 152 x 102	(-45,0,45,90)
Airbus industries [186]	4 x 150 x 100	(45,0,-45,90)
ASTM: [187]	5 x 150 x 100	(45,0,-45,90)
JIS: [188]	5 x 150 x 100	(45,0,-45,90)
JIS Small Coupon: [188]	2.5 x 80 x 50	(45,0,-45,90)
SACMA: [189]	5 x 150 x 100	(45,0,-45,90)
CRAG: [190]	3 x 180 x 50	(45,-45,0,90)
Prichard and Hogg: [191]	2 x 89 x 45	$(-45,0,45,90)_{2S}$

Table 7-1: ***Commonly used CAI Test Methods in Industry***

The most commonly used method to date has been the Boeing standard [185], which shares similar characteristics to the ASTM [187], Airbus [186] and Japanese Industrial Standards [188]. However, all these methods specify large sample dimensions which require a large amount of material, specimen preparation and testing capacity. The Japanese International standard [188] is very similar to the Boeing standard [185] but also includes a provisional guide standard for a reduced sample size, similar in thickness to CRAG [190] and Prichard Hogg [191] methods. Problems exist with the validity of all CAI test methods as to precisely what the

results mean in terms of design. Also, comparisons between results from different test methods will not be directly comparable due to dimensional effects during impact and compression testing [191].

Prichard and Hogg [191] considered a CAI test method suitable for 16ply quasi-isotropic (QI) laminates, similar in design but not dimensions to the Boeing standard [185]. Here it was considered that CAI should be conducted over a range of impact energies, and not just at one level as described by many of the test standards. However, it is recognised that this would be impractical and expensive. It was also recognised that CAI testing does not assess a unique property of the composite, but is merely a complex and expensive indication of the extent of damage introduced during the impact test. Therefore, it is suggested that it may be more advantageous to base materials development on an assessment of the initial damage state after impact. However, the acceptance of the Boeing test method [185] as an ASTM standard [187] reaffirms the general consensus that there is a need for CAI testing in the design and use of advanced engineering composites.

The results from the testing conducted by Prichard and Hogg [191] showed a clear correlation between impact damage width and CAI strength. It also identified that Mode I fracture toughness has no bearing on the residual compression strength, rather it was a material's resistance to initiation and propagation of impact damage that produces superior residual compressive strength.

Dorey et al [192,193] and Curtis [194] found that impact energies causing a decrease of 60% in compression strength had no effect on the tensile strength. Conversely, at higher energy impacts the occurrence of broken 0° fibres, in addition to delaminations, caused a 25% reduction in tensile strength with no further losses in compression strength. This highlights that delaminations caused by low energy impact events are detrimental under compressive loads due to local buckling instabilities. It was also identified that the main load bearing fibres for longitudinal loading (0°) can support compressive loading after fibre failure but cannot support tensile forces. These findings reaffirm the need to use CAI testing in order to assess the detrimental

effects that low velocity, low energy impact energies have on the mechanical performance of composite materials.

Guild et al [195] considered a finite element model in order to assess post-impact performance of composites without invoking fracture mechanics. Their findings maintained compatibility with experimental results indicating comparable performance from laminates with different G_{IC} and G_{IIC} values (strain energy release rate). It was concluded that there is no correlation between interlaminar Mode I fracture toughness and compression after impact performance. Furthermore, interlaminar Mode II fracture toughness was found to affect the CAI performance by influencing the resistance to impact.

Habib [196] considered the construction of a test rig for BAE systems in order to produce CAI results that were more representative of a real structure, and with more flexibility in sample thickness than the standard Boeing [185] CAI test method. The use of this test rig provided an opportunity to compare the performance of 4, 6 and 8mm thickness plates in the same testing rig. The authors also observed that the damage area of a laminate increases with impact energy until it reaches a certain energy level, at which it plateaus.

Hosur et al [197] further developed the findings of Habib [196], relating residual CAI strength and impact energy for T300/C914 QI laminates. The authors identified three distinct phases that occurred with respect to the residual strength and failure strain as the impact energy was increased (see Figure 7-1a):

1. Impact energy entirely absorbed by elastic deformation of laminate with minimal delamination
2. Residual strength and failure strains decrease rapidly with increase in impact energy due to large increase in delamination damage
3. Marginal decrease in strength and failure strains with increase in impact energy, due to highly localised damage and negligible delamination growth

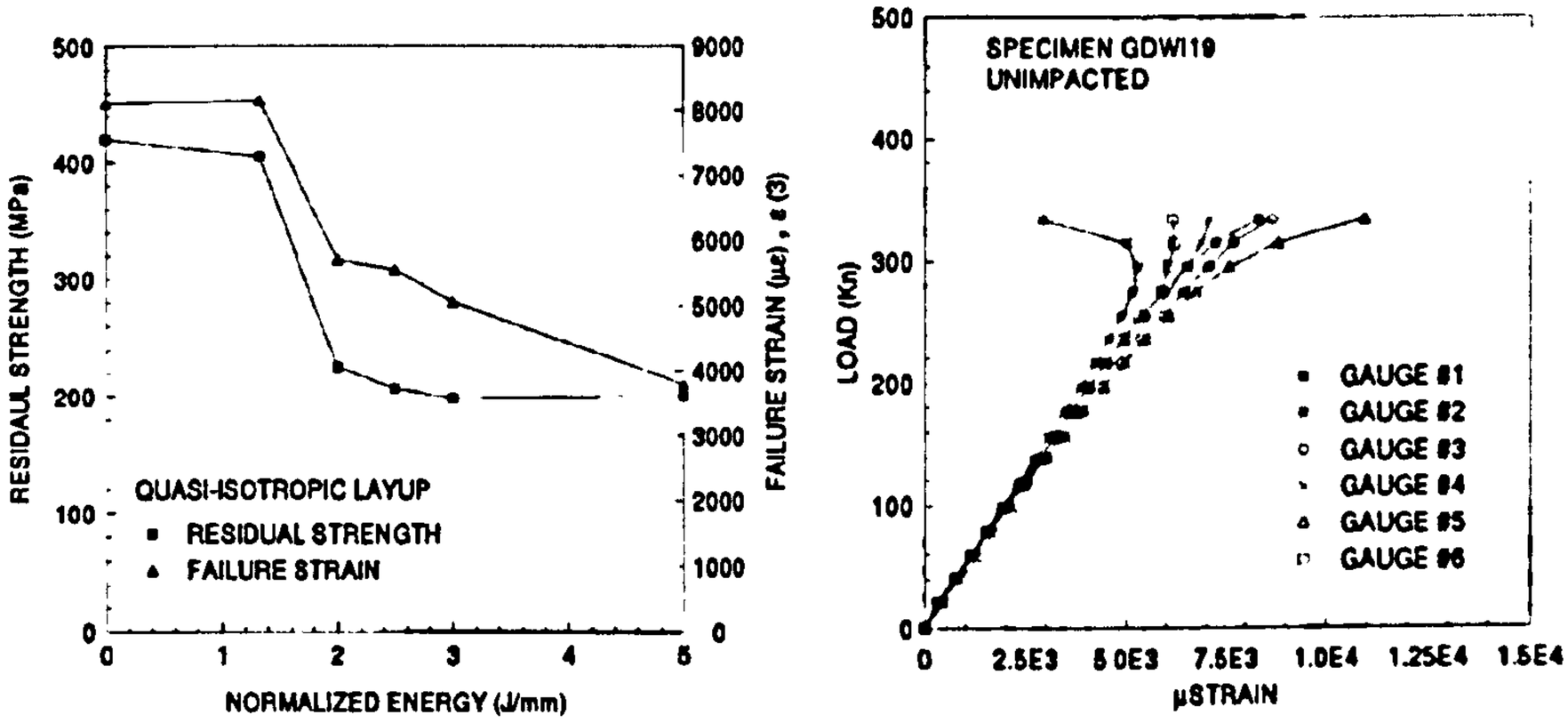

Figure 7-1: ***a) Variation of Residual Strength and Failure Strain with Normalised Impact Energy[197] b) Variation of Specimen Strain with Compressive Load showing Failure due to Bending***

Figure 7-1b) shows a typical strain output from strain gauges located on the front and back faces of specimens during CAI testing. It shows failure of the sample due to buckling as the faces of the laminate deviate.

Hawyes et al [198] considered the validity of the 'open hole' analytical method when compared with experimental results. The 'open hole method' or cohesive zone model applied by Soutis et al [199] considers representing impact damage as an open hole of representative dimensions in order to predict the CAI strength of the laminate. Hawyes [198] used the CRAG method [190] to assess the CAI performance of TMA/924 and IMS/M21 CFRP and compared the results with the theoretical values produced using the open hole method, with good agreement. The authors also found that for 16 ply laminates a 28J impact was too damaging and 3.5J was insufficient resulting in ~7J impact energy being most suitable for CAI testing. It was found that failure modes in compression testing (no damage) were micro-buckling of 0° fibres rather than fibre shear failure, and tended to initiate at free edges where the fibres were unsupported or at material imperfections such as resin rich regions, voids or fibre waviness. This reaffirms the sensitivity of compression performance of laminates to embedded defects.

De Freitas et al [200] used the Airbus CAI standard [186] for 4 different 24ply lay-ups of IM7/977-2 (3.24mm) and T800/5245C (4.56) carbon fibre/epoxy laminates. It

was concluded that the delamination area was a function of absorbed energy and relatively independent of stacking sequence, although it was highly dependant on the number of interfaces within the laminate. An increased number of interfaces reduced the delamination area as compliance between plies is improved. When plies of the same direction are grouped, a larger stiffness mismatch occurred between the blocked plies resulting in a tendency to delaminate.

Cartie and Irving [201] used the Boeing CAI test standard [185] for a comparative study between six carbon fibre/epoxy laminates and found that the resin toughness rather than the fibre's strength or stiffness was the dominating parameter affecting CAI performance for QI CFRP laminates. Furthermore, the increases in delamination area for different laminates were a result of increased damage initiation load (P_C) due to an increased G_{IIC} rather than an increased resistance to delamination.

A number of authors [191, 203-205] have considered the use of CAI testing for small coupon sizes. Generally, measures need to be taken in order to prevent global buckling with the use of anti-buckling guides (Figure 7-2). These guides are stiff metal plates positioned to prevent global instabilities, but have an open region over the damage area so as not to inhibit the local instabilities and delamination growth. CRAG [190] and JIS [188] provide provisions for small coupon testing of 3mm and 2.5mm laminate thickness respectively, although they do not include anti-buckling guides beyond the edge support, as featured in the test standards for larger coupons. Pritchard and Hogg [191] also developed a test method for small sized coupons (3mm) without anti-buckling guides, with notable success.

Sanches-Saez et al [203] developed an anti-buckling guide to allow CAI testing of 2.2mm and 1.6mm laminates (12ply and 6ply respectively) carbon fibre/epoxy. This comprised two C-shaped adjustable plates to support the front face and two fixed plates that were welded to the loading plates. Testing was successfully conducted with specimen failure occurring in the damage zone by local sub-laminate buckling (Figure 7-2c).

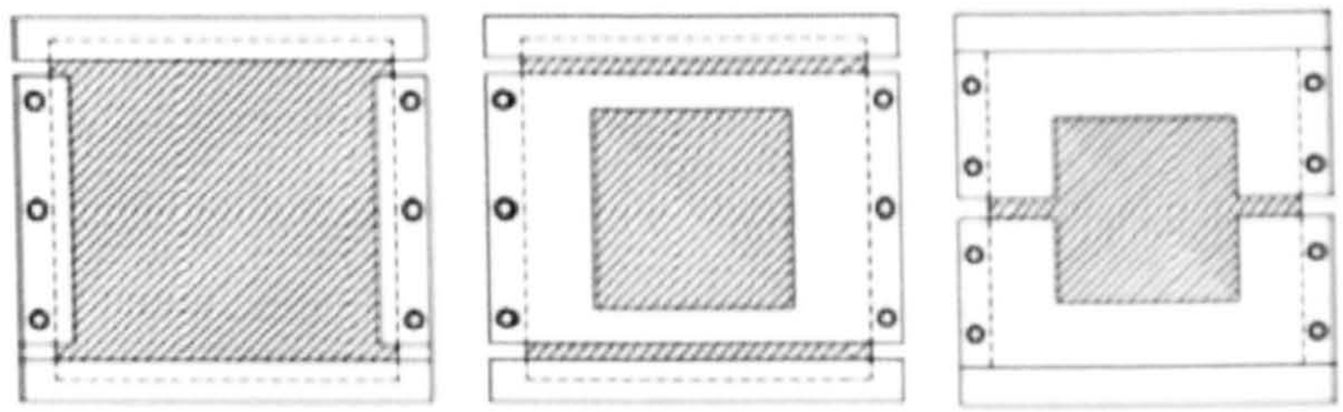

Figure 7-2: ***CAI Anti-buckling Guides Typical of a) ASTM Approach [184-191] b), c) Approaches taken to Ensure Local Instabilities Determine Failure under Compressive loads for Thinner Laminates [203-205]***

Liu et al [204] used the NASA [184] standard for thin laminates and for laminates with varying degrees of damage, with slightly reduced coupon width (175mm to 125mm). It was found that for laminates with little or no impact damage, samples failed due to crushing of the laminate at the top or bottom clamping ends. To avoid this, end tabs were bonded to the specimens. However, for thin laminates these end tabs were extremely long and extended to the damaged region. It was concluded that the NASA method was not suitable for thin laminates of 2.24mm. However, Sanches-Saez explains how the use of end tabs is not generally desirable as they require narrow grips, which may be different to those used for tensile testing and their use makes alignment of the specimen more complex.

Duarte et al [205] tested 16ply QI T300/914C and interleaved carbon fibre/epoxy specimens with a customised CAI test rig. This comprised front and back face plates that covered the entirety of the sample except a circular region over the impact damage and at the loading ends to allow for shortening of the sample during testing. Samples were manufactured to the SACMA standard [189] but with slightly reduced dimensions of 90x115mm and a damage window of 80x90mm. Specimens were impacted at incident energies up to 7J.

This brief review of CAI testing has outlined the current methods employed for CAI testing. The most commonly used methods such as ASTM [187], Boeing [185] etc are costly and time consuming due to their required specimen dimension and thicknesses. It has also been shown [191] that these methods are not suitable for laminates thinner than those specified within the respective standard. Therefore, many authors have

developed or customised methods to allow CAI testing of smaller and thinner specimens. In particular, it was evident that the test method proposed by Prichard and Hogg [191] could be implemented by customising an ASTM standard rig. This method achieved CAI testing without the requirement for extensive anti-buckling guides beyond those already required for the ASTM standard.

It was concluded that this method was most suitable for the purpose of this study. Therefore, an in-house ASTM standard rig was customised (Figure 7-3, Figure 7-4 more detailed drawings can be found in Appendix A). This allowed for smaller coupon sizes and thinner laminates than specified in the standards, which allowed some carry forward of similar laminate specifications used previously in the four point bend flexural strength studies (Chapter 6).

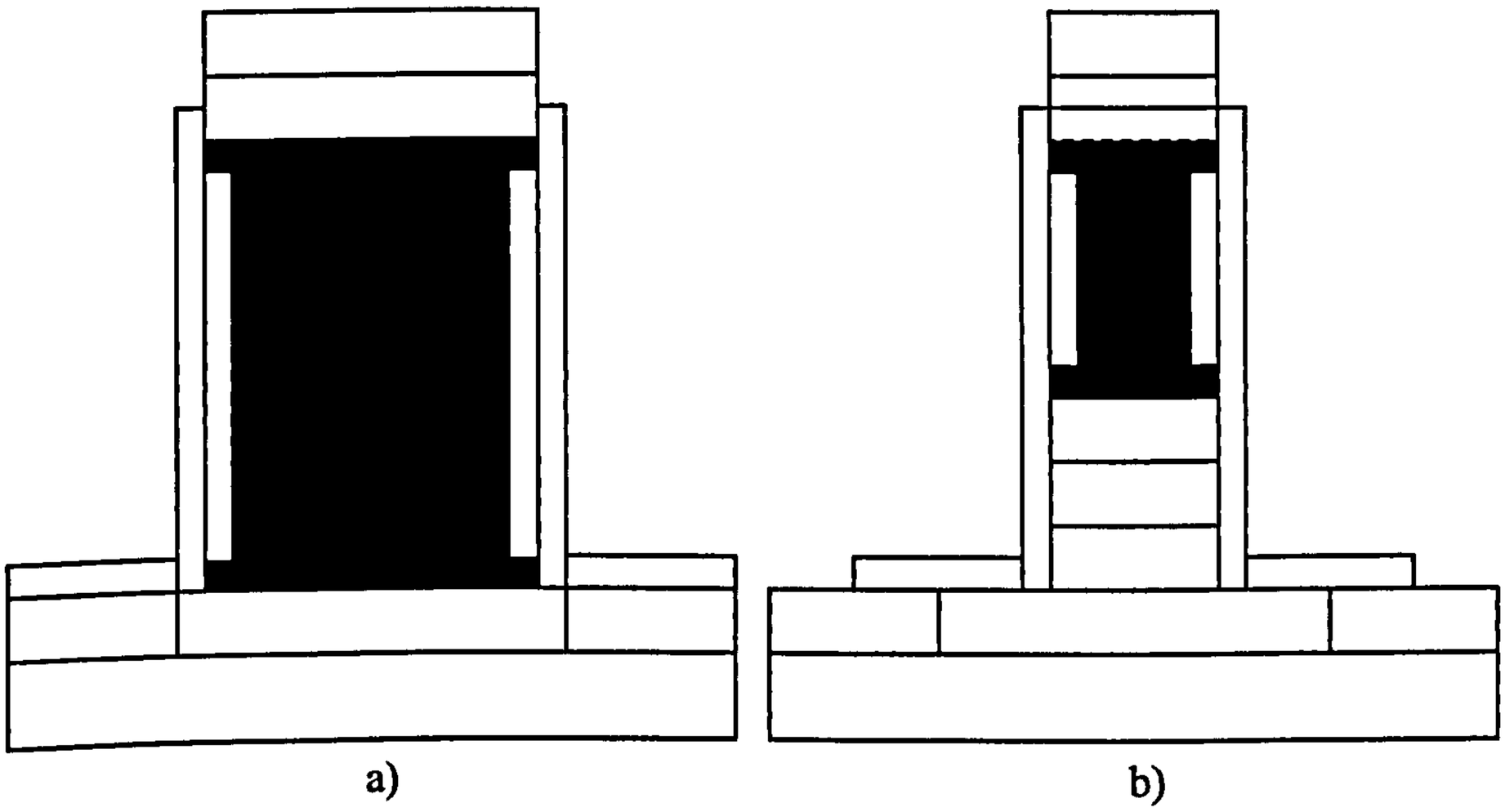

Figure 7-3: ***Comparison of a) Boeing/ASTM Standard Rig [185,187] and b) Modified Rig in Accordance with Prichard and Hogg [191] (Appendix A_2 , A_3)***

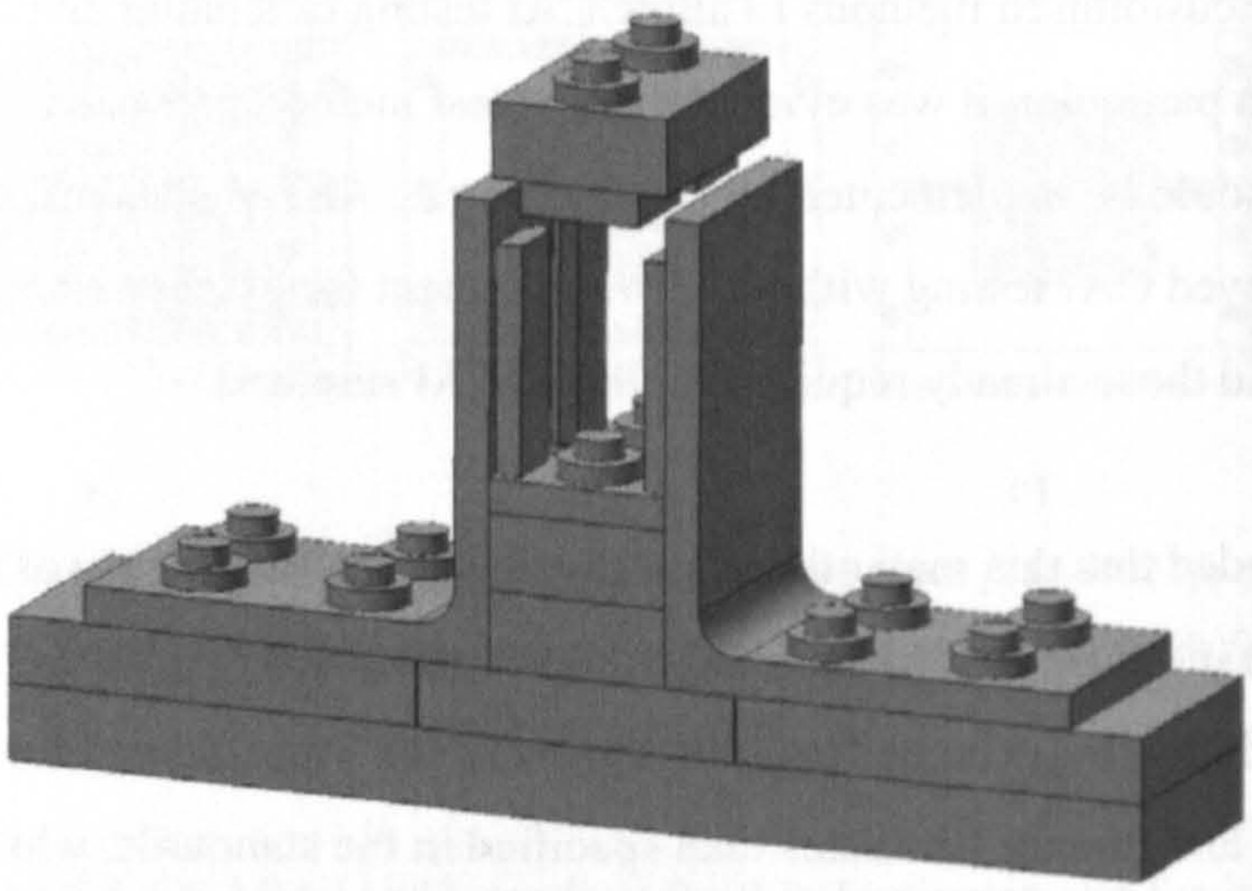

Figure 7-4: ***Modified ASTM CAI Standard Testing Rig [191]***

A quick analytical comparison was made between the ASTM and Prichard & Hogg methods to further justify the decision to choose the latter. Roark [206] was consulted to provide a comparative estimation of the buckling load under compression for the proposed sample dimensions using Eqn. 7-1.

$$\sigma = K\frac{E}{1-\nu^2}\left(\frac{t}{b}\right)^2 \qquad \textbf{Eqn 7-1}$$

This was used as an indicator of the suitability of each method for the required laminate thickness. The boundary conditions (Figure 7-5a) were assumed to be clamped along edges *a,* and simply supported along edges *b*. The sample size for the two methods was clear, however, the boundary conditions also produced an effective window which could also be used for the calculations from Roark (Figure 7-5). Therefore, both total and effective dimensions were used and the results are displayed in Table 7-2. Using the effective dimensions an indication of the subtle differences in boundary conditions between the two methods is considered.

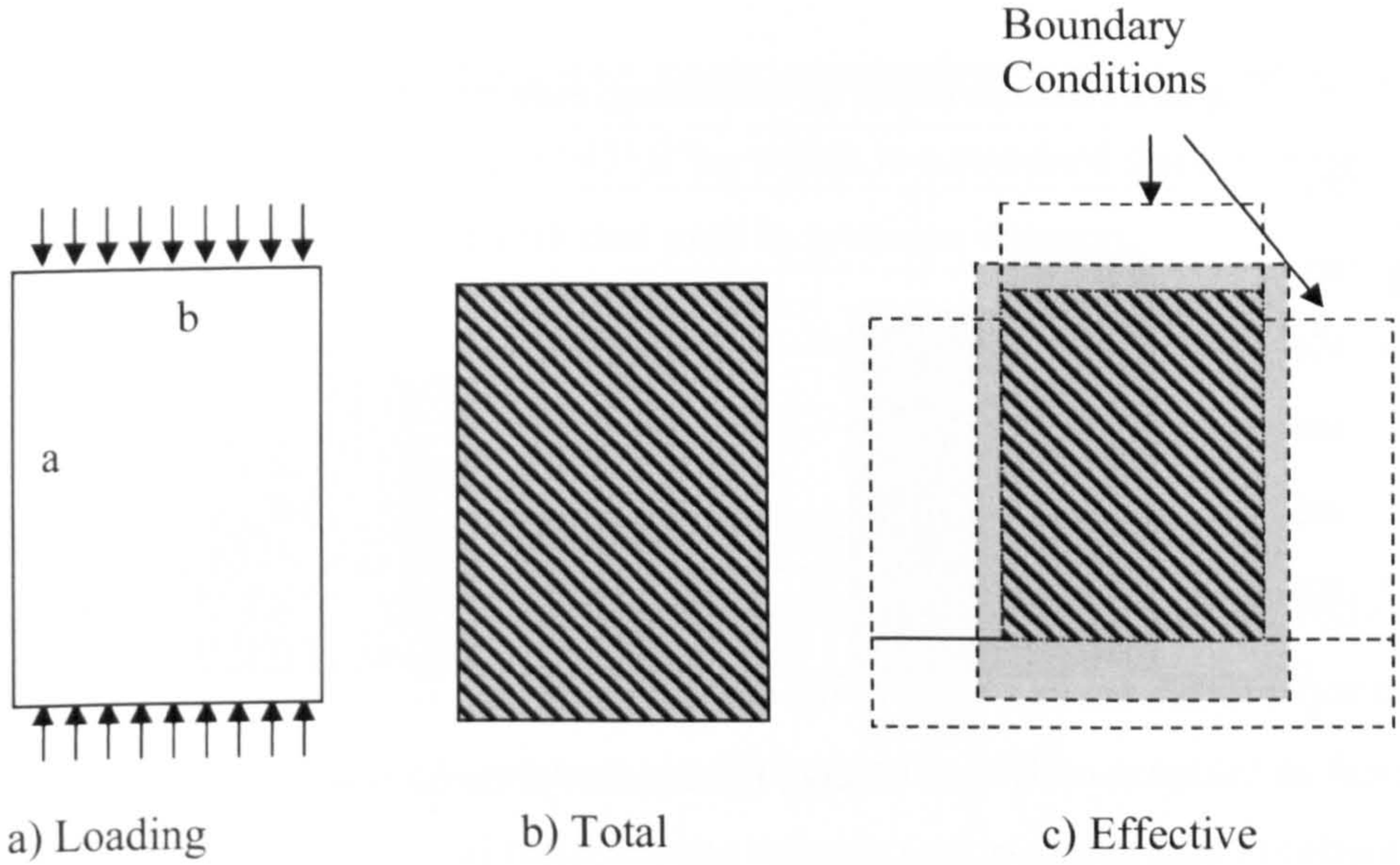

Figure 7-5: ***Schematic Showing a) Total and b) Effective Sample Dimensions***

Standard	No. plies	Dimensions a/b/t (mm)		a/b	K	Compression Strength (MPa)
		Effective (window)	Total (sample)			
ASTM [187]	40	134x84x5		1.595	4.390	1025.5
	16	134x84x2.5		1.595	4.390	256.4
	40		150x100x5	1.500	4.435	731.0
	16		150x100x2.5	1.500	4.435	182.8
Prichard & Hogg [191]	16	66x45x.5		1.467	4.449	905.3
	16		89x55x2.5	1.618	4.390	598.0

Table 7-2: ***Estimation of Compressive Failure Strength for Samples using ASTM [187] and Prichard/Hogg [191] CAI Testing Rigs (using formulae outlined in ROARK [206])***

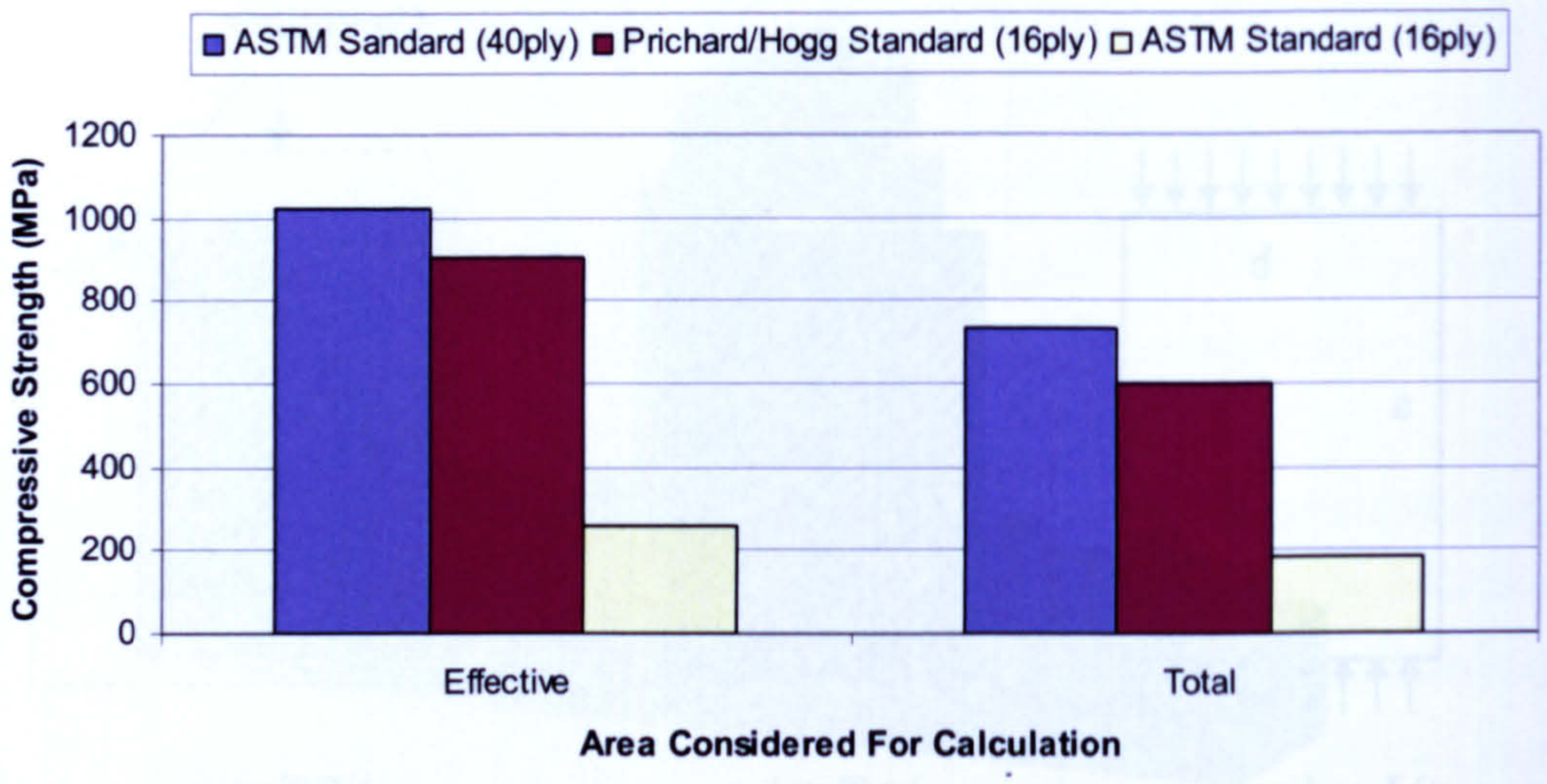

Figure 7-6: ***Estimation of Compressive Failure Strength for Samples using ASTM and Prichard/Hogg CAI Testing Rigs (using formulae outlined in ROARK [206])***

Although quantification of a true compression failure is difficult, it is evident that the ultimate goal was to detect the failure stress of the material irrespective of sample size. Therefore, the goal of the Prichard & Hogg [191] method was to achieve a failure stress approaching that expected from the ASTM standard. It can be seen in Table 7-2 and Figure 7-6 that when data for the modified CAI rig was used with the smaller sample sizes, the calculated failure stress approached those values expected using larger samples in the ASTM standard. It can be seen that this occurred particularly when the effective area calculations were used. It also demonstrated that the ASTM standard was not suitable for thin laminates (i.e. ≤16ply) as an extremely low failure stress would be expected (Figure 7-6). A useful modification for the purposes of this work was the adjustable boundary conditions on all four sides of the sample. This ensured the prerequisite conditions were achieved (clamped top and bottom, simply supported on the sides) and also accommodated variations in laminate thickness as it was found in Chapter 6 that specimen thicknesses experienced slight variation due to the addition of HGF.

7.1 Design

The laminate material used was T300 carbon fibre pre-impregnated with 914 epoxy resin (Hexcel Composites [1]). The manufacturer's cure schedule was 1 hour at 175°C

at 700kN/m^2 (7 bar) pressure followed by a post-cure dwell of 4 hours at 190°C. The laminate lay-up chosen was $(-45°,90°,45°,0°)_{2S}$ which is a standard quasi-isotropic configuration and was consistent with that used in previous chapters.

7.1.1 Configuration

To ensure commonality with the testing undertaken in Chapter 6, tests were conducted to explore similar HGF configurations. However, an intermediate HGF spacing of 140µm (i.e. 2x HGF OD spacing) was investigated as the 210µm spacing alone was deemed inadequate to produce significant healing when assessed in flexural testing. Also, to improve the total resin storage volume and to exploit the excellent embedment of HGF, the 210µm spacing was also included at four interfaces (x_1-x_4) from those identified in the standard lay-up:

$$(-45°/90°/45°/\mathbf{X_5}/0°/\mathbf{X_1}/-45°/90°/45°/\mathbf{X_3}/0°/0°/\mathbf{X_4}/45°/90°/-45°/\mathbf{X_2}/0°/\mathbf{X_6}/45°/90°/-45°)$$

Details of the Configuration assessment tool reported in this section can be found in Chapter 5, section 2.1, the results of which are presented in Figure 7-2. It can be seen from Table 7-3 that the decrease in HGF pitch spacing is proportional to the increase in storage volume and reduction in E_x. It can also be seen that the addition of 210µm spaced HGF at four 0°/±45° interfaces provides a significant increase in storage volume compared to two interfaces but with less anticipated disruption to the laminate as found for lower HGF pitch spacings. It was expected that the 210µm HGF spacing would again result in the smallest reduction in mechanical properties (3% E_x) and that the 70µm HGF spacing configuration would provide the largest volume of resin (131.3mm^3). However, it can be seen that the two additional configurations provided additional benefits. The 140µm HGF spacing configuration was an intermediate step between the extremes of 70-210µm and therefore resulted in an intermediate reduction in mechanical properties and stored resin volume (5% E_x and 98.61mm^3 respectively). Furthermore, the 210µm HGF spacing configuration provided the second largest stored resin volume (131.3mm^3) and although the estimated effect on E_x (7%) was greater than for the 140µm HGF configuration (5%) it must be considered that this estimation only accounts for substitution of load bearing carbon fibre by HGF and does not give an indication of the effectiveness of HGF

embedment. It was expected that the embedment of the 210mm HGF configuration would offer a significant improvement over the 140μm and 70μm. However, this larger spacing may result in limited HGF fracture during an impact event, a key factor in the self-healing approach.

HGF Spacing (µm)	No. Interfaces	CF reduction in 0° (%)	Global CF reduction (%)	New V_{CF} (%)	Stiffness (%)			Healing Resin Vol (mm^3)	Healing Resin V_{FR}
					E_x	E_y	E_{xy}		
70	2	13	3	62	90	99	99	197.5	1.61
	3	19	5	61	85	99	99	296.2	2.42
	4	26	6	60	80	98	98	395.0	3.22
	5	32	8	59	75	98	98	494.0	4.03
	6	39	11	58	65	97	97	592.4	4.30
140	2	6	2	63	95	100	100	98.61	0.80
	3	10	2	62	93	99	99	148.0	1.20
	4	13	3	62	90	99	99	197.2	1.60
	5	16	4	61	88	99	99	246.5	2.01
	6	19	5	61	85	99	99	295.8	2.41
210	2	4	1	63	97	100	100	65.7	0.54
	3	6	2	63	95	99	99	98.5	0.80
	4	9	2	63	93	99	99	131.3	1.07
	5	11	3	62	92	99	99	164.1	1.34
	6	13	3	62	90	99	99	197.0	1.61

Table 7-3: ***Prediction of Laminate Properties for CAI Testing***

7.1.2 Volumetric Assessment

The image shown in Figure 7-7 was created using ultrasonic time of flight techniques in order to assess the damage inflicted by low velocity drop weight impact. This shows the associated delamination diameters that can be measured. Typical delamination diameters were found to be upper surface=22mm and lower surface=36mm for a 6J impact in T300/914 carbon fibre/epoxy. This data was used in derivations to populate Table 7-4 (see Chapter 5 Section 2.2). Details of the process used to select an impact energy level can be found in 7.2.3.

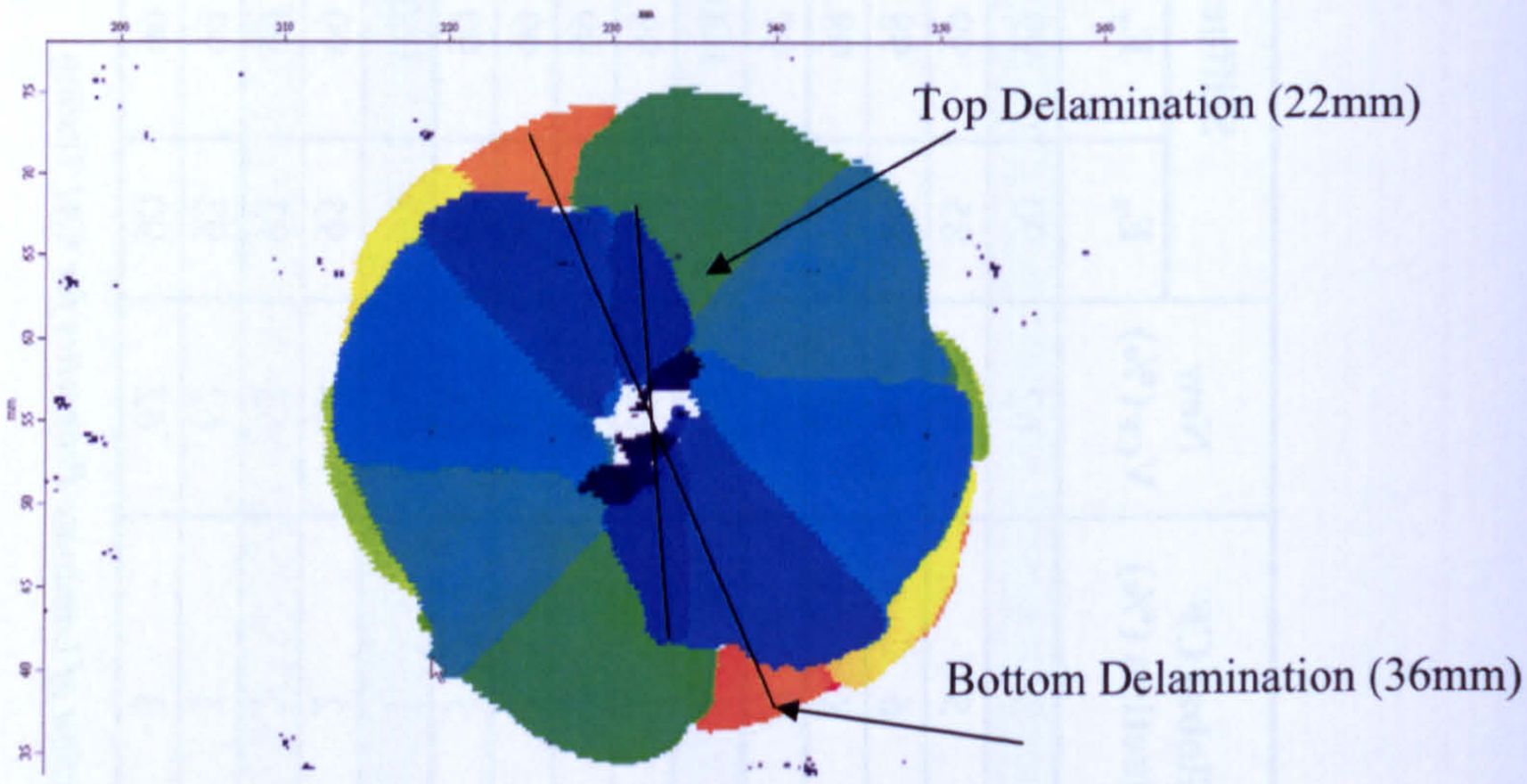

Figure 7-7: ***Ultrasonic TOF Image for 6J Impact of T300/914 CFRP***

HGF Spacing (μm)	No of Interfaces	HGF V_F (%)	HGF Fracture (F_n) / Damage Fill (V_n) (%)					
			F_1	V_1	F_2	V_2	F_3	V_3
70	2	3	46	48	46	17	23	12
140	2	2	46	24	46	8	23	6
210	2	1	46	17	46	6	23	4
210	4	2	45	33	45	11	23	8

Table 7-4: ***CAI_1 Sample Data for Drop Weight Impact (6J) T300/914, Damage Vol. 189.344mm^3***

Details of the *Volumetric Assessment* tool reported in this section can be found in Chapter 5, section 2.2, the results of which are presented in Figure 7-4. It can be seen from Table 7-4 that the 70μm and 210μm HGF spacing configurations were expected to contain the highest volume of healing resin. Referring to Table 7-3, it can be seen

that these configurations were predicted to cause a reduction in E_X of 10% and 7% respectively. Comparatively, it can be seen that initial estimations suggest that the 70μm configuration will be more effective in terms of healing resin supplied for a given level of damage. However, these predictions do not account for instances of manufacturing defects such as HGF clumping and resin rich regions which were found to be widespread in the 70μm and absent from the 210μm HGF configurations (refer to section 7.2.2). Furthermore, the expected increase in sensitivity to internal defects when loaded in compression was not accounted for and could be significant. The distribution of 210μm HGF at four interfaces was expected to supply significantly more resin to the damage site for all three conditions considered in table Table 7-4 and outlined in more detail in Chapter 5 section 2.2. Therefore, it was expected that this configuration would provide significant healing effectiveness. However, it should be noted that the configuration determined to provide the largest volume of healing resin is only able to fill ≈50% of the estimated damage volume for condition 1 of the *Volumetric Assessment*. If Chapter 6, section 2.2 is considered, the 210μm configuration was predicted to fill a similar percentage of the estimated damage volume for quasi-static indentation. Although this configuration was reported to provide excellent healing efficiencies under flexural loading, the increased sensitivity of impact damaged laminates to compressive loading may result in the healing efficiency being more reliant on the volume of resin supplied. Therefore, it may be necessary to ensure that the resin supply can target a higher percentage of the estimated damage volume in order to achieve the desired healing efficiencies that were reported in Chapter 6.

7.2 Experimental

CAI testing was conducted in accordance with the standard ASTM D7137/D 7137M-05 [187] but modified in accordance with Prichard and Hogg [191]. Low velocity drop weight impact damage was inflicted according to ASTM D7136/D 7136M [207] again with modifications in accordance with Prichard and Hogg [191]. Specimen dimensions were defined in accordance with Prichard and Hogg [191] (89mm x 55mm x 2.6mm).

7.2.1 Laminate Manufacture

Four laminate configurations were proposed for mechanical assessment. These were HGF spacings of 70μm and 140μm at two interfaces and 210μm placed at four interfaces. Those located at two interfaces followed a lamination process as outlined in Chapter 6, section 2.1. HGF located at four interfaces required additional consideration.

It was proposed in Chapter 3, Figure 3.1 Global Workflow that the manufacturing process can be subdivided into four distinct sections. These will be considered here.

7.2.1.1 Initial Lamination

The sixteen ply QI lay-up $(-45°/90°/45°/0°)_{2S}$ was selected as the host laminate for consistency with previous chapters. The specimen dimensions were 89mm x 55mm x 2.6 mm, which necessitated a panel dimension of 210mm x 210mm to provide 6 replicates with sufficient material for wastage during the cutting process, as shown in Figure 7-8.

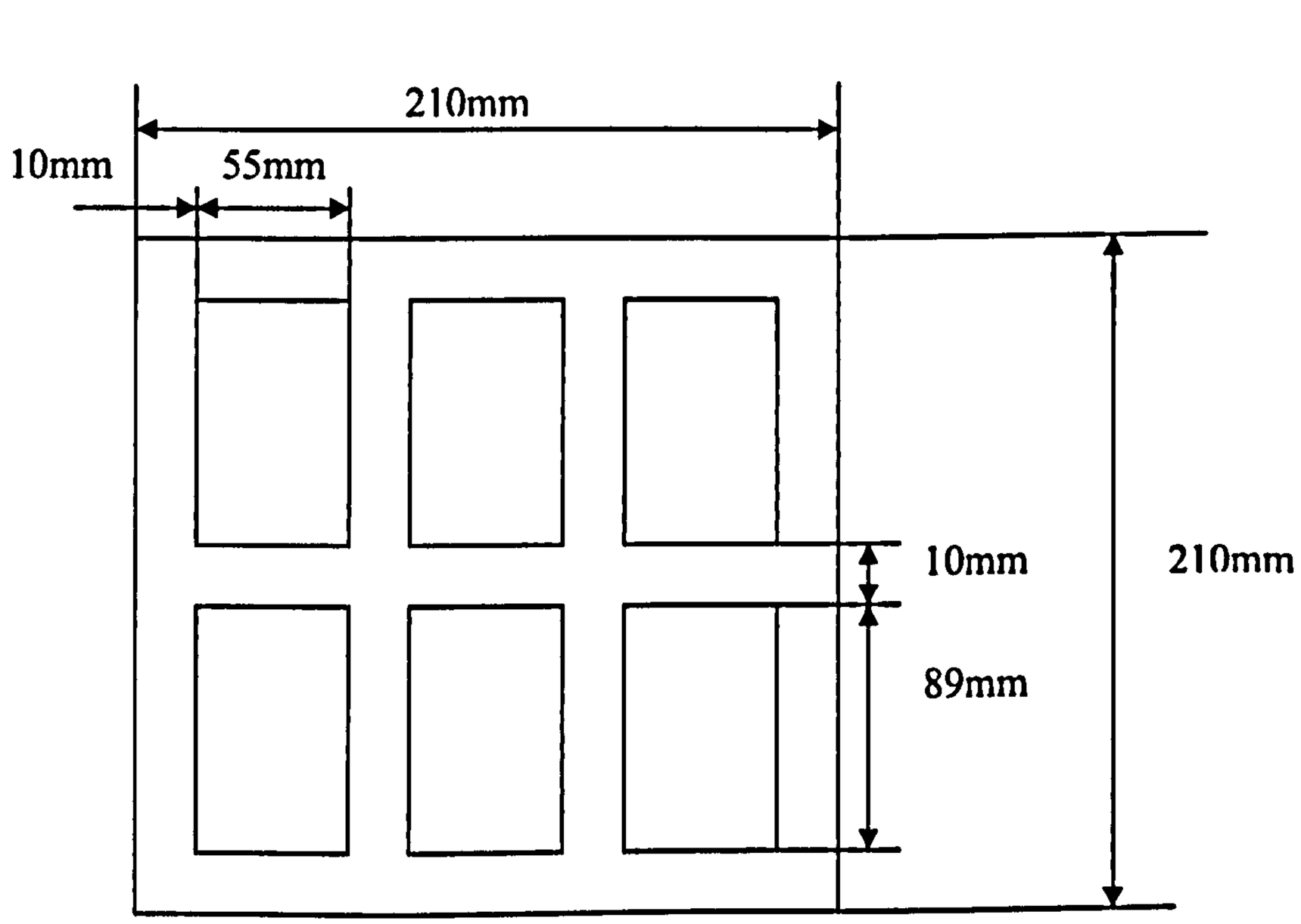

Figure 7-8: ***Schematic Diagram of Laminate Plates from which CAI Samples were Cut***

T300/914 carbon fibre/epoxy pre-preg was removed from storage at -18°C and given adequate time to defrost. Sufficient pre-preg was then cut to the required laminate size.

HGF of the required pitch spacing (210μm) was to be wound directly onto uncured CFRP plies prior to lamination by attaching them directly onto the take-up drum during the HGF manufacturing process, as described in Chapter 6, section 2.1.1 . To achieve this, the overall laminate was divided into three sub-laminates as follows, with HGF fibre located as indicated by H_n and as shown in Figure 7-9:

(-45°/90°/45°/0°/**HGF$_1$**/-45°/90°/45°/0°/0°/45°/90°/-45°/**HGF$_2$**/0°/45°/90°/-45°)

1. *(45°/90°/-45°/0°/**HGF$_2$**)$_{\text{Front Face}}$
2. (-45°/90°/45°/0°/0°/45°/90°/-45°)$_{\text{Middle}}$
3. (-45°/90°/45°/0°/**HGF$_1$**)$_{\text{Back Face}}$

***±45 ply directions reversed**

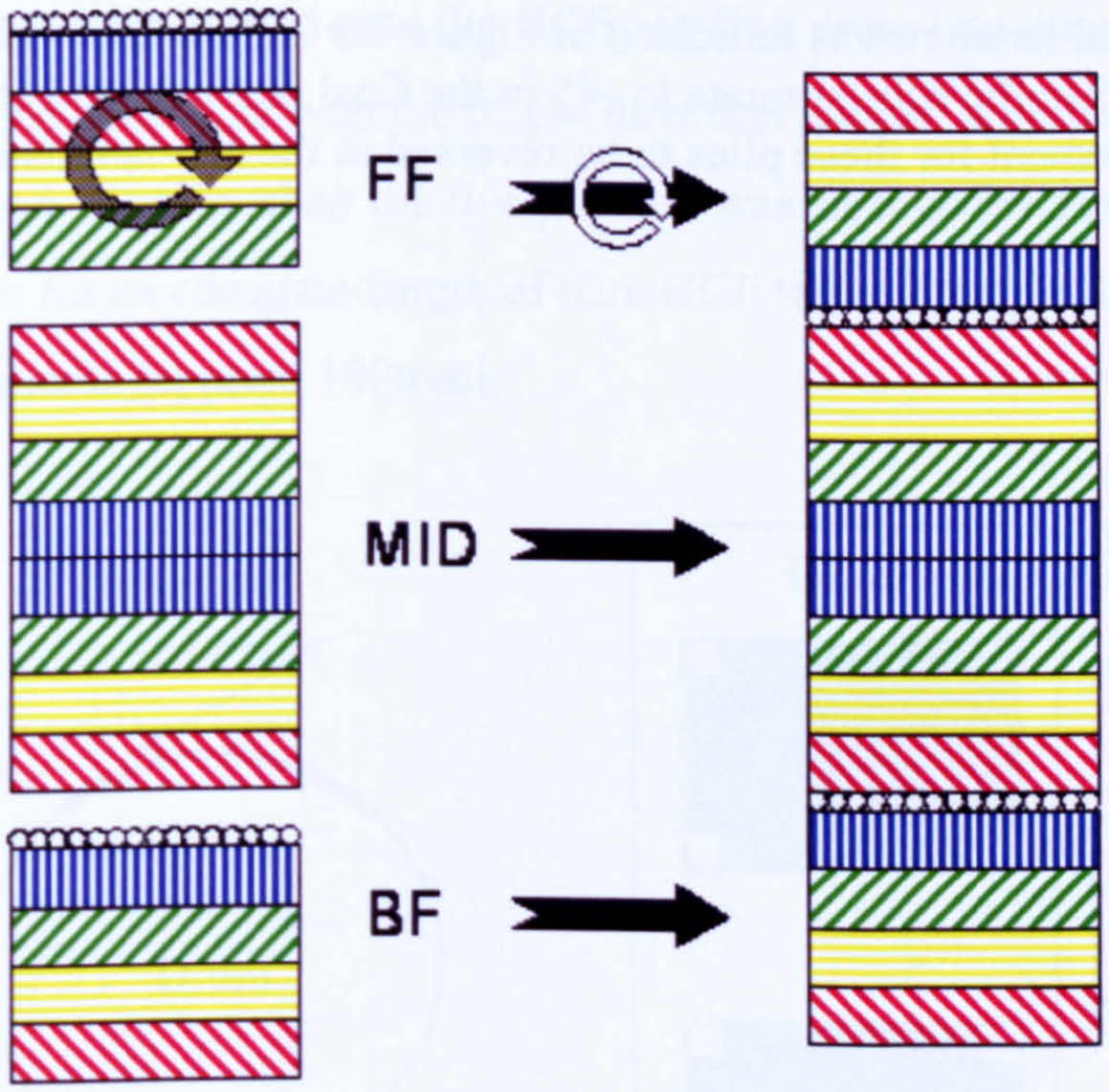

Figure 7-9: ***Construction of Self-Healing Laminate with HGF Embedded at Two 0/45 Interfaces***

To achieve the integration of HGF at four interfaces, the laminate was divided into five sub-laminates as follows, with HGF fibre located as indicated by H_n and as shown in Figure 7-10:

(-45°/90°/45°/0°/**HGF$_1$**/-45°/90°/45°/**HGF$_3$**/0°/0°/**HGF$_4$**/45°/90°/-45°/**HGF$_2$**/0°/45°/90°/-45°)

1. *(45°/90°/-45°/0°/**HGF$_2$**)$_{\text{Front Face 2}}$
2. *(45°/90°/-45°/**HGF$_4$**)$_{\text{Front Face 1}}$
3. (0°/0°/**HGF$_3$**)$_{\text{Middle}}$
4. (-45°/90°/45°)$_{\text{Back Face 2}}$
5. (-45°/90°/45°/0°/**HGF$_1$**)$_{\text{Back Face 1}}$

***±45 ply directions reversed**

It can be seen that the sub-laminates denoted * have their ±45° plies reversed to ensure that the HGF could be drawn directly onto the 0° plies where possible. This improved the embedment of the HGF. Therefore, after HGF manufacture and during final lamination, the laminate sub-stack was rotated to be placed into the overall stack and form the final laminates as indicated in Figure 7-9 and Figure 7-10. This action, translates all +45 in the sub-laminate to -45 in the final laminate and all -45 to +45, hence the requirement for these plies to be reversed in the sub-laminate stack.

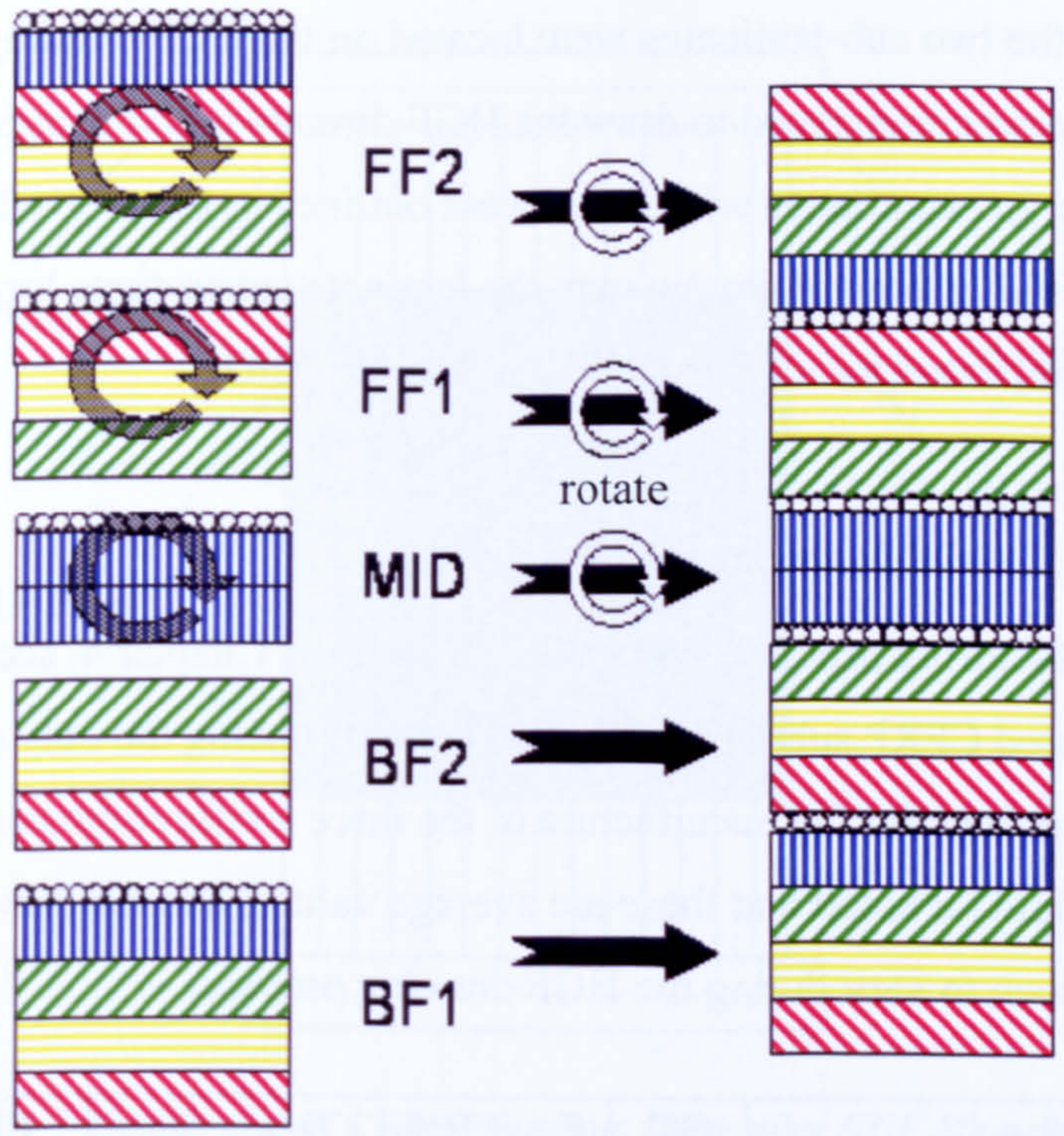

Figure 7-10: ***Construction of Self-Healing Laminate with HGF Embedded at Four Interfaces***

The sub-laminates were located onto the HGF winding drum (maximum of two at a time) using double sided tape with the 0° ply direction aligned with the HGF winding direction (Figure 6-7). Also, their relative position was arranged with sufficient space between to allow for an adequate length of bare HGF to facilitate the later healing resin infusion process (approx. 100mm).

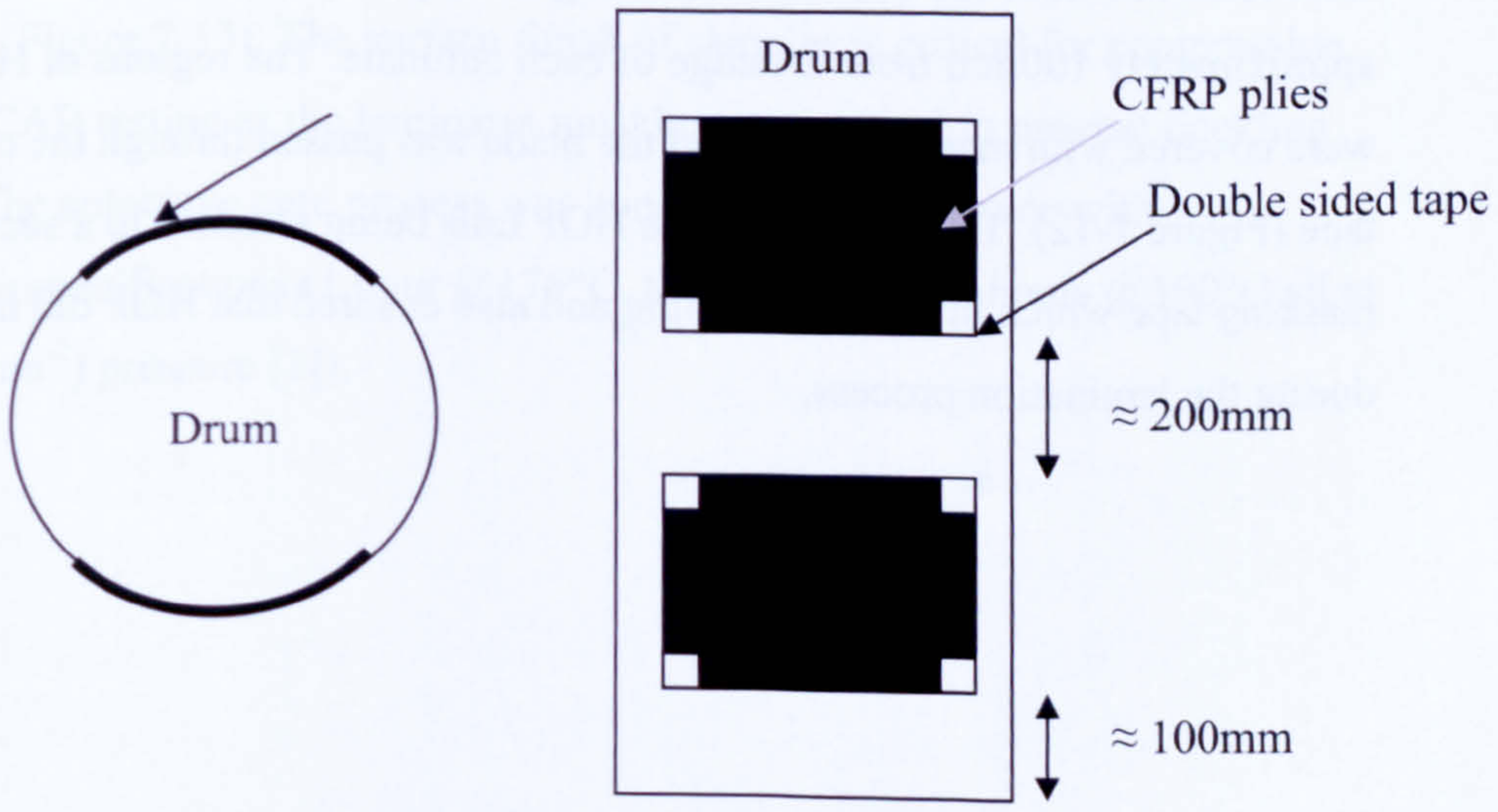

Figure 7-11: ***Placement of CFRP Plies onto Drum during Manufacture***

Once prepared, the two sub-laminates were located on the HGF winding drum, and the drawing process commenced to draw the HGF directly onto the exposed sub-laminate surface, in accordance with the process outlines in Chapter 4.1.4. However, in addition the HGF is drawn directly onto the laminate subsections located on the drum. This was repeated for all sub-laminates requiring HGF.

7.2.1.2 HGF Manufacture

The HGF manufacturing process is described in detail in Chapter 4, section 1.2. The addition of uncured CFRP sub-laminates onto the drum being the only difference. The manufacturing settings for the manufacture of the three configurations are outlined in Table 7-5. It should be noted that these are average values, and the draw rate, in particular, was seen to vary during the HGF drawing process.

Configuration		OD	Feed Rate	Draw Rate	Pitch Rate
70µm	Setting	58	110	180	70
	Reading		29.4 μms^{-1}	1.26 ms^{-1}	-0.8 µm/rev
140µm	Setting	58	110	180	140
	Reading		29.4 μms^{-1}	1.26 ms^{-1}	-1.73 µm/rev
210µm	Setting	58	110	180	200
	Reading		29.4 μms^{-1}	1.26 ms^{-1}	-2.31 µm/rev

Table 7-5: ***HGF Manufacturing Settings for 70µm and 210µm Configurations***

Once the 'top' and 'bottom' sub-laminates were completely covered with HGF, they were removed from the drum surface using a sharp blade to cut the HGF approximately 100mm from the edge of each laminate. The regions of HGF to be cut were covered with masking tape, and the blade was passed through the centre of the tape (Figure 7-12). This resulted in the HGF tails being attached to a section of masking tape which improved handling and also ensured that HGF did not entangle during the lamination process.

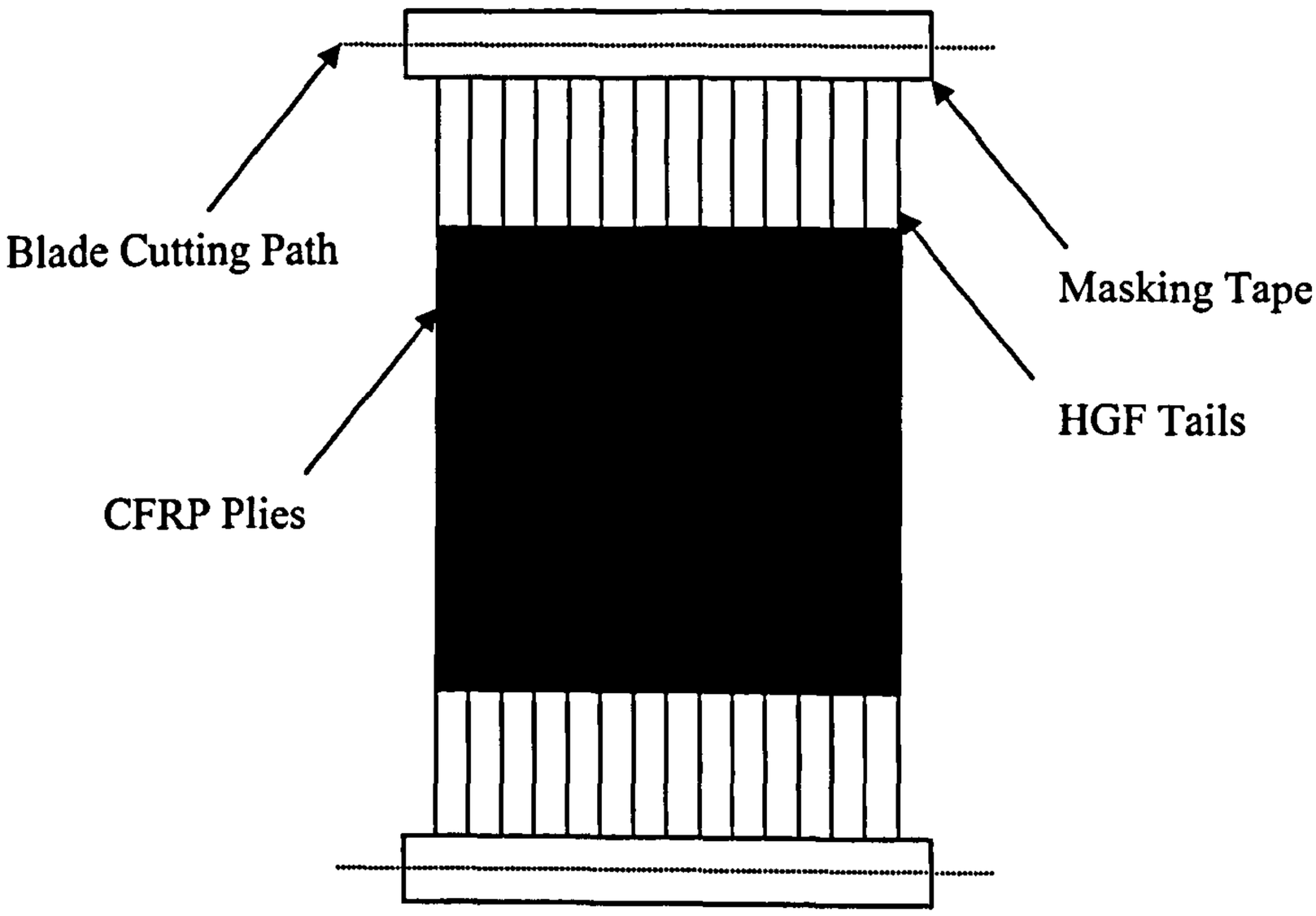

Figure 7-12: ***Removal of CFRP Plies from Drum after HGF Manufacture***

7.2.1.3 Lamination and Cure

After the HGF manufacture, all sub-laminates were then combined (Figure 7-9 and Figure 7-10) using standard hand lay-up techniques and vacuum bagged in preparation for the autoclave. Additional measures were taken during the 'bagging process' to adequately maintain the open ends of the HGF for subsequent healing resin infiltration, as outlined in section 7.2.1.4. Furthermore, a thin aluminium caul plate (210mm x 210mm x 5mm) was placed on-top of the laminates to ensure a good surface finish (Figure 7-13). The surface finish of samples is critical for compression after impact (CAI) testing as the laminates must be symmetrical to prevent buckling instabilities. The autoclave cure process was conducted in accordance with manufacturer's specifications (1 hour @175°C, then post-cured 4 hours @190°C all at 7bar (700kNmm^{-2}) pressure [1]).

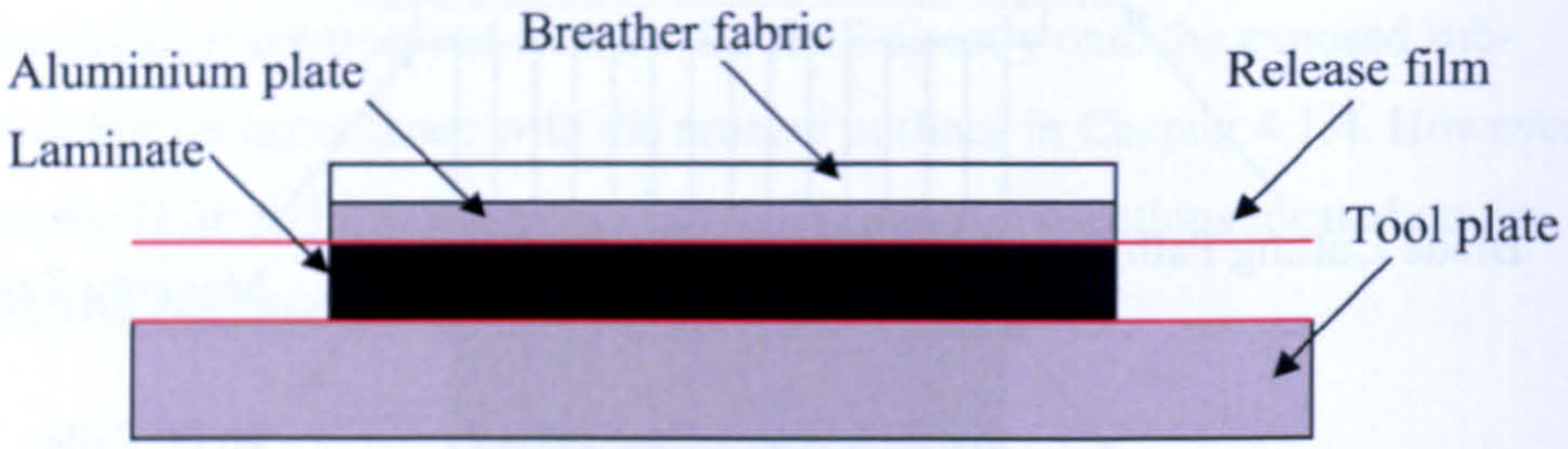

Figure 7-13: ***Schematic Diagram of Vacuum Bag Configuration***

7.2.1.4 Resin Infiltration of HGF

Details of the resin infiltration process are described in detail in section 6.2.1.4. After HGF infiltration was completed, the plate was cut in half using a water cooled diamond saw to form a suitable size to fit the drop weight impactor (Figure 7-14). This allowed three adjacent specimens to be impacted in succession. The specifics of the low velocity impact are described in section 7.2.3. After impact, panels that contained healing resin, were placed in an oven to undergo a two stage accelerated healing cycle:

1. 45 minutes @70°C: *This allowed 15 minutes for the panel to reach the required temperature and then a 30 minute dwell where the viscosity of the healing agent was at a minimum (25cps)*
2. 75 minutes @125°C: *This allowed 15 minutes for the panels to reach the required temperature and then a 60 minute dwell to fully cure the healing agent*

The initial step was an attempt to minimise healing resin viscosity in order to simulate an 'optimised' resin system for this role. The second step accelerated the cure cycle to 60 minutes to simulate the desirable time period for a healing event. It is worth noting that the resin system used is capable of ambient temperature cure within 7-10 days, but such a protracted period was considered impractical in this study. After heat treatment, individual test specimens were cut from the panels (Figure 7-14) using a water cooled diamond saw. Particular attention was paid to the cutting of individual specimens as excellent alignment of the sides is needed to ensure an even load distribution in the subsequent compressive testing. A low feed rate was used with the

diamond saw to ensure an excellent edge finish and to eliminate the need for additional specimen preparation. Local variations in dimensions can lead to an uneven load path, local instabilities and premature failure. Once cut to size, the specimens were stored in a temperature and humidity controlled environment (19.6°C, 52%) until mechanically tested (section 7.2.4).

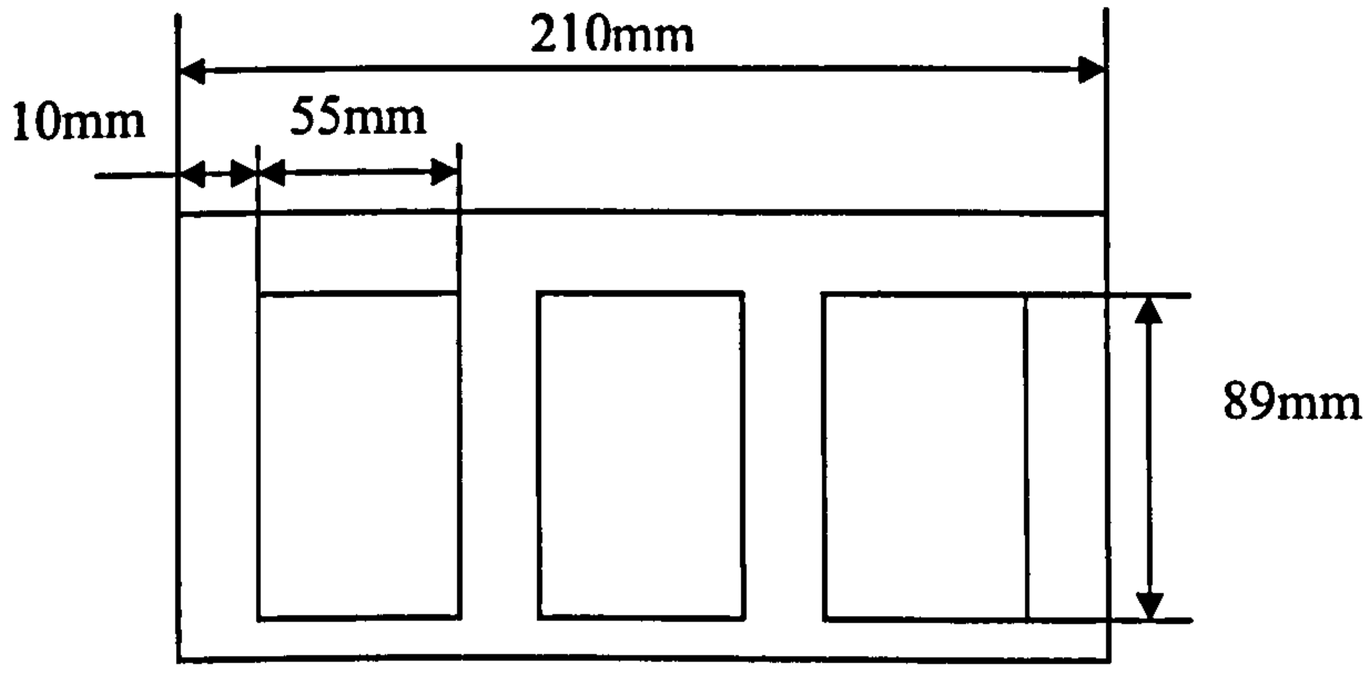

Figure 7-14: ***Schematic Diagram of the Laminate Plates from which CAI Samples were Cut***

7.2.2 Laminate Microstructure

Small sections of waste material from the specimen preparation were potted in a clear two part epoxy resin (SP320, Cytec) which was cured and then ground with SiC paper (P200, P400, P800, P1200 and P2500) and polished with a diamond suspension fluid (particle size 6μm, 3μm and 1μm) on a Metaserv 2000 Grinder/Polisher. A Jenavert Carl Zeiss Jena microscope, with a Pixera Pro 150ES camera and Viewfinder v3.0.1 software from Pixera Corp allowed the microstructure of the different configurations to be visually assessed.

The 70μm, 140μm 210μm HGF spacing configurations can be seen in Figure 7-15, Figure 7-16 and Figure 7-17 respectively. It can be seen that the efficiency of HGF embedment improved as the HGF packing density decreased. This was attributed to the reinforcing carbon fibre having sufficient space to migrate between the large HGF during the consolidation process when the matrix resin is reduced to a sufficiently low viscosity. If the HGF spacing was small, the reinforcing fibres were constrained which resulted in the generation of resin rich regions identified in Figure 7-15c.

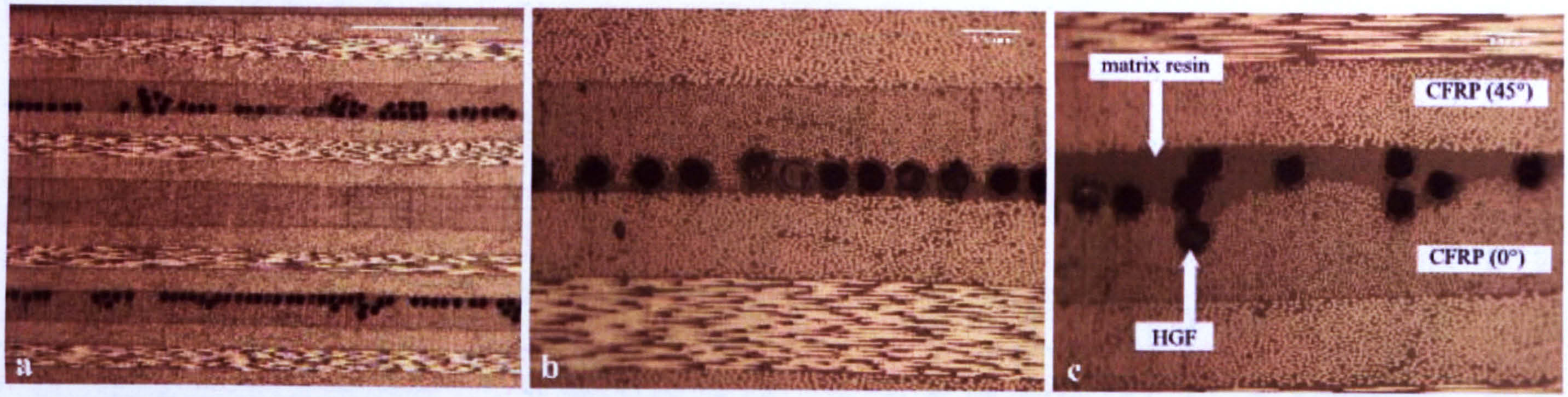

Figure 7-15: ***a) Embedded HGF Spaced at 70μm showing b) Ideally Nestled Side by Side and c) Fibre Clumping and Resin Rich Regions***

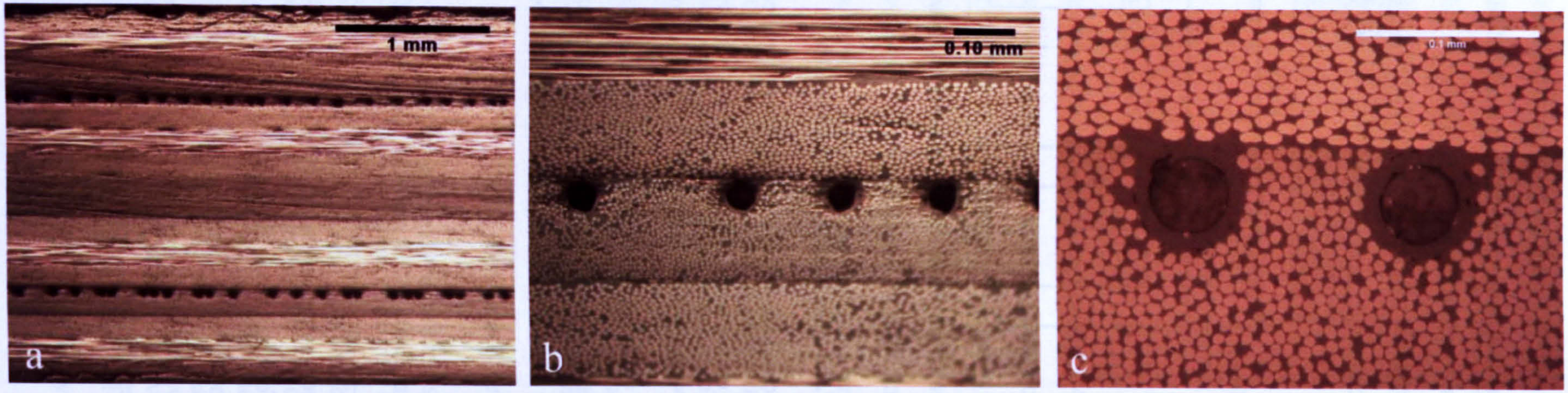

Figure 7-16: ***a) Embedded HGF Spaced at 140μm Showing b) Ideally Spaced at Two HGF Diameters and c) Excellent Embedment***

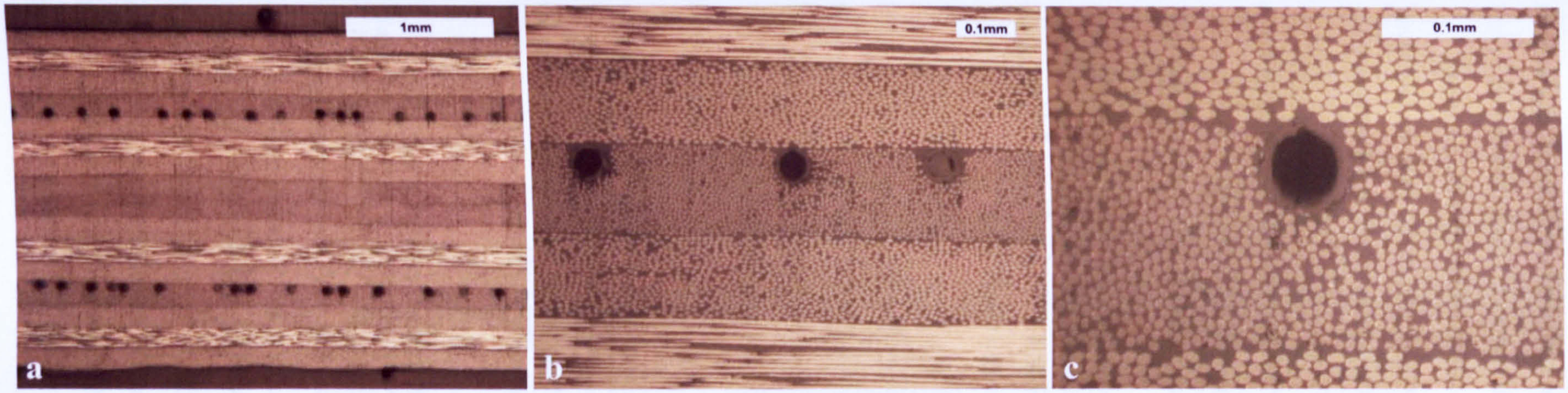

Figure 7-17: ***a) Embedded HGF Spaced at 210μm showing b) Ideally Spaced at Three HGF Diameters and c) Perfect Embedment***

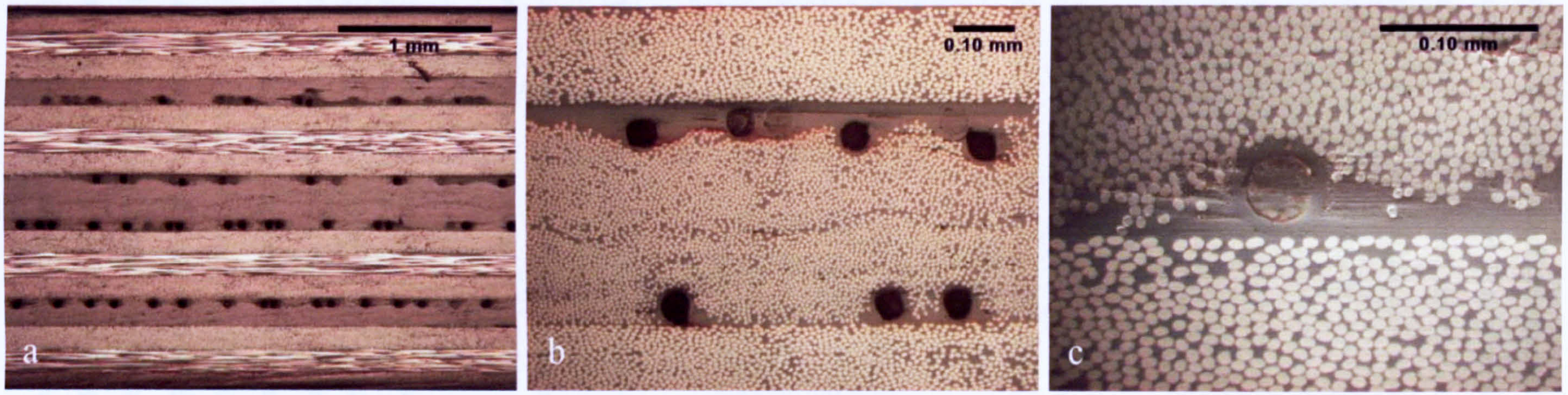

Figure 7-18: ***a) Embedded HGF Placed at Four Interfaces, Spaced at 210μm showing b) Differences in Embedment within Laminate and c) Poor Embedment at One Interface***

It can be seen in Figure 7-18 that the HGF spaced at 210μm on four interfaces embeds very efficiently at all but one interface (Figure 7-18b and c). This interface corresponds to sub-laminate 2 ("TOP1" Figure 7-10) and highlights the problems encountered when HGF is overlaid onto a non 0° CFRP ply. In this case the HGF was overlaid onto a -45° ply direction and as a result, the quality of HGF embedment was significantly reduced. This was attributed to two factors:

1. Fibre drawing tension during HGF manufacture promotes embedment when overlaid onto parallel carbon fibres (0°), as highlighted in Figure 7-19a. However, when overlaid onto off axis directions (±45°, 90°) this effect is lost as highlighted in Figure 7-20a.
2. Misalignment of the HGF with the 0° fibres in the additional sub-laminate when the sub-laminates are combined as demonstrated in Figure 7-20c.

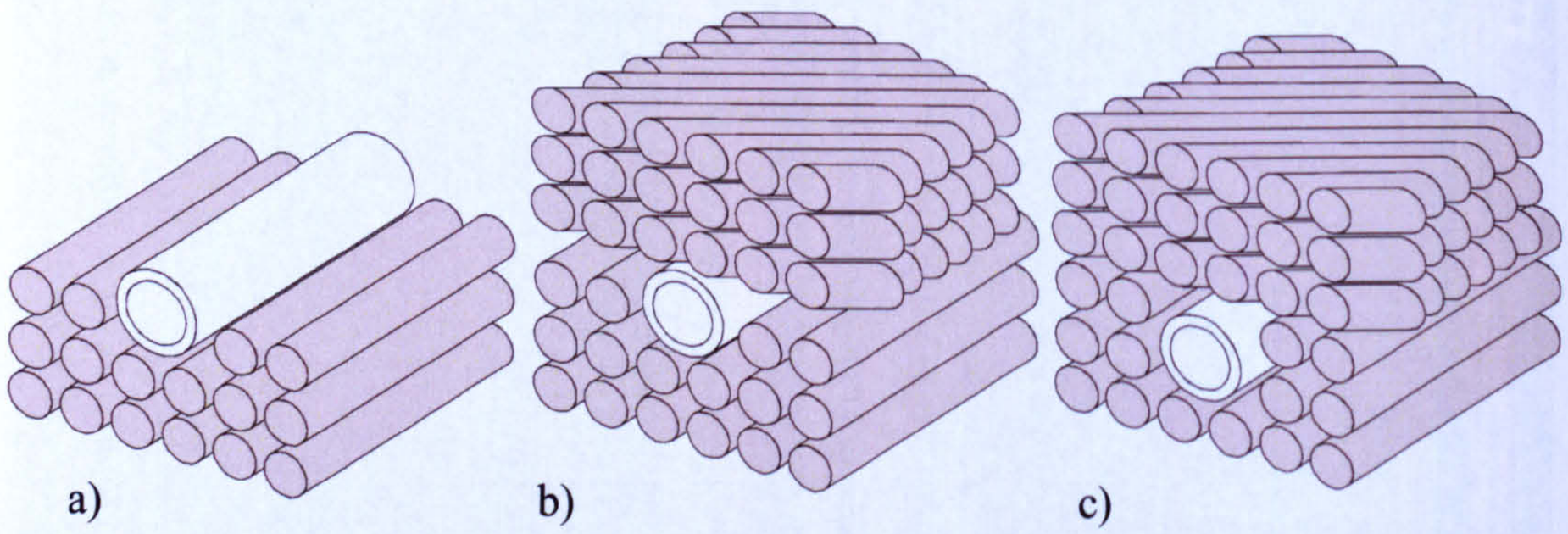

Figure 7-19: ***Schematic Diagram Illustrating the Benefits of Drawing HGF Directly onto the CFRP Plies a) Tension in HGF Forces HGF to Begin to Tessellate with Reinforcing CF b) Plies of Dissimilar Direction are Combined c) During Autoclave Process, High Temperature Reduces Matrix Viscosity and Facilitates Embedment of HGF into 0° Plies***

If Figure 7-19a is considered, it can be seen that the tension created in the HGF drawing process encourages HGF embedment into a 0° ply and improves alignment between HGF and the reinforcing fibre. In contrast, Figure 7-20a indicates that the HGF can not readily embed into a 45° ply due to a mismatch between HGF and reinforcing fibre orientation. When plies are combined during subsequent lamination and placed into an autoclave for consolidation, it can be seen in Figure 7-19c that the low viscosity of the matrix resin facilitates high quality embedment. Figure 7-20c shows this is much more difficult when there is misalignment between the HGF and

the host ply fibres. Thus, resin rich regions are generated where fibre rearrangement is constrained.

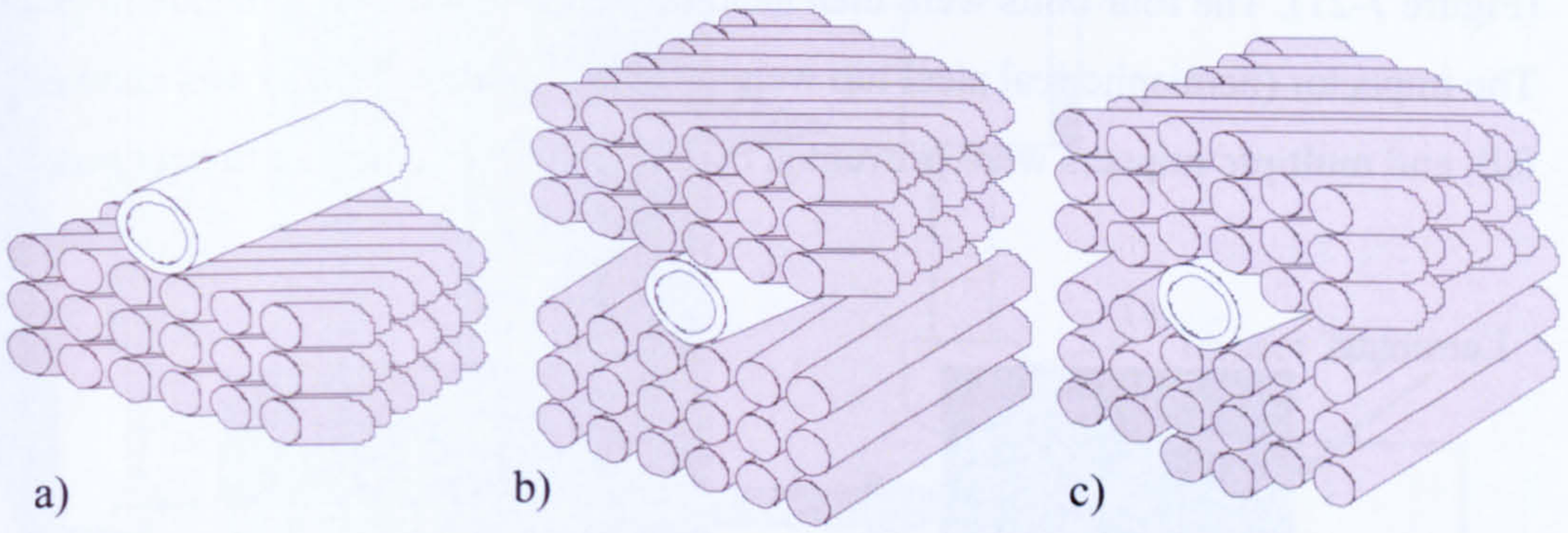

Figure 7-20: ***Schematic Diagram Illustrating the Problem Drawing HGF Directly onto the 45° CFRP Plies a) Tension in HGF can not Facilitate Tessellation with Reinforcing CF b) Plies of Dissimilar Direction are combined c) During Autoclave Process, High Temperature Reduces Matrix Viscosity and Facilitates Embedment of HGF into 0° Plies***

The individual specimen dimensions were measured for the analysis needed in CAI assessment. There was a small increase in the measured thickness of the specimens that contained HGF when compared to those without. The results can be seen in Table 7-6. However, such variations are fully accounted for in the data reduction methods for CAI.

		Average (mm)	S.D (mm)
HGF	Width	55.06	0.09
	Height	88.97	0.17
	Thickness	2.50	0.03
Plain	Width	55.03	0.05
	Height	89.07	0.07
	Thickness	2.46	0.03

Table 7-6: ***Summary of Average Sample Dimensions for CAI Assessment for Comparison between Laminates With and Without HGF (based on 5 measurements of each dimension)***

7.2.3 Drop Weight Impact Testing

Two large steel plates (190mm x 200mm x 12mm) with a circular impact window of diameter 40mm (in accordance with Prichard and Hogg [191]) provided the restraints for impact testing, Figure 7-21. The impact window ensured that the impact damage remained in the centre of the laminate and would not extend to the edges where the

CAI test fixture would provide a clamping force during testing. The centre of each sample was marked with a white pen and located at the centre of the impact window (Figure 7-21). The four bolts were then hand tightened to hold the laminate in place. The impactor (hemispherical steel tup weight=1.68kg, radius 20mm) was allowed to fall, and multiple impacts were prevented by manually retracting the impact mass.

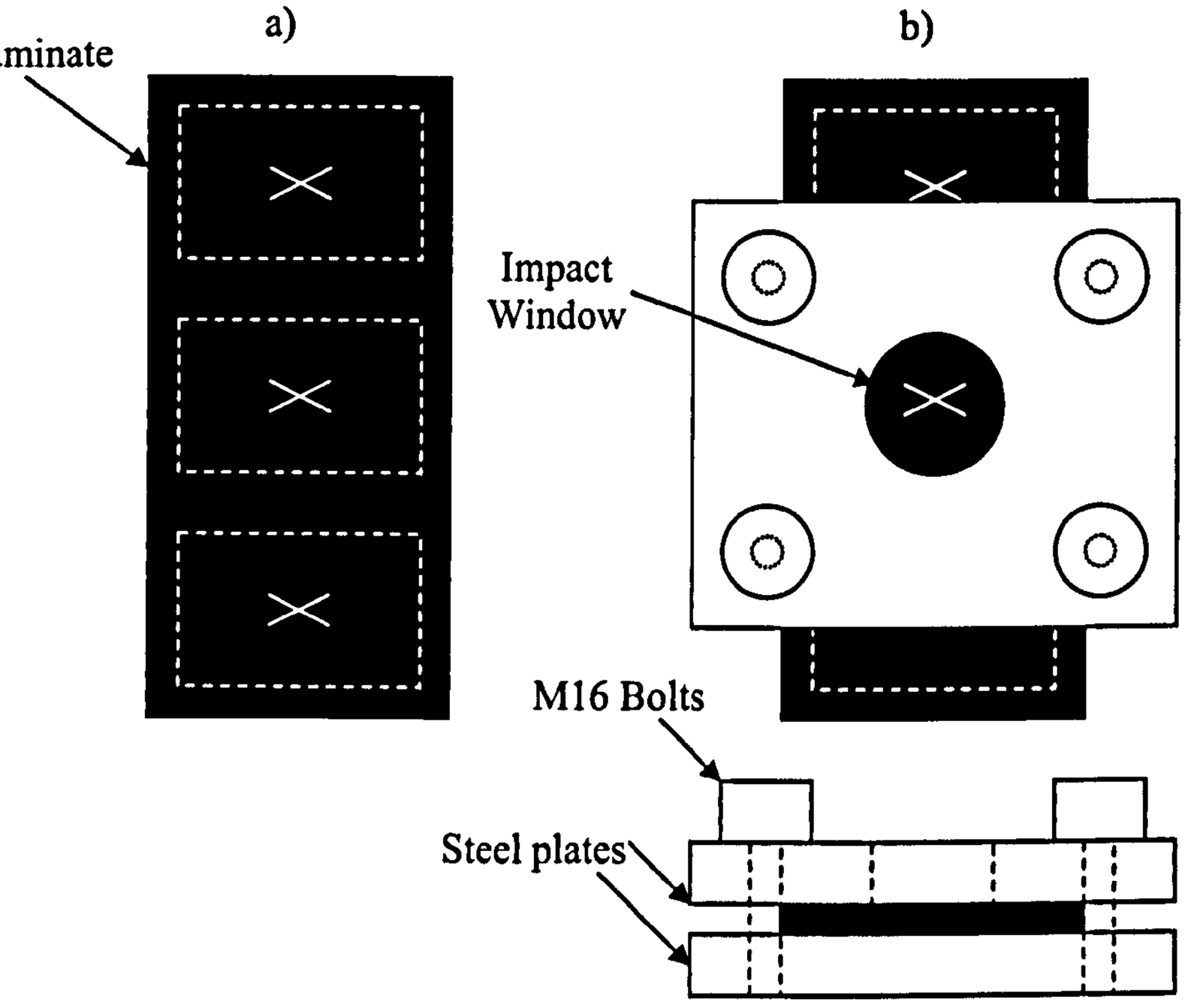

Figure 7-21: ***Set-up for Low Velocity Impact a) CFRP Laminate Marked for Impact b) Plan View and Cross Sectional View of Impact Support Plates***

The impact rig comprised a load cell (5kN) with a hemispherical impact tup (20mm and 1.68kg) attached. The arrangement was raised manually and dropped from the requisite height to achieve a target impact energy. As the mass was released and approached the target, it passed a light sensor which detected the time passage of a known length marker, as indicated in Figure 7-22 and hence the velocity was calculated. This was recorded before and after impact, the difference in velocity being converted to kinetic energy and assumed to represent the energy absorbed by the laminates (other losses assumed negligible).

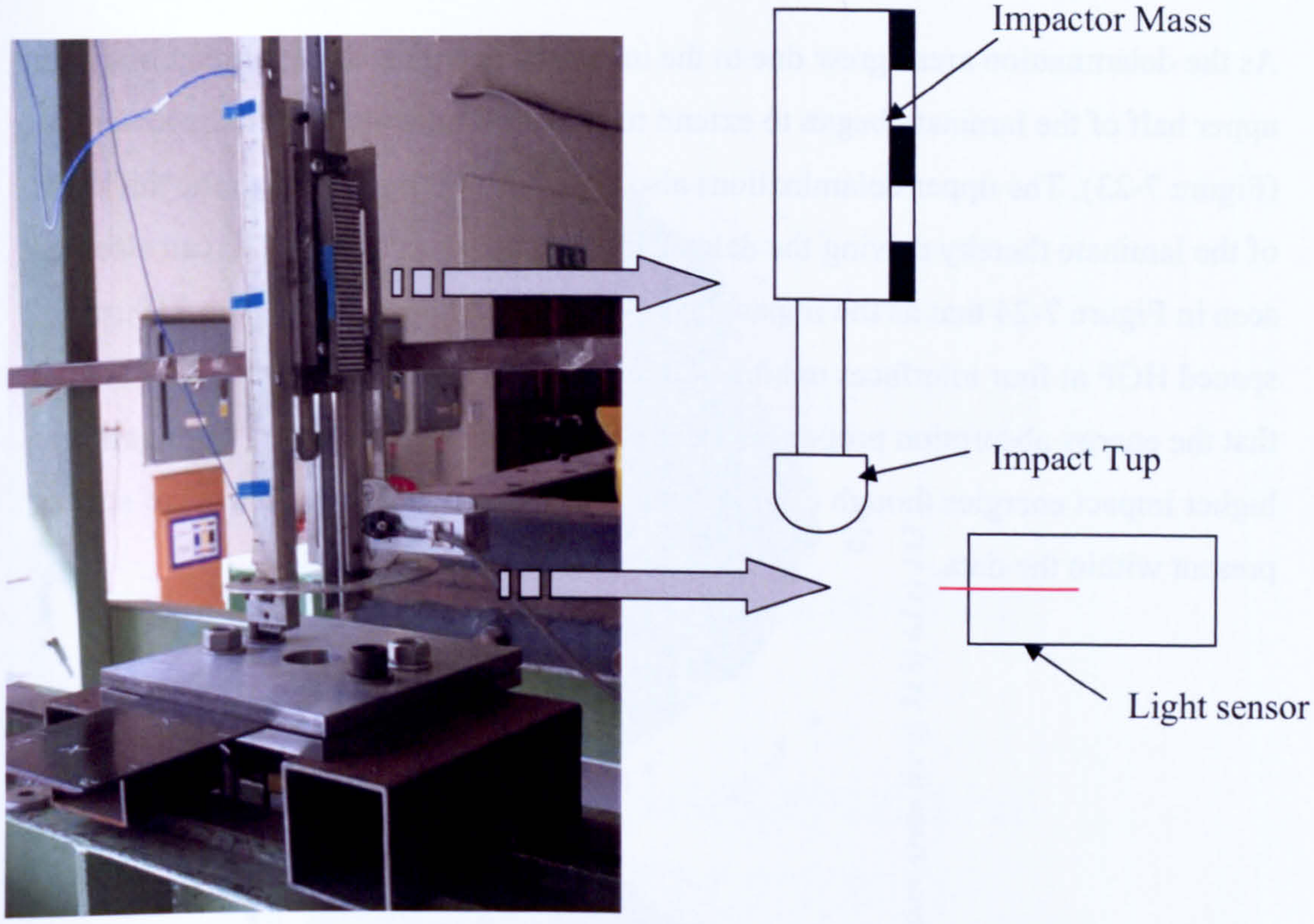

Figure 7-22: ***Photograph and Diagram Showing the Low Velocity Drop Weight Rig and the Mechanism by which Velocity was Measured***

It was necessary to determine the appropriate impact energy to use for CAI testing. Thus, additional panels of identical laminates to those used for CAI testing were exposed to incremental impact energies from 2J to16J. This was to assess whether the incorporation of HGF altered the impact response and damage formation within the laminate. Post-impact, the delamination areas for all laminates were determined using ultrasonic C-Scanning. The results of this impact energy assessment can be seen in Figure 7-24.

It was concluded that the presence of HGF reduced the delamination area even at low impact energies. This effect became less evident as the impact energy increased and the delamination area approached the boundaries of the impact window (Figure 7-21). It was also evident that delaminations did not propagate beyond this boundary (represented in Figure 7-24 by the red dashed line at 1256mm^2) as can be seen for impact energies 12J, 14J and 16J where delaminations were effectively 'pinned' at the impact window boundary. Furthermore, it was evident that this boundary affected the through thickness distribution of higher energy impact damage within the laminates.

As the delamination areas grew due to the increased energies, the delaminations in the upper half of the laminate began to extend to exhibit similar areas as in the lower half (Figure 7-23). The upper delaminations also began to penetrate through the thickness of the laminate thereby driving the delaminated surfaces further apart. It can also be seen in Figure 7-24 that as the impact energy increased, the laminate with 210μm spaced HGF at four interfaces exhibited a reduced delamination area and may suggest that the energy absorption properties from HGF at different interfaces are engaged at higher impact energies though clear conclusions are difficult with the level of scatter present within the data.

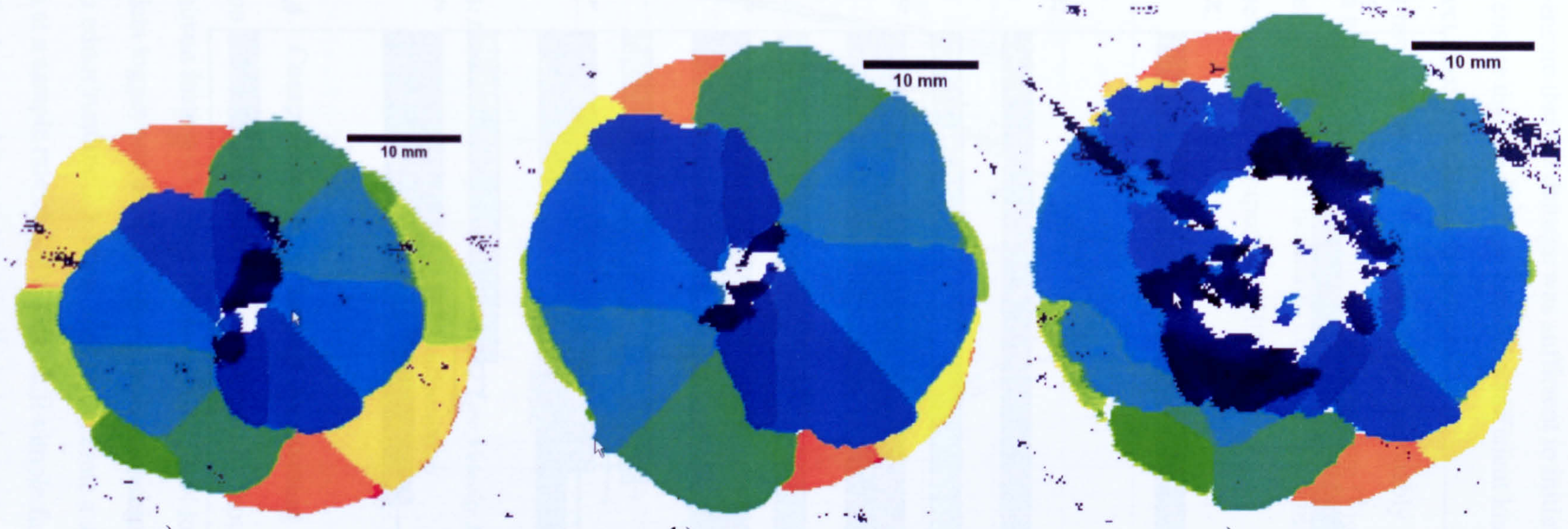

a) b) c)

Figure 7-23: ***Ultrasonic Time of Flight Images of Delamination Areas for a) 3J b) 6J c) 14J***

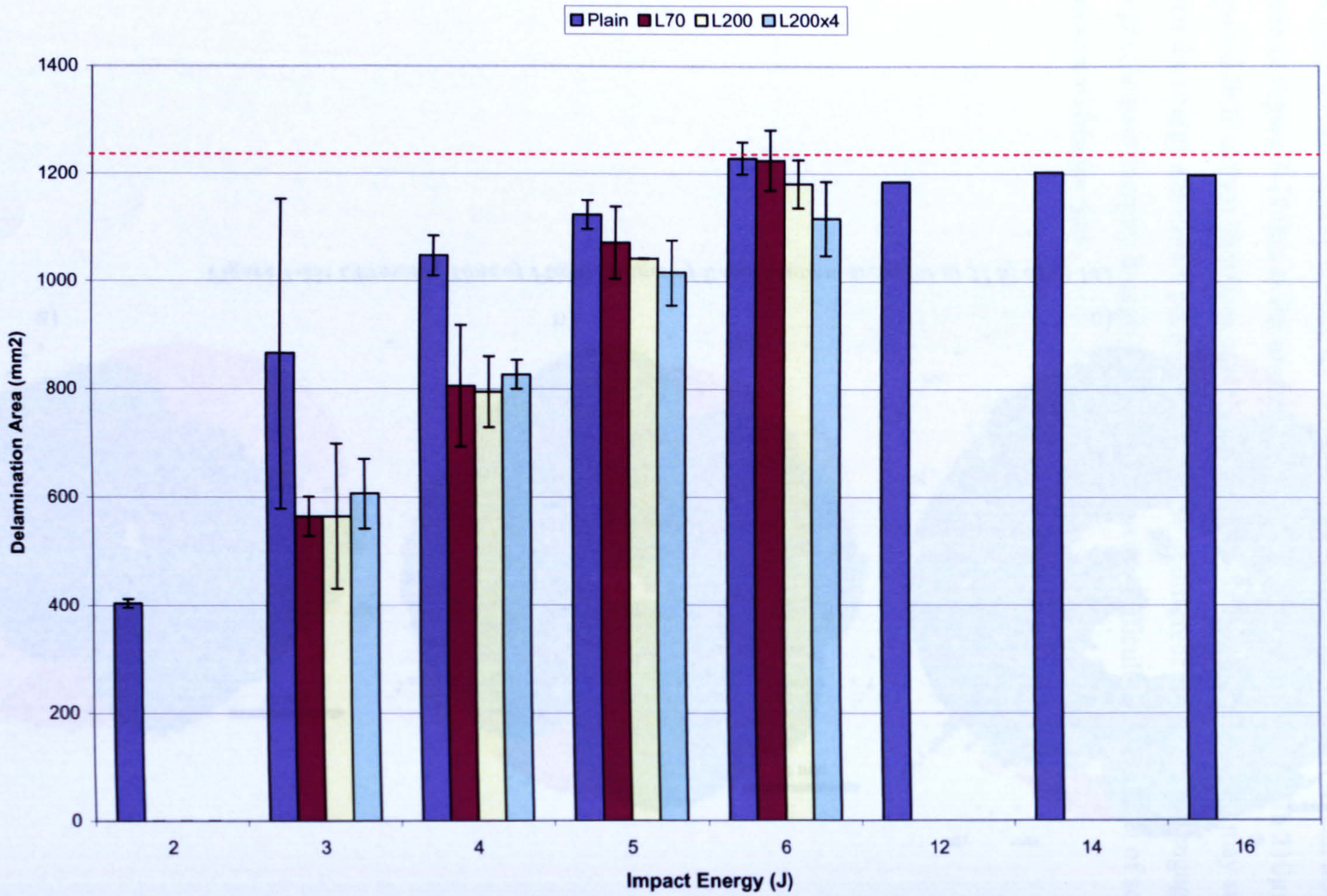

Figure 7-24: ***Variation in Delamination Area with Impact Energy and HGF Configuration***

The 6J impact energy level was selected for the CAI testing for two primary reasons:

1. To ensure that the damage was sufficient to initiate HGF fracture
2. To ensure that the damage created a sufficient knockdown in CAI strength to detect a recovery after a healing event.

The impact response at this energy level was reasonably insensitive to HGF content as can be seen when impact load is plotted against time (Figure 7-25). It was also an energy level where the plain laminate (i.e. no HGF) damage area was equivalent to that of those laminates incorporating HGF.

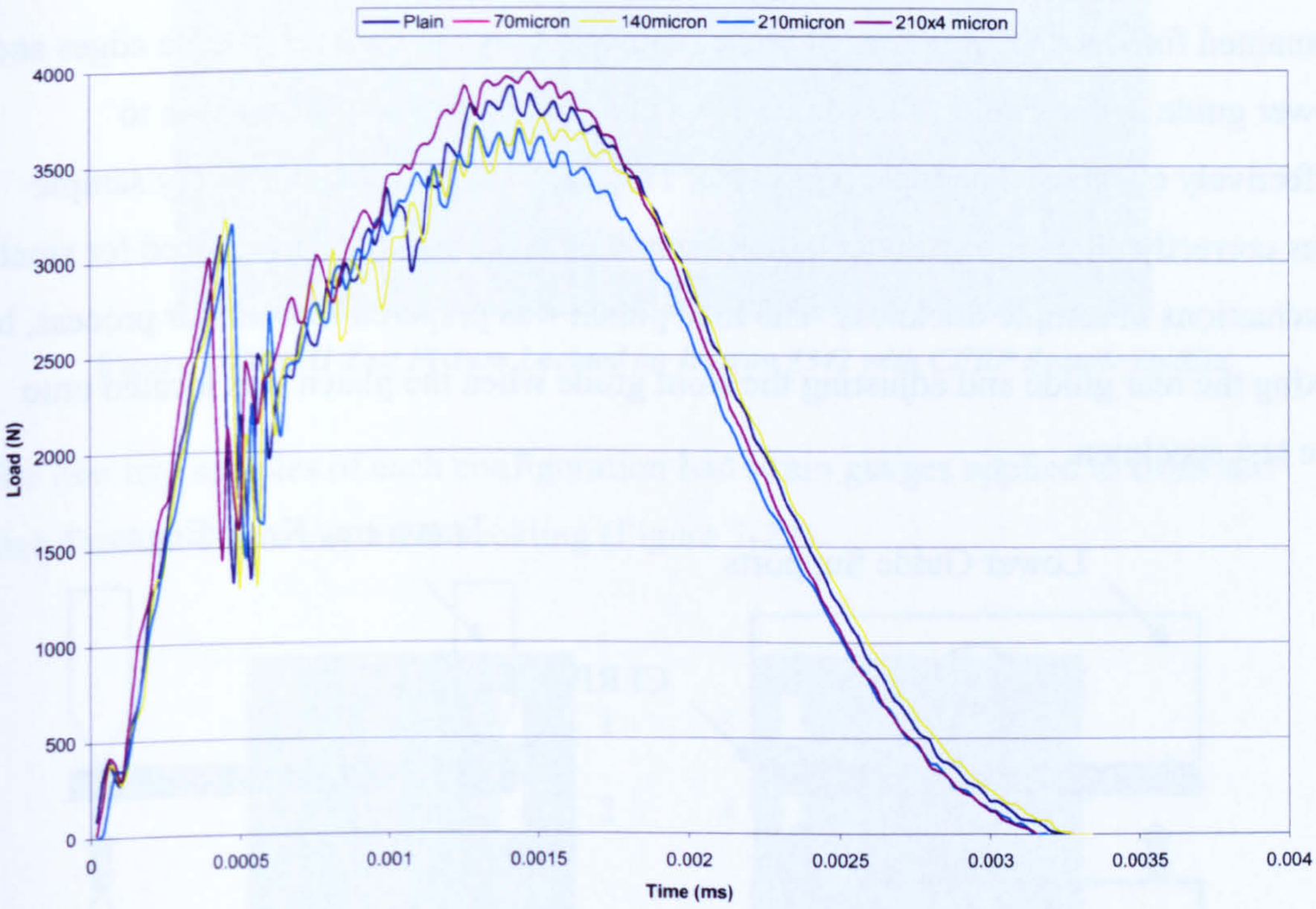

Figure 7-25: ***Load vs Time Representation of a 6J Low Velocity Drop Weight Impact Event for all HGF Configurations***

7.2.4 Compression After Impact Assessment

Compression After Impact testing was conducted by mounting the modified CAI test fixture within an Instron 1342 test frame with a 250kN load cell. An Instron 8800 controller/data logger was used to control the test machine and record the data output. Wavemaker editor/runtime 7.1.1 was used to generate a simple loading ramp of 0.4mm/min at a sample rate of 0.005 kHz until sample failure at which point the crosshead displacement was automatically halted and the crosshead was manually

retracted. A maximum crosshead displacement of 5mm was set as a fail-safe as this represented the maximum displacement before the load platen would impinge upon the knife edge supports which could ultimately cause distortion/failure of the test fixture. It was expected that sample failure would occur before this limit was reached.

Samples were mounted into the fixture by first ensuring that the transverse knife edge supports and lower guides at the rear of the test fixture were well aligned and located in position by tightening all screws (Figure 7-26). Positioning was ensured by use of a spirit level to ensure both vertical and horizontal alignment. The rear supports remained fixed for the duration of the testing, and only the transverse knife edges and lower guide at the front of the fixture were adjusted or moved into position to effectively clamp each sample into place. This approach ensured that every sample was correctly aligned, facilitated quick sample changeover and also allowed for small fluctuations in sample thickness. The load platen was prepared in a similar process, by fixing the rear guide and adjusting the front guide when the platen was located onto the test specimen.

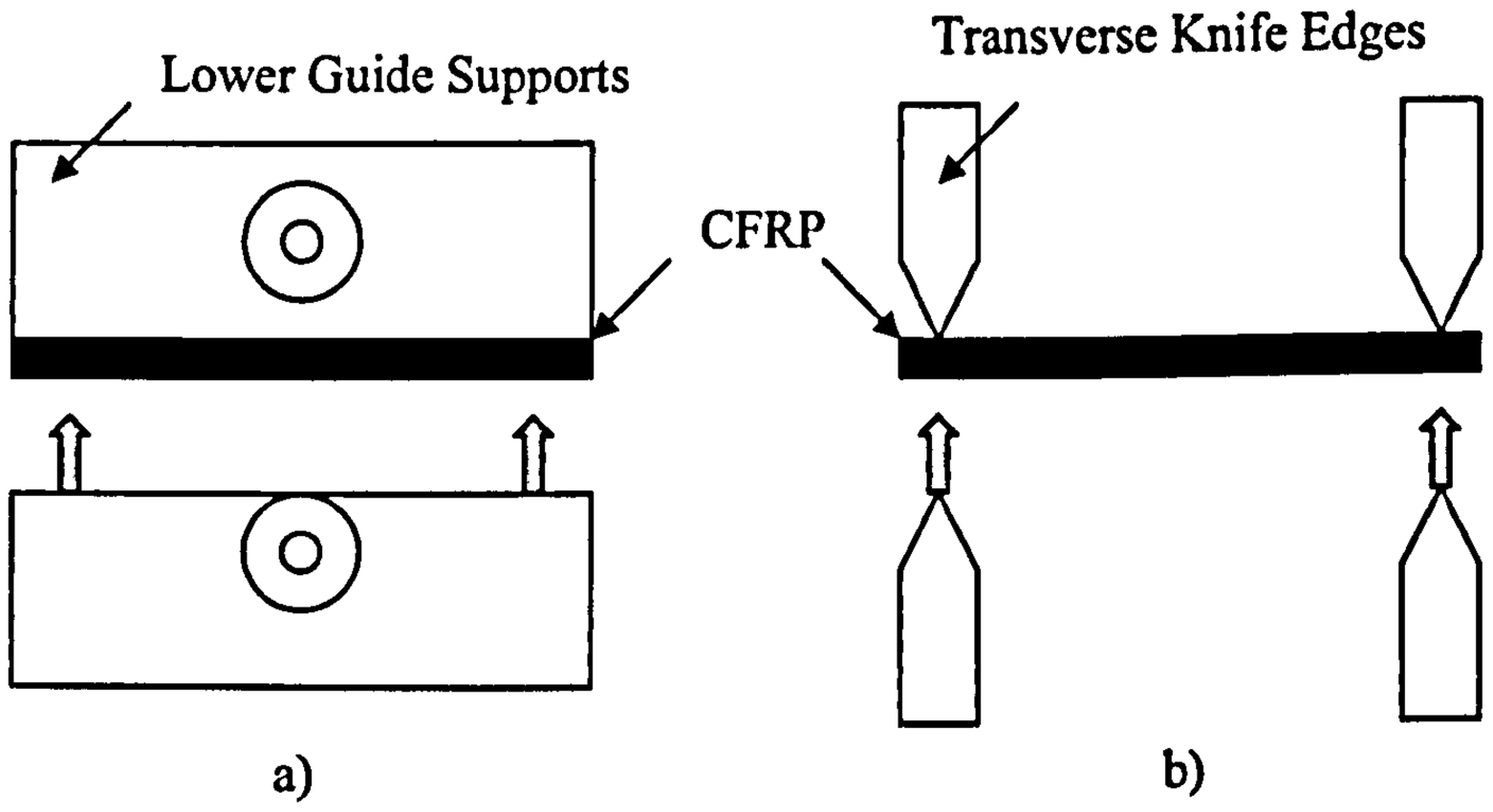

Figure 7-26: ***Schematic Illustration of Supports and Constraints for CAI***

Once the sample was secure and the supports were located, the test machine crosshead was lowered until it contacted the load platen. The crosshead was further lowered to a position where a compressive force was detected in the load cell, which ensured that any initial play in the system was removed, Figure 7-27. The CAI test was then initiated until specimen failure. The crosshead was retracted, the sample removed

from the fixture by loosening the front supports, the next specimen placed into the fixture and the process repeated.

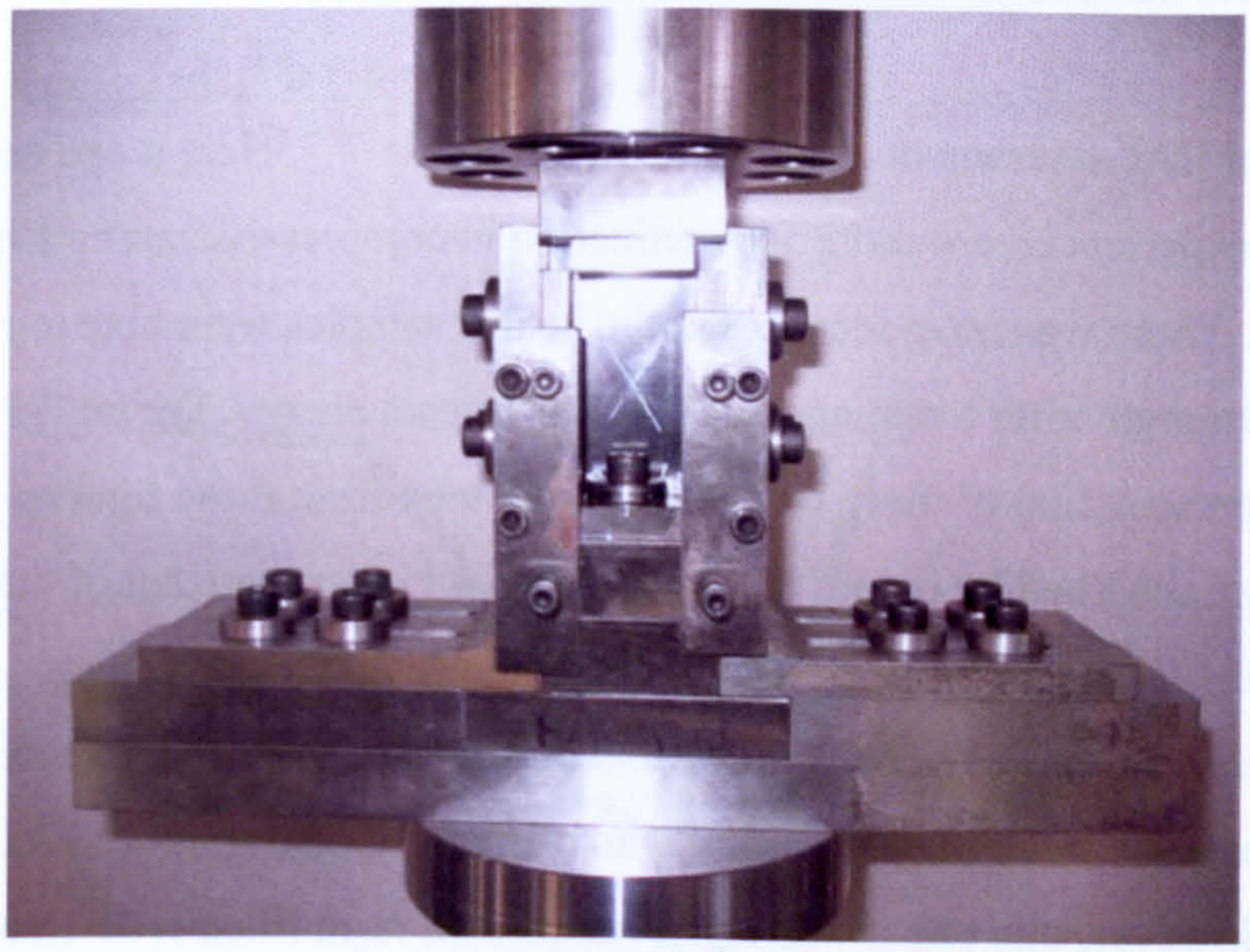

Figure 7-27: ***CAI Test Fixture Located on Instron 1342 with CFRP Sample In-Situ***

The first two samples of each configuration had strain gauges applied to front and back faces to detect any local buckling (Figure 7-28).

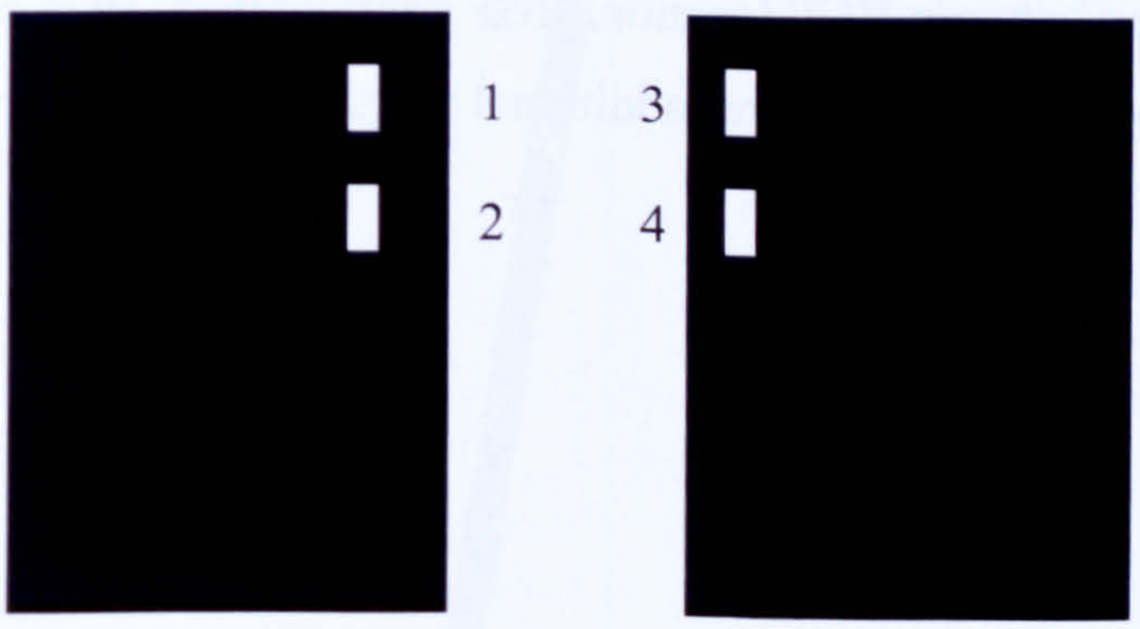

Figure 7-28: ***Location of Strain Gauges on Front and Back Faces of Specimen for CAI Testing***

7.3 Results: Compression Strength

Typical stress-strain plots are shown in Figure 7-29 and Figure 7-30. It can be seen that the laminates experienced local buckling due to the formation of 'sub-laminates' as the delaminations propagated under compressive loading. This divergence is evident when strain gauge pairs (front and back face) are compared. Plots of similar

colour in Figures 7-29 and 7-30 share the same relative position but on opposite faces of the laminate (1-3, 2-4, see Figure 7-28). There was no evidence to suggest that the healed samples delayed the onset of buckling.

The results of CAI assessment are summarised in Table 7-7. Here it can be seen that the samples experienced around a 50% reduction in compressive strength after an impact of 6J. There was no evidence that the healed samples were able to recover any mechanical strength after a damage event at this impact energy. Figure 7-31 shows a graphical representation of these results. It can be seen from these figures, that the impact energy absorbed by empty HGF was slightly higher than that of the plain baseline laminate. In particular HGF located at four interfaces absorbed approximately 15% more energy. It was also observed that the HGF located at four interfaces absorbed more impact energy than other HGF configurations located at two interfaces. However, this effect was less evident with resin filled HGF (healed). Therefore, there is a suggestion that increasing the number of interfaces of HGF and more specifically locating HGF closer to the impact surface increases the energy absorbed by HGF fracture/crushing. However, when HGF are filled with healing resin the difference in energy absorption between configurations is reduced. This suggests that the interaction between HGF location, HGF configuration, HGF content and the impact event is complex and requires additional investigation to improve the understanding.

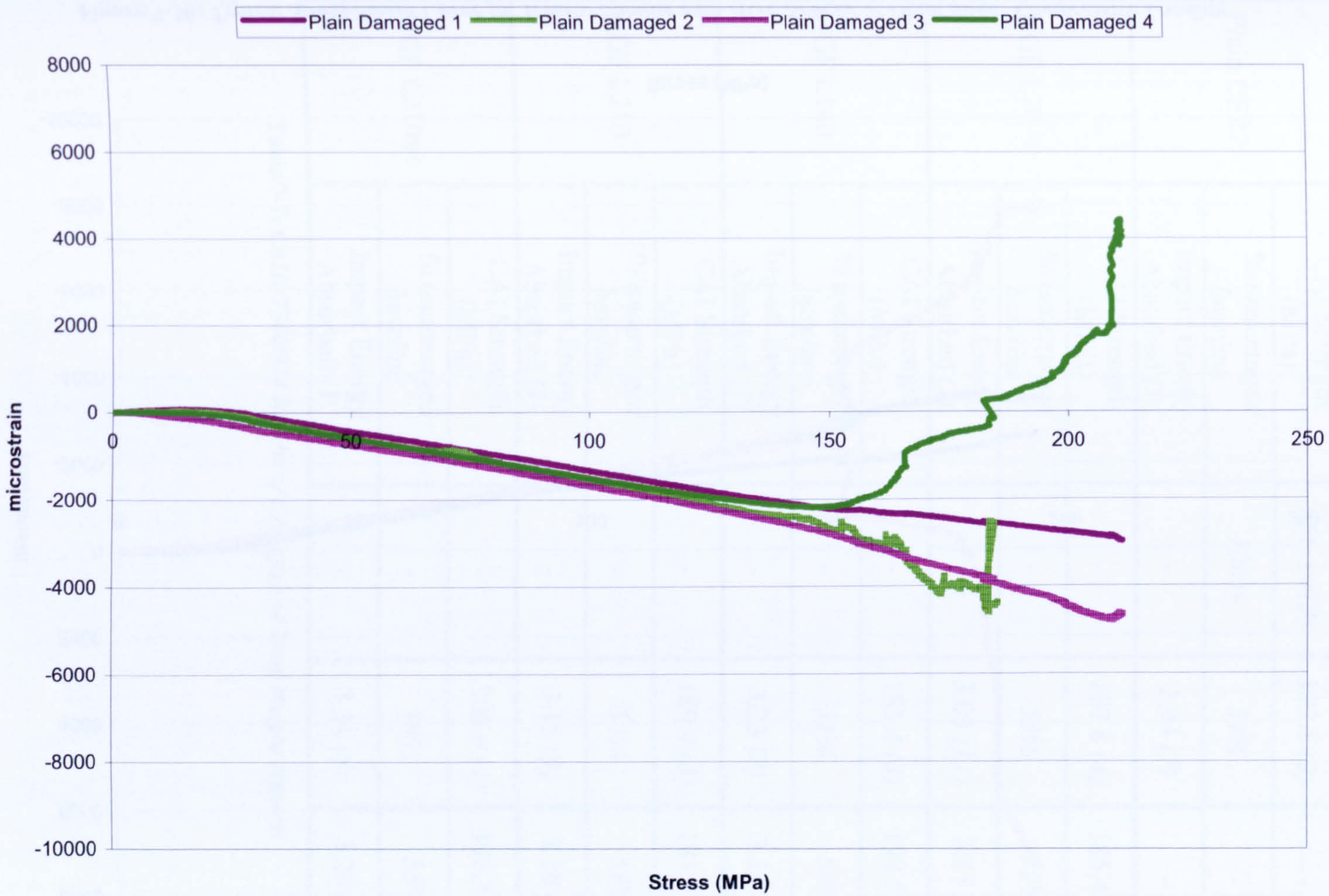

Figure 7-29: ***Typical Stress-Strain Curve for Damaged Sample with No HGF under Compressive Loading***

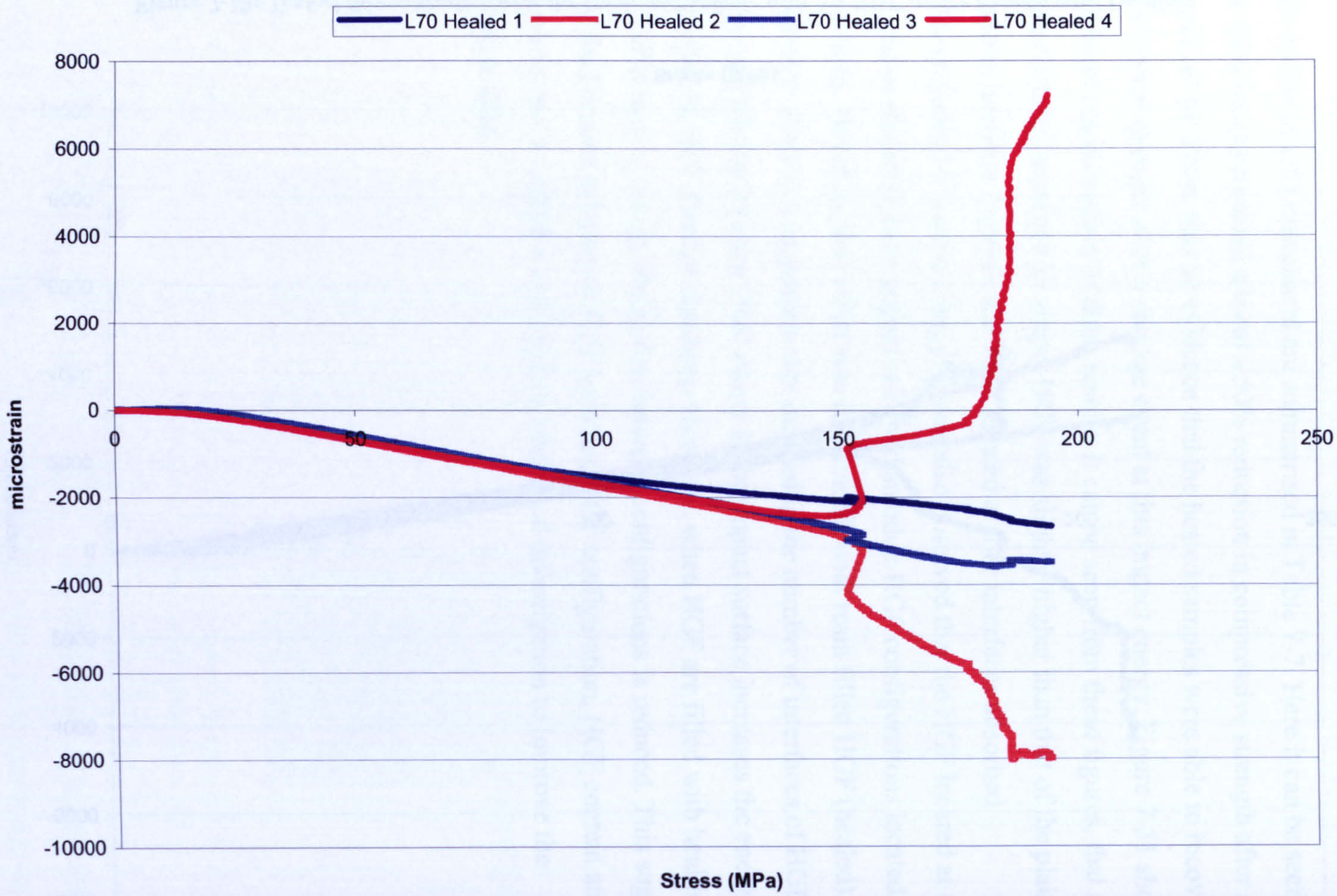

Figure 7-30: ***Typical Stress-Strain Curve for Healed Sample with HGF Spaced at 70μm under Compressive Loading***

Specimen		Undamaged (CV%)	Damaged (CV%)	Healed (CV%)
Plain CFRP	CAI Strength (MPa)	356.1 *(12)*	192.5 *(2)*	-
	% undamaged baseline	*100%*	*54%*	-
	Impact Energy Absorbed (J)	-	2.93 *(7)*	-
HGF L70	CAI Strength (MPa)	-	187.8 *(4)*	185.4 *(2)*
	% undamaged baseline	-	*53%*	*52%*
	Impact Energy Absorbed (J)	-	3.09 *(11)*	3.17 *(3)*
HGF L140	CAI Strength (MPa)	-	181.4 *(3)*	192.5 *(3)*
	% undamaged baseline	-	*51%*	*54%*
	Impact Energy Absorbed (J)	-	3.23 *(2)*	3.22 *(4)*
HGF L210	CAI Strength (MPa)	-	189.4 *(3)*	181.9 *(3)*
	% undamaged baseline	-	*53%*	*51%*
	Impact Energy Absorbed (J)	-	3.15 *(5)*	3.18 *(5)*
HGF L210x4	CAI Strength (MPa)	-	206.6 *(1)*	198.2 *(3)*
	% undamaged baseline	-	*58%*	*53%*
	Impact Energy Absorbed (J)	-	3.34 *(8)*	3.24 *(4)*

Table 7-7: ***CAI1: T300/914 Results of CAI after 6J Drop Weight Impacts***

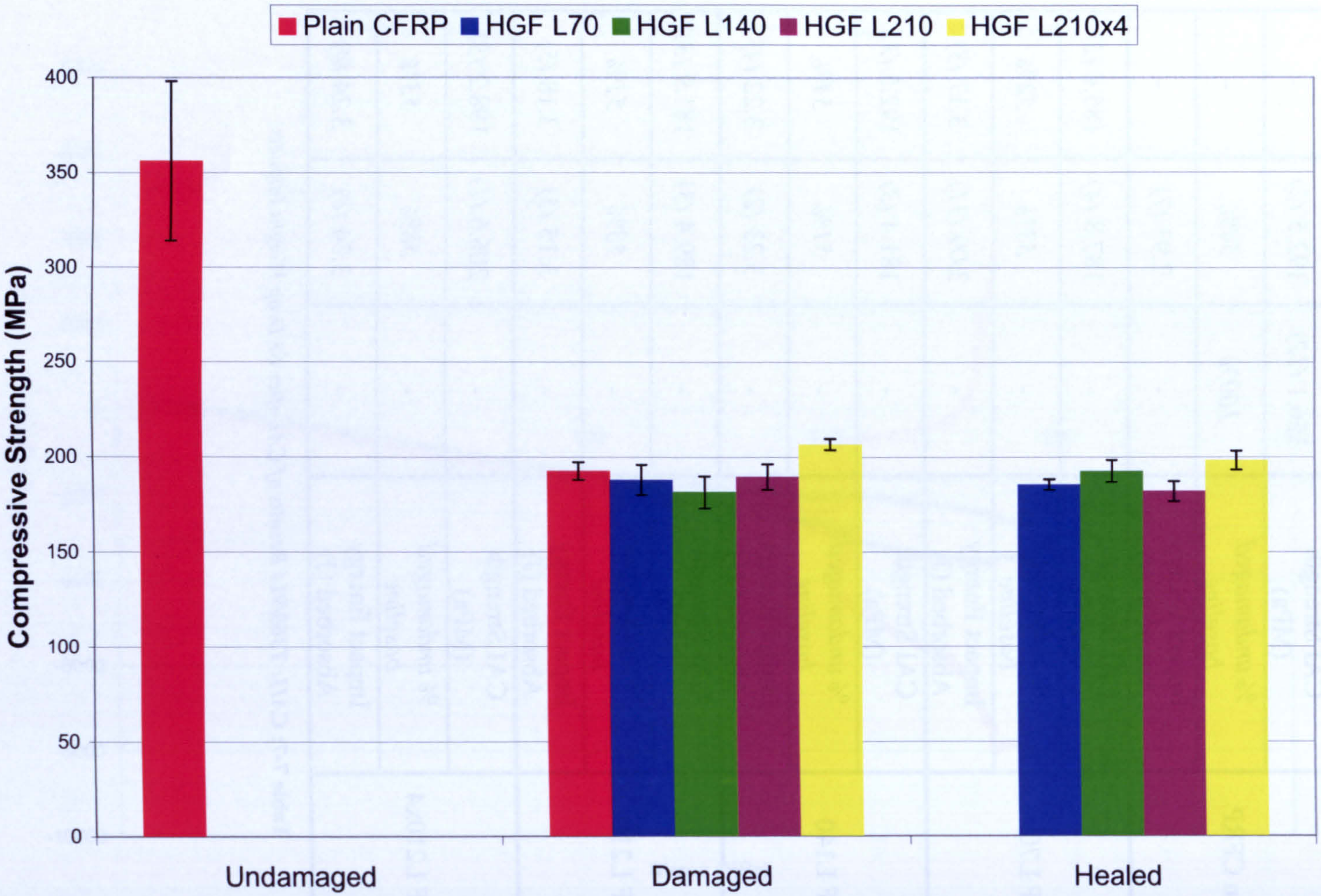

Figure 7-31: ***Graphical Representation of Laminate Performance in Response to Drop Weight Impact and Compressive Loading***

7.4 Fracture Analysis

The results from CAI assessment identified that the HGF laminate configurations proposed were not able to heal the damage level inflicted from a 6J low velocity drop weight impact. In order to identify why this was the case and possible improvements in laminate design, ultrasonic assessment and fractographic analysis were undertaken.

7.4.1 Ultrasonic Assessment

Ultrasonic assessment was undertaken by submerging the laminates in water and placing onto copper blocks in order to separate the target from the bottom of the water tank. Pulse-echo scanning, with a focussed transducer in a two dimensional plane above the laminate surface, was undertaken using ultrasonic waves at a frequency of 10MHz and controlled/recorded using Winspect software supplied by Utex Scientific. The digitiser frequency was set to 100MHz, the number of averages was set to 8 to minimise noise and the voltage level was set for each sample in order to ensure the maximum peak (front face) remained at two thirds of the set value. The transducer was set to 10MHz, with a repetition rate of 5kHz, output voltage of 50V and an amplifier gain of 23dB. In order to assess the laminates, three gates were defined within the software (Figure 7-23):

1. Front Face: *This was positioned at a time period that coincided with the reflected signal from the top surface of the laminate. Therefore, this was positioned at a higher voltage as it would generally be the strongest signal. The positioning of this gate was essential as the other gates were defined at an offset from its position.*
2. Middle: *This was positioned across the central portion of the laminate in order to pick up any reflections generated by internal damage within the laminate. Lowering the voltage threshold of this gate increased its sensitivity. At low voltage settings the fibres and matrix were detected, at higher settings only the larger delaminations were detected, therefore, its location was optimised to detect all damage within the laminate.*
3. Back Face: *This was positioned at a time period that coincided with the reflected signal from the back surface of the laminate. It was essential that this*

was accurately selected to eliminate any signals reflected from the bottom of the water tank.

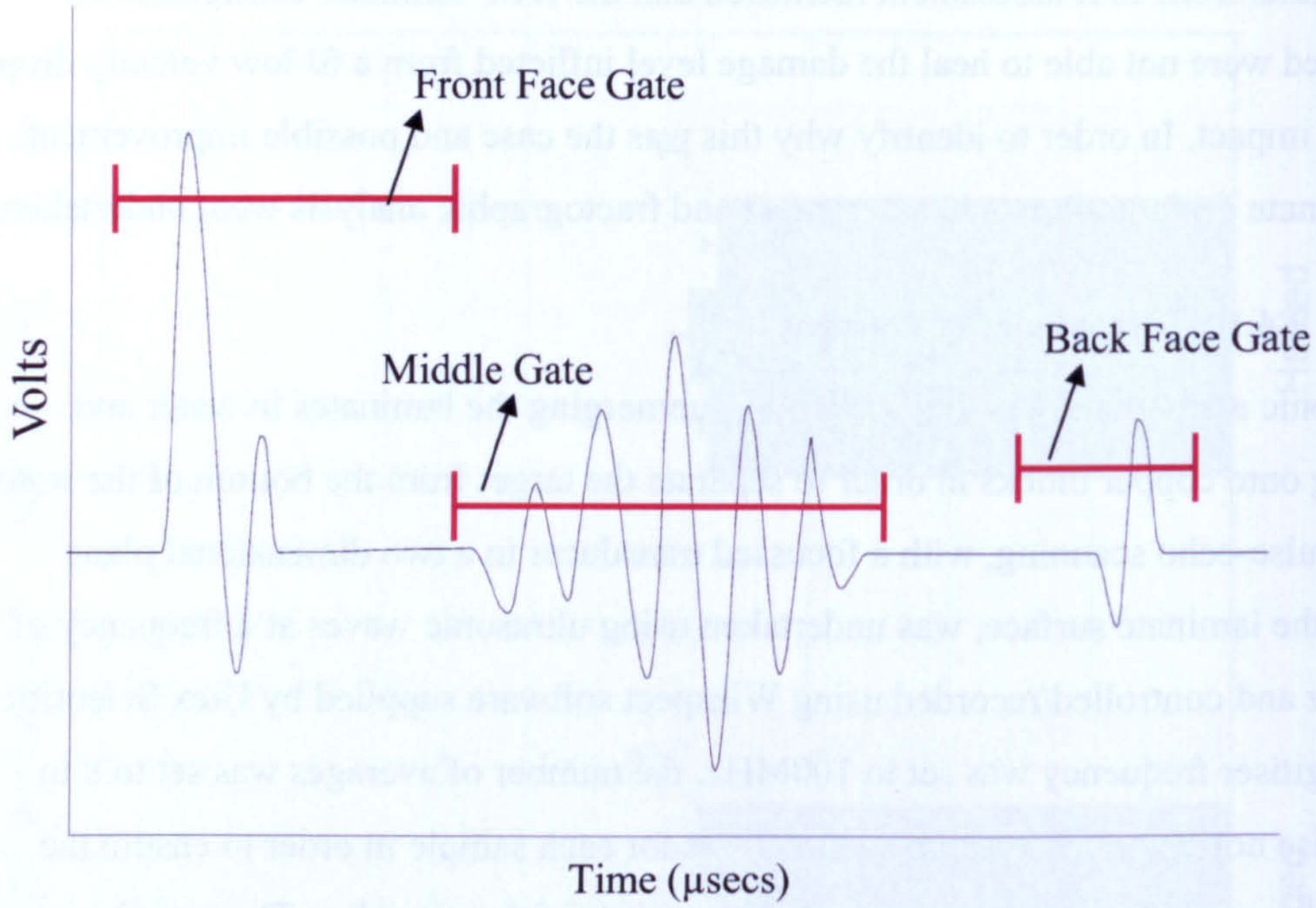

Figure 7-32: ***Gates for Signal Detection of Ultrasonic Assessment***

The ultrasound data can be displayed in a number of graphical representations. For the purposes of these investigations, the most useful for the visualisation of impact damage is 'time of flight'. This produces a graphical representation of each individual delamination and its location through the thickness of the laminate. However, this does result in a shadowing effect where delaminations towards the upper section of the laminate hide the delaminations located below them. Generally this is not a problem due to the 'pine tree' nature of impact induced damage which ensures that those delaminations located towards the back face extend beyond those located above. It can be seen in Figure 7-33a, that with a pine tree damage distribution, delaminations are still detected. However, Figure 7-33b) shows that smaller delaminations can be shadowed and evade detection for atypical damage distributions.

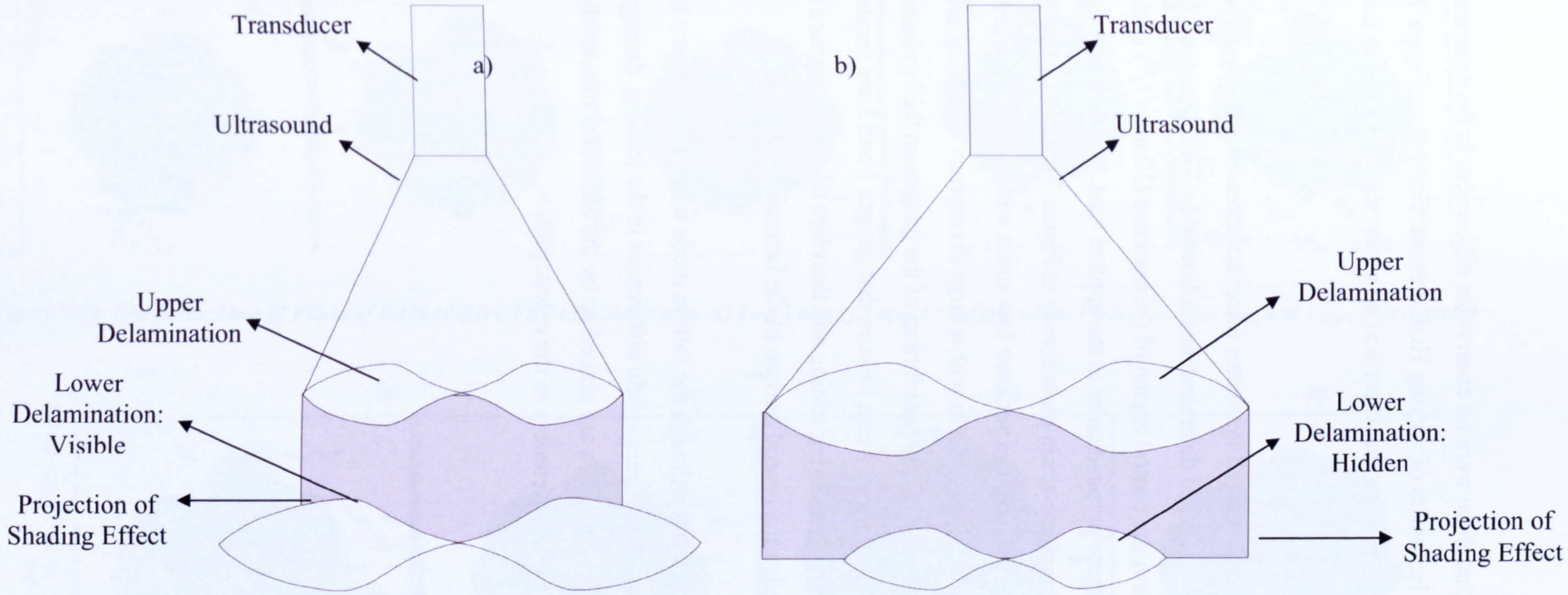

Figure 7-33: ***Demonstration of the Potential Shading Effect of Ultrasonic Time of Flight showing a) Lower Delamination Visible Beyond Shading Effect of Upper Delamination b) Lower Delamination Hidden by Shading Effect of Upper Delamination***

Figure 7-34 shows that there were no observable differences in the delamination areas or distribution with laminates of varying HGF content. Comparing Figure 7-34 and Figure 7-35 it can also be seen that there was no observable reduction in delamination due to a healing cycle.

Figure 7-36 shows that damaged laminates under compressive loading fail due to the propagation of impact induced delaminations followed by local buckling. The local buckling occurs within the central region of the laminate (30mm$\approx^{1}/_{3}^{rd}$) as the delaminations propagate perpendicular to the applied load. This is reinforced by the trends observed in the stress-strain plots shown in Figure 7-29 and Figure 7-30. These show that strain gauges 1 and 3 experience low strain with a small divergence, and gauges 2 and 4 experience high strain with a large divergence indicating local buckling. This is explained by the positioning of the gauges on the laminates as indicated in Figure 7-28, where it can be seen that gauges 1 and 3 are located towards the top edge of the laminate during testing and therefore do not experience the local buckling experienced at the central portion of the laminate.

Figure 7-36 also shows that although the failure mode under compressive loading is similar, each laminate experiences subtle differences in the loading, damage formation and propagation which are picked up by the ultrasonic time of flight images and represented by subtle differences in the colour plots.

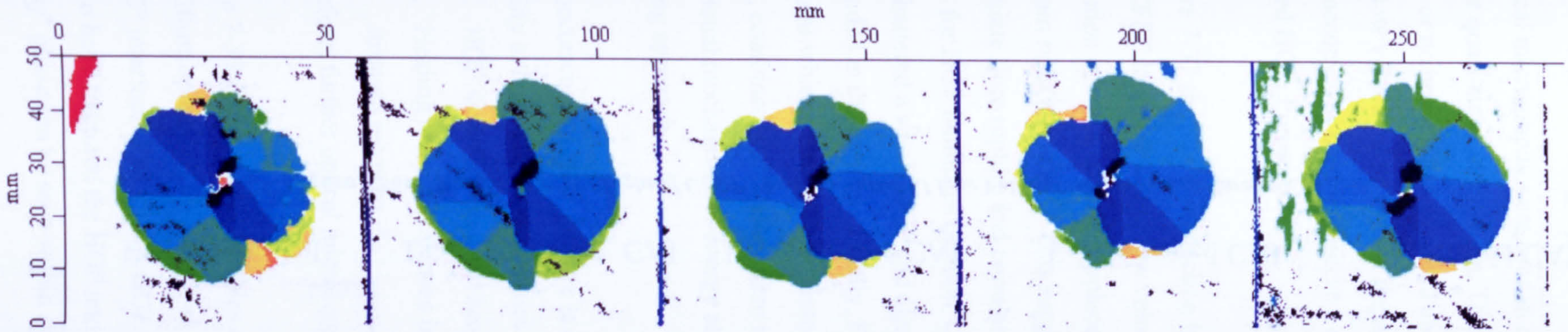

Figure 7-34: ***Ultrasonic Time of Flight of DAMAGED CFRP Laminates after 6J Low Velocity Impact Configurations Plain, L_{70}, L_{140}, L_{210} and L_{210x4} (left to right)***

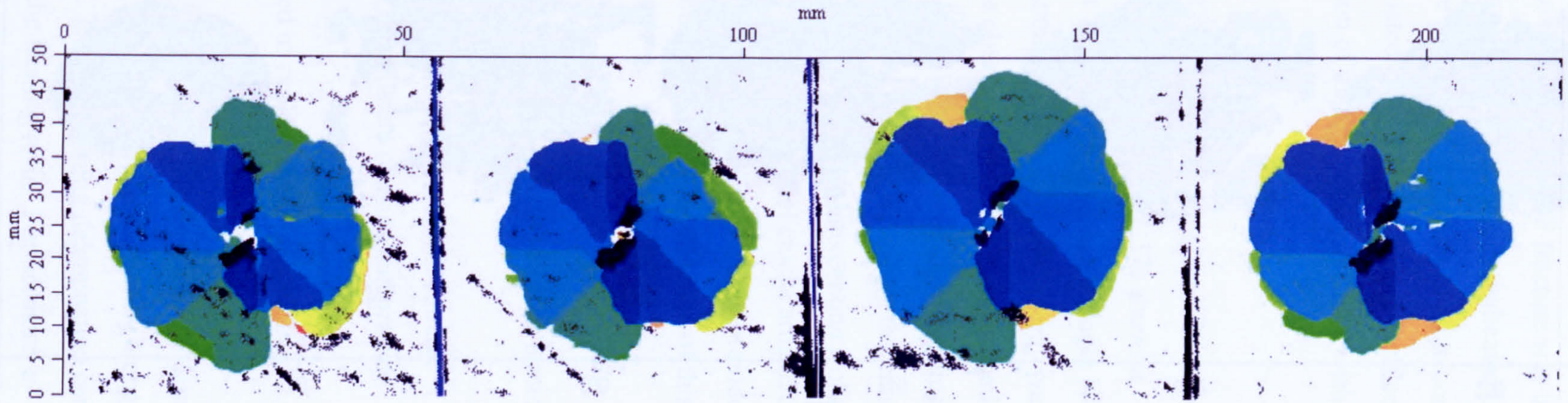

Figure 7-35: ***Ultrasonic Time of Fight of HEALED CFRP Laminates after 6J Low Velocity Impact Configurations Plain, L_{70}, L_{140}, L_{210} and L_{210x4} (left to right)***

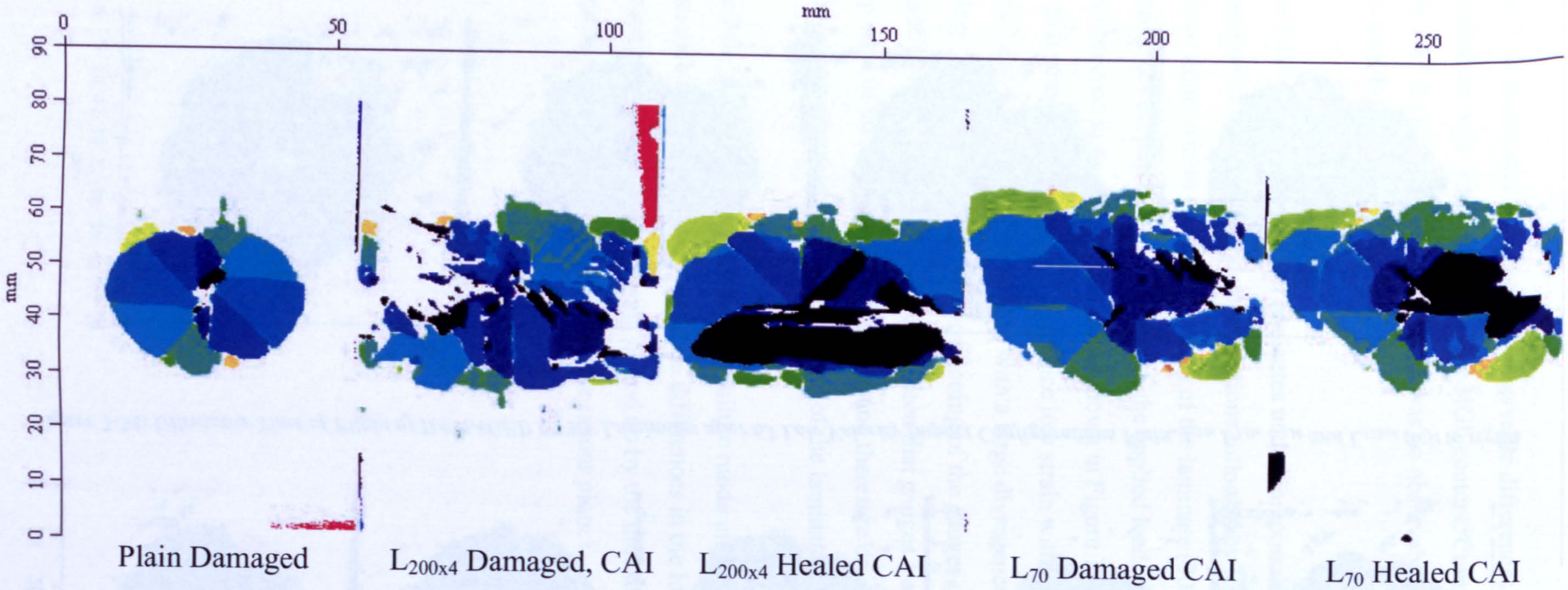

Figure 7-36: ***Ultrasonic Time of Fight of CFRP Laminates after 6J Low Velocity Impact and Failure by CAI***

7.4.2 Fractography

Optical micrographs were used in chapter 6 to identify that HGF fracture was initiated under quasi-static indentation. The CAI testing results reported here indicated that little or no healing had occurred and therefore it was necessary first of all to confirm that low velocity drop weight impact had initiated HGF fracture. Scanning Electron microscopy was used to observe a cross section of impact damaged CFRP with 70μm spaced HGF, Figure 7-37.

Figure 7-37 shows the interaction between HGFs and propagating crack fronts within the CFRP laminate due to low velocity impact damage. Figure 7-37a shows a reduction in crack opening displacement after a crack passes though a single HGF (bottom right to top left). This suggests that some of the propagation energy was used to initiate fibre rupture and correlates with the observed reduction in delamination areas for HGF laminates (section 7.2.3). Figure 7-37b shows how a propagating crack has shattered a single HGF and clearly illustrates the significant energy that must be expended in this process. Finally, Figure 7-37c shows a crack intercepting a cluster of HGFs at which point it divides into both fibre/matrix interfacial cracks around the HGF, combined with further fibre rupture. The rupture of HGF not only provides an additional mechanism for energy absorption but is critical to the function of this self-healing approach.

The occurrence of HGF fracture is evident and thus is not the cause of the laminate's inability to heal. Other possibilities were that:

1. HGF were fractured but healing resin was unable to infiltrate damage
2. Healing resin volume was insufficient to infiltrate damage and provide strength recovery

Therefore, further optical microscopy was used to explore these possibilities.

Figure 7-38 shows some examples of delaminated interfaces within a CFRP laminate with 70μm spaced HGF. Images a), b) and c) show delaminations passing along the -45°/0° interface at which the HGF is located. The propagating delamination can be seen to have fractured the HGF and released the healing resin. Furthermore, a 'glassy' phase can be seen within smaller shear cracks and delaminations which

would suggest that the healing resin has infiltrated these regions. Figure 7-39a) shows an example of this 'glassy' phase in the central delamination alongside small shear cracks. However, it can be seen that significant dark regions remain in the delaminations where it would appear the healing resin was unable to infiltrate. This may be attributed to the distance between delaminated surfaces being too large to facilitate capillary action. Furthermore, there are examples in Figure 7-39b) of HGF that contain cured healing resin. This may be a result of two outcomes:

1. Insufficient surface forces to draw the resin from the ruptured HGF
2. The HGF may have been damaged but not opened; therefore the resin was unable to escape.

Figure 7-39c) shows one ruptured HGF adjacent to another that is intact. The ruptured HGF appears to have released sufficient resin to infiltrate the surrounding damage. It should be noted that all these images are two dimensional 'snapshots' of a three dimensional material. Therefore, it may be that un-damaged HGF observed here are actually fractured at a different location along their length. Furthermore, the damage that appears to have been infiltrated by resin released from local HGF may have been infiltrated by resin released by multiple fibres at different locations.

Figure 7-40 shows scanning electron microscopic images of larger delaminations. Again, a 'glassy' phase, characteristic of a cured resin, can be seen between the delaminated surfaces but of insufficient volume to adequately fill the region. In particular Figure 7-40c) shows a formation within a delaminated surface that could only be formed by the presence of a viscous fluid after the formation of damage and is not characteristic of a brittle fracture surface.

Another possible factor in the laminates inability to heal is evident in Figure 7-41 and Figure 7-42. Here it can be seen that significant damage is present at the back face of the laminates after a 6J impact event. Effectively the laminates are 'saturated' with damage which is a consequence of using 6J impact energy with the specified impact boundary conditions. The 40mm impact window outlined in section 2.3 effectively pins the delaminations that would naturally continue extending beyond this boundary if unconstrained. The result is that the impact energy is dissipated by increased

opening of the delaminated surfaces and increased matrix shear cracks as the back face becomes saturated with damage.

7.4.3 Failure Modes

The failure modes characteristic of each laminate state was observed using ultrasonic assessment in section 4.1. These findings are reinforced in Figure 7-43, where it can be seen that undamaged samples failed by edge brooming and damaged samples failed by central buckling. More specifically, Figure 7-43a) highlights the location of the buckling mode that leads to failure. Here it can be seen that the impact induced delaminations have propagated sufficiently to induce local buckling of the sample and therefore the compression strength is reduced compared to the undamaged laminate as reported in section 3. Figure 7-43b) highlights the location of failure for the undamaged laminate. It can be seen that edge brooming occurs, characterised by the separation of plies at the sample edge due to compressive loading. It was also noted that the healed samples all failed by central buckling which indicated that little or no healing was evident, as reported in section 3.

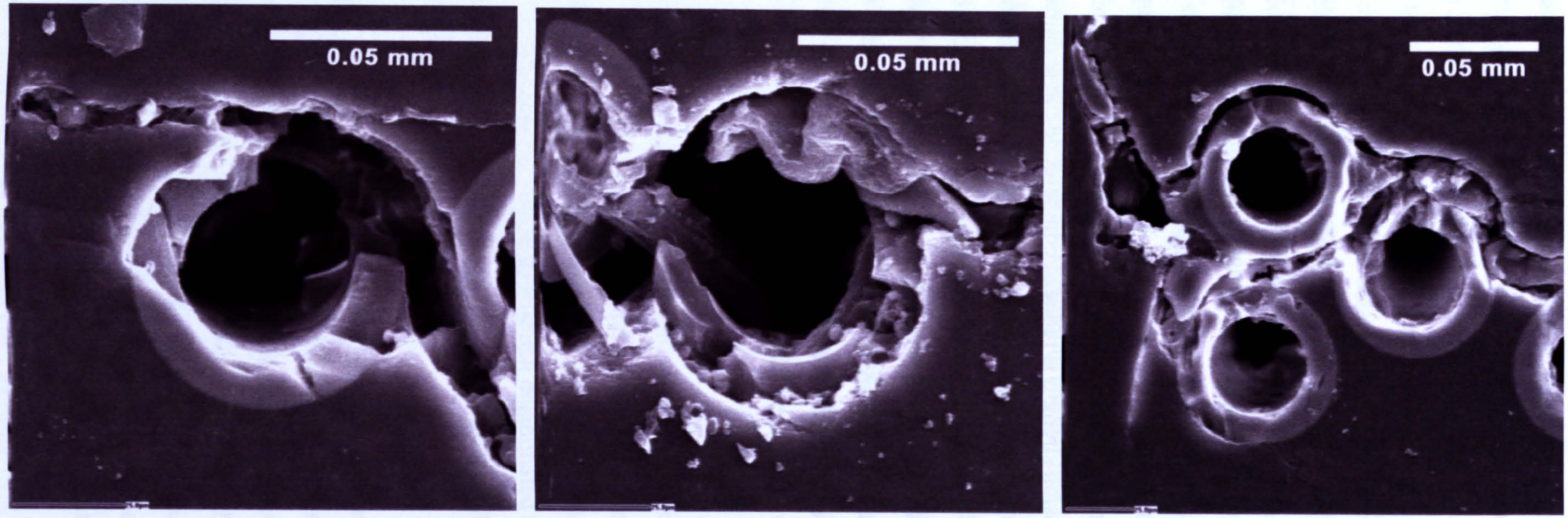

Figure 7-37: ***SEM Images of a) Energy of a Propagating Delamination Dissipated as Crack Passes Around HGF, b) Crack Passing Directly Through HGF c) Crack Passing Around and Through Cluster of HGF***

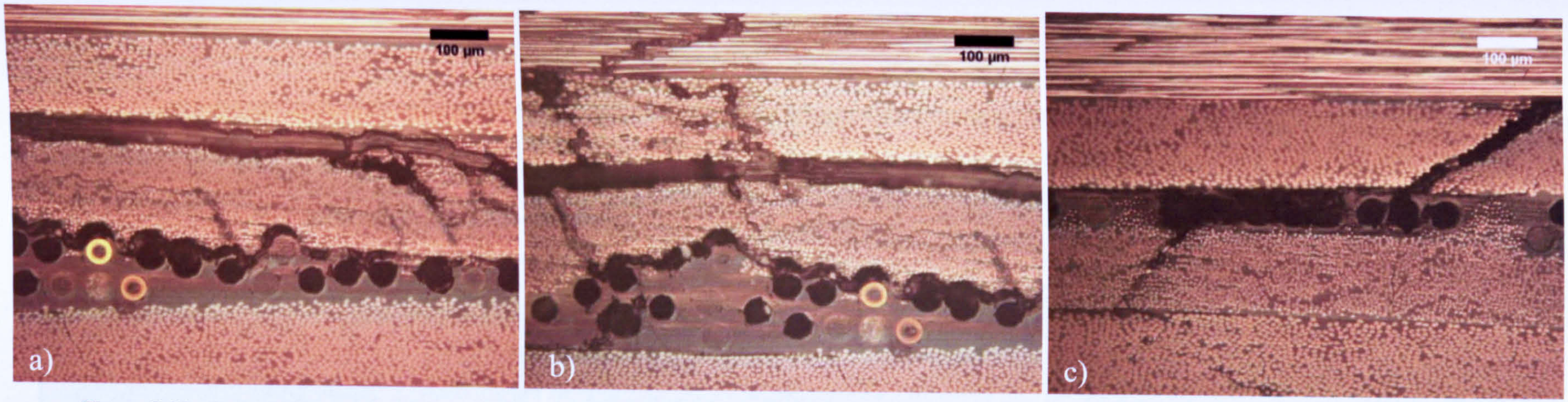

Figure 7-38: ***Optical Micrograph of L_{70} Healed CFRP with 6J Impact Induced Damage Showing HGF Fracture and Incomplete Filling of Fracture Plane***

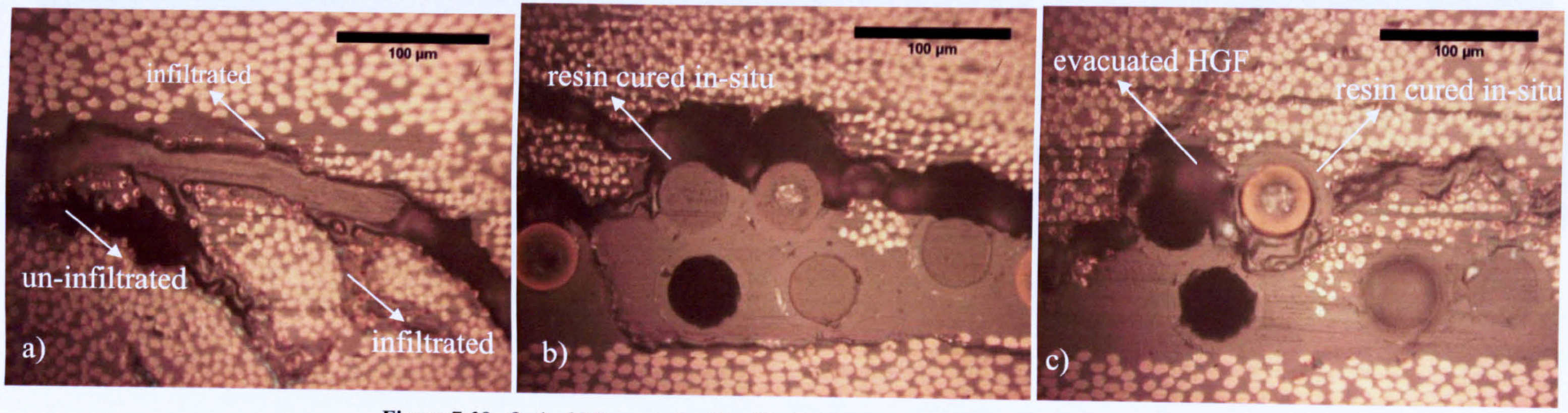

Figure 7-39: ***Optical Micrograph of L_{70} Healed CFRP with 6J Impact Induced Damage***

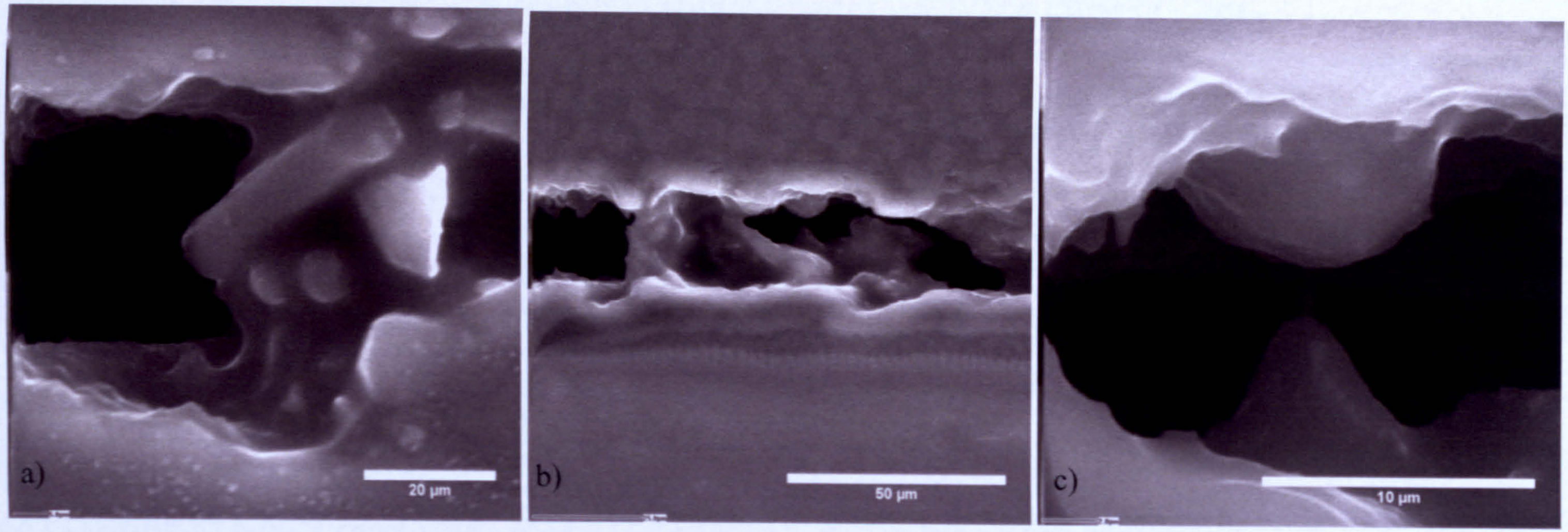

Figure 7-40: ***SEM Images of Fracture Plane after Drop Weight Impact and Compressive Buckling***

Figure 7-41: ***Through Thickness Damage Distribution of L_{70} Damaged after 6J Impact***

Figure 7-42: ***Through Thickness Damage Distribution of L_{70} Healed after 6J Impact***

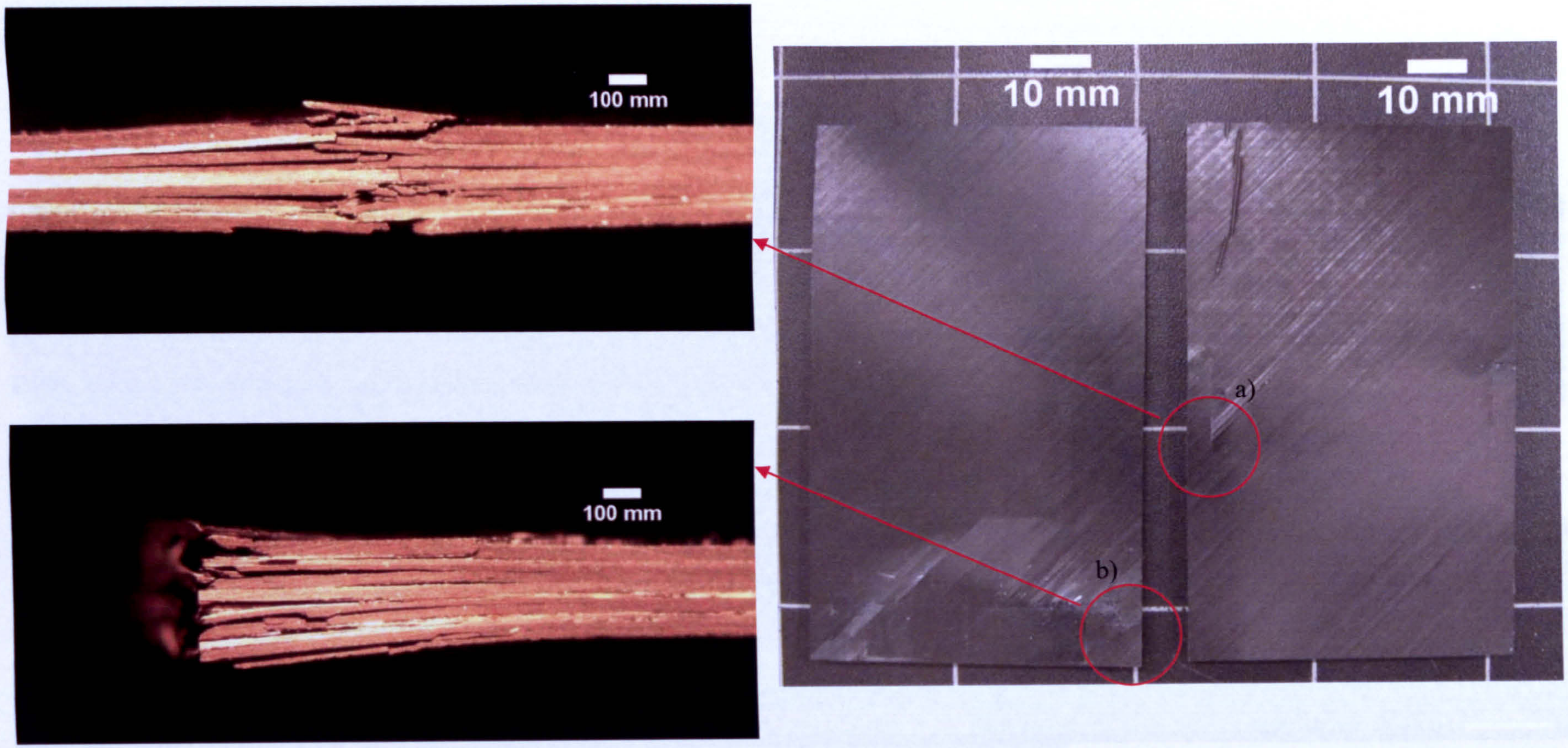

Figure 7-43: ***Failure Modes of Laminates during CAI Assessment for a) Undamaged: Edge Brooming and b) Damaged: Central Buckle***

7.5 Discussion

The testing conducted in this CAI assessment has shown no evidence of strength recovery from a 6J drop weight impact after a healing cycle. The configurations considered were HGF L_{70}, L_{140}, L_{210} placed at 2 interfaces and L_{210} placed at four interfaces. The possible reasons for this failure and possible solutions are discussed below.

1. Impact Energy Level

It was identified in section 7.2.3 that the impact window boundary conditions significantly influence the damage profile within the laminates by preventing the propagation of impact induced delaminations beyond 40mm. This causes a divergence from the usual 'pine tree' damage distribution to a profile that should not be considered as BVID. It was seen that above 4J impact energy, the delaminations towards the front face of the laminate begin to propagate to the same dimension as those towards the back face which had already reached this boundary. This was indicative of the shift in energy absorption mechanisms experienced during the impact events. Delaminated surfaces were driven further apart and an increase in delamination and matrix shear cracking towards the back face resulted in the laminates becoming saturated with damage. Therefore, it is proposed that a less demanding impact energy is selected in the next stage of the testing program.

2. Insufficient Resin Volume

The images shown in sections 7.4.1 and 7.4.2 have highlighted that the volume of healing resin stored in the various laminate configurations was insufficient to address the volume of damage created after 6J impacts. The healing resin was seen to infiltrate small delaminations and matrix shear cracks which were not otherwise detectable using ultrasound. There was evidence that healing resin did infiltrate larger delaminations but with insufficient volume to re-attach the two surfaces. To address this, a new configuration must be developed to increase the HGF content and therefore the volume of resin can be stored but without detrimental effect on the host laminate. The revised HGF configuration should ideally be able to infiltrate a value approaching 100% of the predicted damage volume (*Volumetric Assessment*) summarised in Table 7-3, as was seen for the successfully healed samples in Chapter 6.

3. Insufficient HGF Fracture

Placement of HGF at only two interfaces does not ensure that sufficient HGF are fractured upon impact. Therefore, the revised HGF configuration should be distributed over an increased number of ply interfaces to improve the distribution of healing resin, and reducing the reliance on damage connectivity to provide a path through which the resin can infiltrate. It cannot be assumed that the damage network is sufficiently connected nor can it be assumed that the resin will travel significant distances within the damage. Increasing the number of interfaces for HGF was seen to reduce the delamination area after impact. However, manufacturing issues resulted in poor embedment when HGF was not overlaid directly onto 0° plies which must be considered for any revised HGF configuration.

4. Inadequate Adhesion

It cannot be assumed that the healing resin (Cycom 823) is sufficiently compatible with Hexcel 914 matrix resin to ensure adequate adhesion to inhibit further crack propagation under compressive loading. However, this healing resin was shown to provide 97% recovery of strength under flexural loading in earlier studies (Chapter 6). Thus, it does not seem unreasonable to continue using this resin system for further studies.

The solutions proposed will be incorporated into the laminate design and assessment utilised in Chapter 8. It is clear from the results presented in section 3 and the points of discussion made above that a refined HGF configuration is required. This will be considered in Chapter 8, in order to achieve effective recovery of compressive strength after drop weight induced damage similar to the excellent recovery reported in flexural strength after quasi-static indentation in Chapter 6.

8. Compression After Impact Assessment: Optimised HGF Content

Chapter 7 outlined the second stage of the development of a self-healing system for aerospace grade CFRP. However, none of the HGF configurations investigated were able to deliver any notable recovery in compression strength after a 6J low velocity impact event. A number of ways forward were established from this work, which will be addressed in this chapter of CAI assessment:

1. Decrease impact energy level
2. Increase resin storage volume
3. Increase incidence of HGF rupture under impact

8.1 Design

The host laminate material for the investigation was again T300 carbon fibre within a 914 epoxy matrix (Hexcel composites, properties found in Table 8-1). This was to ensure commonality with the previous stages of investigation. The cure schedule recommended by the manufacturer was 1 hour at 175°C at 700kN/m^2 (7 bar) pressure followed by a 4 hour post-cure dwell at 190°C. The lay-up chosen was $(-45°,90°,45°,0°)_{2S}$ which was a standard quasi-isotropic configuration and was consistent with that used in previous chapters.

	914 Resin	T300 CF
Tens Mod 0° (GPa)	3.9	235
Tens Strength 0° (MPa)	47.7	$4.41x10^3$
Tens Mod 90° (GPa)	3.9	-
Tens Strength 90° (MPa)	47.7	-
Comp Mod 0° (GPa)		-
Comp Strength 0° (MPa)	180	-
Elongation (%)	1.5	1.9

Table 8-1: ***Specification of Component Materials used for CAI Testing***

8.1.1 Optimised HGF Configuration

It was concluded in Chapter 7 that the HGF configurations investigated up to that point were unable to provide notable healing when subjected to drop weight impact followed by compression testing. Therefore, a new revised configuration was proposed which increased the resin storage volume and increased the number of interfaces at which HGF were located. The revised configuration combined two

different HGF densities and was intended to yield a HGF distribution better suited to the profile of the impact induced damage. This was achieved by weighting the number of HGF interfaces and density towards the back face whilst respecting the drive to minimise disruption within the host laminate. Therefore, 140μm HGF were placed at x_6 and x_4 and 70μm were placed at x_1, x_3 and x_5.

$$(-45°/90°/45°/x_5/0°/x_1/-45°/90°/45°/x_3/0°/0°/x_4/45°/90°/-45°/0°/x_6/45°/90°/-45°)$$

- Increased number of interfaces with HGF: For a given impact energy, this increases the number of HGF through the thickness which are exposed to the impact force thereby increasing the incidence of HGF rupture.
- Tailored HGF distribution: An increased concentration of HGF in regions of the laminate exposed to greatest expected damage. It can be seen that towards the back face, the delamination areas are larger and the crack opening displacement between delaminated surfaces is increased. Therefore, increasing the HGF concentration in this region provides a locally increased resin volume. Regions towards the front face experience less damage and thus require lower HGF concentrations thereby limiting the local disruption to the laminate. This approach also reduces reliance on damage connectivity to transport healing resin from the storage site to the damage sites.

Figure 8-1 shows a cross sectional image of a laminate damaged by 3J of drop weight impact. It can be seen that there is a significantly larger proportion of damage located below the neutral axis (NA) as indicated by the dashed line. This confirms the requirement to increase the concentration of HGF within this section of the laminate.

Details of the Configuration assessment tool reported in this section can be found in Chapter 5, section 2.1, the results of which are presented in Table 8-2. Here it can be seen from that the revised design is predicted to give a laminate which essentially has the same mechanical properties as a laminate with HGF spaced at 70μm on four ply interfaces. However, the revised HGF configuration has the benefit of providing a more effective distribution of resin storage, at the risk of introducing asymmetry into the laminate.

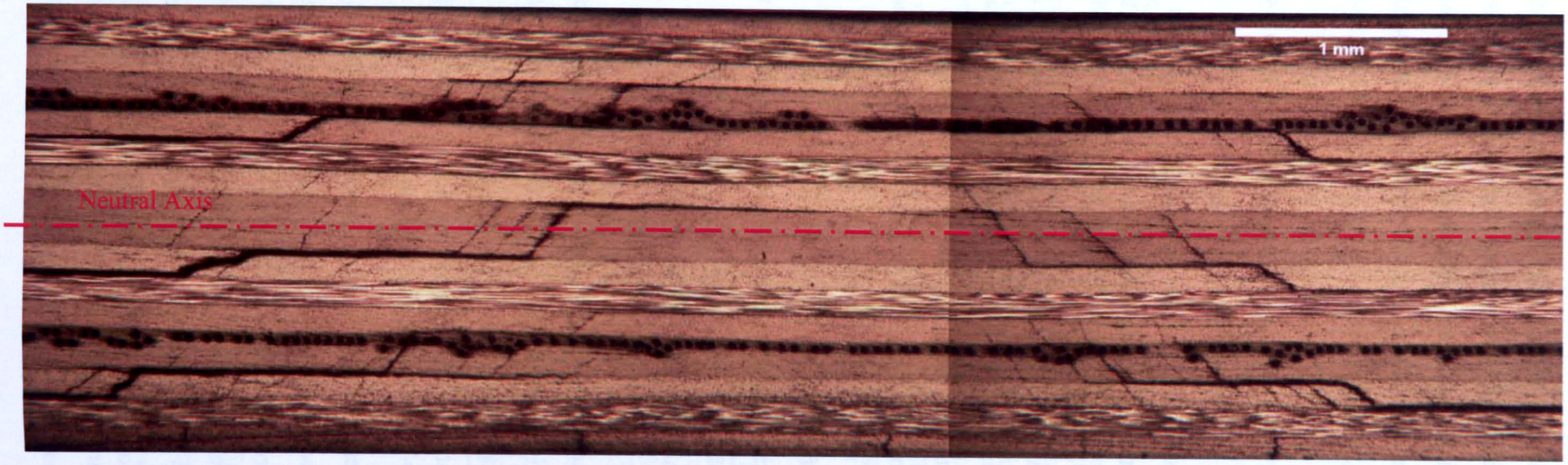

Figure 8-1: ***Impact Induced Damage Distribution for 3J Incident Energy (l_{70} HGF @ 2 Interfaces)***

HGf Spacing (μm)	No. Interfaces	CF reduction in 0° (%)	Global CF reduction (%)	New V_{CF} (%)	Stiffness (%)			Resin Vol	Resin V_{FR}
					E_x	E_y	E_{xy}		
70	3	19	5	61	85	99	99	296.2	2.42
140	2	6	2	63	95	100	100	98.61	0.80
Tot	5	26	7	60	80	98	98	394.8	3.23
70	4	26	6	60	80	98	98	395	3.23

Table 8-2: ***Prediction of Laminate Properties for Refined Design and Equivalent Closest Equivalent L_{70} @ 4 Interfaces***

8.1.2 Volumetric Assessment

Ultrasonic 'time of flight' images were used to assess the damage created by low velocity drop weight impact. Figure 8-2 shows an example of one such image and the associated delamination diameters that were measured. The upper and lower delamination diameters were found to be 20mm and 30mm respectively. Details of how the energy level was determined can be found in section 2.3 and details of the ultrasonic 'time of flight' technique can be found in section 4.1.

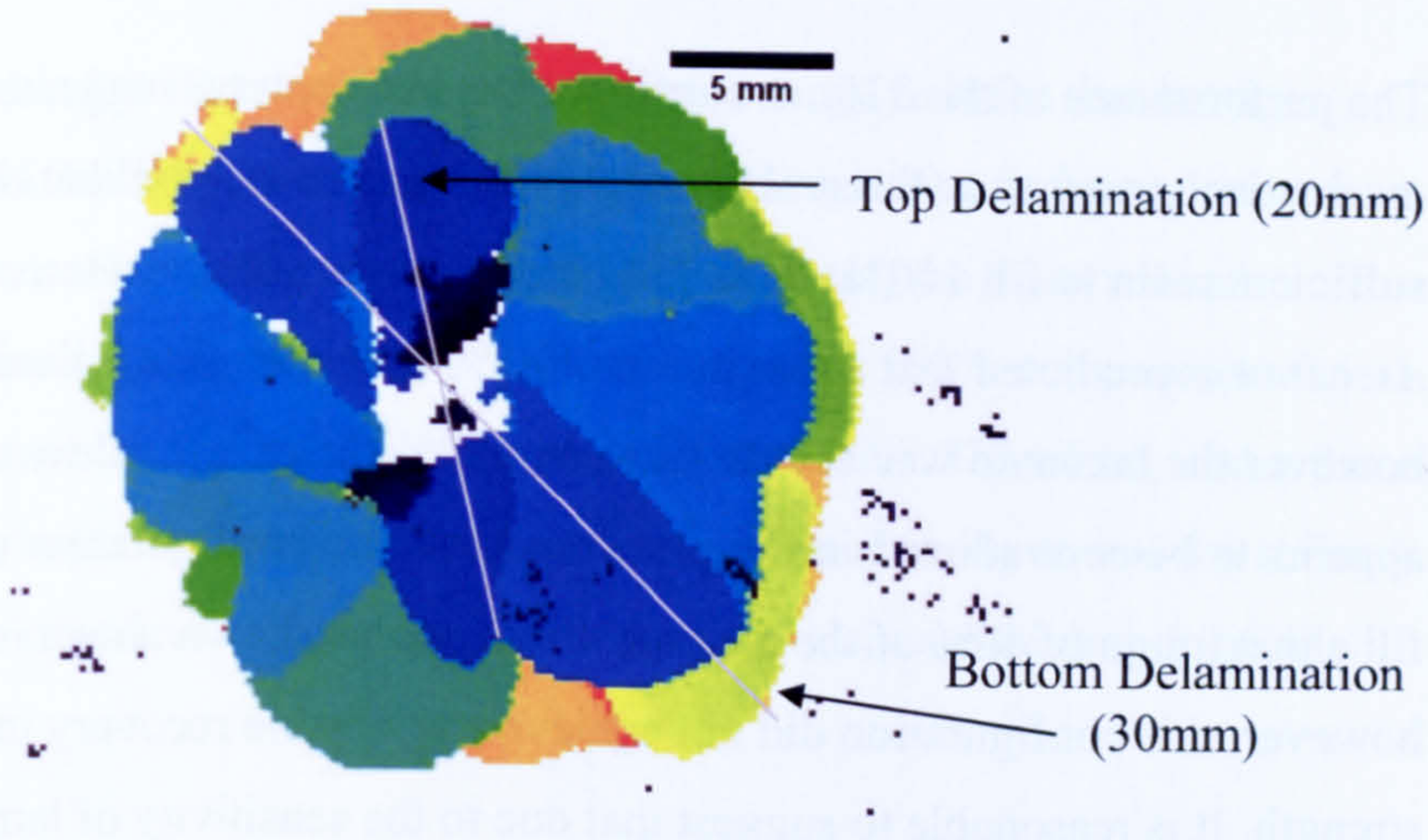

Figure 8-2: ***Ultrasonic TOF Image for 3J Impact of T300/914 CFRP***

The data extracted from the ultrasonic assessment is then used in the *Volumetric Assessment* tool, details of which are reported in Chapter 5, section 2.2. Below can be seen a comparative study between the HGF configurations considered in Chapter 7 (70, 140, 210) and the refined configuration considered herein (70/140). Table 8-3 presents the data for 6J impact energy and Table 8-4 presents the data for 3J impact energy. This allows a comparative assessment of the configurations considered, permitting estimations of the relative performance of the refined configuration considered within this Chapter.

HGF Spacing (μm)	No of Interfaces	HGF V_F (%)	HGF fracture (F_n) / Damage Fill (V_n) (%)					
			F_1	V_1	F_2	V_2	F_3	V_3
70	2	3	46	48	46	17	23	12
140	2	2	46	24	46	8	23	6
210	2	1	46	17	46	6	23	4
210	4	2	45	33	45	11	23	8
70/140	5	7	46	96	46	31	23	24

Table 8-3: ***CAI_1 Sample Data for Drop Weight Impact (6J) T300/914 Damage Vol. 189.344mm^3***

The performance of the 210μm configuration in Chapter 6 suggested that recovery of mechanical properties (flexural strength) is not necessarily reliant on providing sufficient resin to fill 100% of the predicted damage volume. Here, the *Volumetric Assessment* predicted that a maximum of 51% of the damage volume could be filled, however the laminate was able to provide a 12% recovery of flexural strength. This appears to be contradicted in Chapter 7 as the 70μm configuration was predicted to fill a maximum of 48% of the damage volume (also shown above in Table 8-3), however, this configuration did not achieve any notable recovery in compressive strength. It is reasonable to suggest that due to the sensitivity of laminates to impact induced delaminations under compressive loading, a higher percentage of the damage volume must be infiltrated by the healing resin (i.e. approaching 100%).

Although the combined 70/140μm HGF spacing was not tested at this level of impact energy (6J), it was included in Table 8-3 in order to compare its performance with the standard configurations. It can be seen that for condition 1. only the 70/140 configuration was able to provide a resin supply approaching 100% of the damage volume. Therefore it could be suggested that the refined configuration would be able to achieve a notable recovery of compressive strength under these impact conditions. However, for the reasons discussed in Chapter 7, it was decided to reduce the impact energy to 3J (also outlined below in section 2.3).

HGF Spacing (μm)	No of Interfaces	HGF V_F (%)	HGF fracture (F_n) / Damage Fill (V_n) (%)					
			F_1	V_1	F_2	V_2	F_3	V_3
70	2	3	39	56	39	16	20	14
140	2	2	39	28	39	8	20	7
210	2	1	39	18	39	5	20	5
210	4	2	39	37	39	11	19	9
70/140	5	7	40	109	40	31	20	27

Table 8-4: ***CAI_2 Sample Data for Drop Weight Impact (3J) T300/914 Damage Vol. 144.309mm^3***

It can be seen in Table 8-4 that decreasing the impact energy reduces the damage volume by 24% (144.309/189.334mm^3). Therefore, although the configurations are predicted to experience the same percentage of HGF fracture, the resin volume provided by the refined configuration (70/140μm) exceeded 100% compared to the 70μm configuration which was estimated to provide only 56%. Therefore, under these conditions (loading/impact energy), it was deemed appropriate only to test the refined configuration as the others were not expected to provide adequate healing for CAI.

8.2 Experimental

CAI testing was conducted in accordance with the standard ASTM D7137/D 7137M-05 [187] but modified in accordance with Prichard and Hogg [191]. Low velocity drop weight impact damage was inflicted according to ASTM D7136/D 7136M [207] again with modifications in accordance with Prichard and Hogg [191]. Specimen dimensions were defined in accordance with Prichard and Hogg [191] which resulted in a sample size of 89mm x 55mm x 2.6mm.

8.2.1 Laminate Manufacture

The laminate configuration to be assessed comprised of HGF distributed at five interfaces, more specifically with pitch spacing of 140μm at two interfaces above the midline of the stack and pitch spacing of 70μm at three interfaces below the midline of the stack. This arrangement posed some additional manufacturing challenges due to the quantity and asymmetric distribution of HGF.

It was proposed in Chapter 3, Figure 3.1 Global Workflow that the manufacturing process can be subdivided into four distinct sections. These will be considered here.

8.2.1.1 Initial Lamination

A 16 ply QI lay-up $(-45°/90°/45°/0°)_{2S}$ was selected as the laminate to maintain commonality with previous testing (Chapters 6,7). The specimen dimensions were 89mm x 55mm x 2.6 mm, which required a laminate panel of 210mm x 210mm to provide 6 replicates per laminate, with sufficient material for wastage during the preparation process (Figure 7-8).

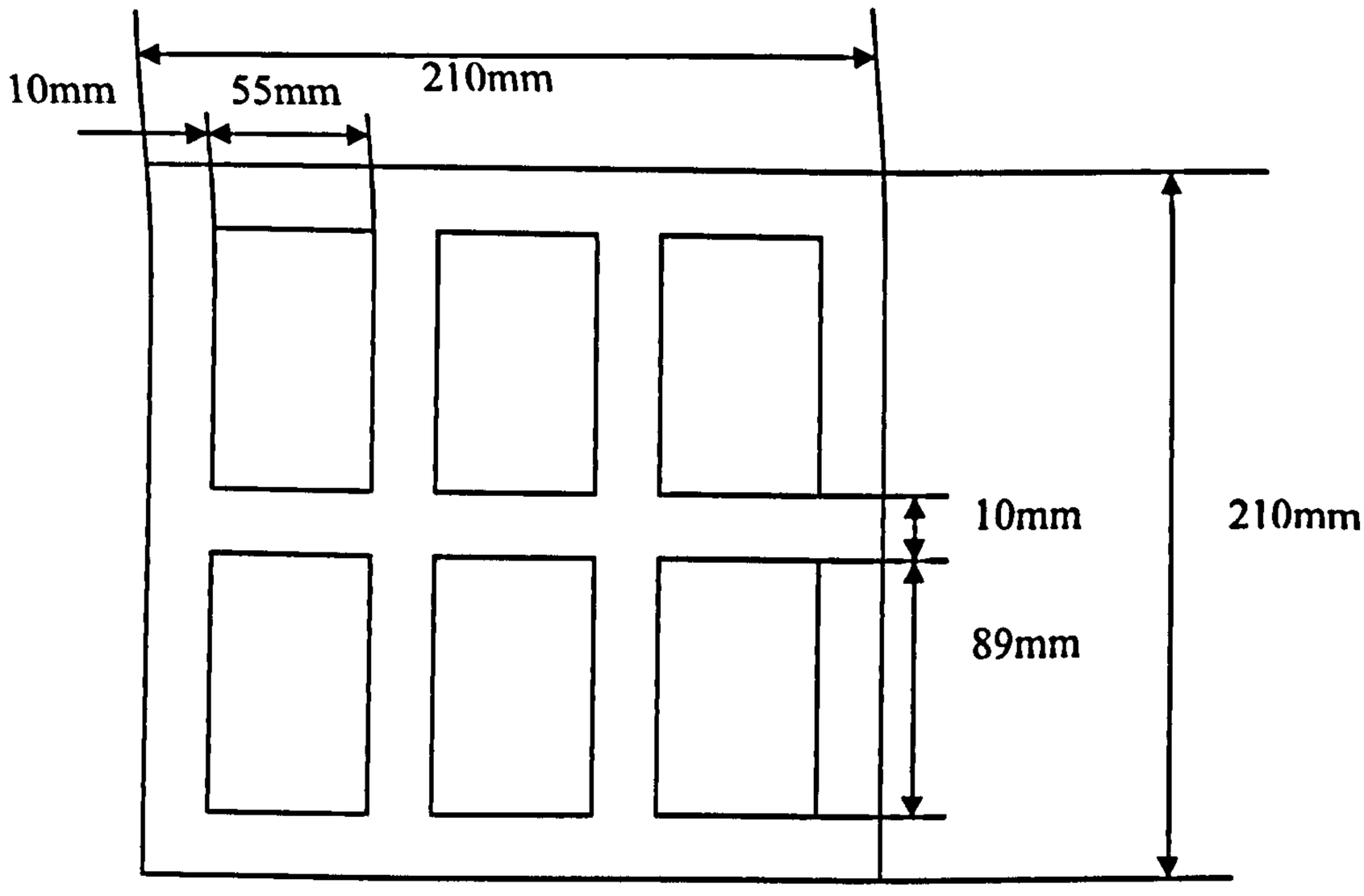

Figure 8-3: ***Schematic Diagram of Laminate Plates from which CAI Samples were Cut***

T300/914 carbon fibre/epoxy pre-impregnated tape was removed from storage at -18°C and given adequate time to defrost. Sufficient pre-preg was then cut to the required laminate size.

HGF of the required pitch spacing was overlaid directly onto uncured CFRP plies prior to lamination as per the procedure described in Chapter 6, section 2.1. To facilitate HGF incorporation, the laminate was divided into six sub-laminates as follows:

$$\underline{(-45°/90°/45°/\mathbf{HGF}_{(70^{1})}/0°/\mathbf{HGF}_{(70^{2})}/-45°/90°/45°/\mathbf{HGF}_{(70^{3})}/0°/0°/\mathbf{HGF}_{(140^{1})}/45°/90°/-45°/0°/\mathbf{HGF}_{(140^{2})}/45°/90°/-45°)}$$

1. $*(45°/90°/-45°/\mathbf{HGF}_{(L140^{2})})_{\text{Front Face 3}}$
2. $*(0°/45°/90°/-45°/\mathbf{HGF}_{(L140^{1})})_{\text{Front Face 2}}$
3. $*(0°/0°/\mathbf{HGF}_{(L70^{3})})_{\text{Front Face 1}}$
4. $*(-45°/90°/45°/\mathbf{HGF}_{(L70^{2})})_{\text{Back Face 3}}$
5. $(0°)_{\text{Back Face 2}}$
6. $(-45°/90°/45°/\mathbf{HGF}_{(L70^{1})})_{\text{Back Face 1}}$

***±45 ply directions reversed**

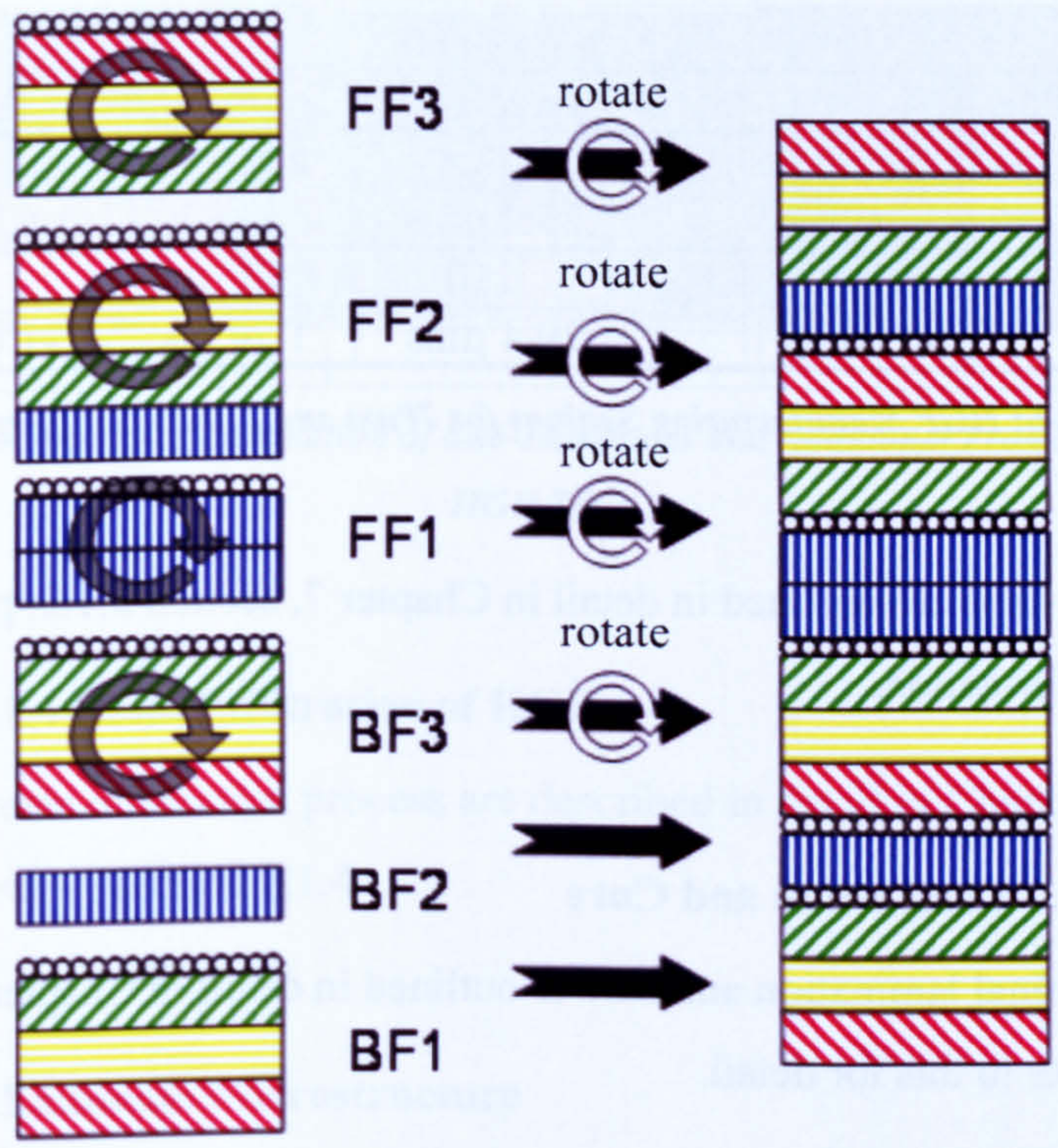

Figure 8-4: ***Construction of Self-Healing Laminate with HGF Embedded at Five Interfaces***

It can be seen that the sub-laminates denoted * have their ±45° plies reversed to ensure that the HGF could be drawn directly onto the 0° plies where possible. This improved the embedment of the HGF. Therefore, after HGF manufacture and during final lamination, the laminate sub-stack was rotated to be placed into the overall stack and form the final laminates as indicated in Figure 8-4. This action, translates all +45

in the sub-laminate to -45 in the final laminate and all -45 to +45, hence the requirement for these plies to be reversed in the sub-laminate stack.

The subsequent steps are outlined in detail in Chapter 7, section 2.1.1, please refer to this for more information.

8.2.1.2 HGF Manufacture

This HGF manufacturing process is described in detail in Chapter 7, section 2.1.. The settings for the manufacture of the two configurations are outlined in Table 7-5. It should be noted that these are average values, and the draw rate, in particular, was seen to vary during the HGF drawing process.

Configuration		OD	Feed Rate	Draw Rate	Pitch Rate
70µm	Setting	58	110	180	70
	Reading		29.4 μms^{-1}	1.3 ms^{-1}	-0.83 µm/rev
140µm	Setting	58	110	170	140
	Reading		29.4 μms^{-1}	1.24 ms^{-1}	-1.61 µm/rev

Table 8-5: ***HGF Manufacturing Settings for 70µm and 210µm Configurations***

The subsequent steps are outlined in detail in Chapter 7, section 2.1.2, please refer to this for more information.

8.2.1.3 Lamination and Cure

The process for final lamination and cure is outlined in detail in Chapter 7, section 2.1.3. Please refer to this for detail.

Figure 8-5 shows a number of images representing each stage of the final lamination and cure for the refined HGF configuration. Images 1-6 show the placement of each sub-laminate in sequence with the addition of PTFE film and breather fabric to protect the HGF tails as outlined in detail in Chapter 6 and 7, sections 2.1.3 and 2.1.4. Image 7 shows the placement of the caul plate to ensure the laminate had a smooth surface finish. Image 8 and 9 show the final layers of breather fabric being placed and then

the laminates bagged on the tool plate before being transferred to the autoclave to undergo the prescribed cure schedule (Chapter 6, section 2.1.3).

Figure 8-5: ***Photographs of Lamination of Sub-Laminates and Additional Protection Provided for HGF Tails***

8.2.1.4 Resin Infiltration of HGF

Details of the resin infiltration process are described in detail in Chapter 6, section 2.1.4 and Chapter 7, section 2.1.4.

8.2.2 Laminate Microstructure

Figure 8-6 shows the distribution of HGF within the optimised self-healing laminate configuration. Regions of uniformity can be observed for HGF spacings of 70μm (Figure 8-6b) and 140μm (Figure 8-6c). However, Figure 8-6a shows that HGF clumping is present for both 140μm Figure 8-7a),b) and 70μm Figure 8-7c) HGF densities. The cause of this defect can be attributed to an un-optimised manufacturing process which could be easily improved to achieve greater uniformity in HGF distribution. However, it was observed in Chapters 6 and 7 that HGF clumping observed at high HGF volume fractions (V_{fHGF}) could be beneficial by increasing the

damage tolerance of laminates. Furthermore, the selected HGF configuration dictated that HGF had to be overlaid onto non 0° plies for one sub-laminate and, as was identified in Chapter 7, section 2.2, this was shown to result in poor embedment of the HGF.

The individual specimen dimensions were measured for the analysis needed in CAI assessment. There was a small increase in the measured thickness of the specimens that contained HGF when compared to those without. The results can be seen in Table 7-6. However, such variations are fully accounted for in the data reduction methods for CAI.

		Average (mm)	S.D (mm)
HGF	Width	54.92	0.01
	Height	89.02	0.05
	Thickness	2.55	0.01
Plain	Width	55.07	0.13
	Height	89.05	0.14
	Thickness	2.44	0.03

Table 8-6: ***Summary of Average Sample Dimensions for CAI Assessment for Comparison between laminates With and Without HGF***

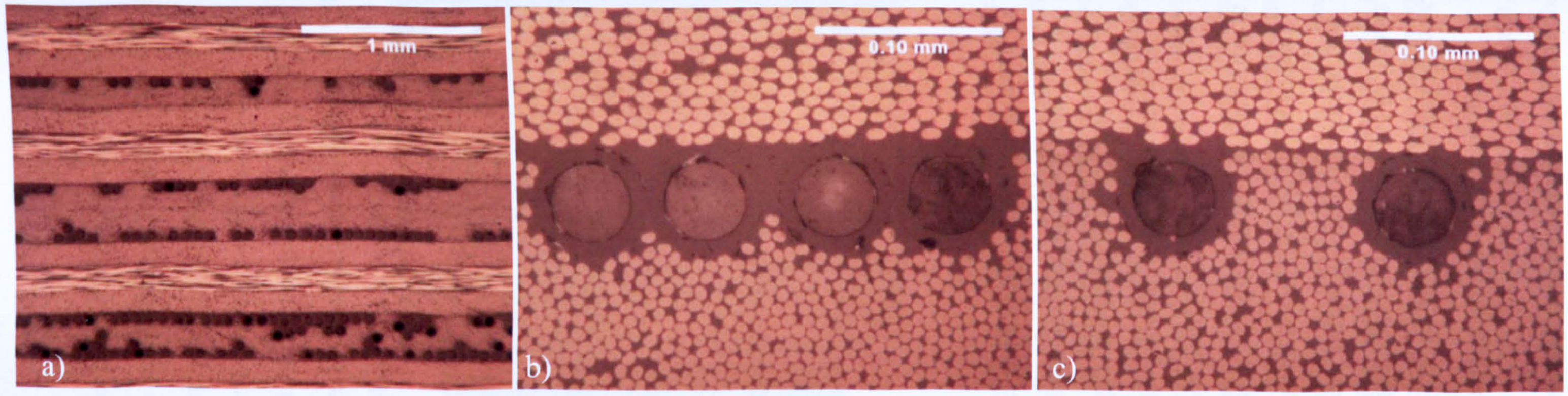

Figure 8-6: ***HGF at five interfaces showing a) overall HGF distribution and optimal spacing at b) 70μm and c) 140μm***

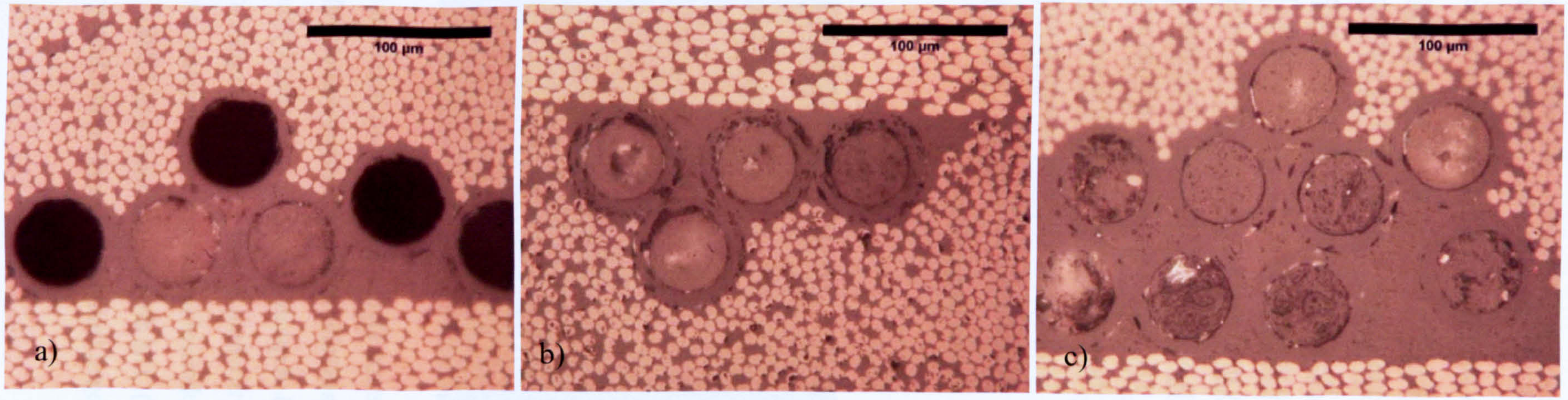

Figure 8-7: ***Laminate with HGF at Five Interfaces showing Ineffective Embedment of a),b) 140μm and c) 70μm Spaced HGF***

8.2.3 Drop Weight Impact Testing

Impacts were imparted to a sample laminate in order to re-assess the appropriate energy level for creating appropriate damage, using the same boundary conditions as outlined in chapter 7, section 2.3. It was concluded from chapter 7 that the 6J impact energy level was inappropriate for CAI assessment, primarily due to the interaction between the damage profile and the impact boundary conditions (BC). The impact window produced a clamped condition which restrained the laminate deformation in response to impact (Figure 8-8), the consequences being:

1. The impact boundary conditions suppressed delamination propagation, therefore the damage profile was not truly representative of BVID
2. The laminates became saturated with damage towards the back face
3. Delaminated surfaces were driven further apart as the impact force began to induce penetration.

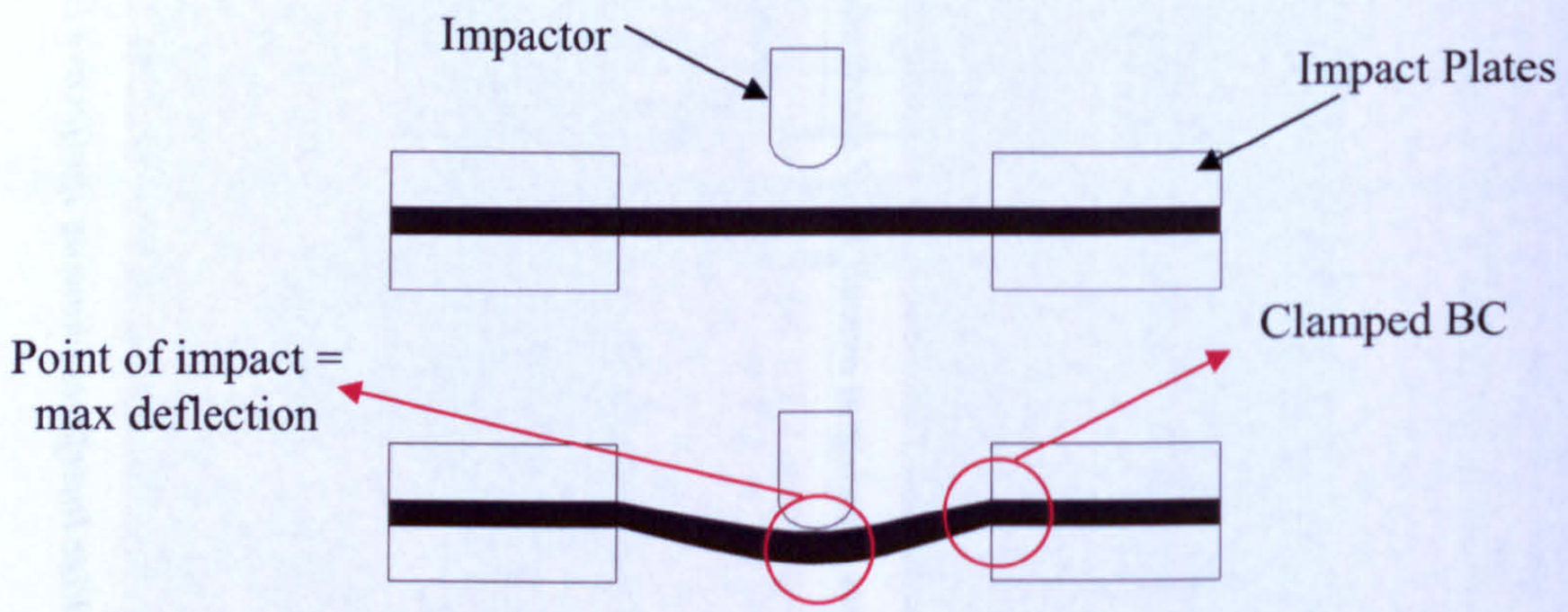

Figure 8-8: ***Boundary Condition Restricting Laminate Deformation in Response to Impact***

The Instron Dynatup 9250K1644 is shown in Figure 8-9. This system is a fully automated and instrumented low velocity drop weight impact test machine (Load cell 1.5kN). Repeated impact is prevented by the deployment of hydraulic activated supports which extend after initial impact to catch the rebounding drop weight. The hemispherical impact tup was consistent with that used in Chapter 7 (diameter = 20mm). The drop weight mass was 5.38kg. The impact boundary conditions were unchanged from those described in Chapter 7, section 2.3, except that the base plate

required additional countersunk fasteners to rigidly attach it to the Dynatup machine (Figure 8-10).

The impact induced delamination areas were assessed at incremental energies from 1-6J using ultrasonic 'time of flight' (Figure 8-11) for plain laminates with no HGF. The areas were measured and can be seen in comparison to the area assessments made in earlier CAI testing, Chapter 7, section 2.3 (Figure 8-12). It can also be seen that the general trends of growth in delamination area highlight the influence of the impact window boundary condition by suppressing delamination propagation as the area approaches 1200mm^2. It can be seen that the 3J impact produced the expected 'pine tree' delamination profile (Figure 8-11) and was located within the linear region of a plot of delamination area increase versus impact energy, Figure 8-12. For these reasons, 3J energy was selected for the final CAI assessment.

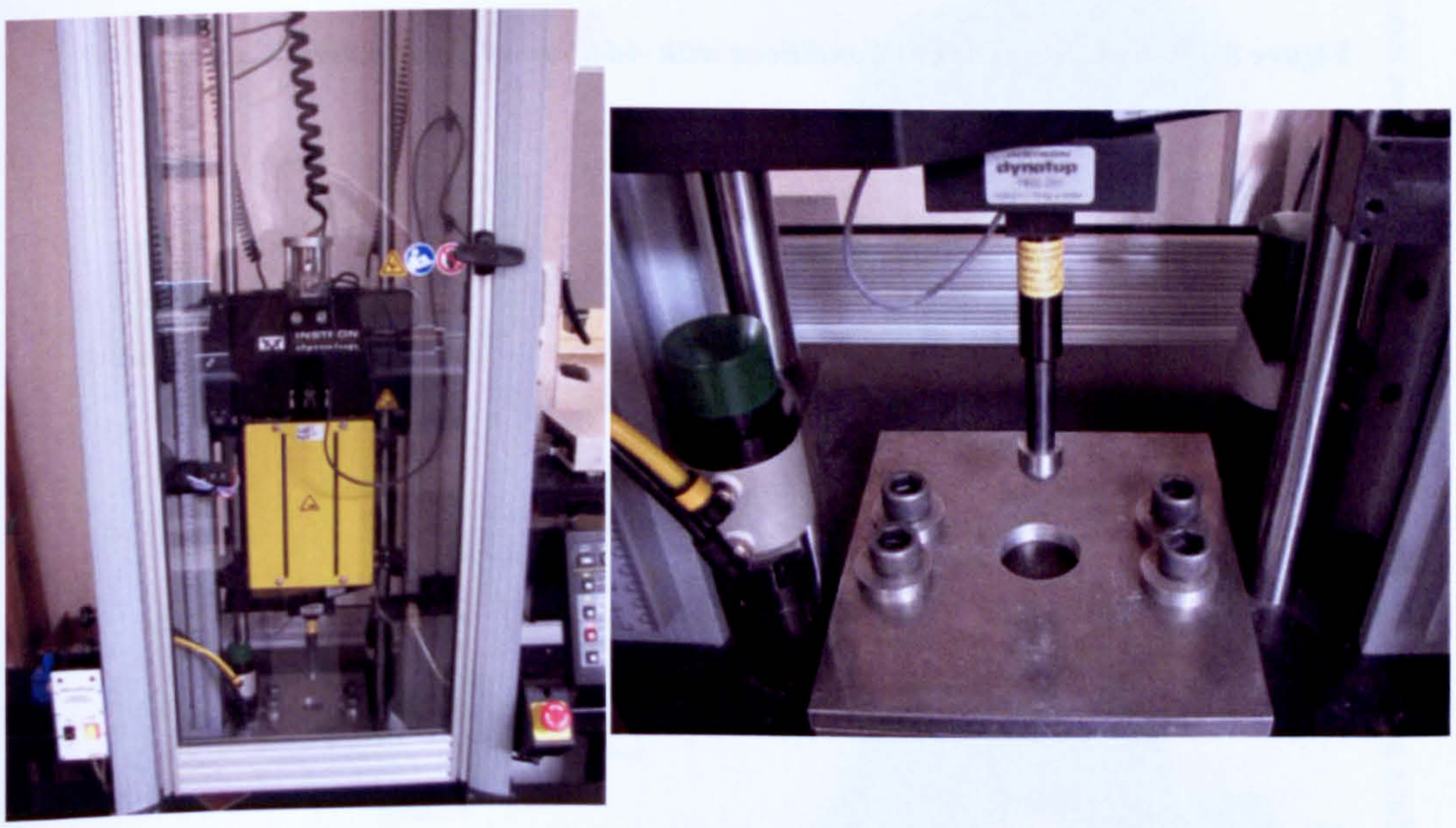

Figure 8-9: ***Images of Instron Dynatup Impact Tester and Impact Support Plates***

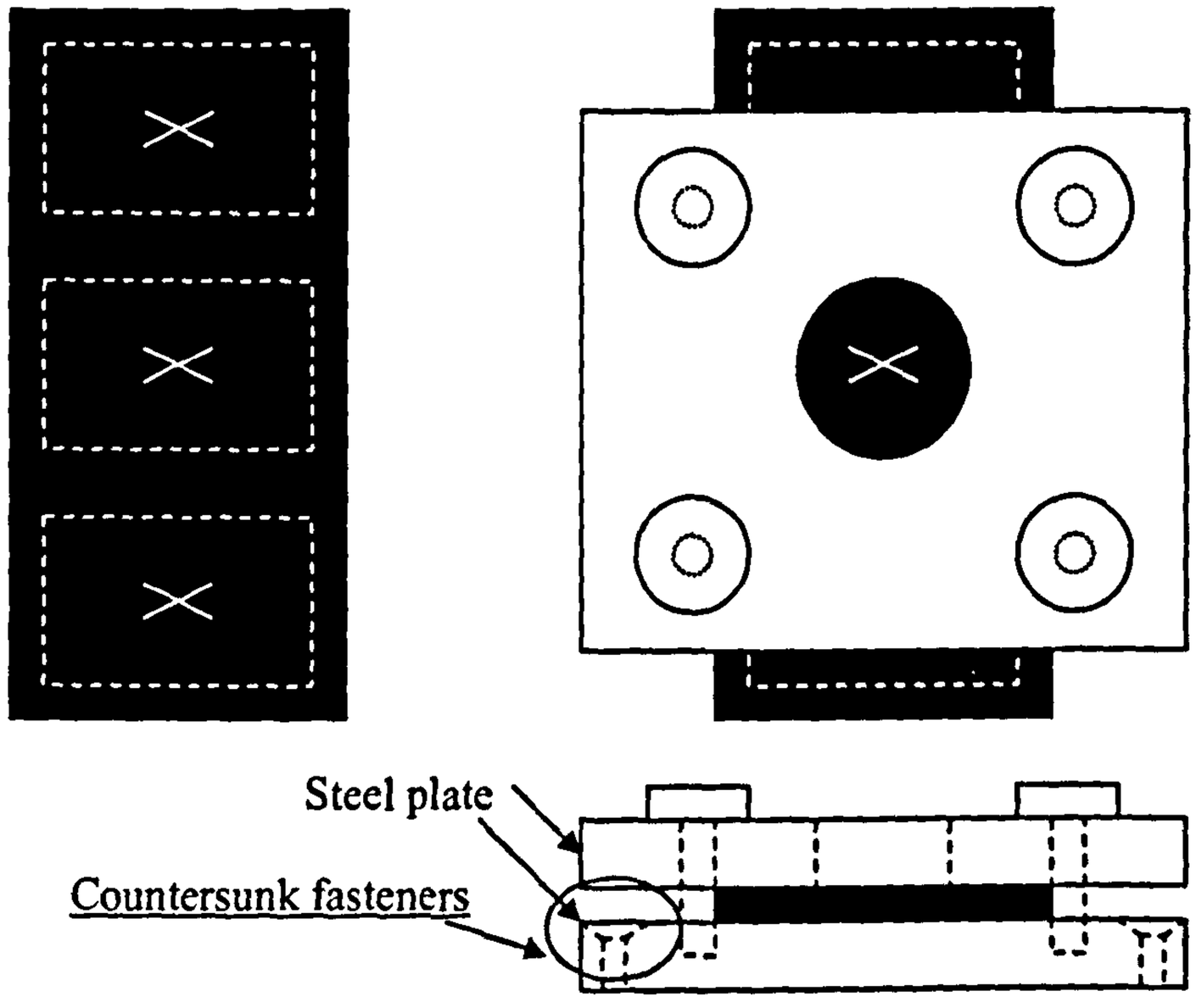

Figure 8-10: ***Impact Boundary Conditions with Addition of Countersunk Fasteners***

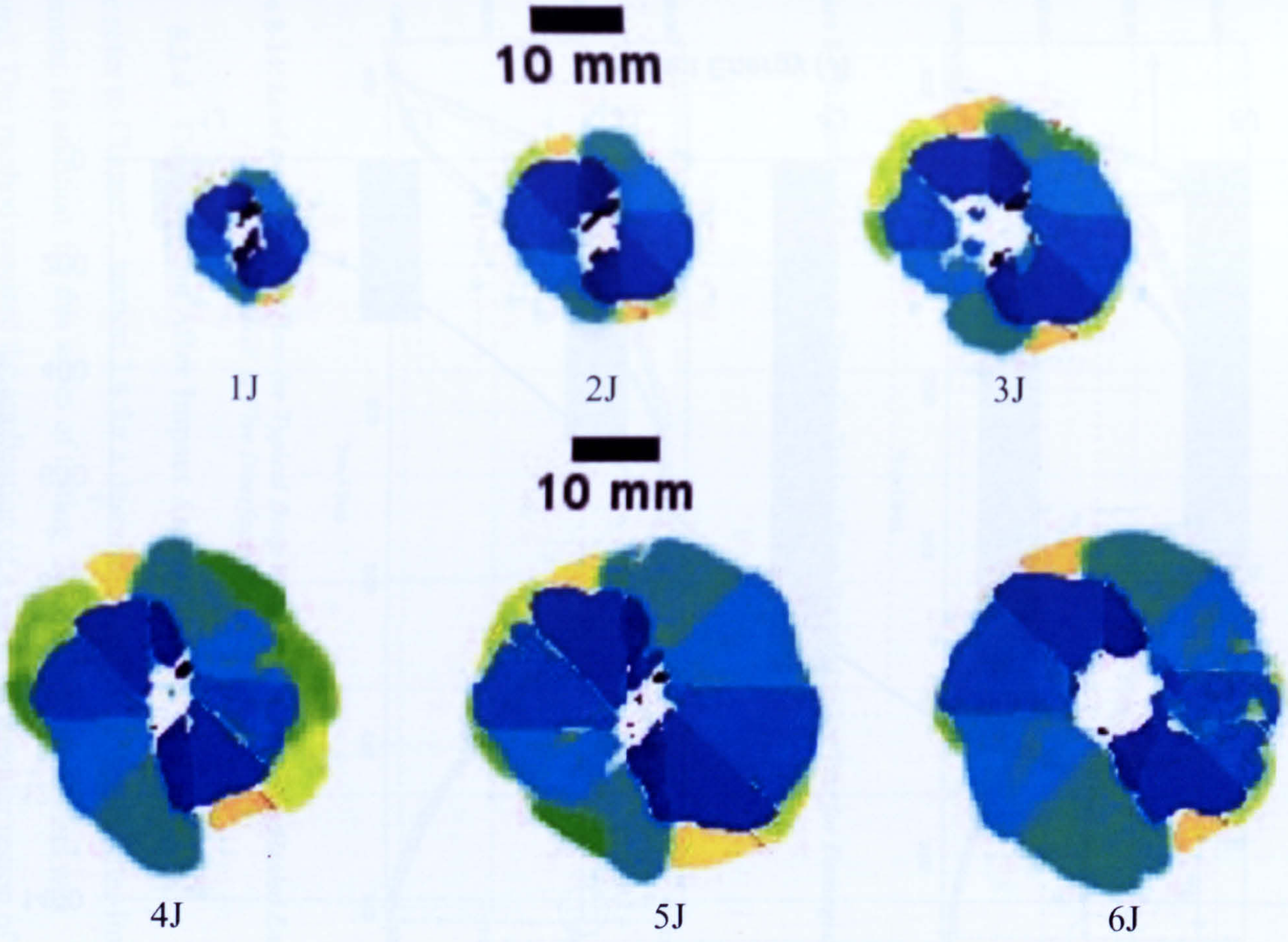

Figure 8-11: ***Ultrasonic Time of Flight Images used to select an Appropriate Impact Energy***

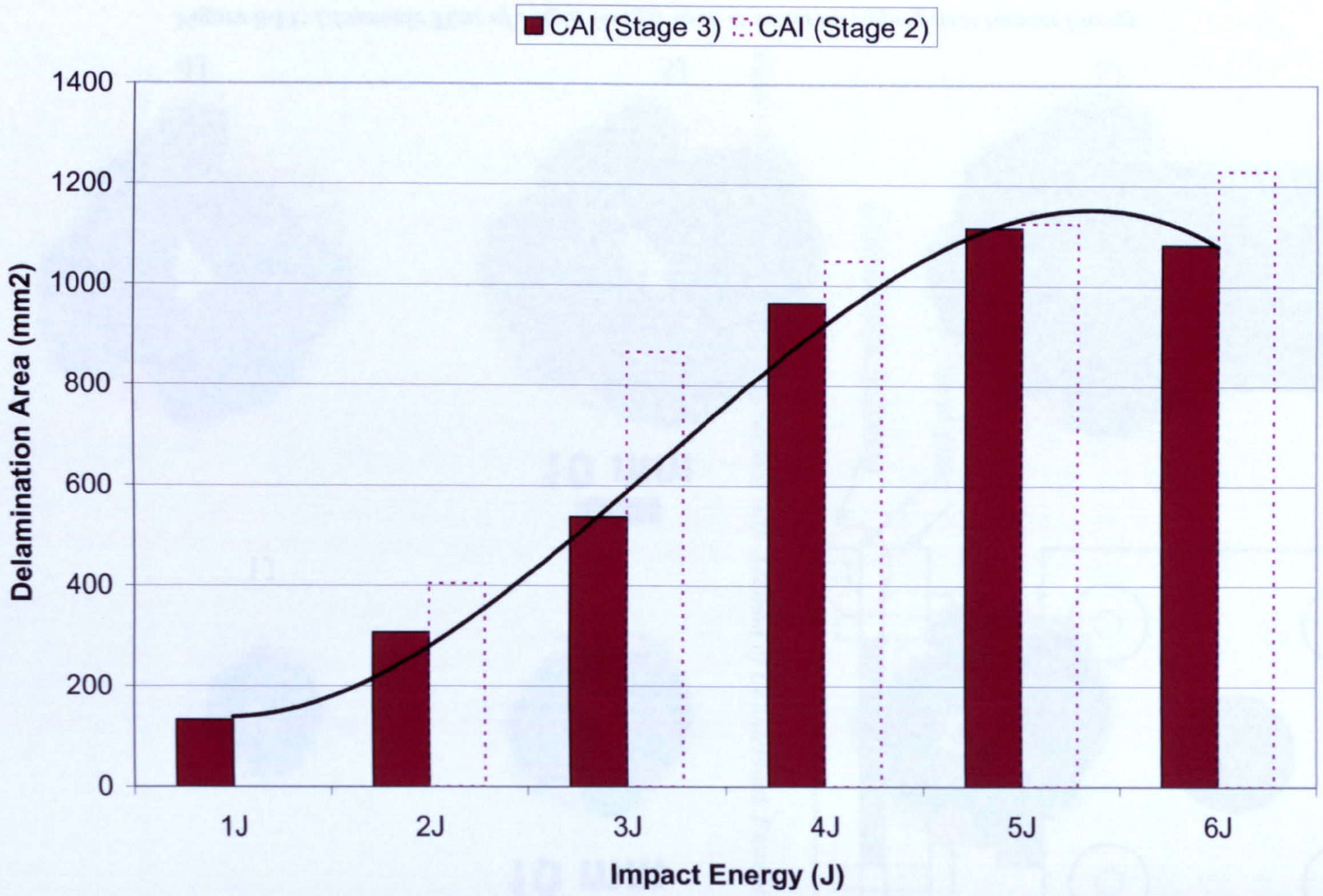

Figure 8-12: ***Variation of Impact Induced Delamination Area with Impact Energy for Plain Laminates for Assessment in Stage 2 and Stage 3 CAI***

The impact response for samples of the same HGF configuration were relatively consistent. However, it can be seen from Figure 8-13 and Figure 8-14 that, although the general response of laminates to drop weight impact was consistent, an increase in absorbed energy was experienced when embedded HGF were infiltrated with healing resin (Healed) indicated by point a).

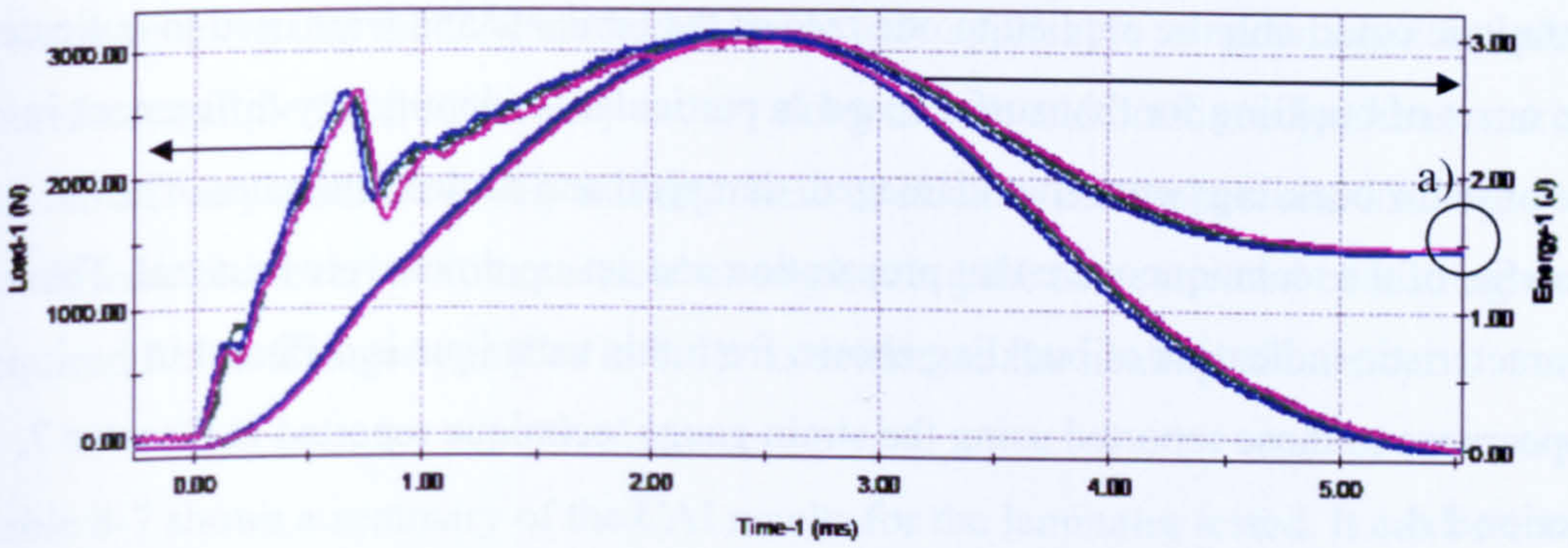

Figure 8-13: ***Load and Energy vs Time for Typical Drop Weight Impact Test for Damaged HGF Laminates***

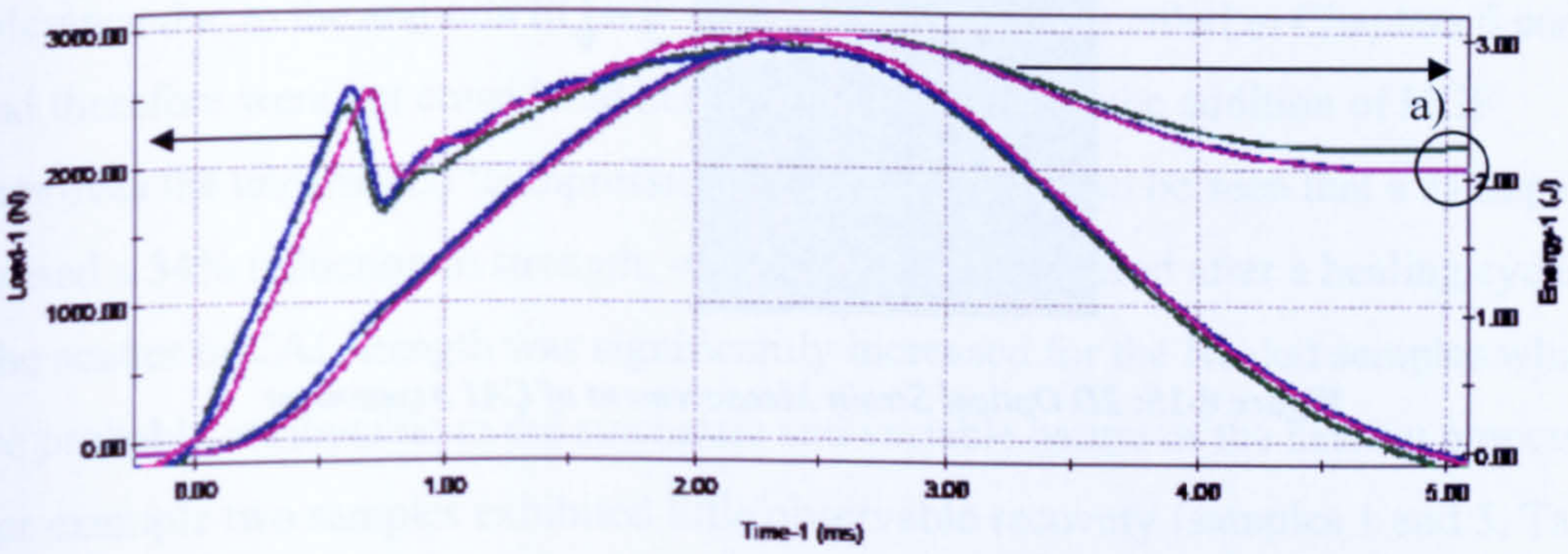

Figure 8-14: ***Load and Energy vs Time for Typical Drop Weight Impact Test for Healed Laminates with HGF at Five Interfaces Resin In-situ***

8.2.4 Compression After Impact Assessment

Please refer to Chapter 7, section 2.4 for a description of Compression After Impact assessment. In addition, for this series of testing, 2D full-field strain data was collected. This method required the application of a small rectangular region of speckled paint to the laminate gauge section. A camera was then focussed onto this area where three unique points were identified at suitable locations for monitoring (Figure 8-15). The system then monitored the displacement of the selected points in order to determine the strain experienced at that location. The relative strain between

the three selected locations was proposed to identify global buckling in the sample as the strain rates of the three points deviated. The first strain reading (strain 1) was the relative change in displacement between point 1 and 2 (300 units displacement), and the second strain reading (strain 2) between point 2 and 3 (600units displacement). Therefore it was expected that a deviation in the strain recorded for strain 1 and strain 2 would indicate the surface of the laminate was experiencing local buckling. This technique could only be applied to one face of the laminate and were used to indicate the onset of buckling for that surface, and in particular to identify any differences in the onset of buckling between undamaged, damaged and healed laminates. The benefits of the technique were that preparation and set-up times were minimal. The characteristic indication of buckling shown from this technique is different in appearance to those reported using the strain gauge technique reported in Chapter 7, section 2.4.

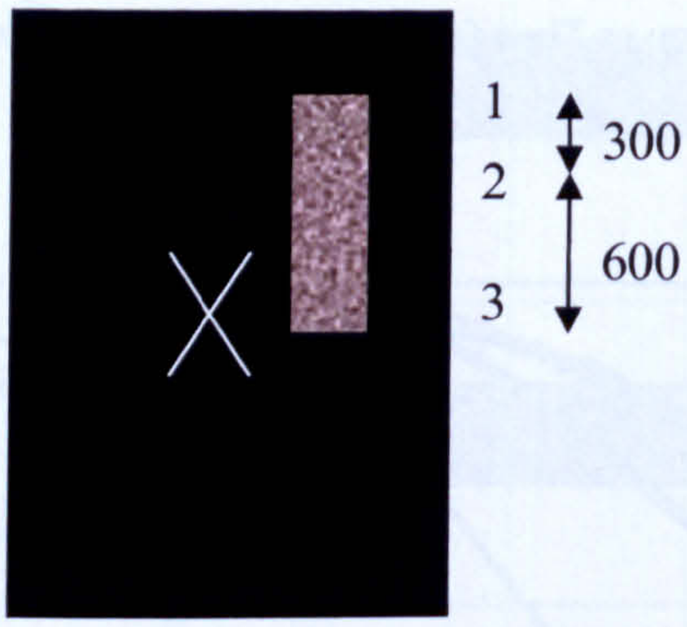

Figure 8-15: ***2D Optical Strain Measurement of CAI Assessment***

8.3 Results: Compression Strength

Characteristic stress-displacement curves can be seen in Figure 8-16 showing the relative performance of the laminates tested. It can be seen that the Plain and HGF Undamaged configurations achieved a high failure stress, as expected. The HGF Damaged configuration can be seen to fail at around 50% of the levels of the undamaged samples. The HGF Healed configuration can be seen to achieve a failure stress and displacement similar to that of the undamaged samples. Moreover, the stress-displacement trace is similar in form to the undamaged sample. However, it should be noted that the Plain undamaged samples showed evidence of some progressive failure. This feature was not observed in the HGF Undamaged

configuration and may be attributed to the increase in laminate thickness (average of 5%) experienced with the addition of HGF. Undamaged samples are extremely sensitive to support/loading conditions when tested in the CAI fixture, therefore the discrepancies in failure may be due to increased stability imparted by the increase in laminate thickness.

It must be noted that the CAI method is not strictly applicable to undamaged samples, therefore, sample failure generally occurs along the top and bottom edges thus making the failure very sensitive to any misalignment or slack in the support and loading conditions. However, a 'compression' strength using the same method of loading was required for undamaged samples in order to determine the healing efficiency.

Table 8-7 shows a summary of the CAI results for the laminates tested. It can be seen that only laminates containing HGF were tested in Undamaged, Damaged and Healed conditions. The plain CFRP laminate was tested Undamaged as a point of reference for the subsequent HGF laminate performance. The improvements in damage tolerance due to the addition of HGF have been well documented in Chapters 6 and 7 and therefore were not considered here. It can be seen that the addition of HGF improves the undamaged 'compression' strength. It can also be seen that a 3J impact caused a 34% reduction in strength, which was then recovered after a healing cycle. The scatter in CAI strength was significantly increased for the Healed samples which are probably attributable to the stochastic and variable nature of the healing process. For example two samples exhibited little observable recovery (samples 1 and 5, Table 8-8).

The absorbed impact energy was recorded for damaged and healed samples. It can be seen in Figure 8-17 that the healed samples absorbed more impact energy than the damaged samples. The only difference between the two configurations was that the Healed samples were infiltrated with liquid resin prior to impact. Therefore, the improvements in absorbed energy may be attributed to the presence of this liquid medium transmitting additional hydraulic loading along the HGF as a result of the impact and consequently initiated more extensive HGF fracture.

Specimen type		Undamaged (CV%)	Damaged (CV%)	Healed (CV%)
Plain CFRP	CAI Strength (MPa)	330.33 *(12)*	-	-
	% undamaged baseline	*100%*	-	-
HGF @5 interfaces	CAI Strength (MPa)	373.33 *(16)*	218.38 *(6)*	315.19 *(22)*
	% undamaged baseline	*113%*	*66%*	*95%*
	Impact Energy Absorbed (J)	-	1.45 *(1)*	2.2 *(4)*

Table 8-7: ***Results of CAI after 3J Impact for T300/914 CFRP Laminates with Embedded HGF***

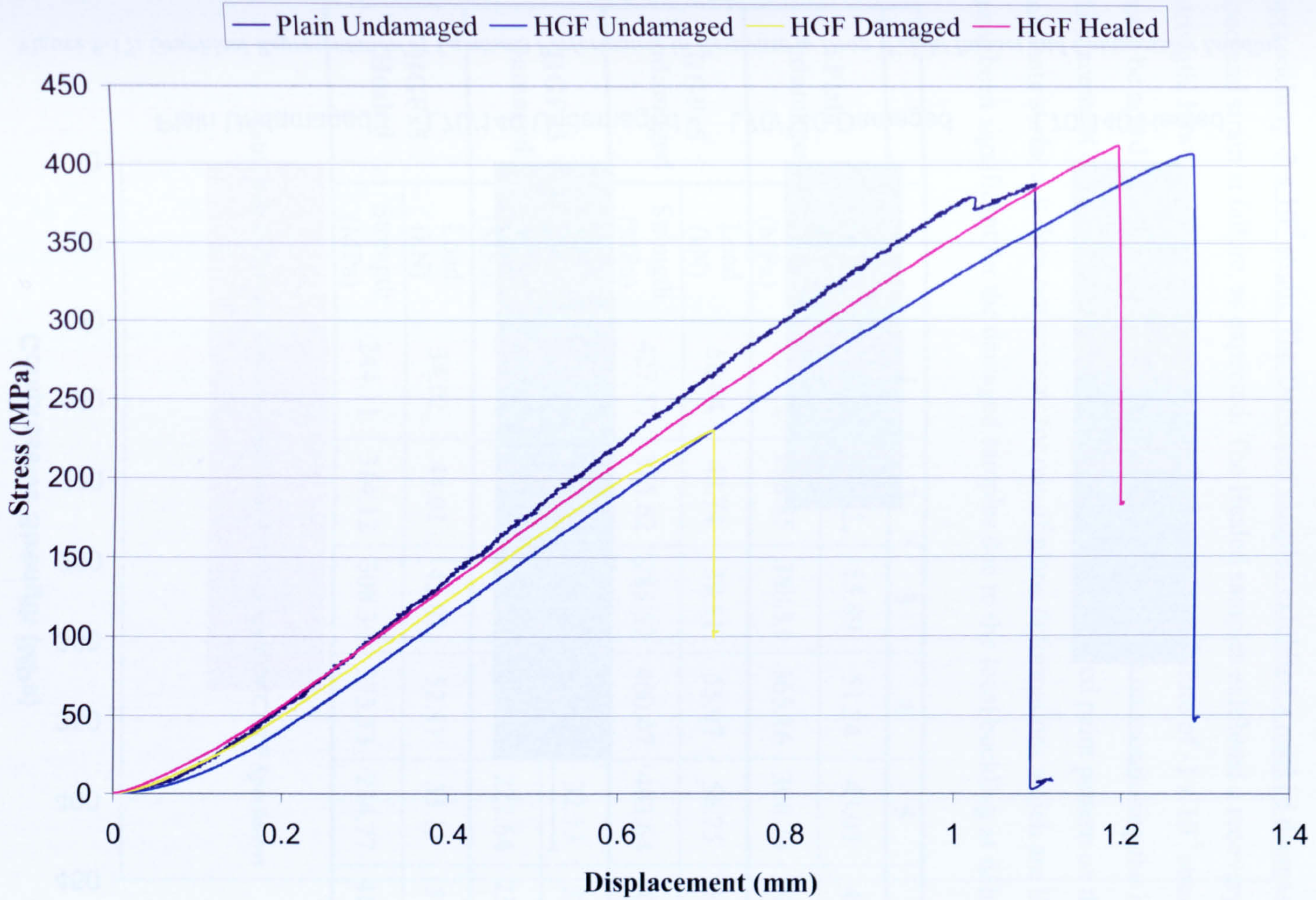

Figure 8-16: ***Typical Stress/Displacement Curves for Plain Undamaged, and Undamaged, Damaged and Healed Laminates with HGF at Five Interfaces***

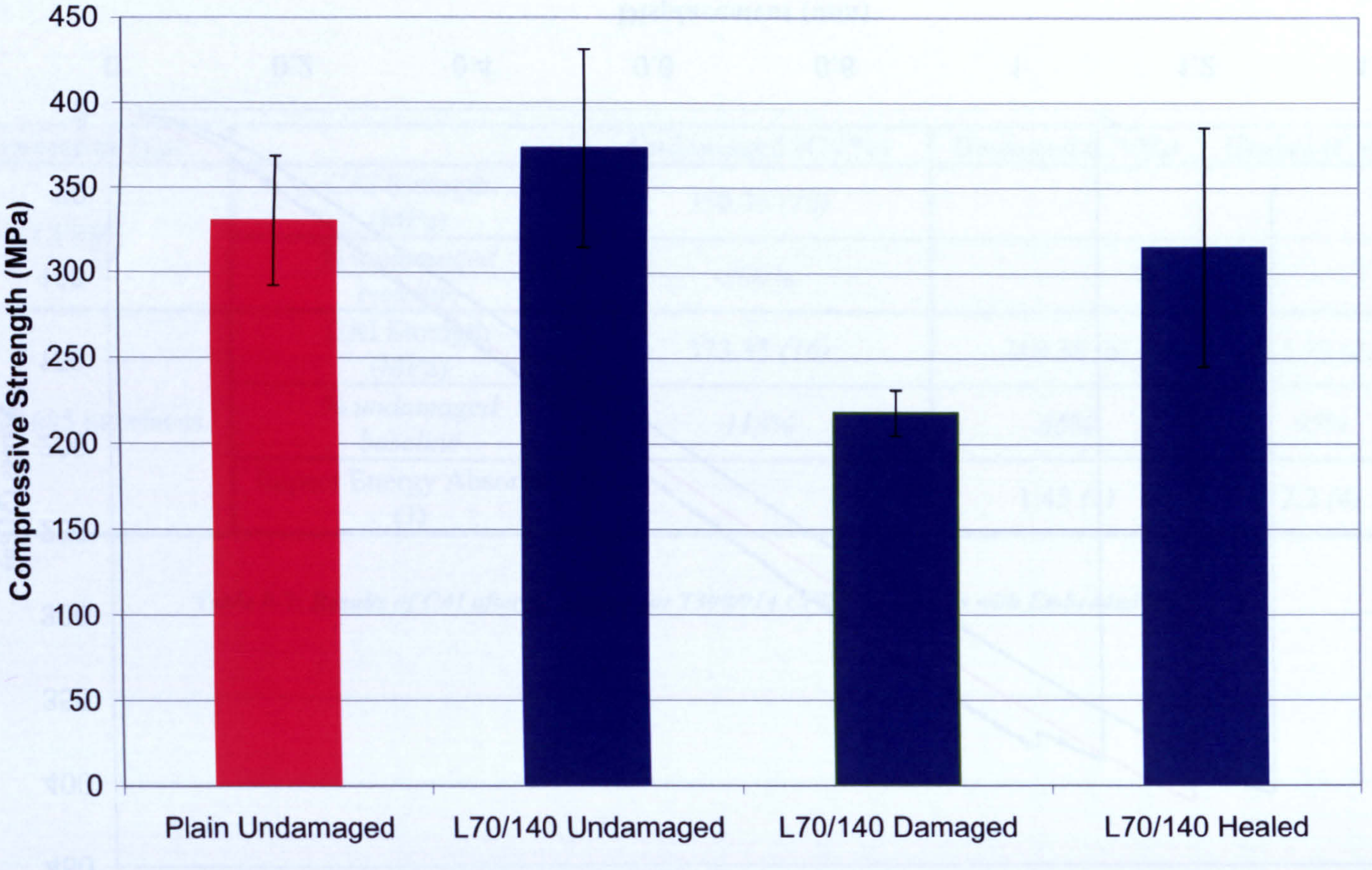

Figure 8-17: ***Graphical Representation of Laminate Performance in Response to Drop Weight Impact and Compressive Loading***

The results of optical strain measurements for Plain Undamaged, HGF Damaged and HGF Healed can be seen in Figure 8-18, Figure 8-19 and Figure 8-20 respectively. The Undamaged HGF samples sustained a peak load of 60kN and a strain at failure approaching -2 x 10^{-3} strain. The Damaged samples exhibited a marked decrease in load and strain at failure, as expected. The Healed samples exhibited a recovery of strength, however, the specimens approached a strain at failure of -1 x 10^{-3} strain. It must be noted that this strain measurement technique relies on monitoring the in-plane displacement of a unique point identified within the speckled paint pattern on the laminate surface, it does not account for out-of-plane deformations which are likely to have been significant for the damaged samples due to the local buckling at failure.

		1	2	3	4	5	6
Plain Undamaged	Load (kN)	45.11	41.41	53.89	51.24	43.03	42.21
	Strength (MPa)	325.72	298.85	388.31	365.16	306.74	294.62
HGFx5 Undamaged	Load (kN)	58.84	43.74	39.51	55.97	56.75	58.01
	Strength (MPa)	427.57	315.62	285.37	400.47	403.64	407.35
HGFx5 Damaged	Load (kN)	29.07	29.12	28.76	31.96	32.13	32.84
	Strength (MPa)	206.35	206.92	205.90	229.76	227.64	233.76
HGFx5 Healed	Load (kN)	34.02	44.01	43.01	52.17	33.13	57.76
	Strength (MPa)	244.11	314.12	308.30	373.33	234.77	412.49

Table 8-8: ***Individual Failure Loads and CAI Strength for CFRP Specimens***

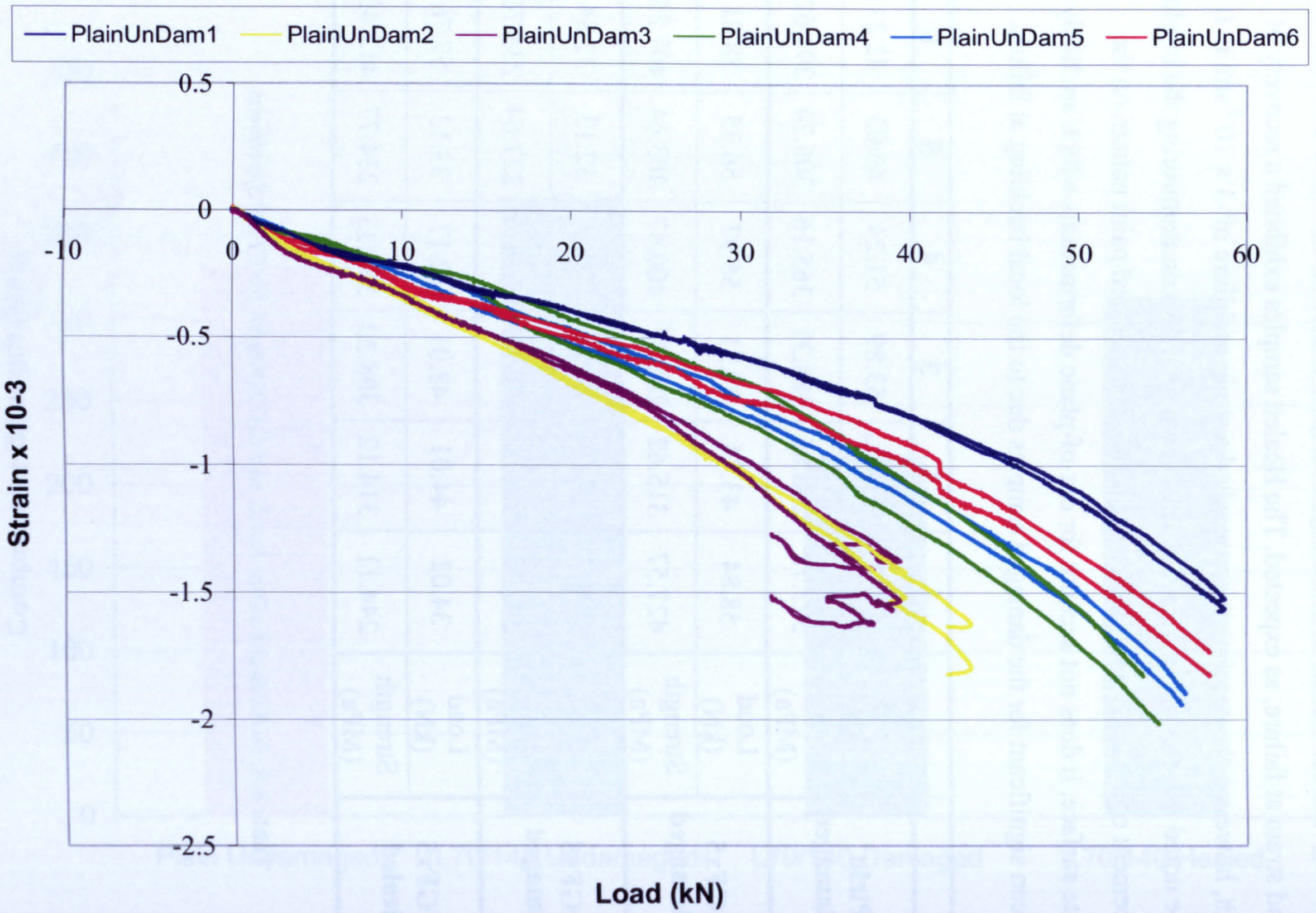

Figure 8-18: Load-Strain Data for Plain Undamaged Samples (Baseline)

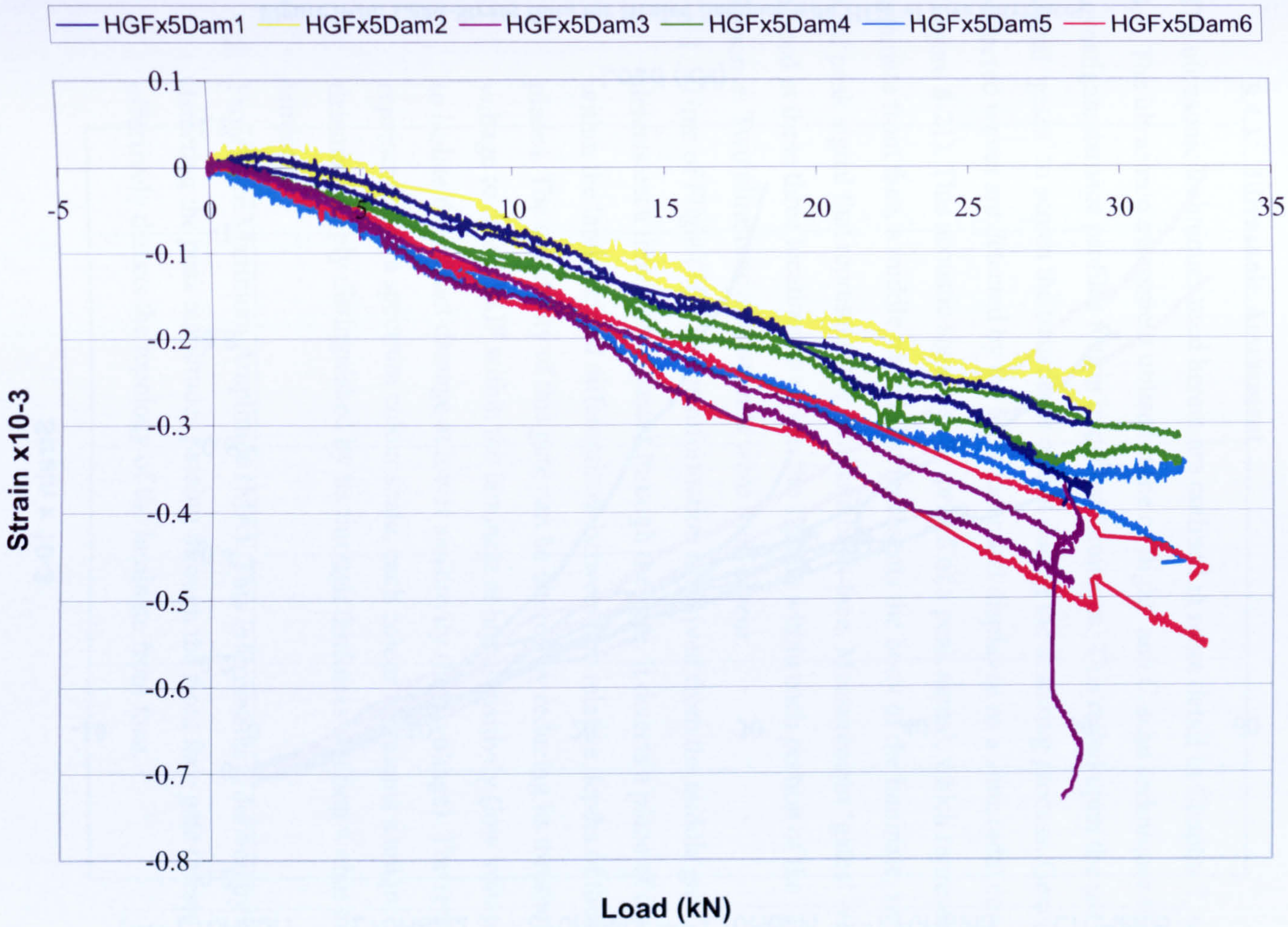

Figure 8-19: Load-Strain Data for Damaged Samples with HGF at Five Interfaces

Figure 8-20: Load-Strain Data for Healed Samples with HGF at Five Interfaces

8.4 Fracture Analysis

The CAI results conclusively demonstrated a recovery in mechanical performance via healing. Following the testing, a number of non-destructive techniques were used alongside optical microscopy to further investigate and explain the results.

8.4.1 Ultrasonic Assessment

The ultrasonic techniques used herein are outlined in more detail in Chapter 7, section 4.1. The ultrasonic assessment utilised 'time of flight' and C-scan techniques to investigate damage profiles within impacted laminates. This relied upon the use of signal 'gates' to screen the transducer output during the scanning process. Generally, reflected waves are detected by the transducer and displayed as a sinusoidal curve (Figure 8-21). This acoustic signal is comprised of a peak signal, which represents the laminate front face, a middle period that represents the body of the laminate, and a final peak signal that represents the laminate back face. Measurement 'gates' were placed at these three locations to screen the signals within each portion of the response. Two ultrasonic assessments were used herein:

1. Time of Flight (TOF): This information is derived from the middle gate, and detects each time a peak passes through the gate. It detects a plane of damage within the laminate and differentiates between the relative depths of these planes. The sensitivity of this gate can be altered by reducing its threshold voltage to detect HGF within the laminate at high sensitivity (low voltage) and to isolate the impact damage at lower sensitivity (high voltage). The results are represented by a spectrum colour scale, each colour represents a unique delaminated ply distinguished by its through thickness position within the laminate.
2. Front Face Maximum Amplitude (MA): This information is derived by detecting the peak amplitudes passing through the front face gate threshold. It effectively detects the topology of the laminate front face.

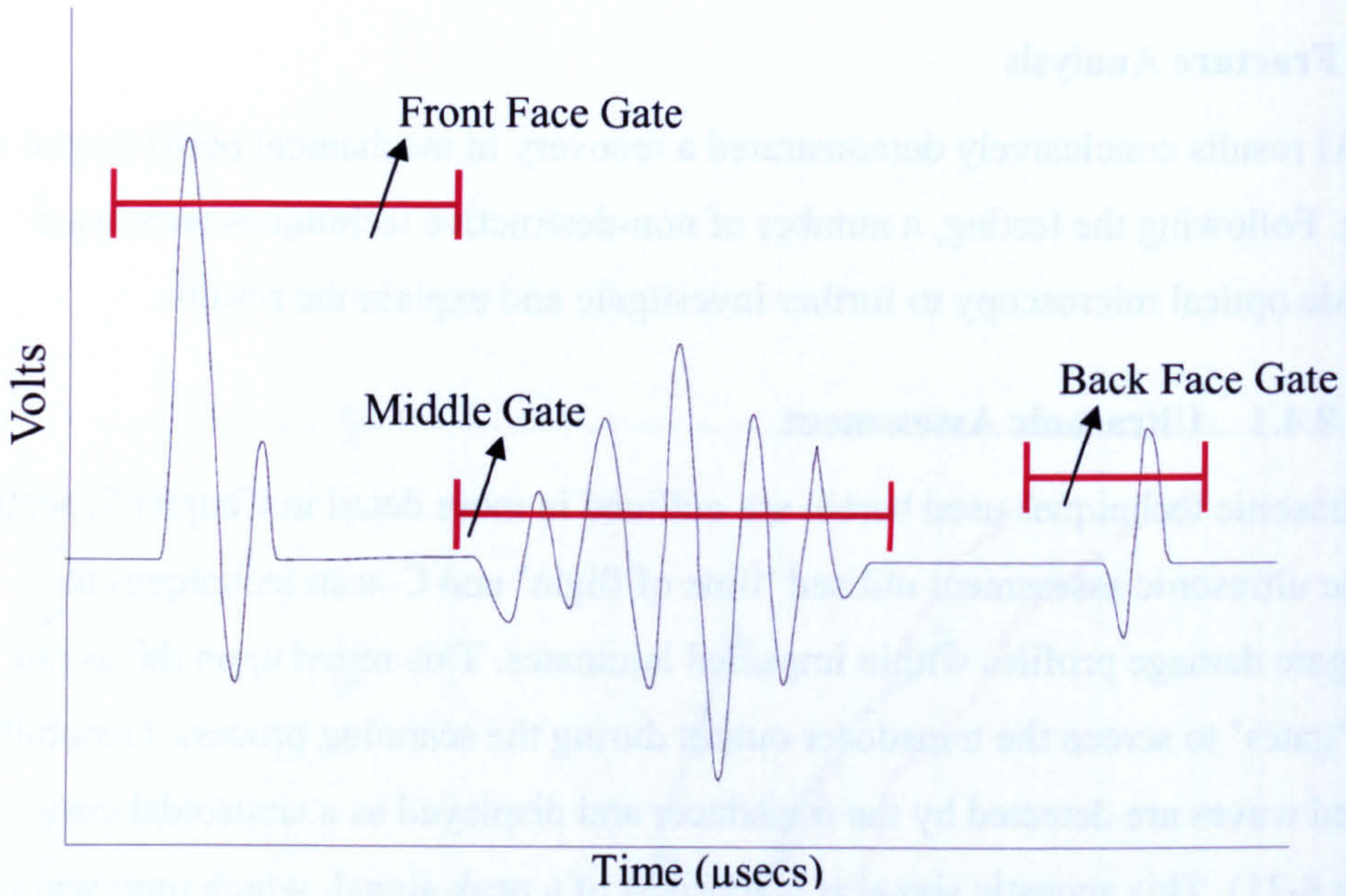

Figure 8-21: ***Sinusoidal Wave Detected by Ultrasonic Transducer and Construction of 'Gates' to monitor the Signal***

Ultrasonic assessment identified the likely failure mechanisms that occurred during CAI testing. The TOF and MA data for the undamaged specimens 1-6 (left to right) are presented in Figure 8-22 and Figure 8-23 respectively. Specimens 1-3 and 6 failed along the upper edge in the region of load application. Specimen 4 failed along the bottom edge and specimen 5 exhibited a mix of upper edge failure and a small central buckle.

Damaged samples can be seen to consistently fail due to a central buckle, where impact induced delaminations propagate orthogonal to the applied load. This can be seen using TOF (Figure 8-24) and MA (Figure 8-25). (Note: the darker regions in the MA images represent where buckling induces significant out of plane displacement of the near surface laminate and the outer carbon fibre are fractured by the knife edge supports at failure).

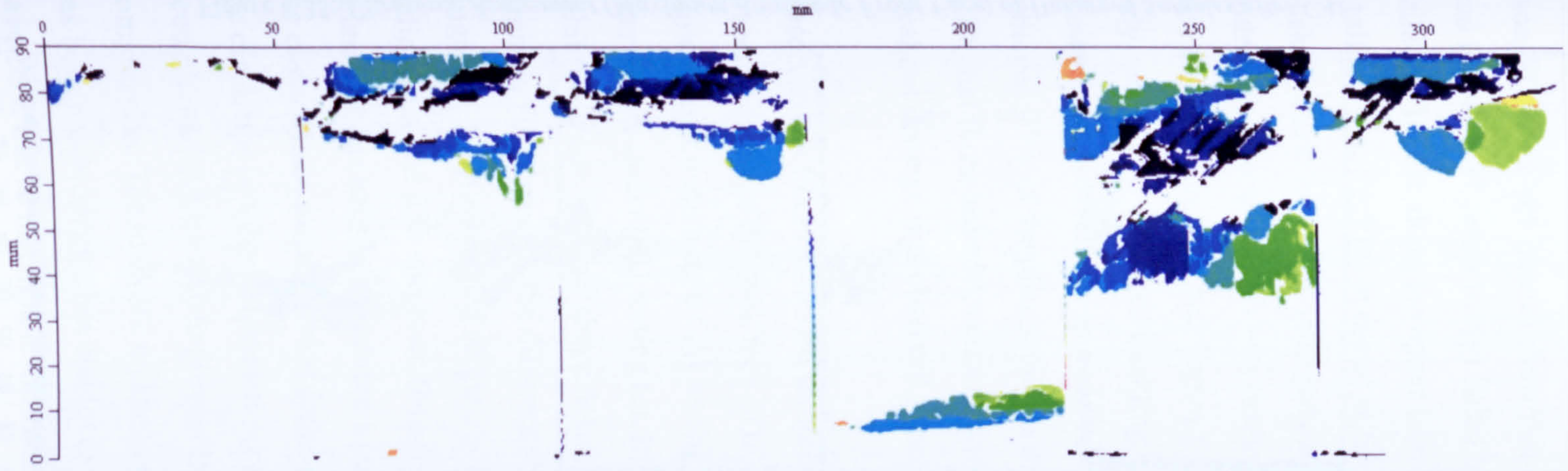

Figure 8-22: ***Ultrasonic Time of Flight Assessment of Undamaged Samples after CAI***

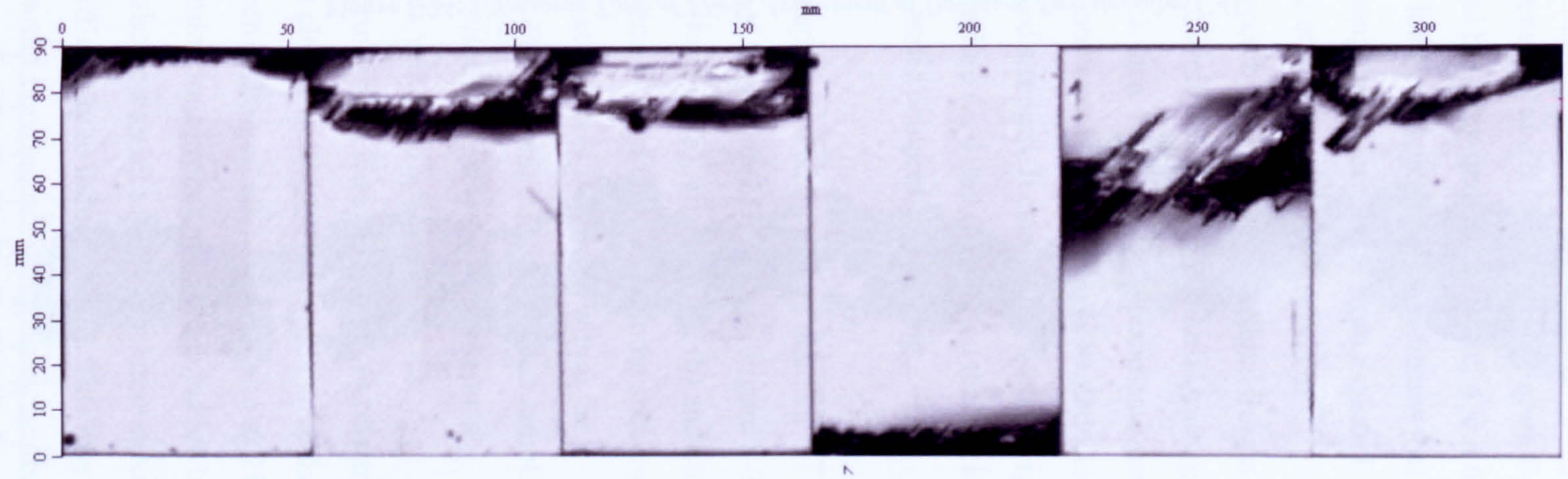

Figure 8-23: ***Ultrasonic Assessment (Maximum Amplitude Front Face) of Undamaged Samples after CAI***

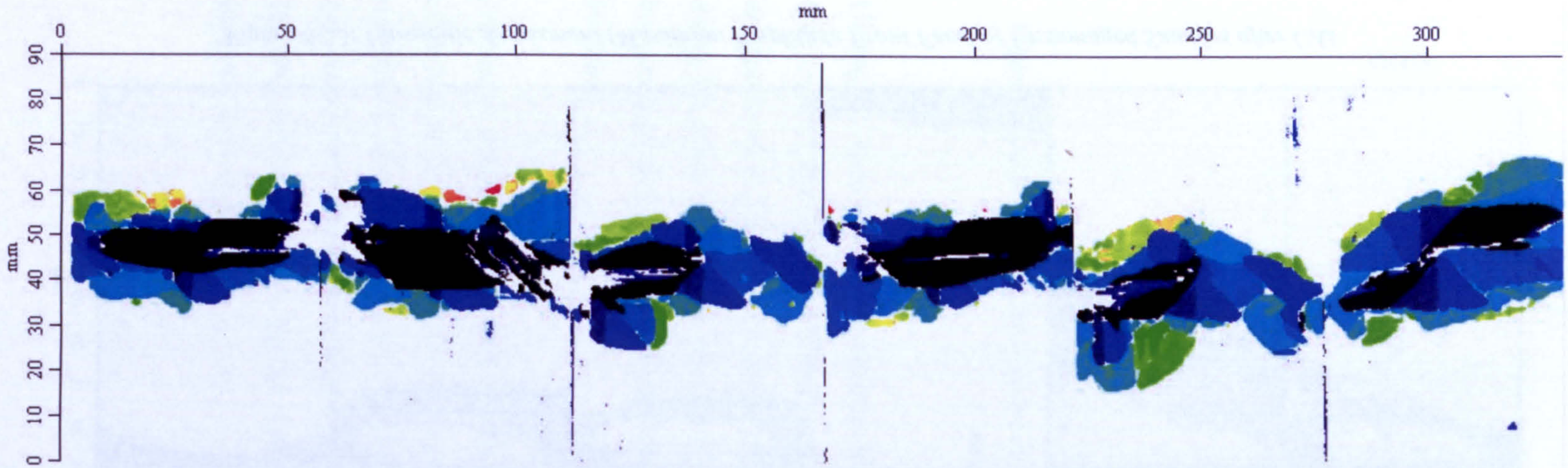

Figure 8-24: ***Ultrasonic Time of Flight Assessment of Damaged Samples after CAI***

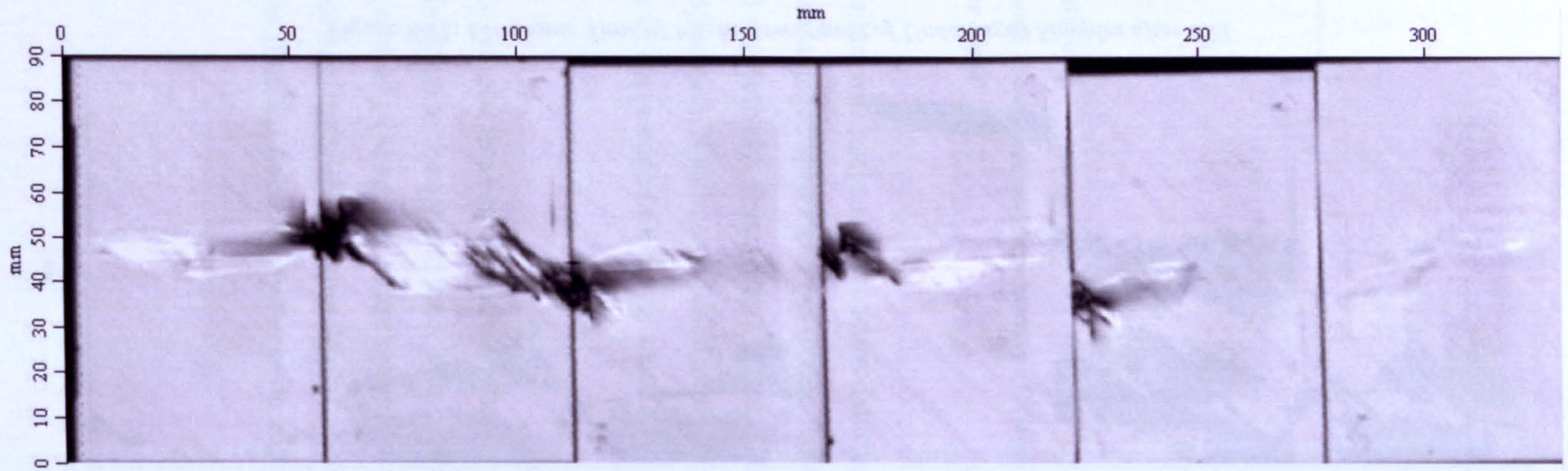

Figure 8-25: ***Ultrasonic Assessment (Maximum Amplitude Front Face) of Damaged Samples after CAI***

Healed samples were assessed using TOF and MA data from both the front face and back face of each specimen, which resulted in improved detail of the two regions by eliminating the shielding effect described in Chapter 7 section 4.1. From the front face, TOF and MA images show that specimens 1, 2 and 3 (left to right, Figure 8-26 and Figure 8-27 respectively) failed by central buckling and specimens 2, 4 and 6 failed by failure along the upper edge where load was applied. This indicates that the healing event (in 50% of cases) initiated a change of failure mode from a central buckle, characteristic of damaged samples, to edge failure, characteristic of undamaged samples. This was further reinforced by TOF and MA images from a back face view (Figure 8-28 and Figure 8-29 respectively). However, for the MA images, only specimen 5 exhibited buckling at the back face. Furthermore, specimen 3 was shown to have failed due to a central buckle, however it was evidently healed as it achieved 93% of the plain laminate undamaged strength. It can also be seen in Figure 8-29, that three healed specimens with edge failure (2, 4 and 6), showed that back face breakout damage was observed to propagate under compressive loading.

Observations from the healed samples were supplemented by a more detailed investigation into the back face TOF images of impacted (3J) coupons. Figure 8-30 shows a specimen before CAI testing with no healing (a), after healing (b) and then after failure under CAI testing (c). It can be seen in Figure 8-30a) that the specimen exhibits classic 'peanut' shape delaminations at different interfaces within the laminate (indicated by the different shading). This is similar for the healed samples (Figure 8-30b)) and failed (Figure 8-30c) specimens. However, at the markers indicated α and β in specimen (b) and markers γ and δ in specimen (c), the delaminations have been reduced in size in comparison with sample (a). Furthermore, the edges of the delaminations are much less clearly defined. This is indicative that the crack tips of these delaminations have been infiltrated with healing resin and have been blunted sufficiently to prevent the delaminations propagating when loaded in compression. The marker ε on specimen (c) shows a small region of delamination that has begun to propagate but did not extend sufficiently to induce failure. This may have been due to incomplete infiltration or partial bonding of the region by healing resin. However, the stress at failure of this specimen achieved 120% of the undamaged failure stress and therefore, this propagation was pinned by the healing action and consequently had no detrimental effect on the failure mode or load.

Coupons that were damaged at 3J impact energy consistently failed between 60% and 70% of the undamaged compressive failure strength by a process of localised buckling at the mid-section. This is illustrated in Figure 8-31 specimen 1 (left) where delaminations can be seen to propagate from the impact centre (a) to extend across the width of the specimens (b). Coupons that were healed after 3J impact (specimen 2, right) were able to sustain loads up to and exceeding the undamaged compressive failure strength and failed in a similar manner to the undamaged samples by edge brooming, as illustrated in Figure 8-31c). It can also be seen that the delaminations present at the impact centre did not propagate under compressive loading Figure 8-31a). However, there was a significant degree of scatter in the results as two of the coupons showed only a limited degree of compressive strength recovery. It is not evident whether healed damage was entirely infiltrated by healing resin or whether only the crack tips of the delaminations were infiltrated to give some degree of 'crack blunting' effectively preventing further damage propagation.

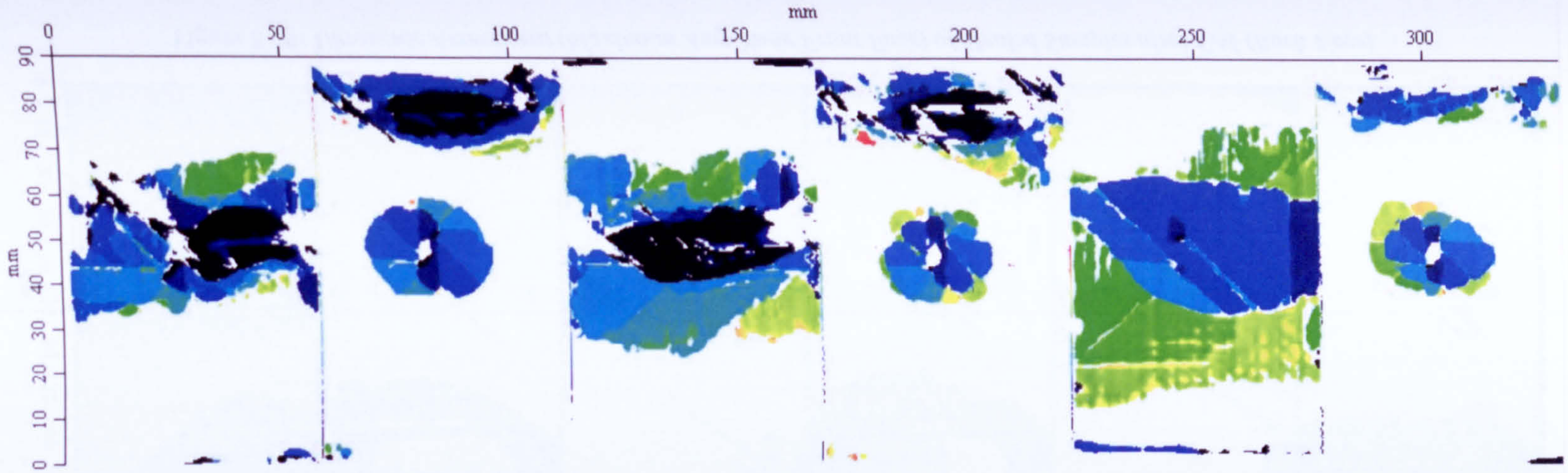

Figure 8-26: ***Ultrasonic Time of Flight Assessment of Healed Samples after CAI (Front Face)***

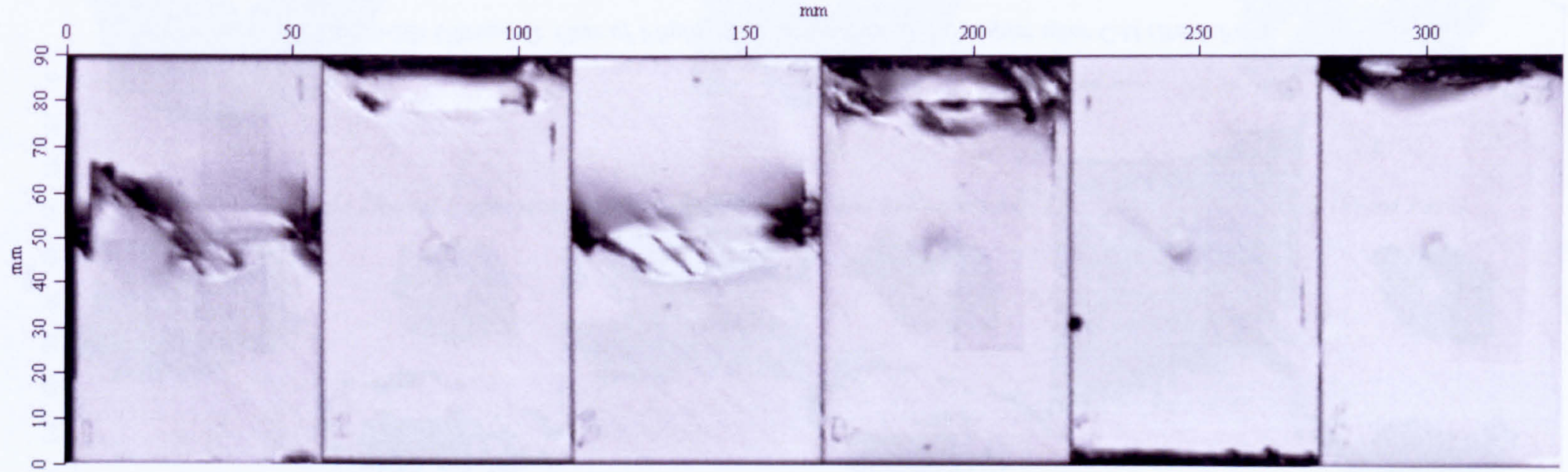

Figure 8-27: Ultrasonic Assessment (Maximum Amplitude Front Face) of Healed Samples after CAI

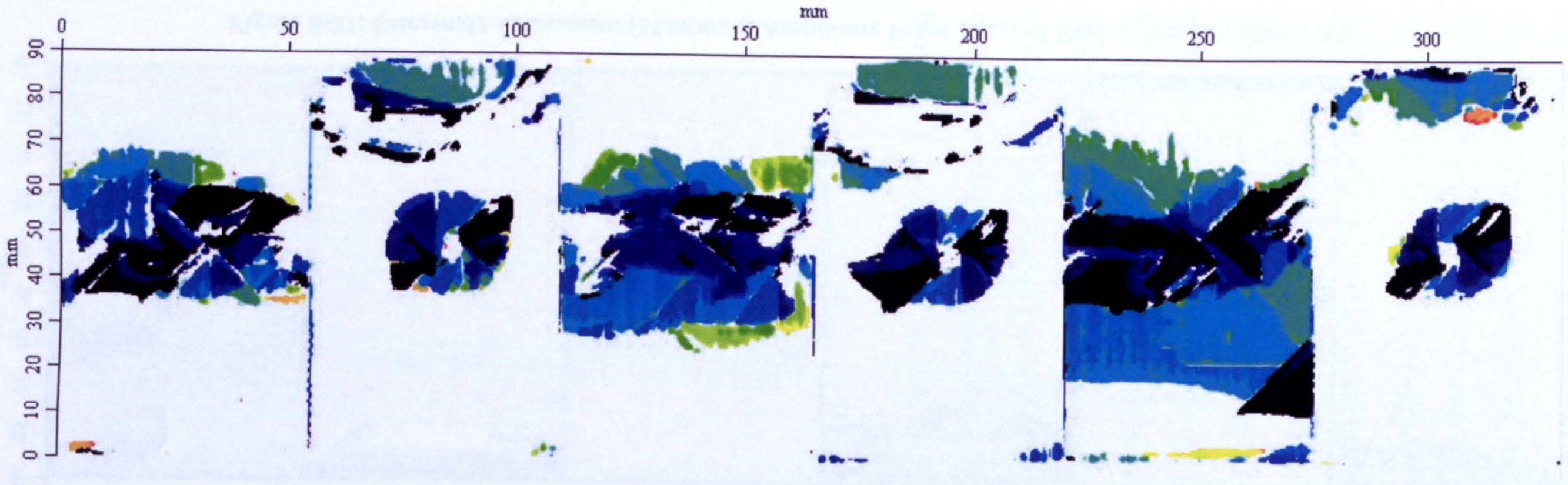

Figure 8-28: ***Ultrasonic Time of Flight Assessment of Healed Samples after CAI (Back Face)***

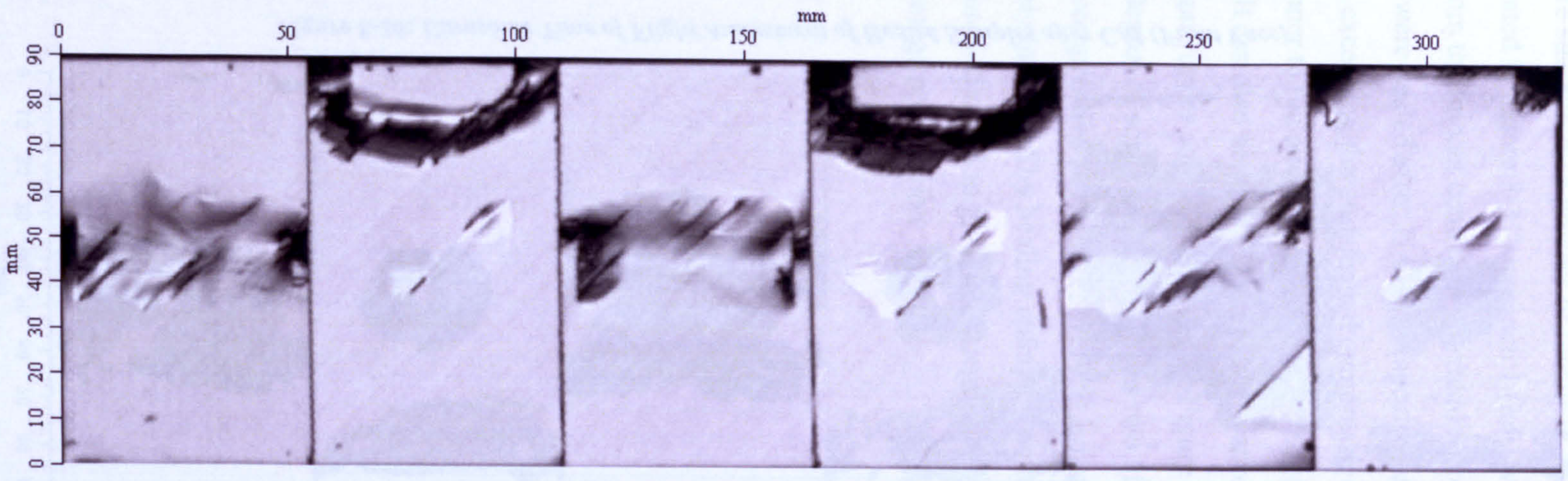

Figure 8-29: ***Ultrasonic Assessment (Maximum Amplitude Front Face) of Healed Samples after CAI (Back Face)***

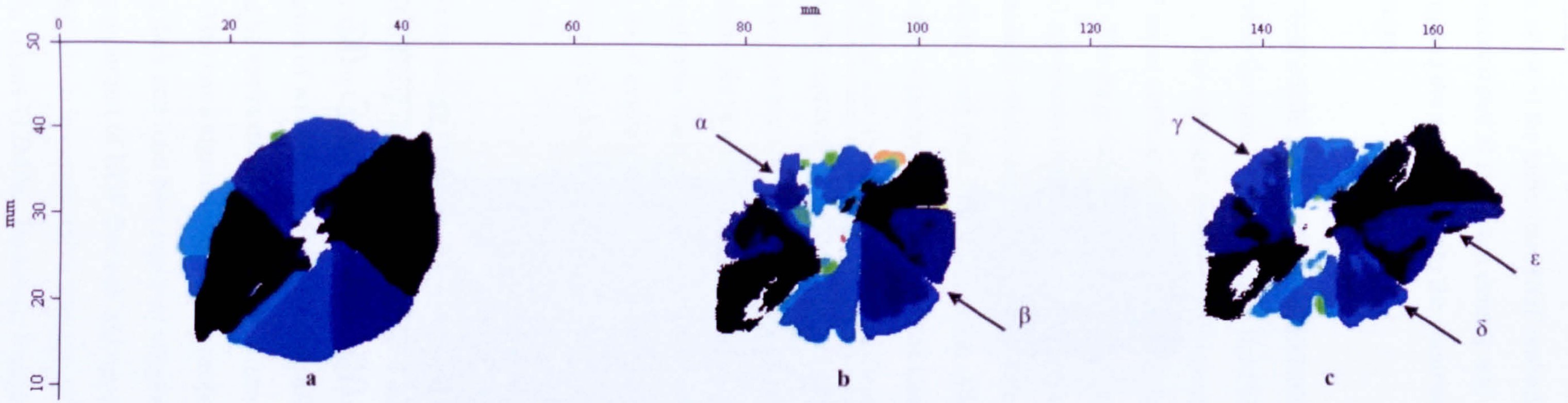

Figure 8-30: ***Ultrasonic Time of Flight Assessment of a) Undamaged and b) Successfully Healed Samples after CAI (Front Face)***

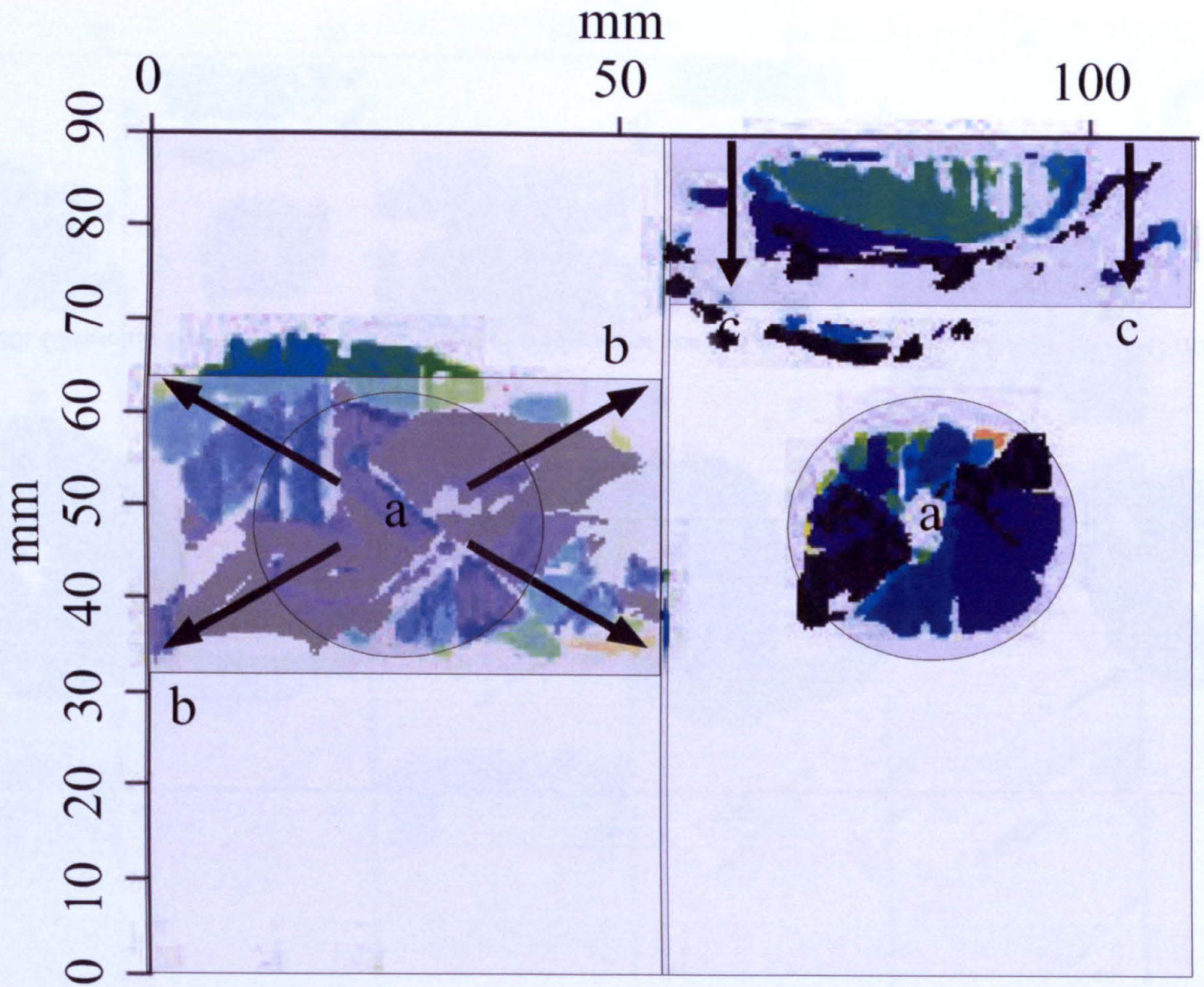

Figure 8-31: ***Characteristic Failure Modes of Damaged and Undamaged/Healed Samples under Compressive Loading***

Increasing the sensitivity of the TOF gate produced the images shown in Figure 8-32 and Figure 8-33. This allowed the individual HGF embedded within the laminate to be detectable when concentrated at sufficient density and un-infiltrated with healing resin. This was used to acquire an insight into the occurrence of HGF fracture and infiltration of the damage.

Figure 8-32 shows a comparison between a) plain undamaged laminate and b) damaged and then healed laminate. The dark blue, light blue, turquoise, orange and red colours in Figure 8-32a) represent the five HGF layers within the laminate. This verified that the HGF are at sufficient density at all interfaces to be detectable with ultrasonic assessment. The large red and multicoloured portion towards the top of Figure 8-32 sample b) represents an edge failure or 'brooming' under compressive loading. The central delaminations are also clearly visible and small regions of HGF can be observed, primarily with dark blue colouration. The absence of colour in the remainder of the laminate suggests that the pre-mixed healing resin within the HGF has cured and thus the HGF are no longer detectable. Several instances of HGF can be observed in Figure 8-32b) represented by the dark and light blue, which suggests that the HGF in these regions has been emptied of healing resin after the damage event. This does not however, imply that these are the only regions of HGF emptied of healing resin, just that at these locations the empty HGF are of sufficient density to be detectable. Individual HGF evacuated of resin interspersed with HGF containing cured healing resin will not be detected and it was expected that this would be the most common condition.

Figure 8-33 shows a comparison between a) healed, then failed by central buckling and b) healed then failed along upper edge. The central buckling region can be clearly observed in sample a) and so too can the edge failure in sample b). These images assist in the identification of whether the lower healing effectiveness for the specimen in Figure 8-33a) could be attributed to a reduced occurrence of HGF fracture. The specimen in Figure 8-33b) has a significantly higher proportion of empty regions of HGF (indicated by the dark and light blue regions) suggesting that this specimen experienced a higher proportion of HGF fracture and egress of healing resin, which may account for the difference in compressive strength achieved by the two specimens i.e. 244MPa versus 412MPa . However, it must be re-stated that the HGF

were only discernible with ultrasound when empty and when packed to a high density. Sparsely distributed, empty HGF are not detectable.

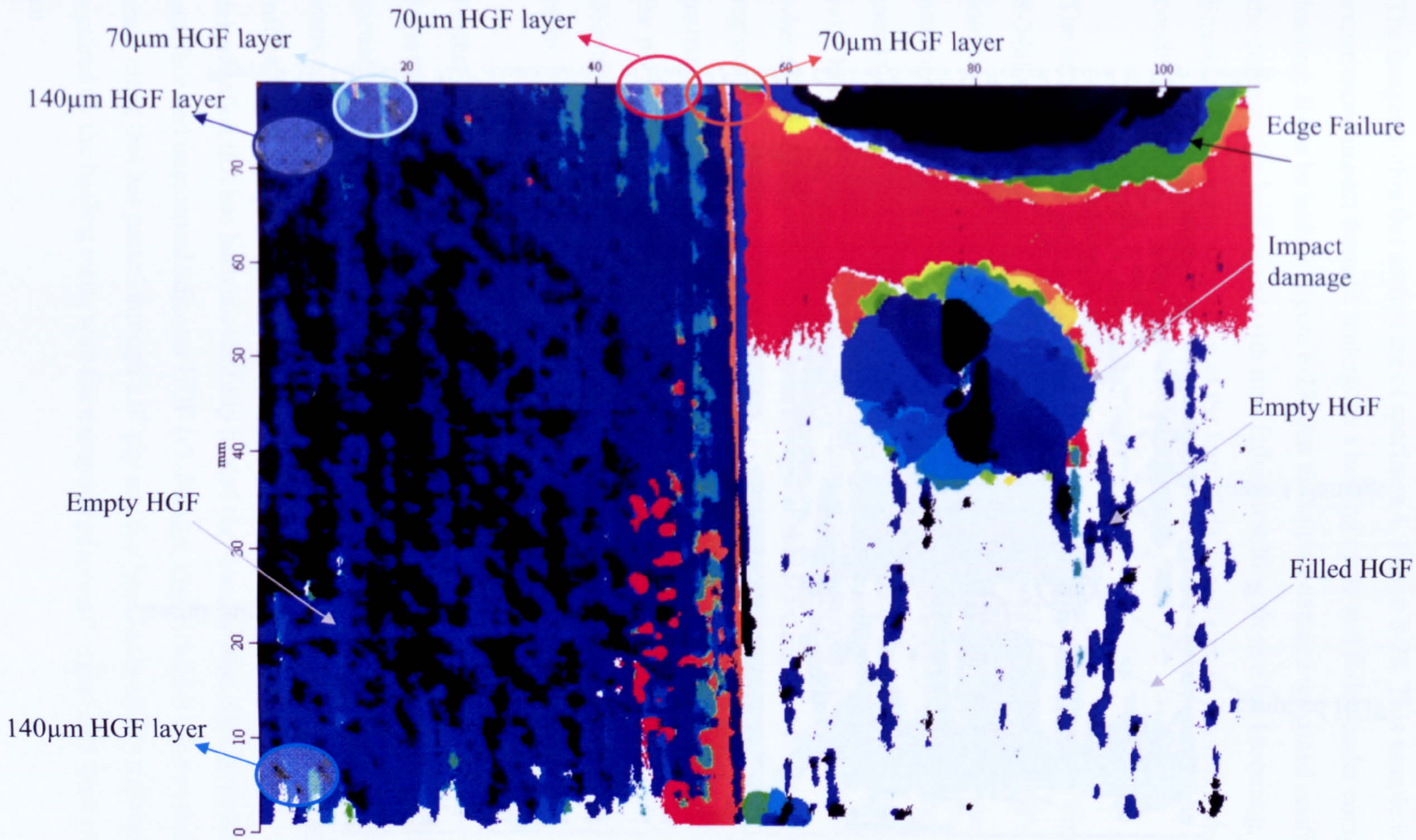

Figure 8-32: ***Ultrasonic TOF Assessment of a) Plain Undamaged and b) Damaged, Healed Laminates Showing Presence of HGF***

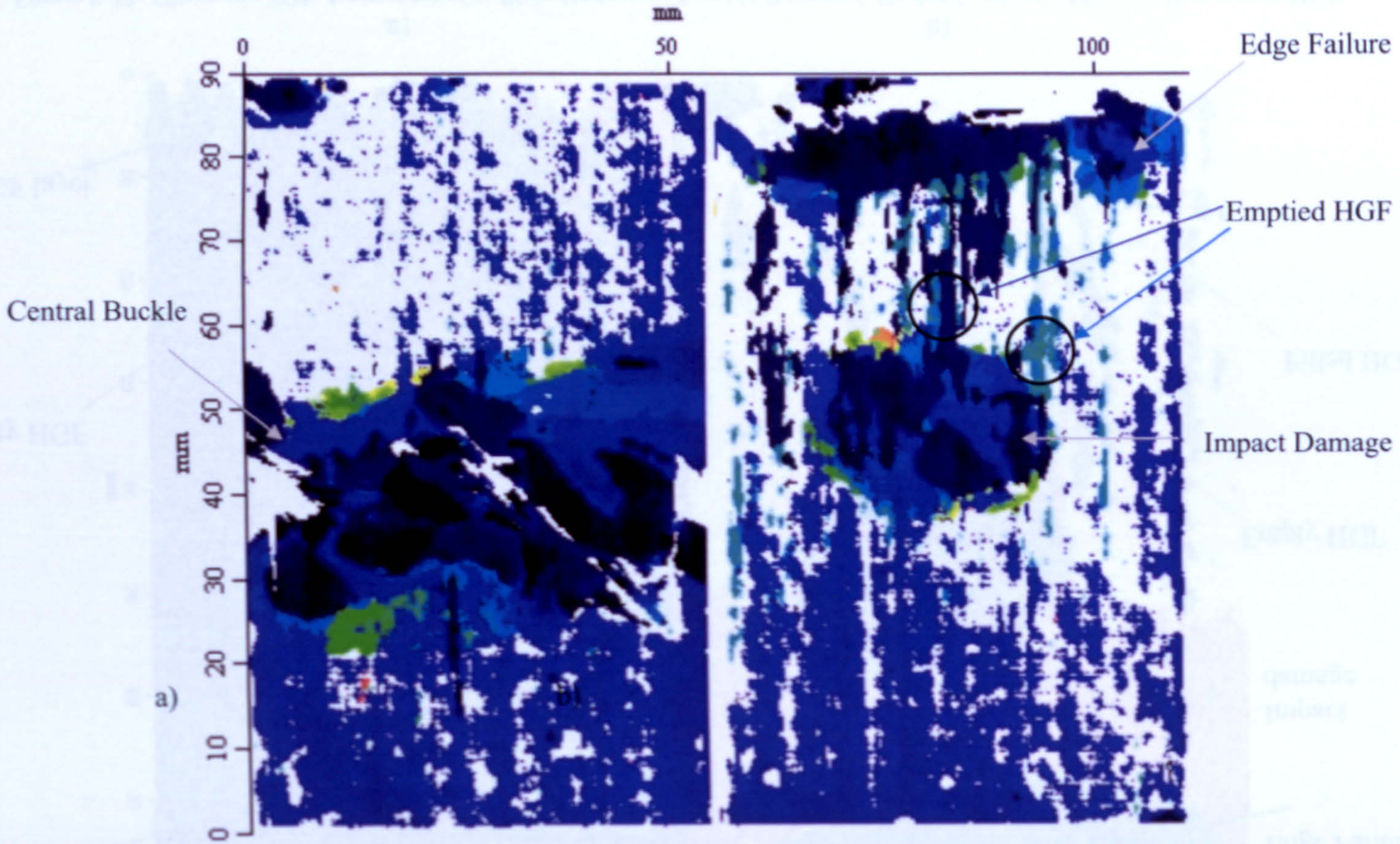

Figure 8-33: ***Ultrasonic TOF Assessment of a) Healed Failed by Central Buckle b) Healed Failed by Edge Failure***

8.4.2 Fractography

The images within this section are of specimen 4, Figure 8-28. This sample has experienced impact damage, undergone a healing cycle and failed under compressive loading. It can be seen in Figure 8-28, that the impact damage remained unaffected by the compressive loading and with final failure resulting from edge brooming. Fractographic images were taken of the impact damaged area to determine the condition of the HGF and the extent of the damage.

The images presented in Figure 8-34 are located near the point of impact. Figure 8-34a) shows an example of a delamination that has propagated along the 0°/-45° interface, intercepting a HGF at i). At ii) the delamination has been infiltrated by healing resin which has subsequently cured and repaired the damage. Further examples of this healing can be seen in the matrix shear cracks indicated at iii) and iv). These points of interest can be seen at a higher magnification in Figure 8-34b) where the healed damage is almost indistinguishable from adjacent undamaged regions of laminate. A further example of this is shown in Figure 8-34c) where a matrix shear crack can is seen passing through a HGF (v) before propagating through the ply and initiating a delamination at the ply interface (vi). Both the shear crack and delamination appear to have been successfully infiltrated and repaired by the healing resin.

Further examples of self-healed impact damage can be observed in Figure 8-35. Figure 8-35a) shows a large delamination (i) passing along a ply interface with only partial healing. At ii) the delamination has developed into a matrix shear crack that intercepts a local cluster of HGF, and the damage within this region has been fully infiltrated and repaired by the healing resin (iii). Figure 8-35b) shows that a delamination that has been successfully healed (iv) has deviated slightly from the ply interface and intercepted adjacent HGF (v). Finally, Figure 8-35c) shows a matrix shear crack that has passed through a 0° ply and has been successfully infiltrated and repaired by the healing resin, with the exception of a small region indicated at point vii.

Figure 8-36 provides additional evidence of successful healing within the laminate. It can be seen in Figure 8-36a) that a number of damaged regions are present but have been infiltrated with healing resin: i) shows a small delamination that has propagated along the ply interface and ii) shows a similar delamination that has propagated into the ply to form a matrix shear crack before intercepting a region occupied by HGF. The damage has propagated through the HGF located on this interface causing significant HGF rupture at point iii). Figure 8-36b) shows this region of ruptured HGF in more detail. Point iv) shows that a number of HGF have been fractured, which has released a large volume of healing resin to infiltrate the damage. Point v) shows a single HGF that has a small section of its wall shattered by local damage which has subsequently been suspended in the cured healing resin. This is shown in more detail in Figure 8-36c) where point vi) indicates the HGF and point vii) indicates the fractured HGF wall.

This is clear evidence that there is extensive rupture of HGF during impact and release of encapsulated healing resin. The resin appears to have been supplied in sufficient volume to fully infiltrate damage and entrain any residual debris.

8.4.3 Failure Modes

Further images of the failure modes after CAI assessment are presented in Chapter 7, section 4.3. In addition to this, three of the healed samples reported in Chapter 8 share the edge brooming (Figure 8-28 specimens 2, 4 and 6) shown in Chapter 7 that is characteristic of the undamaged samples. This is discussed in more detail in Chapter 8, section 4.2.

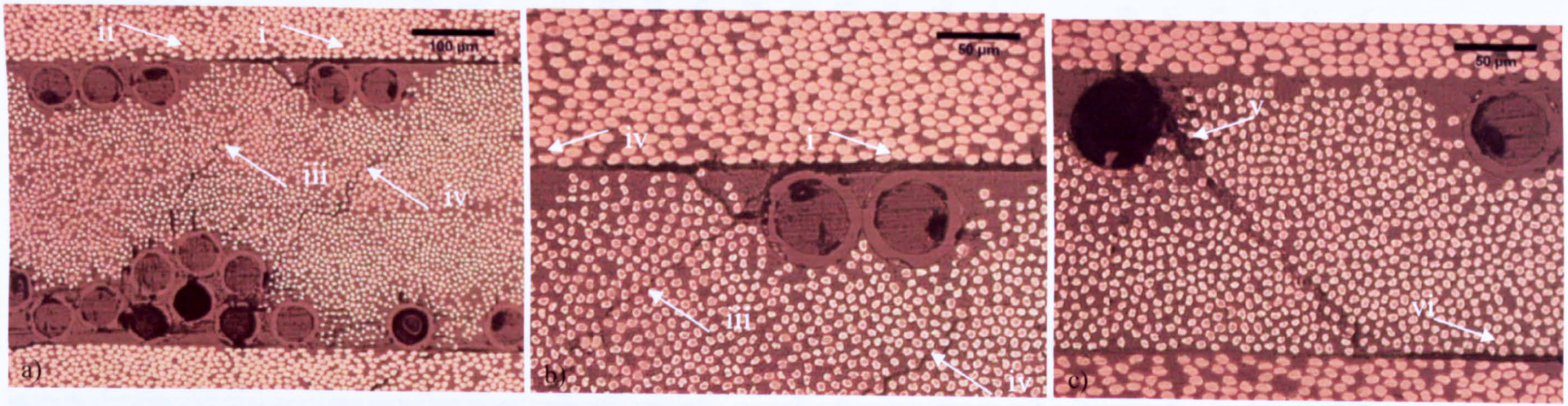

Figure 8-34: ***Healed Laminate after CAI Assessment showing Shear Cracks and Delaminations Infiltrated with Healing Resin***

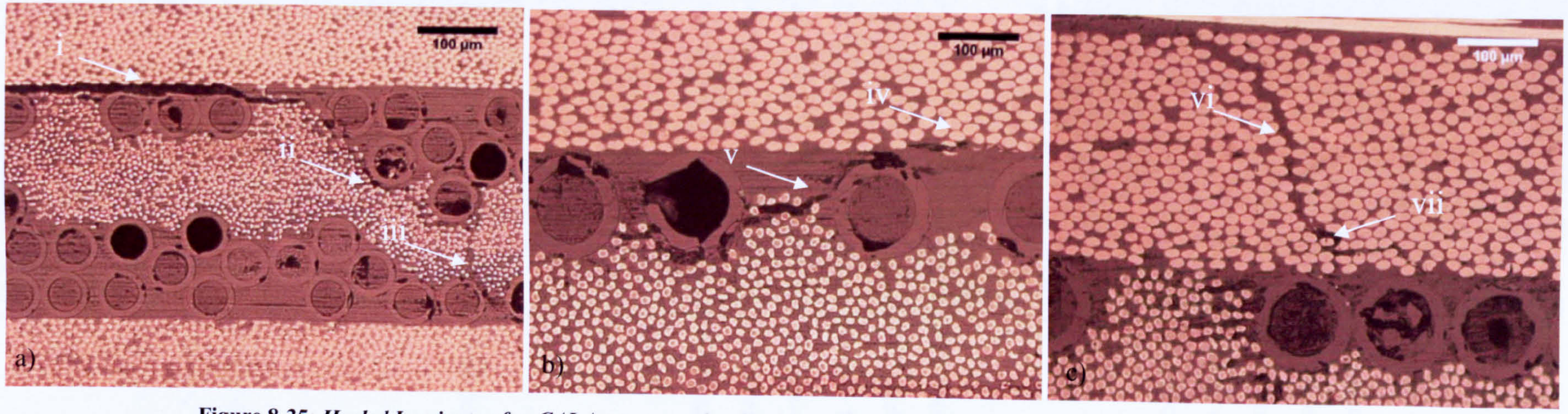

Figure 8-35: ***Healed Laminate after CAI Assessment showing Shear Cracks and Delaminations Infiltrated with Healing Resin***

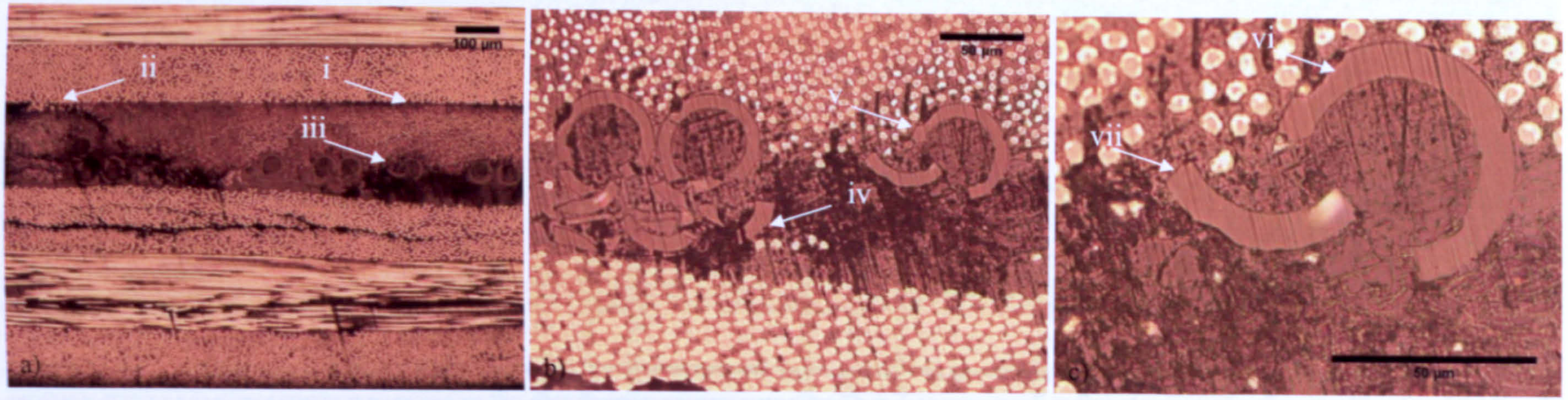

Figure 8-36: ***Healed Laminate after CAI Assessment showing a) Shear Cracks and Delaminations Infiltrated with Healing Resin b), c) Ruptured HGF Surrounded by Damage Infiltrated with Healing Resin***

8.5 Discussion

8.5.1 Overview

The process of self-healing described throughout this study invariably relies upon the occurrence of HGF fracture initiated by a damage event, and connectivity between HGF and the subsequent damage network generated within the laminate. Therefore, the location and number of HGF within the laminate would be expected to have a significant effect on the healing effectiveness. Thus far, the embedment of HGF has been optimised to meet the following requirements:

1. Minimise disruption to the host laminate
2. Maximise the volume of resin available for each HGF fracture

The latter requirement is partially a function of specimen dimensions which determine the maximum length of HGF achievable in a given laminate. For the specimens reported in this chapter, the maximum length was aligned with the 0° ply direction, however this would obviously increase significantly for real components as opposed to coupon testing. In practice, the method employed for incorporating HGF (section 2.1.2) allows orientation of HGF with the reinforcing fibre direction in any ply direction therefore allowing the HGF placement, in the self-healing laminate, to be optimised as required. Furthermore, it may be beneficial in practice, to locate the HGF away from the 0° interfaces to minimise detrimental effects to the laminate (primary load bearing fibre direction).

The optimised HGF configuration developed in Chapter 8 incorporated the best features from Chapter 7, plus two new features:

1. HGF placed at five interfaces
2. Two different HGF spacings

This configuration provided a self-healing solution that met a requirement to increase the volume of healing resin, whilst minimising the disruption to the laminate. The key factor that enabled these two requirements to be met was the variation in HGF spacing between interfaces. This provided two direct benefits:

1. Resin supply tailored to damage distribution: increased concentration of HGF towards the back face of the laminate improved the overall volume of resin supplied. This also reduced the reliance on connectivity between delaminations to transport healing resin.
2. Minimised disruption to host laminate: the tailored HGF distribution provided an overall performance equivalent to HGF spaced at 70μm on four interfaces but with the added advantage of being concentrated towards the back face.

It has been demonstrated that HGF can be embedded at five interfaces within a CFRP laminate without significant reduction in compression performance. However, it should be noted that the CAI test fixture is not specifically intended for assessing undamaged specimens. For a more comprehensive and representative assessment of the effects of embedded HGF on the compression properties of CFRP, a different test standard must be adopted. The addition of HGF at many interfaces required adjustment of the manufacturing process which resulted in laminates relatively uncompromised at the micro-scale. Some increased HGF clumping was observed, however, this can be improved with further optimisation of the manufacturing process and careful selection of the interfaces at which the HGF are embedded.

The impact response of the CFRP laminates with embedded HGF was consistent between specimens. There was some minor evidence to suggest that the energy absorption of the laminates was increased when the HGF were infiltrated with liquid resin. This may be attributable to an improved load transmission via hydrostatic pressure in the presence of an encapsulated incompressible fluid.

It has been demonstrated that resin filled HGF embedded within CFRP laminates can impart a capability to restore significant compression strength after low velocity impact. The average recovery of compression strength after impact was 95% even though two samples showed limited evidence of healing. Furthermore, effective healing was sufficient to restore the primary failure mode typical of an undamaged specimen.

Closer inspection of damaged regions after CAI testing provided evidence of a reduction in delamination area suggesting that the healing resin had infiltrated the cracks to a sufficient extent to prevent detection by ultrasound. This does not imply that the remaining

delaminations were not infiltrated with healing resin, but that the ultrasound was still able to discern a change in signal response.

The use of optical microscopy identified regions of impact induced damage that had been infiltrated and successfully repaired by the healing resin. The images presented in section 4.2, highlighted examples of matrix shear cracks and delaminations that were visually reduced to the extent that they were almost indistinguishable from the surrounding laminate. Other images identified regions of fractured HGF where the fibre debris was suspended in the cured healing resin after it had infiltrated the damage. Although this evidence is not conclusive, it is reasonable to suggest that the majority of damage generated within the laminate was infiltrated and repaired by the healing resin.

It was not possible to ascertain from this investigation if 100% infiltration of the damage was necessary to achieve an efficient heal or whether it was sufficient to create a crack blunting effect by infiltrating the perimeter of the impact damage delaminations. However, the probability of complete infiltration of the impact damage volume would be low as estimations suggest that all HGF within the cone of damage must be fractured and completely emptied of resin for this to be achieved (*Volumetric Assessment,* condition 1: V_1 and F_1 Table 8-4). As would be expected, the extremities of the impact damage cracks and delaminations were infiltrated due to the greater capillary forces generated by the small surface separations between delaminated plies at those locations. Generally, the surface separation of the delaminations would be expected to increase towards the centre of the impact site as this was the location of maximum deflection. Therefore, it would be reasonable to assume that the healing mechanism provides crack blunting combined with partial infiltration of the opening between delaminated interfaces.

8.5.2 Wider Significance

The results reported in this chapter have shown that for these damage conditions, loading conditions and sample sizes the placement of the HGF has performed well, producing almost 100% healing and minimal disruption to the laminate microstructure. This has extended work reported in Chapters 6 and 7 and also that reported in previous work reported by Pang et al [141,142] and Trask et al [147] who also considered the use of HGF for self-healing in FRP's. Furthermore, the *Configuration* and *Volumetric Assessment* tools

have been verified by enabling a refined HGF configuration to be designed to address specific conditions and achieve excellent results.

It has been shown that HGF can be integrated as discrete units instead of continuous plies in order to minimise the disruption to the host laminate and maintain its mechanical performance. This has significance as the material used as the host laminate was CFRP in preference to GFRP reported in previous work [141,142,147]. This material is more widely used for structural applications due to its higher specific strength and stiffness, therefore it was essential to demonstrate that HGF could be integrated without significant degradation to these properties.

The work reported in this chapter has demonstrated similar healing efficiencies to those reported in Chapter 6, those presented by Pang et al [141,142] and Trask et al [147] using a HGF based approach and also Kessler et al [148,149] and Yin et al [151,152] using a microcapsule based approach.

This work has demonstrated the suitability of a HGF delivery system to address low velocity impact damage within CFRP. Additionally, the use of compression after impact assessment has demonstrated that HGF can be embedded in sufficient numbers to provide an acceptable recovery in compressive strength with minimal disruption to the host laminate. Furthermore, this method of testing verified the resilience of a healed laminate to compressive loading, determined to be the most critical assessment of laminates with impact damage or inclusions.

It could be suggested that the use of microcapsules as a delivery system [148,149,150,152] would not be able to provide healing resin of sufficient volume to address the large scale damage characteristic of low velocity impact events. The disruption caused by embedded microcapsules currently limits their suitability for use in unidirectional pre-preg technology. Furthermore, the disruption generated within woven laminates would be inherently sensitive to compressive loading and therefore may result in significant reductions in compressive strength. Therefore the work presented in this report verifies the suitability of embedded HGF as a delivery system for self-healing CFRP.

9. Conclusions

The susceptibility of laminated FRPs to transverse impact loading is well documented in the open literature. Approaches taken to compensate for this, such as damage tolerant designs, are reported to be problematic in their application and can result in severe consequences for laminate performance. Likewise, the need for regular non-destructive inspection and repair to minor damage carries severe practical and economic penalties. The emerging technology of imparting some form of self-healing to a composite has shown potential in providing a more efficient solution to these challenges.

Numerous self-healing approaches have been documented in the literature, some of which have been used successfully for the purpose of addressing damage in FRPs. The benefits of using a HGF delivery system were particularly evident in terms of their ease of integration into fibre reinforced pre-impregnated tape composite technology and the relatively high volume of storage for a liquid healing agent when compared to competing technologies (i.e. microcapsules). However, there has been limited success thus far in integrating and demonstrating a self-healing system within CFRP. Therefore, after an extensive review of the literature (Chapter 2), the primary aim of this research was defined to be (Chapter 3):

"To develop and optimise an efficient HGF delivery system to facilitate a Self-Healing function in a representative Carbon Fibre Reinforced Plastic, ensuring minimal disruption to the laminate's innate mechanical performance."

A number of specific objectives were derived from this aim within Chapter 3. These provided the focus of the research and will be addressed individually within this chapter.

9.1 Resin System Selection

The healing resin system is of primary importance to the development of an effective self-healing CFRP laminate. It was recognised that the healing efficiency would be inherently dependent on the performance of the system in terms of its ability to:

1. Infiltrate the damage: *Ensure sufficient resin will exit from the HGF and infiltrate the damage*
2. Compatibility with the host matrix: *Ensure sufficient adhesion between the healing resin and the damaged surfaces*

3. Mechanical performance: *Ensure the mechanical performance of the cured resin is sufficient to inhibit further crack propagation from a damage site during subsequent mechanical loading*

A 'wish list' was derived to reflect the requirements for a self healing system. However, it was recognised that these requirements were specific to this application and that no current 'off the shelf' commercial system would fulfil every aspect. (Note: The development of a bespoke healing resin system was beyond the scope of this research)

Three fundamental requirements were identified to be of prime importance when assessing the suitability of an off-the shelf system as discussed in Chapter 4, section 2.

1. Long term stability: *Environmental resistance, storage life, volatiles content*
2. Structural efficiency: *Mechanical performance of cured resin*
3. Practical Requirements: *Resin viscosity, stoichiometric sensitivity, cure stimulus*

Four commercial systems were initially identified that met these requirements, and the relative benefits of each system were assessed (Chapter 4). The system finally selected was a two-part RTM epoxy resin, Cycom 823. This system had the added benefit that it had been previously used for research into self-healing GFRP [147] and therefore its suitability for this application had already been verified.

It was recognised that the use of this resin system in a pre-mixed form (i.e. one-part) prevented demonstration of an autonomous self-healing approach. However for the purposes of this study, it was recognised that employment of this system and the use of temperature to manipulate its viscosity would simulate the properties required from a 'yet to be developed' bespoke self-healing system. This allowed the HGF delivery system to be rigorously assessed and the viability of its application within a representative aerospace structure, after impact damage, to be explored.

9.2 Design and Optimisation of a HGF resin Delivery System

The integration of HGF within CFRP posed new challenges over and above those previously considered in the work on GFRP [141,142,147]. Specifically, the HGF could

not be integrated as entire HGF plies within the CFRP due to the gross detrimental effect this was likely to have in terms of hybridisation of the resulting laminate. Therefore, it was determined that the HGF would need to be embedded as discrete entities at predefined spacing along specific interfaces in the laminate. This generated two competing drivers in the configuration of a HGF delivery system:

- To minimise detrimental effects on host laminate mechanical performance:
    1. Minimise HGF outer diameter
    2. Utilise common direction interface
    3. Minimise number of HGF (minimise no. interfaces on which HGF present)
    4. Minimising HGF density (maximise HGF spacing)

- To maximise healing efficiency:
    1. Maximise HGF outer diameter
    2. Maximise HGF hollowness fraction
    3. Locate HGF at interfaces subjected to damage (non common direction)
    4. Maximise number of HGF (maximise no. interfaces on which HGF present)
    5. Maximise HGF density (minimise HGF spacing)

All these factors were taken into consideration during the design of laminate configurations for mechanical assessment. Two analytical tools were developed to give an initial indication of the likely performance of the resulting laminate configurations (Chapter 5):

- Configuration tool (Chapter 5, section 2.1)

This determined the number of HGF present, the number of carbon fibres replaced, the resin storage volume and the predicted effect on in-plane stiffness. The variables were the number of interfaces and the spacing between HGF.

- Volume Assessment tool (Chapter 5, section 2.2)

This estimated the volume of damage and related that to the volume of healing resin stored within each configuration. Ultrasonic measurement was used to determine the damage volume and the resin storage volume was determined within the configuration tool.

The outer diameter of the HGF was fixed at 60μm for ease of manufacture and to provide a reasonable storage volume per unit fibre length. Therefore, the spacing between HGF within an interface was defined in terms of multiples of the HGF outer diameter. Also, the interfaces at which the HGF were located were restricted to those adjacent to 0° CF plies to improve the embedment, this provided seven possible interfaces for the sixteen ply QI laminate used throughout this research (Chapters 6,7,8).

9.3 HGF Manufacture and Incorporation within a Laminate

Manufacture of HGF at Bristol has been widely described in the open literature [141-147]. The specific manufacturing parameters within this study enabled the reliable manufacture of 60μm OD HGF, with a hollowness fraction of around 60%. HGF spacing was controllable in the ranges defined (i.e. 70μm to 210μm) to a reasonable degree of accuracy. However, problems were observed at low HGF spacing due to fibre clumping. The resulting resin rich regions contributed to an increase in laminate thickness and a reduction in undamaged mechanical performance. However, this also appeared to improve the impact damage tolerance of the laminates by reducing the induced delaminations. Improvements to the manufacturing process to improve fabrication quality were identified as follows;

1. A clean, temperature and humidity controlled environment
2. More precise controls to improve accuracy of HGF spacing thereby reducing clumping
3. A hollowness monitor with real-time feedback to reduce reliance on operator skill and allow generation of HGF with high hollowness
4. Larger diameter winding drum to increase laminate size and reduce curvature to avoid HGF detachment during manufacture.

An efficient method of resin infiltration into the HGF has been developed which raises the resin temperature, reducing viscosity and hence the time required for complete infiltration. It was recognised that this could be a limiting factor for large structural applications with complex geometry.

9.4 Mechanical Assessment

A mechanical assessment of self-healing laminates was essential to determine the effectiveness of the various HGF configurations and the overall efficiency of the self-healing process. Three stages of assessment were undertaken:

4. **Stage 1**: Flexural Assessment (Chapter 6)
   Laminates were configured for damage inflicted by quasi-static indentation.
5. **Stage 2**: CAI Assessment – Effect of HGF Content (Chapter 7)
   Laminate configurations from Stage 1 were subject to low velocity drop weight impact testing before being mechanically assessed under compressive loading.
6. **Stage 3**: CAI Assessment – Optimised HGF Content (Chapter 8)
   The results from stage 1 and stage 2 were formulated into an optimised design for further CAI testing.

Laminates were assessed in three states:

- **Undamaged**: *Assessed the disruption to the laminate caused by presence of HGF by measuring the mechanical properties of the undamaged laminate.*
- **Damaged**: *Assessed the reduction in laminate mechanical properties due to the presence of damage. This also determined if there were any improvements to damage tolerance caused by embedded HGF or if they acted as nucleation sites for damage.*
- **Healed**: *Assessed the recovery in mechanical properties due to healing, after being damaged. This was essential to determine the effectiveness of the healing system and to support development of self-healing composite materials for structural applications.*

9.4.1 Stage 1. Flexural Assessment

Two configurations of self-healing laminate that consisted of HGF located at two interfaces and fibre spacing of either 70μm or 210μm were investigated under four point bend flexure. The microstructure of both configurations was investigated to relate the mechanical performance with any anomalies caused by the presence of HGF.

Quasi-static indentation was used to impart damage to the laminates. Ultrasonic inspection and optical microscopy verified that this damage was a valid representation of low velocity impact damage and more specifically BVID. However, it was recognised that the support conditions generated a concentrated load.

Flexural testing was used to assess the performance of the two configurations in the undamaged, damaged and healed states. The 70μm HGF spacing configuration was observed to result in the most significant disruption to the host laminate. Regions of significant HGF clumping were observed which generated resin rich regions and contributed to an 8% reduction in undamaged flexural strength. Imparting damage caused a reduction in flexural strength of 24%. Although a significant reduction, this was a 7% improvement over the residual strength of a damaged plain CFRP laminate. This indicated an increased degree of damage tolerance and was attributed to the energy absorbed by HGF fracture under impact loading. After healing, the 70μm HGF configuration achieved a recovery of 14%, equivalent to 97% of the undamaged strength or 89% of the undamaged plain CFRP strength.

The 210μm HGF spacing configuration was observed to cause significantly less disruption to the host laminate. No HGF clumping was observed, and the spacing between fibres was sufficient such that the embedment was extremely efficient. There was, however, a 2% reduction in the undamaged strength though this was within experimental scatter. The laminate showed no signs of improved damage tolerance upon indentation. However, after healing it was able to achieve a recovery of 12%, equivalent to 82% of the undamaged strength or 80% of the undamaged plain CFRP strength.

In both configurations, there was no evidence to suggest that the presence of HGF within the laminate affected the propagation of damage under flexural loading. The failure modes for laminates with and without HGF were not distinguishable under flexural loading.

UV fluorescent dye was combined with healing resin to highlight the damage infiltration under quasi-static impact. Optical microscopy was used to identify delaminations and shear cracks that were successfully infiltrated with this pigmented healing resin. It was shown that the majority of damage was infiltrated to some extent. However, damage with small surface separations such as shear cracks appeared to be completely infiltrated, in contrast

to delaminations with larger surface separations which were not. This highlighted the criticality of the capillary action in driving the healing process.

9.4.2 Stage 2. CAI Assessment Effect of HGF Content

It was identified in the literature that laminates were more sensitive to inclusions when under compressive loading. Although flexural testing induces a compressive force on the plies above the laminate neutral axis, it was decided that compression after impact testing provided a more stringent assessment of laminate performance. Furthermore, drop weight impact testing imparted more representative damage typical of that expected from low velocity impact.

The laminate configurations assessed in Stage 1 were also investigated for this analysis. However, two additional configurations were proposed:

1. 140μm HGF spacing at two interfaces
2. 210μm HGF spacing at four interfaces

The purpose of these configurations was to explore the balance between increased resin storage volume and improvements in HGF embedment. Improved distribution of HGF through the laminate, by increasing the number of HGF interfaces, was intended to reduce the reliance on damage connectivity to transport healing resin where required.

The CAI assessment method was based on a specification outlined in research conducted by Prichard and Hogg [191]. This addressed the primary issue for current CAI standards, their unsuitability for thinner/smaller sample sizes. Additional boundary conditions were required for the drop weight impact in order to ensure the impact damage was confined to the central region of the laminates, thereby eliminating its interaction with the boundary conditions of the CAI test fixture.

A 6J low velocity impact event reduced the residual strength to 50-60% of the undamaged strength. Ultrasonic assessment identified that the presence of HGF improved the impact damage tolerance of the laminates. This was evident by a reduction in delamination area for laminates with embedded HGF in comparison to plain laminates and an increase in absorbed energy (average 10% increase). In particular, the laminate configuration with

HGF at four interfaces experienced improved impact damage tolerance compared to other configurations.

Strain gauges located on the CAI specimens indicated the expected buckling failure of impact damaged samples under compressive loading. A central buckling failure mechanism was consistent for both damaged and healed laminates. This indicated that the healing that had occurred was not sufficient to suppress this failure mechanism.

It was concluded that there were four possibilities as to why no apparent recovery in mechanical properties was observed:

1. Impact energy level was too high
2. Healing resin volume was too low
3. Insufficient HGF fracture
4. Inadequate adhesion between healing resin and matrix resin

9.4.3 Stage 3. CAI Assessment Optimised HGF Content

Conclusions drawn from Stage 2 identified the need to further optimise the configuration of HGF within the laminates. Two primary drivers were identified:

1. Increased healing resin storage volume
2. Increased number of interfaces at which HGF are present

Therefore, a revised laminate configuration was proposed that included 140μm spaced HGF at two interfaces above the centreline and 70μm spaced HGF at three interfaces below the centreline. This configuration effectively doubled the healing resin storage volume of the best configuration in Stage 2 (70μm@ 2 interfaces). Furthermore, it increased the number of interfaces containing HGF and tailored the distribution of these to match the profile of the impact induced damage. Improving the through thickness distribution of HGF within the laminate reduced the reliance on damage connectivity to transport healing resin to damaged interfaces.

Optical microscopy highlighted areas of HGF clumping that occurred on both 140μm and 70μm HGF spacing interfaces. This was to be expected due to the number of interfaces required for HGF embedment. It had been concluded previously (Chapter 4, section 3) that

to ensure optimum embedment the HGF must ideally be incorporated directly into the 0° reinforcing fibre plies. However, practical constraints dictated that this was not possible and therefore an optimal embedment was not achievable. Regions of consistent HGF spacing/embedment were observed and therefore, could be consistently achieved with improvements to the manufacturing process.

The impact energy for CAI testing was reduced to 3J to ensure that delaminations were unaffected by the boundary conditions of the impact test fixture. This impact energy was sufficient to reduce residual strength to 58% of the undamaged strength. There was no observable change in the impact response of the laminate due to the presence of the additional HGF with the exception that coupons with fully infiltrated HGF fibres absorbed an increased amount of impact energy compared to laminates with empty HGF (50%). This was attributed to increased HGF fracture stimulated by increased load transmission via hydrostatic forces within the incompressible resin in-situ. Though this effect was not observed for the higher impact energy (6J) considered in Stage 2.

The effect of HGF on the undamaged strength of the laminates proved inconclusive. The use of a CAI test fixture was not appropriate for this purpose and further testing with a better suited test arrangement would be necessary. However, a 'baseline' undamaged strength was measured and was useful for comparative purposes within this assessment of self-healing effectiveness and efficacy.

Laminates that underwent a self-healing cycle achieved an average of 95% of the plain undamaged strength, equivalent to a 29% recovery. It was also observed that in the majority of cases, damage within coupons was healed sufficiently to alter the failure mechanism from central buckling (typically experienced by damaged samples) to edge brooming (typically experienced by undamaged laminates). Ultrasonic C-scan inspection provided further evidence for this change in failure mode. For undamaged specimens, large regions of damage were generated towards the top or bottom edge of the laminates which directly resulted in failure. For damaged specimens, the central buckling, initiated by the transverse propagation of the impact induced delaminations, initiated failure.

It was also observed that the areas of delaminations, identified by ultrasonic inspection, were visibly reduced after healing. This was most evident towards the peripheral regions of

the delaminations where the crack surface separation was minimal. It was not ascertained whether the remainder of the delaminations were also infiltrated or whether a crack blunting effect was sufficient to prevent significant damage propagation. However, optical microscopy has shown evidence that delaminations and matrix shear cracks were completely infiltrated and successfully repaired by the healing resin. The effectiveness of this infiltration was such that, in some cases, the damage was almost indistinguishable from the surrounding laminate. This evidence would suggest that the majority of the damage within the laminate is successfully filled by a healing resin, and any incomplete filling is still sufficient to prevent the damage propagating under compressive loading.

In conclusion, it has been shown that embedding HGF within a CFRP composite laminate is a viable method to create a storage vessel for a liquid resin system for the purpose of self-healing. It has been shown that the minor disruption caused to the CFRP laminate microstructure is outweighed by the improved impact damage tolerance and the subsequent recoverable mechanical properties after a healing event. Recovery to around 90% of the undamaged strength has been demonstrated for flexural and compressive loading. Such a concept is well suited to address the typical damage profile created by BVID in aerospace structures.

10. Further Work

As part of the studies described herein, a number of areas within the development of self-healing CFRP have been identified for further investigation.

10.1 Autonomy

The current research has focussed on the design of a delivery system for a 'healing agent' rather than the healing agent itself. As such, the healing agent selected for this demonstration study was the most suitable 'off the shelf' system available at this time. One of its major limitations was that it required the application of heat to achieve cure within a practical time period of a few hours. It is fully acknowledged that a new 'bespoke' resin system is required that will fully meet the specification and desirable features of a practical and effective self-healing resin system. One major requirement is that it should possess a high level of autonomy in terms of its ability to cure under a variety of environmental conditions, mix ratios and time spans. However, the delivery system described herein is eminently suitable for and adaptable to use with a wide range of potential healing resin chemistries.

10.2 Healing Resin Infiltration of Damage

Efforts were made to identify the volume and extent of damage that was infiltrated by the healing resin, whether these areas were completely or partially filled and whether crack blunting was sufficient to prevent impact damage propagation. Additional higher fidelity techniques, such as micro CT scanning, need to be explored to provide a clearer insight. The use of finite element analysis combined with appropriate experimental studies would help to identify the critical parameters of damage infiltration that are required for effective healing. For example, the extent of infiltration and the properties of the adhered healing agent are likely to have important effects.

10.3 Assessment of HGF Fracture

A critical aspect of the proposed self-healing mechanism is the fracture of embedded HGF under impact loading. The effect of HGF distribution and volume fraction on the probability of interaction with progressing cracks is of paramount importance for refinement of the self-healing technique. High fidelity inspection techniques such as micro

CT scanning could possibly be used to determine the occurrence of HGF fracture (and the egress of healing resin into the crack) in real-time.

10.4 Self-Healing after Multiple Impacts

It remains to be demonstrated that using this approach can achieve self-healing after repeated impact at the same location. Initial indications have shown that HGF are not necessarily emptied completely of healing agent after being ruptured. Therefore the possibility remains for further healing function. A key limitation in demonstrating repeat healing capability to date has been the unavailability of an optimised healing agent.

Two possible multiple impact scenarios are envisaged for further study:

1. Multiple impacts at a single location: This would determine the number of repeat impacts that could be tolerated and how the healing efficiency reduces with the number of impacts.
2. Multiple impacts over a localised area: This would determine how the close proximity of additional impacts affects the healing efficiency.

10.5 Enhanced Damage Visualisation

The incorporation of a conspicuous indicator (e.g. dye or particulate dispersion) as an additive to the healing system or within HGF as an additional surface layer on the laminate presents the opportunity for enhanced damage visualisation. This would facilitate easier damage detection (especially with regard to BVID) and perhaps provide some additional means of gauging the remaining healing potential within the material.

10.6 Compression Testing of Undamaged Self-Healing Laminates

This research has used a CAI test protocol for testing undamaged samples. This was known to provide an inaccurate assessment of the disruption to the laminates caused by embedded HGF. Thus, a more appropriate method of compression testing is needed to assess the true effect of HGF on the host laminate mechanical performance.

10.7 Interactions between Propagating Cracks and HGF

Further investigation is needed to fully characterise the impact response of HGF within CFRP. The interaction of HGF with propagating shear cracks and delaminations created by impact needs to be characterised and understood. Such crack propagation may result from cyclic loading which brings into question the response of this self-healing approach under fatigue.

Some observations have indicated that the presence of HGF within a laminate confers improved impact damage tolerance on the structure. This possibility needs to be confirmed and the mechanisms by which this occurs need to be identified.

10.8 Optimised Manufacture of Self-Healing Laminates

A number of manufacturing deficiencies in the laminates produced for testing have been highlighted previously (Chapters 6,7,8) Further optimisation of the process is needed to improve both the quality of the laminate and the robustness of this self-healing approach. Improvements include;

a. Improved HGF embedment to minimise resin rich regions
b. Review of HGF geometry and dimensions to optimise their structural integration
c. Review HGF properties in terms of materials selection, manufacturability, handle-ability and fracture characteristics

Considerations also need to be undertaken with regard to how a resin filled HGF self-healing approach could be manufactured and integrated into structural CFRP components on a larger (commercial) scale.

11 References

[1] www.Hexcel.com

[2] Peters, S.T. *"Handbook of Composites"*, second edition (1997)

[3] Spillman, W.B., Sirkis. J.S., Gardiner, P.T., (1996) *"Smart materials and structures: What are they?"* Smart Materials and Structures..5:247-301.

[4] Wlezien, R.W., Horner, G.C., McGowan, A.R., Padula, S.L., Scott, M.A., Silcox, R.J., Simpson, J.O. (1998) *"The Aircraft Morphing Program,"* NASA Langley Research Centre, 39th Structures, Structural Dynamics and Materials Conference and Exhibit

[5] Loewy, R.G., (1997), *"Recent developments in smart structures with aeronautical applications,"* Smart Materials & Structures 6: R11-R42.

[6] Etches J.A., Scholey, J.J., Williams G.J., Bond I.P., Mellor P.H., Friswell M.I. and Lieven, N.A. (2007) *"Exploiting Functional Fibres in Advanced Composite Materials"* Journal of Intelligent Material Systems and Structures 18(5):449-458

[7] Beckert, W., Kreher, W.S., (2003) *"Modelling piezoelectric modules with interdigitated electrode structures"* Computational Materials Science 26: 36-45.

[8] Schulz, M.J., Pai, P.F., Inman, D.J. (1999) *"Health monitoring and active control of composite structures using piezoceramic patches,"* Composites: Part B-Engineering 30: 713-725.

[9] Straub, F.K., Merkley, D.J. (1997) *"Design of a smart material actuator for rotor control"* Smart Materials & Structures 6: 223-234.

[10] Straub, F.K., Ngo, H.T., Anand, V., Domzalski, D.B., (2001) *"Development of a piezoelectric actuator for trailing edge flap control of full scale rotor blades,"* Smart Materials & Structures 10: 25-34.

[11] Brei, D. and Cannon, B.J. (2004) *"Piezoceramic hollow fibre active composites"*, Composites Science and Technology 64: 245-261.

[12] Gude, M. and Hufenbach, W. (2006) *"Design of Novel Morphing Structures Based on Bi-stable Composites with Piezoceramic actuators"*. Mechanics of Composite Materials, 42(4): 339-346

[13] Dano, M.L. and Hyer, M.W. (2002), *"Snap-through of unsymmetric fibre-reinforced composite laminates"*. International Journal of Solids and Structures 39: 175-198

[14] Potter, K., Weaver, P., Seman, A.A. and Shah, S. (2006), *"Phenomena in the bifurcation of unsymmetric composite plates"*. Composites: Part A 38: 100-106

[15] Wang, S.Y., Tai, K. and Quek, S.T. (2005) *"Topology optimisation of piezoelectric sensors/actuators for torsional vibration control of composite plates"*. Smart Materials and Structures 15: 253-269

[16] Simeos, R.C., Hagopian, J.D. and Mahfoud, J. *"Modal Active Vibration Control of a Rotor Using Piezoelectric Stack Actuators"*. Journal of Vibration and Control 13(1): 45-64

[17] Choi, Y.T. and Wereley, N.M. (2005), *"Semi-Active Vibration Isolation Using Magnetorheological Isolators"*, Journal of Aircraft 42(5): 1244-1251

[18] Dominguez, A., Sedaghati, R. and Sitharu, I. (2004) *"Modelling of the hysteresis phenomenon of magnetorheological dampers"*. Smart Materials and Structures 13: 1351-1361

[19] Bailey, C.D., Hamilton, J.M. and Pless, W.M. (1976), *"AE monitoring of rapid crack growth in a production-size wing fatigue test article"*, NDT International 9: 298-304

[20] Bailey, C.D. and Pless, W.M. (1977), *"Acoustic-Emission of impact damaged graphite-epoxy composites"*, Materials Evaluation 35: S8-S8

[21] Bailey, C.D. and Pless, W.M. (1981), *"Acoustic Emission an emerging technology for assessing fatigue damage in aircraft structure"*, Materials Evaluation 39: 1045-1050

[22] Lindahl, D. and Knuuttila, M. *"Acoustic emission monitoring of the JAS 39 Gripen combat aircraft"*, www.ndtsweden.com/artiklar.htm

[23] Badcock, R.A. and Fernando, G.F. (1995) *"An intensity based optical fibre sensor for fatigue damage detection in advanced fibre-reinforced composite materials"*, Smart Materials and Structures", 4: 223-230.

[24] Lee, DG, Mitrovic, M, Friedman, A, Carman, GP and Richards, L. (2002) *"Characterization of Fiber Optic Sensors for Structural Health Monitoring"*, Journal of Composite Materials 36: 1349-1365.

[25] Baker, A.A., Jones, R. and Callinan, R.J. (1985) "*Damage Tolerance of Graphite/Epoxy Composites"* Composite structures 4: 15-44

[26] Prevorsek, D.C., Chin, H.B. and Bhatnagar, (1993) "*Damage tolerance: design for structural integrity and penetration"* Composite Structures 23: 137-148

[27] Hull D and Shi YB, (1993) "*Damage mechanism characterisation in composite damage tolerance investigations"* Composite structures 23: 99-120

[28] Richardson, M.O.W. and Wisheart, M.J. (1996) "*Review of low-velocity impact properties"* Composites Part A 27:1123-1131

[29] Serge Arbrate *"Impact on composite structures"* Cambridge University press 1998

[30] Choi, H.Y., Downs, R.J. and Chang, F.K. (1991) *"A new approach towards understanding damage mechanisms and mechanics of laminated composites due to low velocity impact: Part 1-Experiments"* Journal of Composite Materials 25: 992-1011

[31] Choi, H.Y., Wu, H.Y.T. and Chang, F.K. (1991) *"A new approach toward understanding damage mechanisms and mechanics of laminated composites due to low velocity impact: Part 2 Analysis"* Journal of Composite Materials 25: 1012-1038

[32] Liu, S., Kutlu, Z. and Chang, F.K. (1993) *"Matrix cracking and delamination in laminated composite beams subjected to a transverse concentrated line load"* Journal of Composite Materials 27(5): 436-470

[33] Sjoblom, P.O., Hartness, J.T. and Cordell, T.M. (1998) *"On low velocity impact testing of composite materials"* Journal of composite materials 22: 30-52

[34] Shivakumar, K.N., Elber, W. and Illg, W. (1985) *"Prediction of low-velocity impact damage in thin circular laminates"* AIAA J. 23(3): 442-449

[35] Abrate, S. (1991) *"Impact on laminated composite materials"* Applied Mechanics Review 44(4): 155-190

[36] Liu, D. and Malvern, L.E. (1987) *"Matrix Cracking in impacted glass/epoxy plates"* Journal of Composite Materials 21: 594-609

[37] Joshi, S.P. and Sun, C.T. *"Impact Induced fracture initiation and detailed dynamic stress field in the vicinity of impact"* Proc. American Society of Composites 2nd Tech Conf DE 23-25 September 1987 pp177-185

[38] Cantwell, W. and Morton, J. (1985) *"Detection of impact damage in CFRP laminates"* Composite structures 3, 241-257

[39] Liu, D. (1988) *"Impact-induced delamination-a view of bending stiffness mismatching"* J. Composite Materials 22: 674-692

[40] Takeda, N., Sierakowski, R.L. and Malvern, L.E. (1982) *"Microscopic observations of cross sections of impacted composite laminates"* Composites Technology Reviews 4(2): 40-44

[41] Cantwell, W.J., Curtis, P.T. and Morton, J. (1983) *"Low velocity impact damage tolerance in CFRP laminates containing woven and non-woven layers"* Composites 14: 301-305

[42] Jones, R., Paul, J., Tay, T.E. and Williams, J.F. (1988) *"Assessment of the effect of impact damage in composites: some problems and some answers"* Composite Structures 10(1): 51-73

[43] Cantwell, W.J. and Morton, J. (1991) *"The impact resistance of composite materials- a review"* Composites 22(5): 347-362

[44] Cantwell, W.J., Curtis, P.T. and Morton, J. (1986) *"An Assessment of the Impact Performance of CFRP Reinforced with High-strain Carbon Fibres"*. Composites Science and Technology 25: 133-148

[45] Chikhi, N., Fellahi, S. and Bakar, M. (2002) *"Modification of epoxy resin using reactive liquid (ATBN) rubber"*. European Polymer Journal 38: 251-264

[46] Chen, P., Shen, Z. and Wang, J.Y. (2001) *"Damage Tolerance Analysis of Cracked Stiffened Composite Panels* Journal of Composite Materials 35: 1815-1843

[47] Roudolff, F. and Gadke, M. (2000) *"Damage tolerance of composite structures for large transport aircraft"* Aerospace Science Technology 4: 23-32

[48] Zhou, G. (1998) *"The use of experimentally-determined impact force as a damage measure in impact damage resistance and tolerance of composite structures"* Composite Structures 42: 375-382

[49] Hughes, J.D.H, (1991) *"The Carbon Fibre/Epoxy Interface –A Review"*. Composites Science and Technology 41: 13-45

[50] Christoforou, A. (2001) *"Impact dynamics and damage in composite structures"* Composite Structures 52: 181-188

[51] Elder, D.J., Thomson, R.S., Nguyen, M.Q. and Scott, M.L. (2004) *"Review of delamination predictive methods for low speed impact of composite laminates"*. Composite Structures 66: 677-683

[52] Hull, D. and Shi, Y. (1993) *"Damage Mechanism characterisation in composite damage tolerance investigations"*. Composite Structures 23: 99-120

[53] Fuoss, E., Straznicky, P. and Poon, C. (1998) *"Effects of stacking sequence on the impact resistance in composite laminates. Part 1. Parametric study"*. Composite Structures 41: 67-77

[54] Greenhalgh, E. and Hiley, M (2003) "The assessment of novel materials and processes for the impact tolerant design of stiffened composite aerospace structures". Composites: Part A 34: 151-161

[55] Tanimoto, T. (2002) *"Damage tolerant behaviours of a biomimetic CFRP laminate"* Advanced Composite Materials 11(1): 11-19.

[56] Todoroki, A. and Haftka, R.T. (1998) *"Stacking sequence optimisation by a genetic algorithm with a new recessive gene like repair strategy"* Composites Part B 29(B): 277-285

[57] Mouritz, A.P., Leong, K.H. and Herszberg, I. (1997) *"A review of the effect of stitching on the in-plane mechanical properties of fibre reinforced polymer composites"*. Composites: Part A 28(A): 979-991

[58] Kelkar, A.D., Tate, J.S. and Bolick, R. (2006) *"Structural integrity of aerospace textile composites under fatigue loading"*. Materials Science and Engineering B 132: 79-84

[59] Dransfield, K., Baillie, C. and Mai, Y.W. (1994) *"Improving the delamination resistance of CFRP by stitching- A review"*. Composites Science and Technology 50: 305-317

[60] Cartie, D.D.R., Dell' Anno, G., Poulin, E. and Partridge, I.K. (2006) *"3D reinforcement of stiffener-to-skin T-joints by Z-pinning and tufting"*. Engineering Fracture Mechanics 73: 2532-2540

[61] Freitas, G. Magee, C., Dardinski, P. and Fusco, T. (1994) *"Fiber insertion process for improved damage tolerance in aircraft laminates"* Journal of advanced materials 25(4): 36-43

[62] Mouritz, A. (2007) *"Review of z-pinned composite laminates"*. Composites Part A 38: 2383-2397

[63] Gilbert, E.N., Hayes, B.S. and Seferis, J.C. (2003) *Interlayer toughened unidirectional carbon prepreg systems: effect of preformed particle morphology"*. Composites: Part A 34: 245-252

[64] Groleau, M.R., Shi, Y.B., Yee, A.F., Bertram, J.L., Sue, H.J. and Yang, P.C. (1996) *"Mode II fracture of composites interlayered with nylon particles"*. Composites Science and Technology 56: 1223-1240

[65] Sela, N. and Ishai, O. (1989) *"Interlaminar fracture toughness and toughening of laminated composite materials: a review"*. Composites 20(5): 423-435

[66] Dorey, G., Sidey, G.R. and Hutchings, J. (1978) *"Impact Properties of carbon fibre/Kevlar 49 fibre hybrid composites"*. Composites 9(1): 25-32

[67] Garg, A.C. and Mai, Y.W. (1988) *"Failure Mechanisms in Toughened Epoxy Resins- A Review"*. Composites Science and Technology 31: 179-223

[68] Huang, Y. and Kinloch, A.J. (1992) *"Modelling of the toughened mechanisms in rubber-modified epoxy polymers"*. Journal of Materials Science 27: 2753-2762

[69] Kinloch , A.J., Yuen, M.L. and Jenkins, S.D. (1994) *"Thermoplastic-toughened epoxy polymers"*. Journal of Materials Science 29: 3781-3790

[70] Schauer, E., Berglund, L., Pena, G., Marieta, C. and Mondragon, I. (2002) *"Morphological variations in PMMA-modified epoxy mixtures by PEO addition"*. Polymer 43: 1241-1248

[71] Pearson, R.A. and Yee, A.F. (1993) *"Toughening mechanisms in thermoplastic-modified epoxies: 1. Modification using poly(phenylene oxide)"*. Polymer 34: 3658-3670

[72] Lange, F.F. and Radford, K.C. (1971) *"Fracture Energy of an Epoxy Composite System"*. Journal of Materials Science 6: 1197-1203

[73] Mallick, P.K. and Broutman, L.J. (1975) *Mechanical and Fracture Behaviour of Glass Bead Filled Epoxy Laminates"*. Materials Science and Engineering 18: 63-73

[74] Kim, H.S. and Khamis, M.A. (2001) *"Fracture and impact behaviours of hollow micro-sphere/epoxy resin composites"*. Composites: Part A 32: 1311-1317

[75] Morri, T., Hamada, H., Desaeger, M., Gotoh, A., Yokoyama, A., Verpoest, I. and Maekawa, Z. (1995) *"Damage tolerance of glass mat/epoxy laminates hybridized with flexible resin under static and impact loading"* Composite structures 32: 133-139

[76] Xian, X.J. and Choy, C.L. (1994) *"Fatigue fracture behaviour of carbon-fibre-reinforced modified bismaleimide composites"* Composites Science and Technology 52: 93-98

[77] Godwin, E.W. and Mathews, F.L. (1980) *"A review of the strength of joints in fibre-reinforced plastics Part 1. Mechanically fastened joints"*. Composites 11(3): 155-160

[78] Mathews, F.L., Kitty, P.F. and Godwin, E.W. (1982) *"A review of the strength of joints in fibre-reinforced plastics Part 1. Adhesively bonded joints"*. Composites 13(1): 29-37

[79] Chan, W.S. and Vedhagiri, S. (2001) *"Analysis of Composite Bonded/Bolted Joints used in Repairing"*. Journal of Composite Materials, 35(12): 1045-1061

[80] Baker, A.A. *"Composite Materials for Aircraft Structures"* Second Edition American Institute of Aeronautics and Astronautics

[81] Dodd, S.M. and Smith, H. Jr., (1989) *"Expert Systems for Design of Battle Damage Repairs"* Advanced Materials: the Big Payoff; Atlantic City, New Jersey; USA; 25-28 Sept. 1989. pp. 239-248.

[82] Baker, A.A. and Jones (Eds.), *"Bonded Repair of Aircraft Structures"*, Martinus Nijhoff Publishers, 1988.

[83] Baker, A.A., Callinan, R.J., Davis, M.J., Jones, R. and Williams, J.G. (1984) *"Repair of mirage iii aircraft using BFRP crack patching technology"*, Theoretical and Applied Fracture Mechanics 2: 1–16.

[84] Baker, A.A. (1984) *"Repair of cracked or defective metallic components with advanced fibre composites an overview of Australian work"*, Composite Structures 2: 153–181.

[85] Baker, A. A., Rose, L.R.F. and Walker, K.F., Wilson, E.S. (1999) *"Repair Substantiation for a Bonded Composite Repair to F111 Lower Wing Skin"* Applied Composite Materials 6:251-267

[86] Baker, A A *(1999) "Bonded composite repair of fatigue-cracked primary aircraft structure"* Composite Structures 47: 431-443

[87] Chui, W.K., Koh, Y.L., Galea, S.C. and Rajic, N. (2000) "Smart structure application in bonded composite repairs", Composite Structures 50: 433-444

[88] Koh, Y.L. and Chiu, W.K. (2003) *"Numerical study of detection of disband growth under a composite repair patch"*Smart Materials and Structures 12: 633-641

[89] Koh, Y.L., Rajic, N., Chiu, W.K. and Galea, S. (1999) *"Smart structure for composite repair"* Composite Structures 47: 745-752

[90] Koh, Y.L. , Chiu, W.K. and Rajic, N. (2002) *"Integrity assessment of composite repair patch using propagating Lamb waves" Composite Structures* 58: 363-371

[91] Y L Koh, W K Chiu, I H Marshall, N Rajic and S C Galea (2001) *"Detection of disbonding in a repair patch by means of an array of lead zirconate titanate and polyvinylidene fluoride sensors and actuators"* Smart Materials and Structures 10: 946-962

[92] Tsamasphyros, G., Furnarakis, N., Kanderakis, G and Mariolo-Riga, Z (2003) *"Optimization of Embedded Optical Sensor Location in Composite Repairs"* Applied Composite Materials 10: 129-140

[93] Wang, X. (2002) "Shape memory alloy volume fraction of pre-stretched shape memory alloy wire-reinforced composites for structural damage repair"11: 590-595

[94] Russel, A.J. and Bowers, C.P. (1991)*"Resin Requirements for successful repair of delaminations, In. Proceedings of the 36th international SAMPE symposium, San Diego, CA, 15-18th April*

[95] Russel A.J. and Ferguson, J.S. (1994) *"Composite Repair Issues on the CF-18 Aircraft,"* AGARD Conference Proceedings, vol. 550, pp. 14-1 to 14-8.

[96] Dehm, S. and Wurzel, D. (1989) *"Fast, In-situ repair of aircraft panel components"* Journal of Aircraft 26(5): 476-481

[97] Tzetzis, D. and Hogg, P.J. (2008) "The Influence of Surface Morphology on the Interfacial Adhesion and Fracture Behaviour of Vacuum Infused Carbon Fibre Reinforced Polymeric Repairs". Polymer Composites 29(1): 92-108

[98] Tzetzis, D. and Hogg, P.J. (2007) "Experimental and finite element analysis on the performance of vacuum-assisted resin infused single scarf repairs", Materials and Science 29: 436-449

[99] Abbott, D et al "Development and Evaluation of Sensor Concepts for Ageless Aerospace Vehicles: Development of Concepts for an Intelligent Sensing System", Prepared by NASA Research Centre Langley.

[100] Hougie, C. (2004) *"The waterfall-cascade and autoprothombin hypotheses of blood coagulation: personal reflections from an observer"* Journal of Thrombosis and Haemostasis 2:1225–33

[101] Macfarlane, R.G. (1964) "An Enzyme Cascade in the Blood Clotting Mechanism, and its function as a Biochemical Amplifier" Nature 202: 498-499

[102] Davie, E.W. and Ratnoff, O.D. (1964) *"Waterfall Sequence of Instrinsic Blood Clotting"*. Science, New Series 145(3638): 1310-1312

[103] Davies, K.A. and McNicol, G.P. (1983) *"Haemostasis and Thrombosis"*. Oxford Textbook of Medicine (Weatherall D J, Ledingham J G G and Warrel D A eds), Chapter 19 Oxford, UK: Oxford University Press.

[104] Biggs, A.R. (1985) *"Suberized Boundary Zones and the Chronology of Wound Responses in Tree Bark"*. Phytopathology 75 (11): 1191-1195

[105] Biggs, A.R. (1992) *"Anatomical and physiological responses of bark tissues to mechanical injury. In: Defense Mechanisms of Woody Plants Against Fungi."* Blanchette, R.A. and Biggs, A.R. Eds. Springer-Verlag (Berlin) 13-40

[106] Shigo, A.L. (1984) *"Compartmentalization: A conceptual framework for understanding how trees grow and defend themselves"* Annual Review of Phytopathology 22:189-214

[107] Bostock, R.M. and Stermer, B.A. (1989) *"Perspectives on wound healing in resistance to pathogens"*. Annual Review of Phytopathology 27: 343-371.

[108] McCulloh, K.A., Sperry, J.S. and Adler, F.R. (2003) *"Water transport in plants obeys Murray's law"* Nature 421: 939-942

[109] Gosline J, Lillie M, Carrington E, Guerette P, Ortlepp C and Savage K (2002) *Elastic Proteins: biological roles and mechanical properties* Philosophical Transactions of the Royal Society of London 357: 121-132

[110] Vaccaro E and Waite J (2001) "*Yield and Post-Yield behaviour of Mussel Byssal Thread: A Self-Healing Biomolecular Material"* Biomacromolecules 2(3): 906-911

[111] Dry, C (1994) "Matrix cracking repair and filling using active and passive modes for smart timed release of chemicals from fibres into cement matrices", Smart Materials and Structures 3: 118-123

[112] Dry, C and McMillan, W (1996) *"Three-part methylmethacrylate adhesive system as an internal delivery system for smart responsive concrete"*, Smart Materials and Structures 5:297-300

[113] Dry, C and McMillan, W (1997) *"A novel method to detect crack location and volume in opaque and semi-opaque brittle materials"* Smart Materials and Structures 6:35-39

[114] Dry, C (1998) "A time-release technique for corrosion prevention", Cement Concrete Research 28: 1133-1140

[115] Dry, C (2000) "Three designs for the internal release of sealants, adhesives and waterproofing chemicals into concrete to reduce permeability", Cement Concrete Research 30: 1969-1977

[116] United States Patent, Number 6,261,360, November 1999

[117] Li, V.C., Lim, Y.M. and Chan, Y.W. (1998), *"Feasibility study of a passive smart self-healing cementitious composite"*, Composites Part B 29B: 819-827.

[118] Dry, C (1996) *"Procedures Developed for self-repair of polymer matrix composites"*, Composite Structures 35: 263-269

[119] White, S.R. et al, (2001), *"Autonomic healing of polymer composites"*, Nature 409: 794-797

[120] Brown, E.N., Kessler, M.R., Sottos, N.R, and White, S.R. (2003), *"In situ poly(urea-formalehyde) microencapsulation of dicyclopentadiene"*, Journal of Microencapsulation 20: 719-730

[121] Cho, H, Andersson, M, White, S.R., Sottos, N.R. and Braun, P.V. (2006) *"Polydimethylsiloxane-Based Self-Healing Materials"*. Advanced Materials 18: 997-1000

[122] Kessler, M.R. and White, S.R. (2002), *"Cure Kinetics of the Ring-Opening Metathesis Polymerization of Dicyclopentadiene"*, Journal of Polymer Science: Part A: Polymer Chemistry 40: 2373-2383

[123] Rule, J.D. and Moore, J.S. (2002), *"ROMP Reactivity of endo- and exo-Dicyclopentadiene"*, Macromolecules 35: 7878-7882

[124] Mauldin, T.C., Rule, J.D., Sottos, N.R., White, S.R. and Moore, J.S. (2007) *"Self-healing kinetics and the stereoisomers of dicyclopentadiene"*. Journal of the Royal Society Interface 4: 389-393

[125] Jones, A.S., Rule, J.D., Moore, J.S., White, S.R. and Sottos, N.R. (2006) *"Catalyst Morphology and Dissolution Kinetics of Self-Healing Polymers"*. Chemistry of Materials 18: 1312-1317

[126] Brown, E.N, Sottos, N.R and White, S.R, (2002), *"Fracture Testing of a Self-Healing Polymer Composite"*, Experimental Mechanics 42: 372-379

[127] Brown, E.N, White, S.R. and Sottos, N.R, (2004), *"Microcapsule induced toughening in a self-healing polymer composite"*, Journal of Materials Science 39: 1703-1710

[128] Rule, J.D., Brown, E.N., Sottos, N.R., White, S.R. and Moore, J.S. (2005) *"Wax-protected catalyst microspheres for efficient self-healing materials"*. Advanced Materials. 17(2): 205-208.

[129] Brown, E.N., White, S.R. and Sottos, N.R., (2005), *"Retardation and Repair of fatigue cracks in a microcapsule toughened epoxy composite – Part I: Manual infiltration*". Composites Science and Technology 65:2466-2473.

[130] Brown, E.N., White, S.R. and Sottos, N.R. (2005) *"Retardation and Repair of fatigue cracks in a microcapsule toughened epoxy composite – Part II: In-Situ Self-Healing*". Composites Science and Technology 65:2474-2480.

[131] Brown, E.N., White, S.R., and Sottos, N.R. (2006) *"Fatigue crack propagation in microcapsule toughened epoxy"*. Journal of Materials Science 41(19): 6266-6273.

[132] Jones, A.S., Rule, J.D., Moore, J.S., White, S.R. and Sottos, N.R. (2006) *"Life extension of self-healing polymers with rapidly growing fatigue cracks"*. Journal of the Royal Society Interface 4: 395-403

[133] Chen, X et al, (2002), "A Thermally Re-mendable Cross-Linked Polymeric Material", Science 295, 1698-1702

[134] Plaisted TA et al, (2003), "Self-healing structural composites with electromagnetic functionality", Smart Structures and Materials 2003, Proceedings of SPIE, editor: Aderson EH, 5054, 327-381

[135] Nemat-Nasser SC et al, (2002), *"Structural composites with integrated electromagnetic functionality"*, Smart Structures and Materials 2002, Proceedings of SPIE, editor: McGowan AMR, 4698, 237-245

[136] Santos C, (2004), *"Modelling and testing of temperature behaviour and resistive heating in a multi-functional composite"*, Smart Structures and Materials 2004, Proceedings of SPIE, 5387, 24-26

[137] Hayes, S.A., Zhang, W., Branthwaite, M and Jones, F.R. (2007) *"Self-healing of damage in fibre-reinforced polymer-matrix composites"*. Journal of the Royal Society Interface 4: 381-387

[138] Hayes, S.A., Jones, F.R., Marhiya, K. and Zhang, W (2007) *"Self-Healing Composite Materials"*, Composites A 38(4): 1116-1120

[139] Motoku, M, Vaidya, U.K and Janowski, G.M. (1999), *"Parametric studies on self-repairing approaches for resin infused composites subjected to low velocity impact"*, Smart Materials and Structures 8: 623-638.

[140] Bleay, S.M. et al, (2001), *"A smart repair system for polymer matrix composites"*, Composites: Part A 32: 1767-1776

[141] Pang, J.W.C. and Bond, I.P. (2005) *"'Bleeding composites'—damage detection and self-repair using a biomimetic approach"* Composites Part A 36:183-188

[142] Pang, J.W.C. and Bond, I.P. (2005) *"A hollow fibre reinforced polymer composite encompassing self-healing and enhanced damage visibility"* Composites Science and Technology 65:1791-1799

[143] Hucker, M., Bond, I., Foreman, A. and Hudd J. (1999) *"Optimisation of hollow glass fibres and their composites"*. Advanced Composites Letters 8(4): 181-189.

[144] Hucker, M.J., Bond, I.P., Haq, S., Bleay, S. and Foreman, A., (2002) *"Influence of manufacturing parameters on the tensile strengths of hollow and solid glass fibres"*. Journal of Materials Science 37(2): 309-315.

[145] Hucker, M.J., Bond, I., Bleay, S., and Haq, S., (2003) *"Experimental evaluation of unidirectional hollow glass fibre/epoxy composites under compressive loading"*. Composites A Vol. 34(10): 927-932.

[146] Hucker, M.J., Bond, I., Bleay, S., and Haq, S. (2003) *"Investigation into the behaviour of hollow glass fibre bundles under compressive loading"*. Composites A 34(11): 1045-1052.

[147] Trask, R.S. and Bond, I.P. (2006) *"Biomimetic Self-Healing Of Advanced Composite Structures Using Hollow Glass Fibres"*. Smart Materials and Structures 15(3): 704-710.

[148] Kessler, M.R. and White, S.R (2001), *"Self-activated healing of delamination damage in woven composites"*, Composites: Part A 32: 683-699

[149] Kessler, M.R, Sottos, N.R and White, S.R, (2003), *"Self-healing structural composite materials"*, Composites: Part A 34: 743-753

[150] Zako, M., and Takano, N., (1999), *"Intelligent materials systems using epoxy particles to repair microcracks and delamination in GFRP"*, Journal of Intelligent Material Systems and Structures 10: 836-841

[151] Yin, T., Rong, M.Z., Zhang, M.Q. and Yang, G.C. (2007) "Self-healing epoxy composites – Preparation and effect of the healant consisting of microencapsulated epoxy and latent curing agent". Composites Science and Technology 67: 201-212.

[152] Yin, T., Zhou, L., Rong, M.Z., and Zhang, M.Q. (2008) "Self-healing woven glass fibric/epoxy composites with the healant consisting of micro-encapsulated epoxy and latent curing agent". Smart Materials and Structures 17: 1-8

[153] Verberg. R., Dale. A., Kumar. P., Alexeev. A and Balazs. A. (2007) "*Healing substrates with mobile, particle-filled microcapsules: designing a 'repair and go' system"* Journal Royal Society Interface 4:349-357

[154] Alexeev. A., Verberg. R. and Balazs. A (2005) "*Modelling the motion of microcapsules on compliant polymeric surfaces"* Macromolecules 38:10244-10260

[155] Alexeev. A., Verberg. R. and Balazs. A (2006) *"Designing compliant substrates to regulate the motion of vesicles"* Physics Reviews Letters 96:148103

[156] Lee JY, Buxton GA and Balazs AC, (2004), *"Using nanoparticles to create self-healing composites"*, Journal of Chemical Physics 121, 5531-5540

[157] Siefert, R.F. (1963) *"Hollow Glass Fibres"*, The Glass Industry 321-322, 356

[158] Burgman, J.A., (1965) *"Hollow Glass Fibres"* Symposium on Polymers in Construction, September 12-17 Atlantic City, American Chemical Society

[159] Niederstadt, G., Gadke, M., and Bauml, H (1977) *"Investigation of hollow glass fibres for development of reinforced plastics"* European Space Agency Technical Translation ESA TT-360 Report Number DLR-FB 76-45

[160] Watson, J.C. and Farrow, I.R. (1995) *"Hollow Glass Fibre Composites in Aerospace" Proc. ICCE-2 Second International Conference on Composites Engineering, New Orleans 21-24th August, University of New Orleans*

[161] Boniface, L., Foreman, A. and Hitchen, S. (1997) *"Comparative evaluation of solid and hollow S2 glass fibre-epoxy laminates"* Proceedings of the Fourth International Conference on Deformation and Fracture of Composites, UMIST 24-26th March, Institute of Materials 39-48

[162] Bleay, S.M., and Humberstone, L., (1999) *"Mechanical and electrical assessment of hybrid composites containing hollow glass reinforcement"* Composites Science and Technology 59: 1321-1329

[163] Carman, G.P. and Sendeckyj, G.P. (1995) *"Review of the Mechanics of Embedded Optical Sensors"* Journal of Composites Technology and Research 17(3): 183-193

[164] G Zhou and L M Sim (2002) *"Damage Detection and Assessment in fibre-reinforced composite structures with embedded fibre optic sensors- Review"* Smart Materials and Structures 11: 925-939

[165] Satori, K., Ikeda, Y., Kurosawa, Y., Hongo, A. and Takeda, N. (2000) *"Development of small-diameter optical fibre sensors for damage detection in composite laminates"* Proc. SPIE 3986

[166] Tsutsui, H., Kawamata, A., Sanda, T.and Takeda, N (2000) *"Detection of impact damage of stiffened composite panels using embedded small-diameter optical fibres"* Smart Materials and Structures 13: 1284-1290

[167] Yashiro, S., Takeda, N., Okabe, T. and Sekine, H. (2005) *"A new approach to predicting multiple damage states in composite laminates with embedded FBG sensors"* Composites Science and Technology 65:659-667

[168] Takeda, S., Okabe, Y. and Takeda, N. (2002) *"Delamination detection in CFRP laminates with embedded small-diameter fiber Bragg grating sensors"* Composites Part A 33:971-980

[169] Takeda, S., Minakuchi, S., Okabec, Y. and Takeda, N. (2005) *"Delamination monitoring of laminated composites subjected to low-velocity impact using small-diameter FBG sensors"* Composites: Part A 36:903-908

[170] Skontrop, A. (1999) "Structural integrity of Quasi-isotropic Composite Laminates with Embedded Optical Fibres" Journal of Reinforced Plastics and Composites 19(13): 1056-1077

[171] Case, S.W. and Carman, G.P. (1994) "Compression Strength of Composites Containing Embedded Sensors or Actuators" Journal of Intelligent Material Systems and Structures 5(1): 4-7

[172] Shivakumar, K. and *Emmanwori, L. (2004) "Mechanics of Failure of Composite Laminates with an Embedded Fiber Optic Sensor"* Journal of Composite Materials 38(8): 669-680

[173] Leka, L.G. and Bayo, E (1989) *"A close look at the embedment of OF's into composite structures"* Journal of Composites Technology Research 11(3): 106-112

[174] Skontrop, A. (2002) *"Composites with Embedded Optical Fibres at Structural Details with Inherent Stress Concentrations" 36: 2501-2515*

[175] Lee, D.C., Lee, J.J. and Yun, S.J. (1995) *"The Mechanical Characteristics of Smart Composite Structures with Embedded Optical Fibre Sensors"* Composite Structures 32: 39-50

[176] Jensen, D.W., Pascual, J. and August, J.A. (1992) *"Performance of Graphite/Bismaleimide Laminates with Embedded Fibre-Optic Sensors Part 1: Uniaxial Tension"* Smart Materials and Structures 1: 24-30

[177] Jensen, D.W., Pascual, J. and August, J.A. (1992) *"Performance of Graphite/Bismaleimide Laminates with Embedded Fibre-Optic SensorsPart 2: Uniaxial Compression"* Smart Materials and Structures 1: 31-35

[178] Surgeon, M. and Wevers, M. (1999) *"Static and dynamic testing of a quasi-isotropic composite with embedded optical fibres"* Composites Part A 30: 317-324

[179] Surgeon, M. and Wevers, M. (2001) *"The Influence of Embedded Optical Fibres on the Fatigue Damage Progress in Quasi-Isotropic CFRP Laminates"* Journal of Composite Materials 35: 931-940

[180] Jeon, B.S., Lee, J.J., Kim, J.K. and Huh, J.S. (1999) *"Low velocity impact and delamination buckling behavior of composite laminates with embedded optical fibers"* Smart Materials and Structures 8: 41-48

[181] D.L.Hart-Smith "The Ten-Percent Rule" Aerospace Materials Vol5 No.2 p10-16, A Shephard Press publication, August-October 1993.

[182] Anon, Standard test method for flexural properties of un-reinforced and reinforced plastics and electrical insulating materials by four-point bending. ASTM International, D 6272-02

[183] Anon, Standard Test Method for Measuring Damage Resistance of Fiber-Reinforced Polymer-Matrix Composite to Concentrated Quasi-Static Indentation Force. ASTM International, D 6264-98

[184] 'Standard tests for toughened resin composites' NASA Reference Publication 1092 (1982)

[185] Boeing Company, Boeing Specification Support Standard BSS7260, Revision C, Seattle, WA USA 1988

[186] Airbus Industrie, Airbus Industry Test Method, Issue 2 AITM 1.0010, France, June 1994

[187] Anon, ASTM International, *Standard test method for compressive residual strength properties of damaged polymer matrix composite plates*, D 7137/D 7137M-05

[188] Japanese Industrial Standard *Testing method for compression after impact properties of carbon fibre reinforced plastics* K7089-1996

[189] SACMA 'Test method for compression after impact properties of oriented fibre resin composites SRM 2-88' (Suppliers of Advanced Composite Materials Association)

[190] Curtis, P.T. 'CRAG test methods for the measurement of the engineering properties of fibre reinforced plastics' RAE TIC 88012 (Royal Aerospace Establishment, UK, 1988)

[191] Prichard, J.C. and Hogg, P.J. (1990) *"The role of impact damage in post-impact compression testing"* Composites 21(6): 503-511

[192] Bishop, S.M. and Dorey, G. in AGARD Conference Proceeding No. 355, London, i~14 April, 1983, 10, 1-10, 10.

[193] Dorey, G, in "*Structural Impact and Crashworthiness*", Vol. 1, Keynote Lectures, edited by Davies, G.A.O. (Elsevier Science Publishers, London, 1984) pp. 155-192.

[194] Curtis, P.T., (1989) *"Composite materials selection for damage tolerance"* RAE Technical Report 89053, Royal Aerospace Establishment, UK.

[195] Guild, F.J., Hogg, P.J. and Prichard J.C. (1993) *"A model for the reduction compression strength continuous fibre composites after impact damage"* Composites 24(4):333-339

[196] Habib, F.A.,(2001) *"A new method for evaluating the residual compression strength of composites after impact"*, Composite Structures 53: 309-316

[197] Hosur, M.V., Murthy, C.R.L. and Ramurthy, T.S. (1999) *"Compression After Impact Testing of Carbon Fiber Reinforced Plastic Laminates"* Journal of Composites Technology and Research, 21(2): 51-64

[198] Hawyes, V.J., Curtis, P.T. and Soutis, C. (2001) *"Effect of impact damaged on the compressive response of composite laminates"* Composites Part A 32: 1263-1270

[199] Soutis, C. and Curtis, P.T. (1996) *"Prediction of the post-impact compressive strength of CFRP laminated composites"* Composites Science and Technology 56: 677-684

[200] de Freitas, M. and Reis, L. (1998) *"Failure mechanisms on composite specimens subjected compression after impact"* Composite Structures 42: 365-373

[201] Cartie, D.D.R. and Irving, P.E. (2002) *"Effect of resin and fibre properties on impact and compression after impact performance of CFRP"* Composites: Part A 33:483-493

[202] Davies, G.A.O. and Zhang, X. (1995) *"Impact damage prediction in carbon composite structures"* International Journal of Impact Engineering 16[1]:149-170

[203] Sanchez-Saez, S., Barbero, E., Zaera, R. and Navarro, C. (2005), *"Compression after impact of thin composite" laminates* Composites Science and Technology 65:1911-1919

[204] Liu, D., Raju, B. and Dang, X. (1998) *"Size effects on impact response of composite laminates"* International Journal of Impact Engineering 21[10]:837-854

[205] Duarte, A., Herszberg, I. and Paton, R. (1999) *"Impact resistance and tolerance of interleaved tape laminates"* Composite Structures 47:753-758

[206] Young, W.C., "ROARK's Formulas for Stress and Strain" Sixth edition, McGraw-Hill International Editions

[207] Anon, ASTM International *Measuring the damage resistance of a fibre-reinforced polymer matrix composite to a drop-weight impact event,* D 7136/D 7136M -05$^{\epsilon 1}$

A. Appendix

A_1 Cycom 823 Data Sheet

A_2 Hexcel 914 Data Sheet

A_3 ASTM/Boeing CAI Fixture

A_4 Modified CAI Fixture

CYCOM® 823 RTM Liquid Epoxy Resin

TECHNICAL DATASHEET

Description

CYCOM 823 RTM is a liquid epoxy resin system. It is primarily available as a one-part system, with one working week out-life at room temperature so as to remove the requirement for customers to carry out resin mixing and its associated quality control processes. Its frozen storage shelf-life is 6 months at -18°C (0°F). If extended ambient storage is required then the resin could be supplied as a 2 part system.

CYCOM 823 RTM's viscosity is low enough at room temperature to allow injection without having to heat either the resin or the transfer pipework. When the resin is heated to the cure temperature its viscosity is further reduced, helping to ensure full wet-out of the reinforcing fibres.

CYCOM 823 RTM is fully cured after one hour at 125°C (255°F) giving a continuous dry service performance of 110°C (230°F), and a continuous hot/wet service performance of 90°C (195°F).

CYCOM 823 RTM neat resin has high elongation, high G_{IC} and high K_{IC} values, all of which are indicative of a tough material.

CYCOM 823 RTM is compatible with the usual range of reinforcing fibres utilised for the manufacture of composite components, i.e., carbon, glass, aramid etc.

For reinforcement preforming operations a fully compatible binder system, CYCOM790 RTM, has been developed for use with CYCOM 823 RTM. The binder is available pre-coated onto fabrics of the customers choice. A separate datasheet for CYCOM790 RTM is available on request.

Features and benefits

- **Available as a one or two-part system**
- **4-5 day out-life at room temperature, indefinite as 2-part system**
- **Six month shelf-life at 18°C (0°F)**
- **Room temperature injectable**
- **250 cps initial injection viscosity**
- **< 20 cps minimum viscosity**
- **One hour at 125°C (255°F) cure**
- **110°C (230°F) continuous dry service performance**
- **90°C (195°F) continuous hot/wet service performance**
- **High neat resin toughness**
- **Fully compatible, toughness enhancing binder, CYCOM 790 RTM, available**

For more information, contact:
Cytec Engineered Materials
Technical Service
Wrexham, United Kingdom
(+44) 1978-665253

Viscosity data

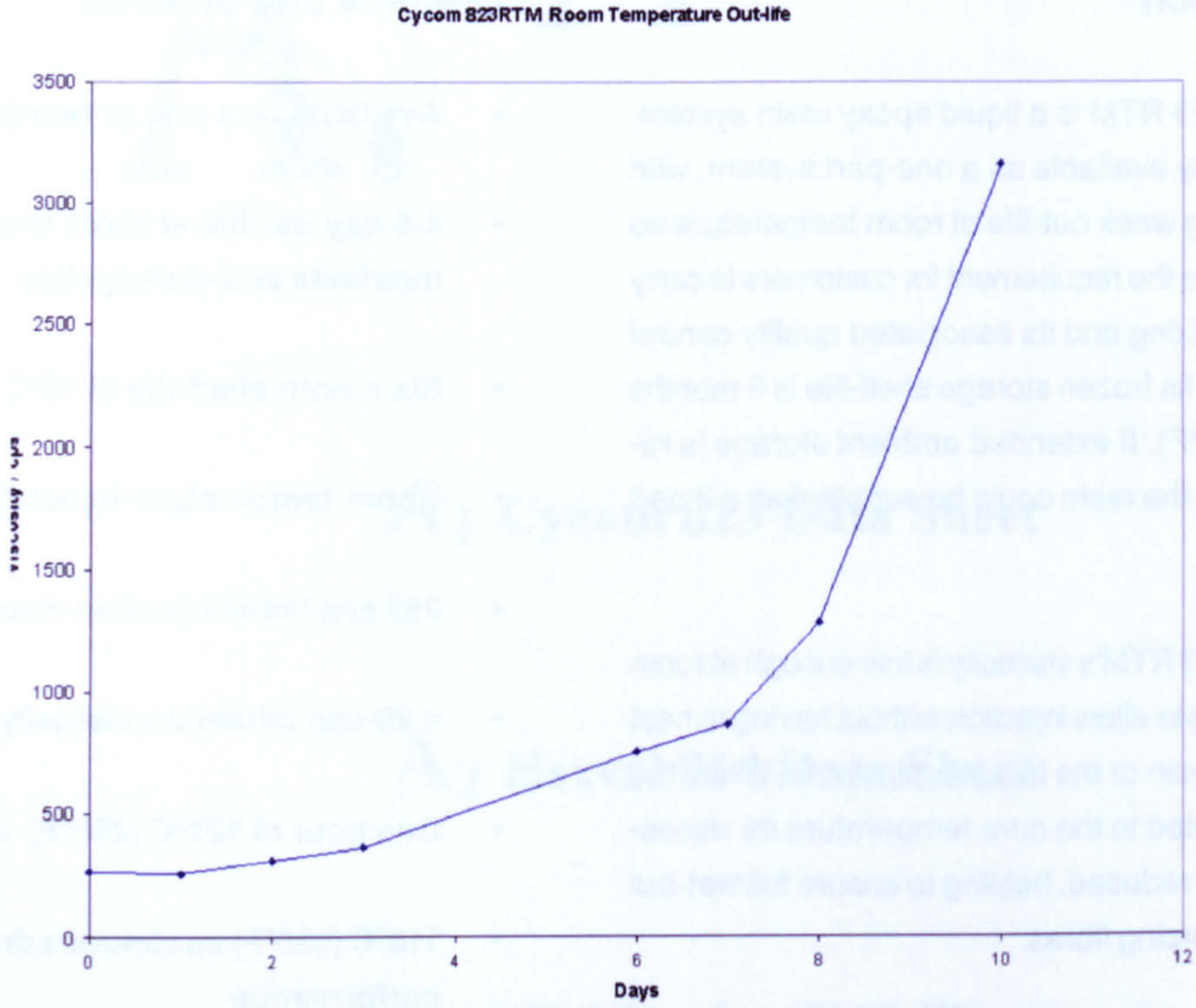

Initial viscosity = 250cps • Time below 500cps = 4 days at RT • Time below 1000cps (Gel) > 7 days at RT

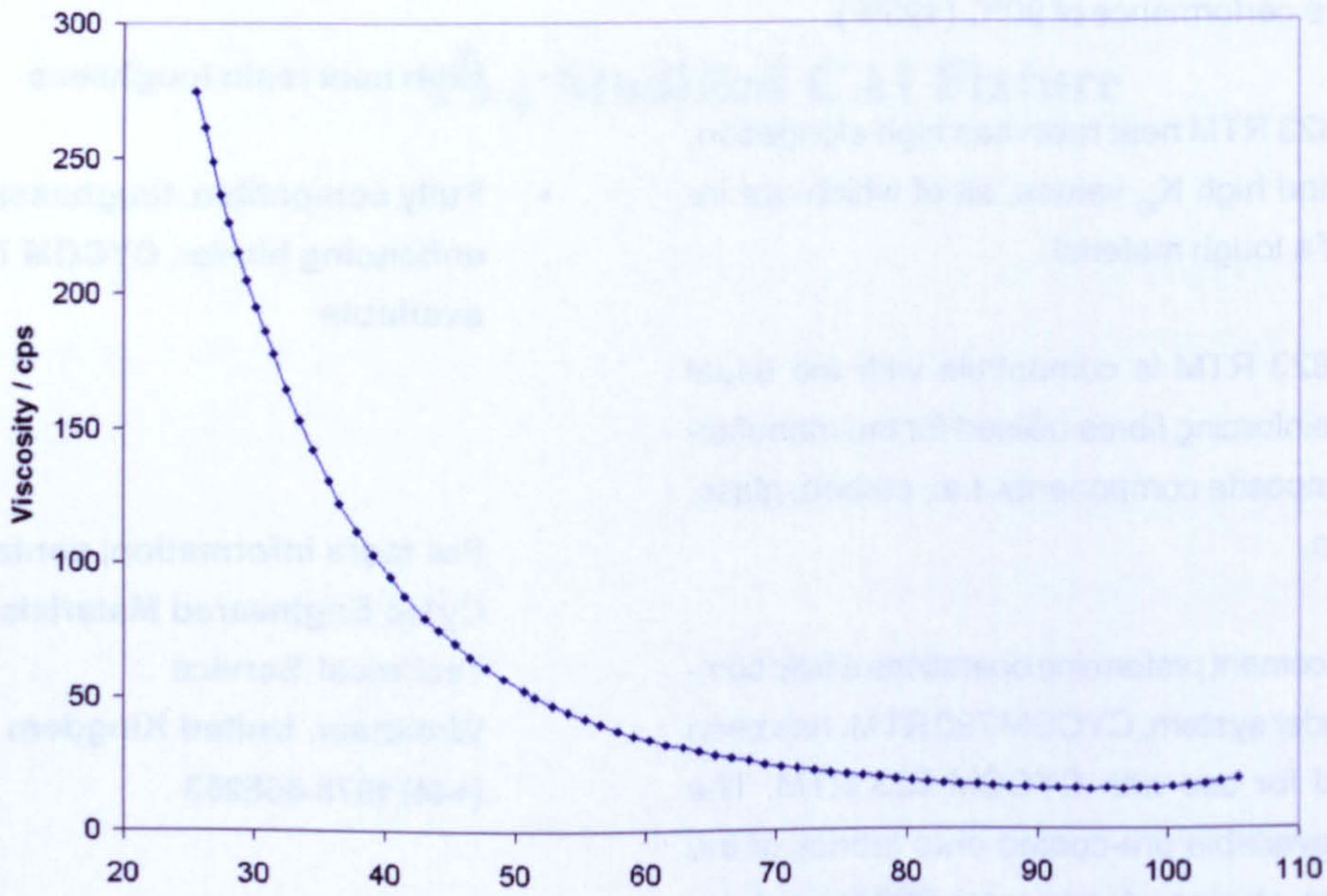

Heating rate = 2°C/min • Minimum viscosity = 15cps at 95°C. Gel Times:> 30 min at 95°C • 15 min @ 125°C (cure temp).

CYCOM 823 RTM Liquid Epoxy Resin

D.M.T.A. data

For neat resin casts cured for 1 hour at 125°C (250°F)

See page 4 for Tg values derived from these curves.

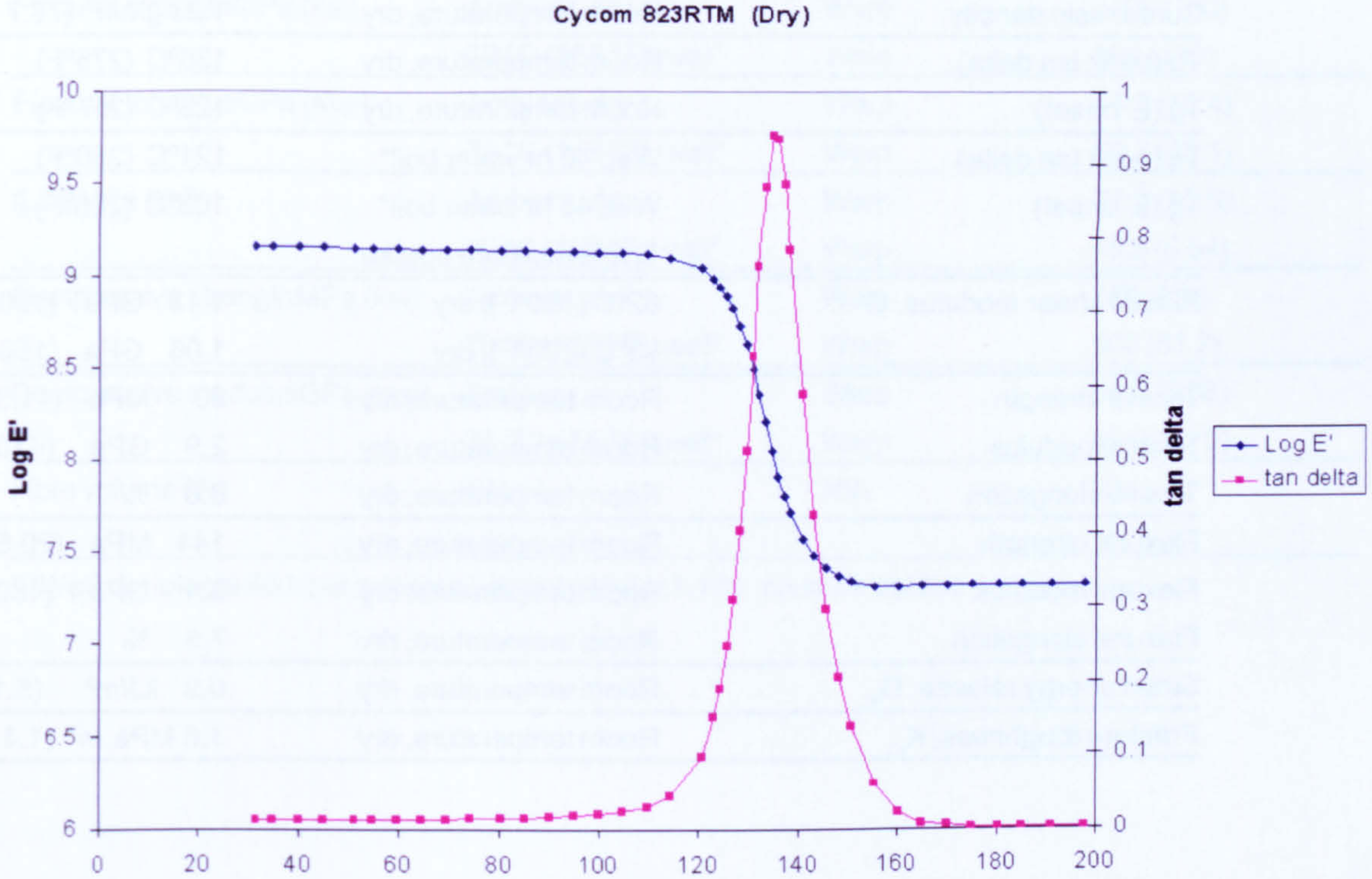

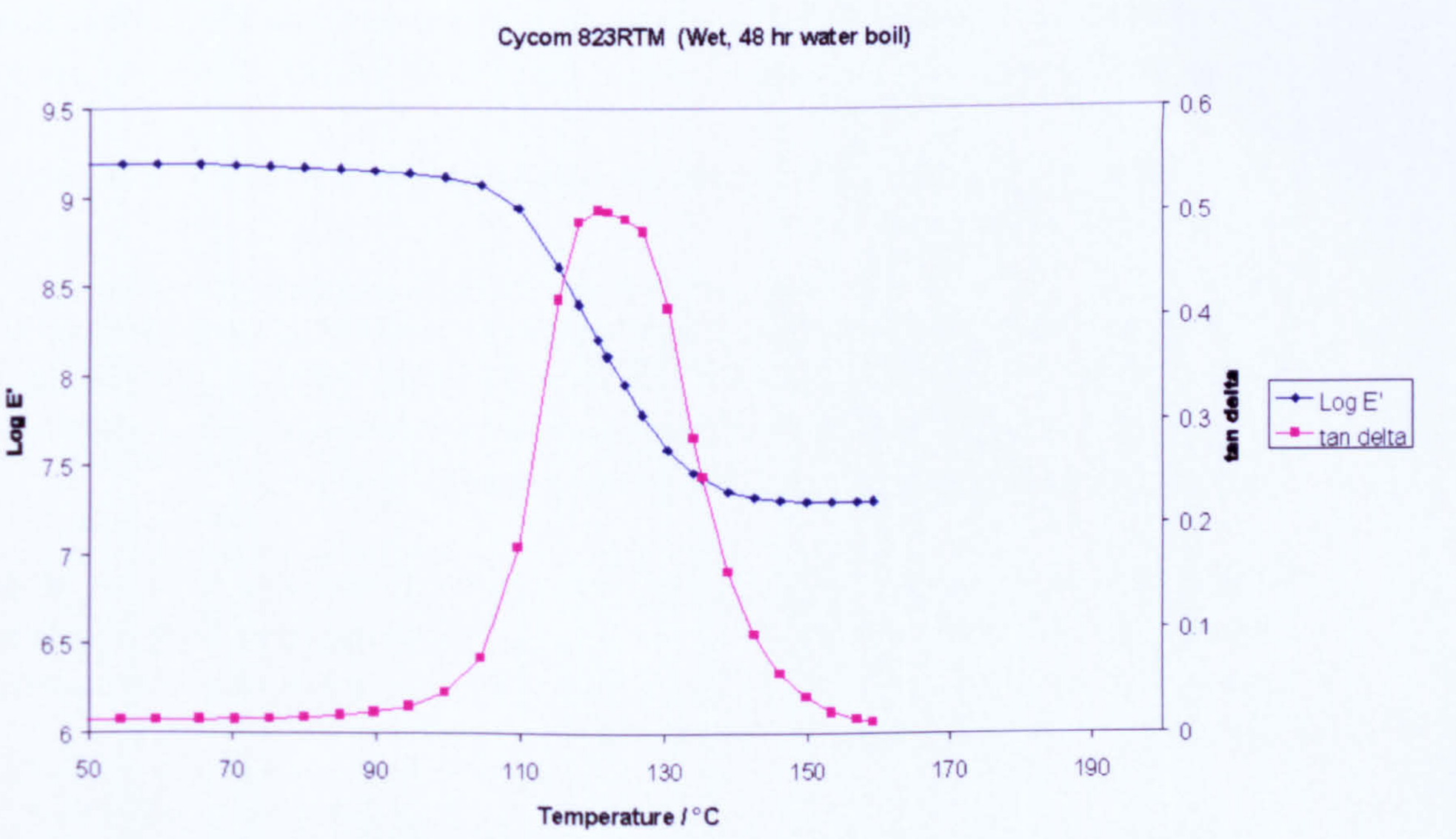

Neat resin data

Property	Specimen conditioning	Value
Cured resin density	Room temperature, dry	1.23 g/cm³ (76.7 lb/ft³)
Tg (peak tan delta)	Room temperature, dry	135°C (275°F)
Tg (E' onset)	Room temperature, dry	125°C (257°F)
Tg (peak tan delta)	Wet, 48 hr water boil*	121°C (250°F)
Tg (E' onset)	Wet, 48 hr water boil*	108°C (226°F)
	*1.2% moisture uptake	
Elastic shear modulus, G'	82°C (180°F), dry	1.13 GPa (160 ksi)
	93°C (200°F), dry	1.06 GPa (150 ksi)
Tensile strength	Room temperature, dry	80 MPa (11.3 ksi)
Tensile modulus	Room temperature, dry	2.9 GPa (410 ksi)
Tensile elongation	Room temperature, dry	8.8 %
Flexural strength	Room temperature, dry	144 MPa (20.5 ksi)
Flexural modulus	Room temperature, dry	3.4 GPa (480 ksi)
Flexural elongation	Room temperature, dry	7.6 %
Strain energy release, G_{IC}	Room temperature, dry	0.9 kJ/m² (5.1in.lb/in²)
Fracture toughness, K_{IC}	Room temperature, dry	1.6 MPa.m^{½} (1.4 ksi.in^{½})

Composite mechanical data

Property	Conditioning	Orientation	6K-5HS-HTA-370
Flexural strengthMPa (ksi)	Ambient, dry	Warp	1106 (160)
	70 °C (158 °F), wet*	Warp	894 (130)
Flexural modulusGPa (Msi)	Ambient, dry	Warp	71.7 (10.4)
	70 °C (158 °F), wet*	Warp	69.7 (10.1)
ILSSMPa (ksi)	Ambient, dry	Warp	72.7 (10.5)
	70 °C (158 °F), wet*	Warp	45.8 (6.64)
Compressive strengthMPa (ksi)	Ambient, dry	Warp	788 (114)
	70 °C (158 °F), wet*	Warp	560 (81.2)
Compressive modulusGPa (msi)	Ambient, dry	Warp	59.2 (8.58)
	70 °C (158 °F), wet*	Warp	60.0 (8.70)
Fibre volume (%)	N/A	N/A	52

* "Wet" denotes a 48 hour water boil prior to test – 1.1 % moisture uptake

Suggested processing parameters

- CYCOM 823 RTM resin has an initial viscosity of 250 cps at room temperature. At this viscosity it is easily transferable to the RTM equipment injection system (i.e. pressure pot, piston ram etc.) without the need for further heating.

- De-gas resin in homogeniser for a minimum of 30 minutes at room temperature, under a minimum of 25" Hg vacuum, prior to injecting.

- Apply full vacuum to tool, containing the preformed reinforcement, ensuring that there is no vacuum loss.

- Preheat tool to 125 + 5°C (255 + 8°F). At this temperature the resin will gel in 15 mins. after injection has been completed.

Depending upon total cure cycle time requirements, degree of heating control on the tool, component size and geometry etc., it is possible to inject the resin under alternative conditions in order to ensure full wet-out of the reinforcement. The resin may be injected into a tool at any temperature from room temperature to 125°C (255°F), and then the tool may be heated to 125°C at 2-3°C/minute (3-5°F/minute) after injection has been completed.

- Close off the vacuum line and open the homogeniser to start injecting, then increase homogeniser pressure (typically to 1-2 bar) to fill the tool.

- When the resin appears in the vent lines, close off the vent lines and continue injecting under pressure until the resin has gelled (15 mins), then shut off the inlet valve to trap the pressure.

- Dwell at 125 + 5°C (255 + 9°F) for 1 hour before cooling to 60°C (140°F) or below before attempting to release part from tool.

* The above cure parameters have been used at Cytec to mould test panels (280mm x 530mm x 2mm) for process and mechanical performance evaluation. A Plastech Hypaject system was utilised to inject resin into a steel tool held in a heated platen press. Some parameters may require adjustment depending upon the nature of the part being moulded and the equipment being used.

For larger or thicker parts, some parameters may require adjustment to avoid the risk of exotherm. Injection pressure for larger parts/alternative tooling may require adjustment to ensure filling of the tool cavity within the resin gel time (if injecting into a pre-heated tool) and to ensure full consolidation of the component.

Different injection equipment may require alternative conditions for degassing.

Safety

WARNING – CYCOM 823 RTM contains epoxy resin. May cause allergic skin reaction or primary skin irritation. Avoid prolonged or repeated contact with skin. Wash thoroughly after handling. Over exposure to vapour during heat curing may cause irritation or injury of the respiratory tract and eye irritation.

FIRST AID – In case of skin contact, wash skin with soap and water. In case of eye contact, immediately irrigate with plenty of water for 15 minutes. If heated vapour is inhaled, remove from exposure. Administer oxygen if there is difficulty breathing.

VENTILATION REQUIRED – Use mechanical exhaust ventilation when heat curing resin system.

DETAILED HANDLING INSTRUCTIONS – Refer to the Cytec Engineered Materials Material Safety Datasheet (available on request) and product labels for this material.

IMPORTANT NOTICE

Contact us

Cytec Engineered Materials Inc. North American Facilities

Anaheim, California
714 630-9400 • Fax 714 666-4345

Havre de Grace, Maryland
410 939-1910 • Fax 410 939-8100

Greenville, Texas
903 457-8500 • Fax 903 457-8598

Winona, Minnesota
507 454-3611 • Fax 507 452-8195

Orange, California
714 639-2050 • Fax 714 639-2033

D Aircraft Products, Inc.
Anaheim, California
714 632-8444 • Fax 714 632-7164

Cytec Carbon Fibers LLC
Piedmont, South Carolina
800 222-2448 • Fax 864 299-9333

GLOBAL HEADQUARTERS
Tempe, Arizona
480 730-2000 • Fax 480 730-2390

Cytec Engineered Materials, Ltd.
United Kingdom

Wrexham, UK
+44 1978 665200
Fax +44 1978 665222

Cytec Engineered Materials (GmbH)
Germany

Ostringen, Germany
+49 7523 912800
Fax +49 7523 912899

HexPly® 914

175°C curing epoxy matrix

Product Data

Description

HexPly 914 is a highly successful modified epoxy matrix which is used extensively in high temperature resistant primary aircraft structures. The controlled melt viscosity and excellent matrix rheology of 914 permits a wide range of processing conditions for high quality components.

Benefits and Features

- High melt viscosity giving easy processing characteristics
- Tolerant to a wide variation of processing conditions
- Latitude for low to high pressure laminating or moulding processes
- Medium tack level giving excellent drape characteristics
- Good shelf life

HexPly 914 is easily processed by press or autoclave for optimum composite properties and is also suitable for vacuum-bag cure of high quality thin components.

Resin Matrix Properties

Rheology

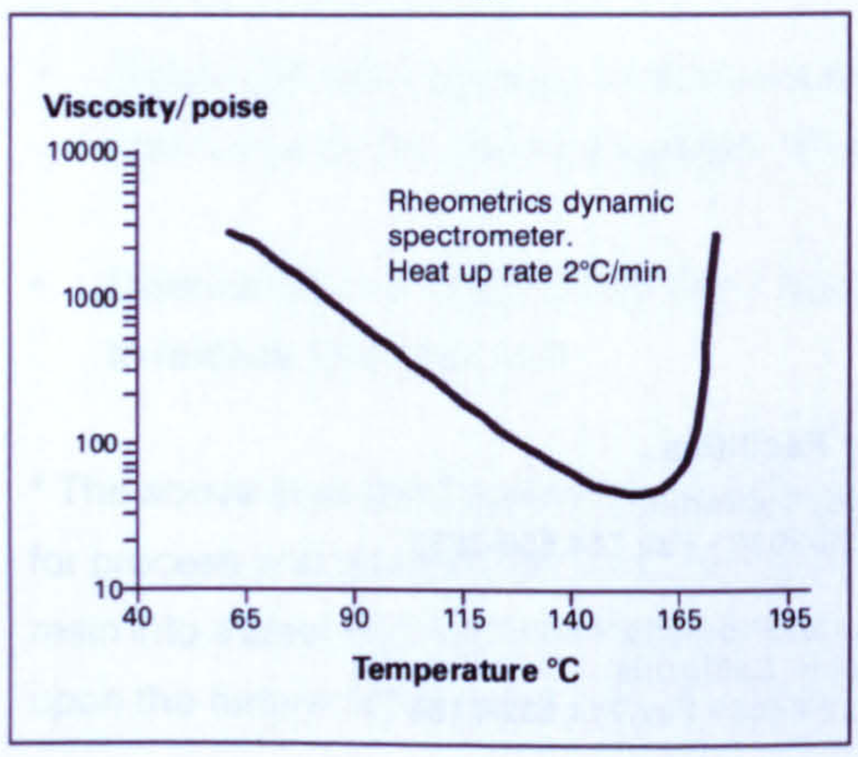

Gel Time

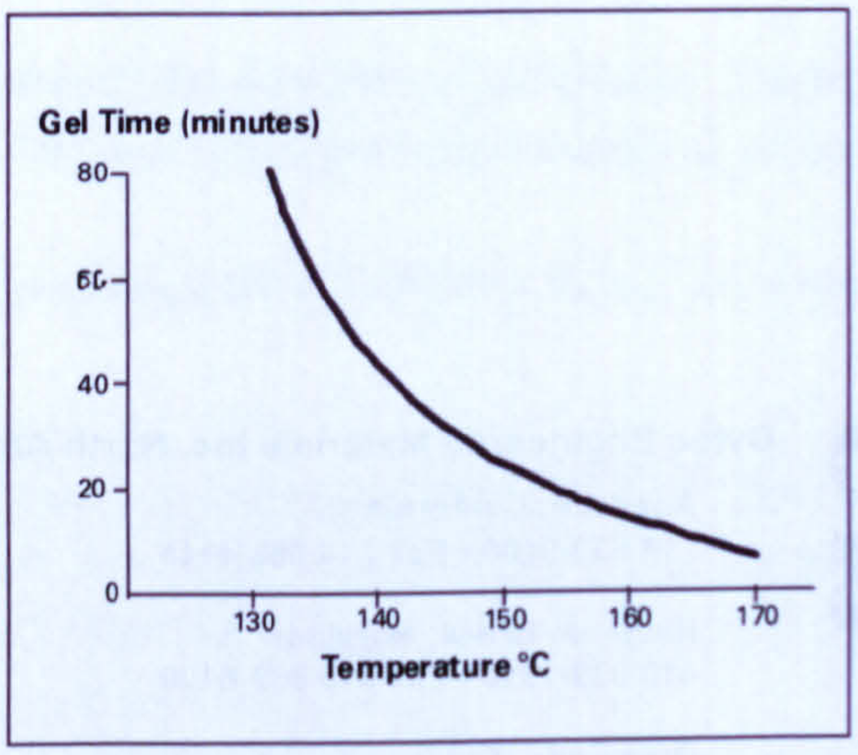

Prepreg Curing Conditions

1 hour at 175°C and 700kN/m² (7 bar) pressure plus 4 hours postcure at 190°C.

Heat up rate 2°C to 5°C.

Components up to 2 mm thick can be cured without a dwell in the cure schedule, provided a maximum heat up rate of 2°C/minute is used. For thicker components a dwell temperature between 120-135°C is recommended to avoid the possibility of an exotherm in the matrix. (Thicker components need longer dwells at the lower temperature).

HexPly® 914 *Product Data*

Cured Matrix Properties (cured at 175°C)

		Method
Tensile strength	47.7 MPa	ISO R527 type 1
Tensile modulus	3.9 GPa	ISO R527 type 1
Tensile strain	1.5%	ISO R527 type 1
Poisson's ratio	0.41	ISO R527 type 1
Calculated shear modulus	1.40 GPa	ISO R527 type 1
Compression strength	180 MPa	ISO 604
Toughness K_{1C}	0.7 MPa √m	Tested in accordance with
Toughness G_{1C}	103 J/m²	EGF Task Group on Polymers and Composites protocol.
Glass transition temperature (Tg)	190°C	DMTA
Cured density	1.29 g/cm³	

Prepreg Storage Life

- Tack Life @ 23°C 60 days
- Guaranteed Shelf Life @ -18°C 12 months

- Storage conditions.

HexPly 914 prepregs should be stored as received in a cool dry place or in a refrigerator. After removal from refrigerator storage, prepreg should be allowed to reach room temperature before opening the polythene bag, thus preventing condensation. (A full reel in its packaging can take up to 48 hours).

Precautions for Use

The usual precautions when handling uncured synthetic resins and fine fibrous materials should be observed, and a Safety Data Sheet is available for this product. The use of clean disposable inert gloves provides protection for the operator and avoids contamination of material and components.

Important

All information is believed to be accurate but is given without acceptance of liability. Users should make their own assessment of the suitability of any product for the purposes required. All sales are made subject to our standard terms of sale which include limitations on liability and other important terms.

Publication FTA053a (Oct 2002)

For further information, please contact your nearest sales office, or visit our website at **www.hexcelcomposites.com**

Australia
Suite 2, 86 Grimshaw Street
Greensborough, Victoria 3088
Tel: **61** 3 9432 7100
Fax: **61** 3 9432 7200

Austria
Industriestrasse 1
A-4061, Pasching
Tel: **43** (0)7229 7720
Fax: **43** (0)7229 772299

Belgium
Rue Trois Bourdons, 54
B-4840 Welkenraedt
Tel: **32** 87 307 411
Fax: **32** 87 882 895

Brazil
Av. J. Guilhermino, 474/72
S.J.Campos, SP 12210-130
Tel: **55** 12 3941 2242
Fax: **55** 12 3923 1186

China
Room B707, Yin Hai Bldg.
250 Cao Xi Rd
Shanghai 200233
Tel: **86** 21 6483 6741/2
Fax: **86** 21 6483 6744

France
ZI La Plaine, B.P.27 Dagneux
01121 Montluel CEDEX
Tel: **33** (0)4 72 25 26 27
Fax: **33** (0)4 72 25 27 30

Germany
Postfach 1560
21655 Stade
Tel: **49** 4141 7879-00
Fax: **49** 4141 7879-01

Italy
Via San Cristoforo, 44
21047 Saronno (VA)
Tel: **39** 02 96709082
Fax: **39** 02 9600809

Japan - *Joint Venture*
DIC - Hexcel Limited
Room 603, Santsu-Mori Bldg.
2-22-1 Nishi - Shimbashi
Minato-Ku, Tokyo 105
Tel: **81** 3 5401 0271
Fax: **81** 3 5401 0270

Spain
Bruselas, 10 - 16
Polig. Ind. "Ciudad de Parla"
28980 Parla, Madrid
Tel: **34** 91 664 4900
Fax: **34** 91 698 4914

United Kingdom
Duxford, Cambridge
CB2 4QD
Tel: **44** (0)1223 833141
Fax: **44** (0)1223 838808

USA
11711 Dublin Blvd.
Dublin, CA 94568-2832
Tel: **1** 925 551 4900
Fax: **1** 925 828 9202

USA
101 East Ridge Drive, Suite 102
Danbury, CT 06810
Tel: **1** 203 798 8311
Fax: **1** 203 798 8161

USA
42705 Grand River
Suite 201
Novi, MI 48375
Tel: **1** 248 344 8688
Fax: **1** 248 305 9760

USA
2350 Airport Freeway, Suite 550
Bedford, TX 76022-6027
Tel: **1** 817 315 3939
Fax: **1** 817 571 8629

USA
16310 NE 80th Street, Suite 102
Redmond, WA 98052
Tel: **1** 425 558 4400
Fax: **1** 425 861 5847

IAN FARROW x 9780

13.7.00

NOTES.

1. ENSURE THAT ALL ITEMS ARE CLEAN AND UNDAMAGED PRIOR TO ASSEMBLY.
2. MATING FACES TO BUTT TRUELY TOGETHER.
3. TORQUE TO 25 N.m.
4. DRILL AND REAM FOR DOWELS. ONLY AFTER INITIAL SPECIMEN HAS BEEN FITTED AND CORRECTLY ALIGNED
5. EXISTING ITEMS.

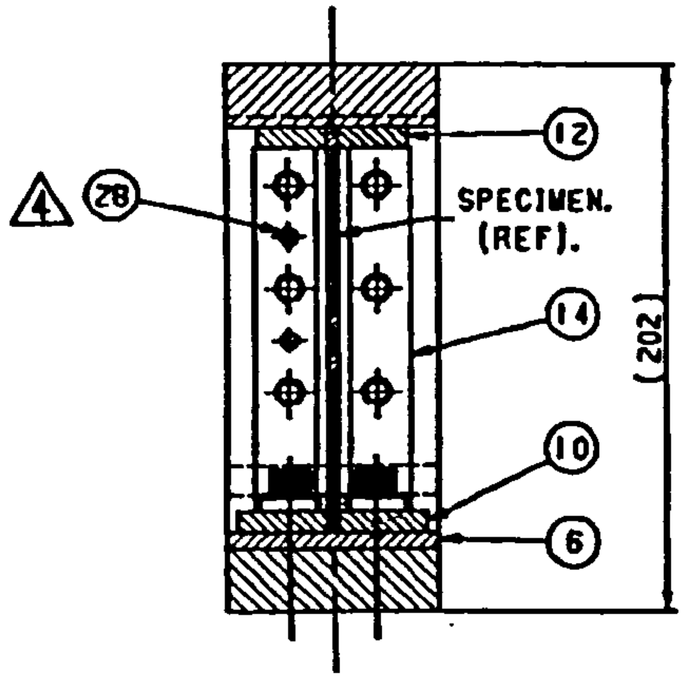

SECTION "A-A"

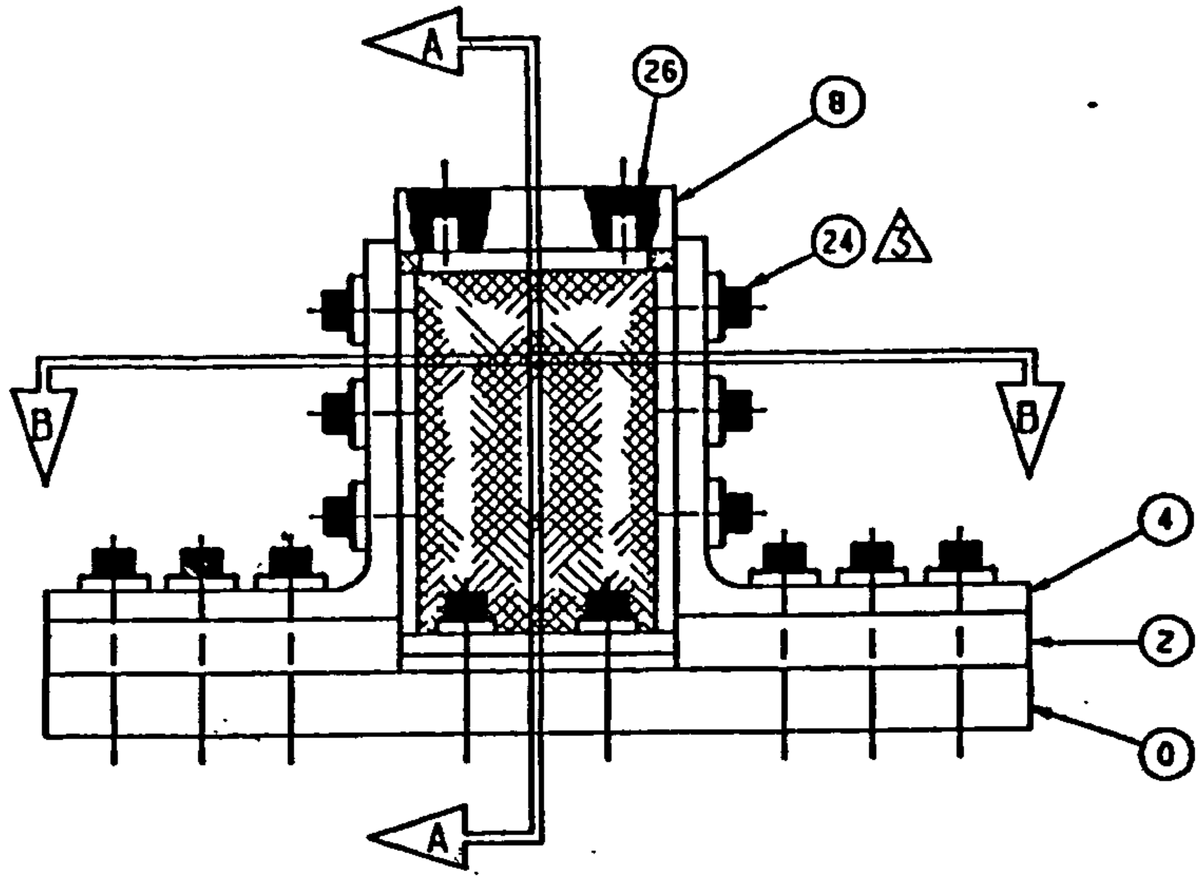

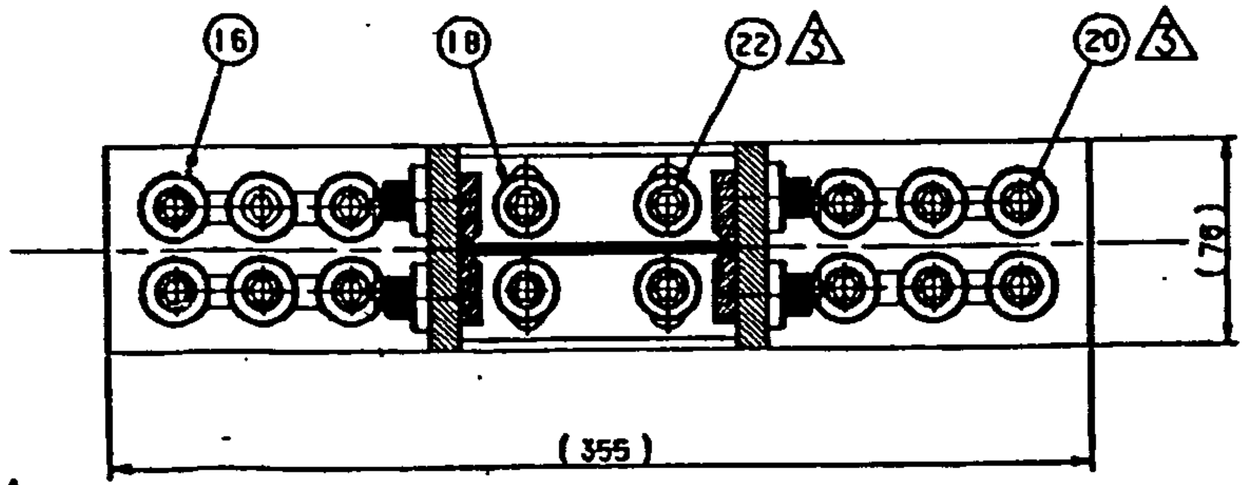

SECTION "B-B"

ALL CAP SCREWS 3/8" BSW.

4	01E07	26	-026		DOWEL.	MTS.	Ø8.0 x 19 LONG.
4	01F04	28	-028		SOCKET HD. CAP SCREW.	MTS.	UNBRAKO-1936 5/8"BSW.x0.75"
12	01F03	24	-024		SOCKET HD. CAP SCREW.	MTS.	UNBRAKO-1936 5/8"BSW.x1.0"
4	01D03	22	-022		SOCKET HD. CAP SCREW.	MTS.	UNBRAKO-1936 5/8"BSW.x1.5"
12	01D02	20	-020		SOCKET HD. CAP SCREW.	MTS.	UNBRAKO-1936 5/8"BSW.x2.0"
4	01D02	18	704-9848-202	A	WASHER.		
24	01C01	16	704-9848-200	A	WASHER.		
4	01E08	14	704-9840-200	A	SIDE GUIDE.		
2	01F05	12	704-9841-200	A	TOP GUIDE.		
2	01E08	10	704-9838-200	A	BOTTOM GUIDE.		
1	01F05	08	704-9842-200	A	LOAD PLATEN.		
1	01D06	06	704-9847-200	A	LOWER REACTION.		
2	01E02	04	704-9837-200	A	ANGLE SUPPORT.		
2	01E02	02	704-9845-200	A	PACKER.		
1	01D02	00	704-9838-200	A	BASE.		
			-000	A	G.A.COMPRESSION TEST FRAME.		

A	INITIAL ISSUE		
	R.JAMES.	P.SAVILLE.	16-07-96
B			

	R.JAMES.	P.SAVILLE.	

COMPRESSION TEST FRAME-ASSEMBLY.

704 9844 A

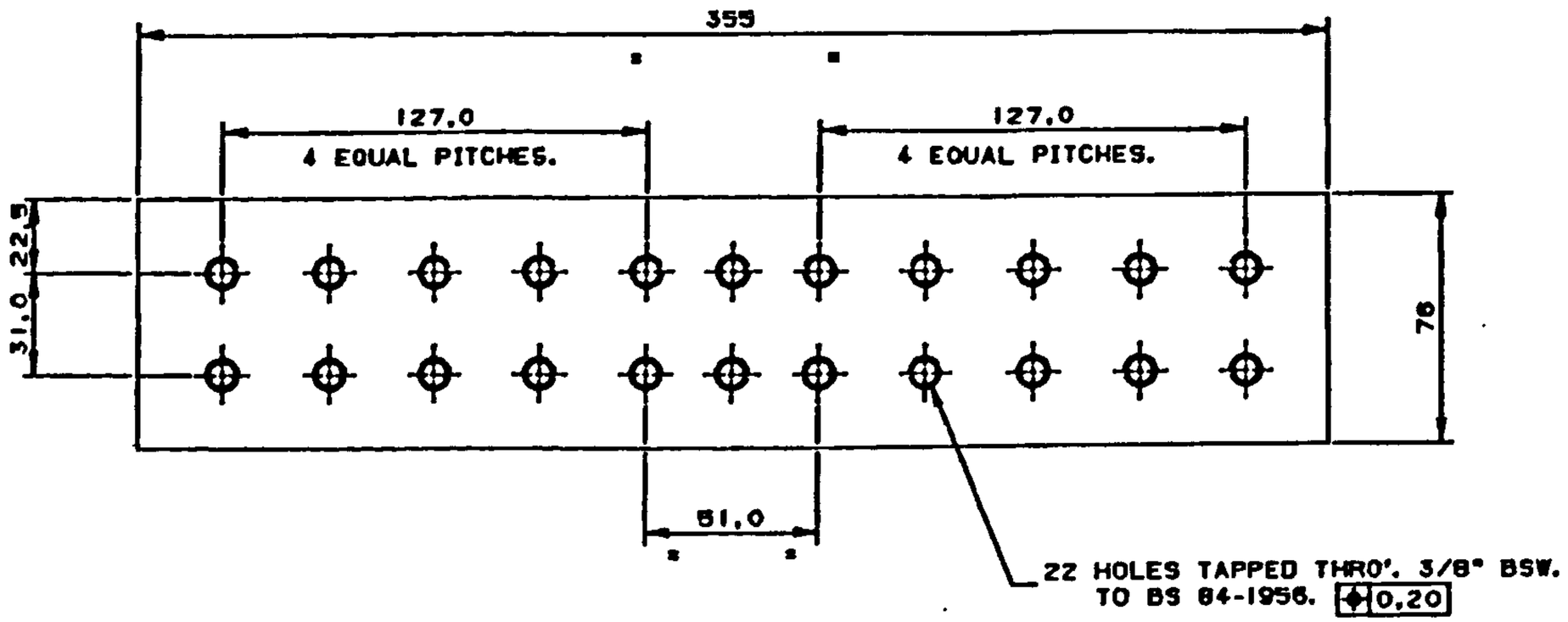

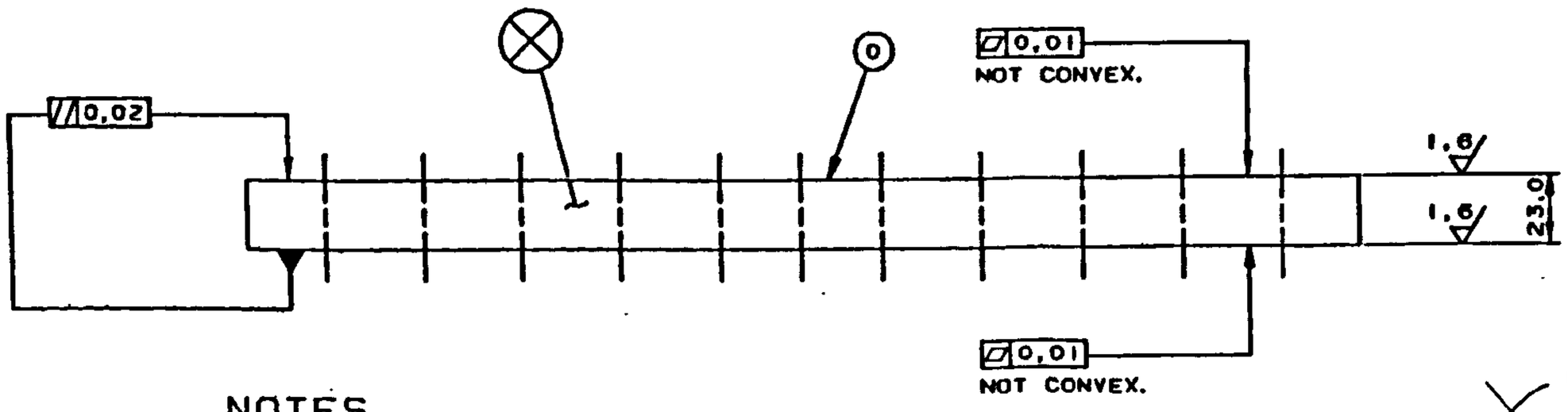

X1 ENZ4ET

NOTES,

1. THIS DRAWING IS RETROSPECTIVE. TO RECORD EXISTING ITEM.
2. MATERIAL :- HTS.
3. LIGHTLY OIL AND PROTECT FROM DAMAGE.
4. USED ON Z04-9844. COMPRESSION TEST FRAME FOR FIBRE REINFORCED IMPACT SPECIMENS.

MODIFICATIONS		
A	INITIAL ISSUE	
DRN	R.AMES.	APPROVAL DATE
CHK	I.P COOK.	
APP	P.J.SPILLER.	16-07-96
B		

DRN		APPROVAL DATE
CHK		
APP		

MILLIMETRES 0 10 20 30 40 50 60 70 80

INCHES 0 1 2 3

ALL DIMENSIONS IN MILLIMETRES UNLESS OTHERWISE STATED

		01004	0	-200	A	BASE	SEE NOTE 2	HTS.	
N° OFF	N° OFF	MAP REF	LINE REF	PART NUMBER	ITEM IND	KEYWORD - DESCRIPTION MAX 27 CHARACTERS - ADM LIMIT	MATERIAL	SPECIFICATION OR REMARKS	MUL.DIM	PROT. TREATMENT	GENERAL CODES
	A/D	10080									
		155									

PART NUMBER

PROTECTIVE TREATMENT CHART ASP 0-1015

GENERAL MANUFACTURING PROCESSES LISTED IN ASP 0-0008 APPLY

PICTURE SHT.No 1 ISSUE A

PICTURE SHT.No ISSUE

THIS SCHEDULE CARRIES THE ISSUE OF PICTURE SHEET 1

COMPUTER PRODUCED DRAWING USING ANVIL 4000

NO MANUAL ALTERATION

DIMENSIONS IN *ITALICS* MAY NOT BE TO SCALE. PART FILE MONETRY SHOULD BE BORNE VERIFIED PRIOR TO USE.

THIS DRAWING IS SIMILAR TO :-

PART No.	INITIALLY USED ON

LIMITS NOT STATED ASD-0001 ± 0.50

SURFACE FINISH 3.2 UOS. ASD-0002

IDENTIFICATION MARKING ASD-0003 ENGRAVE

INTERCHANGEABLE PART YES NO DRAWING NO.

SCALE VALID FOR MASTER DRAWING ONLY 1 : 1

DRN. R.AMES. CHKD. I.P.COOK. STRESS SYST.

D.O.R/B. APPD. P.J.SPILLER. WTS. PROCESS

TITLE AIRBUS BASE.

FIRST ANGLE PROJECTION A1

SHEET OF SHEETS

Z04 9836 A ISSUE

D.A.I.

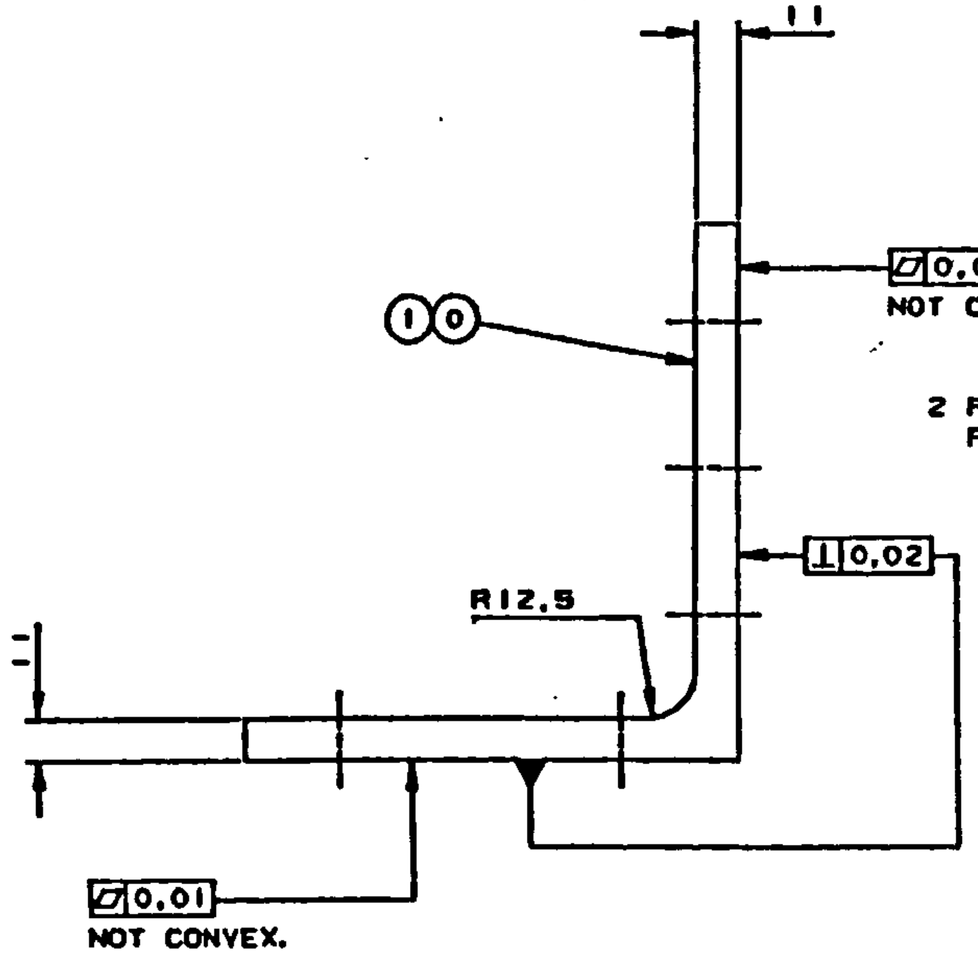

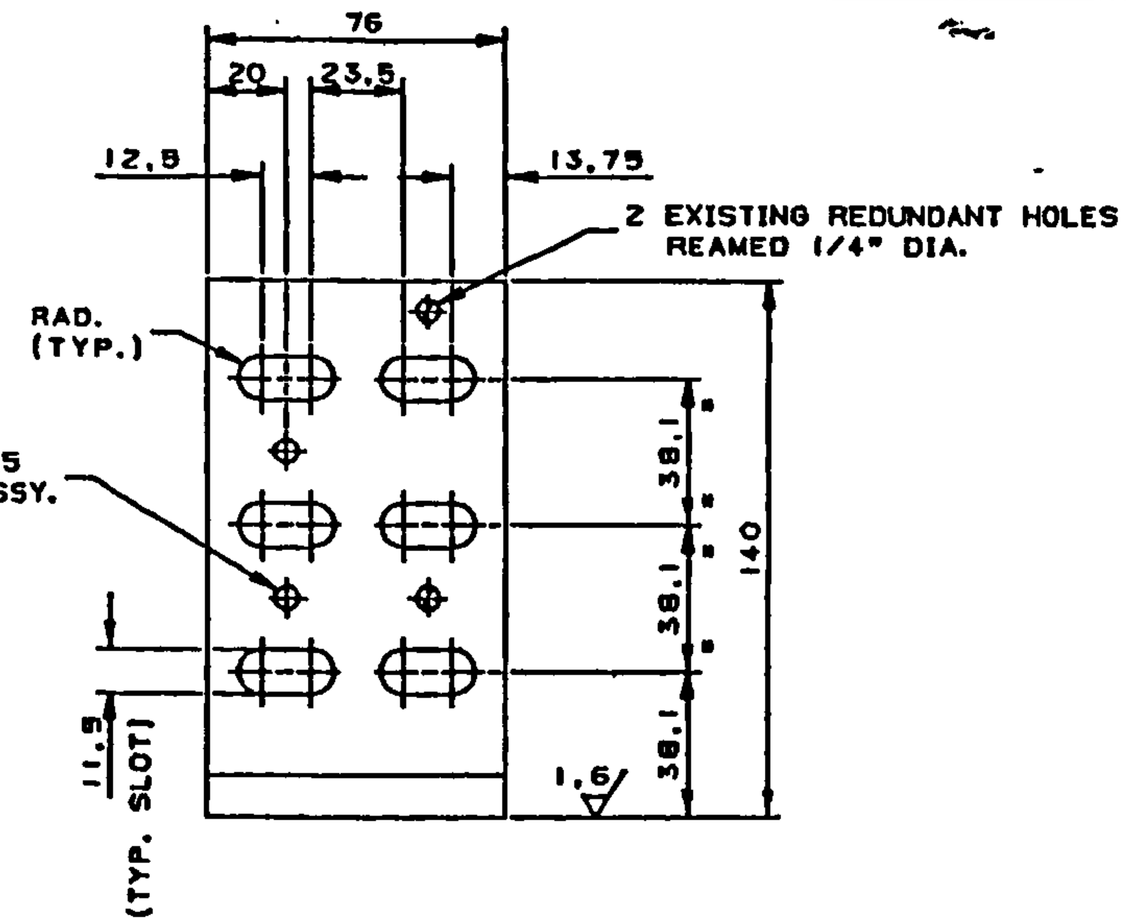

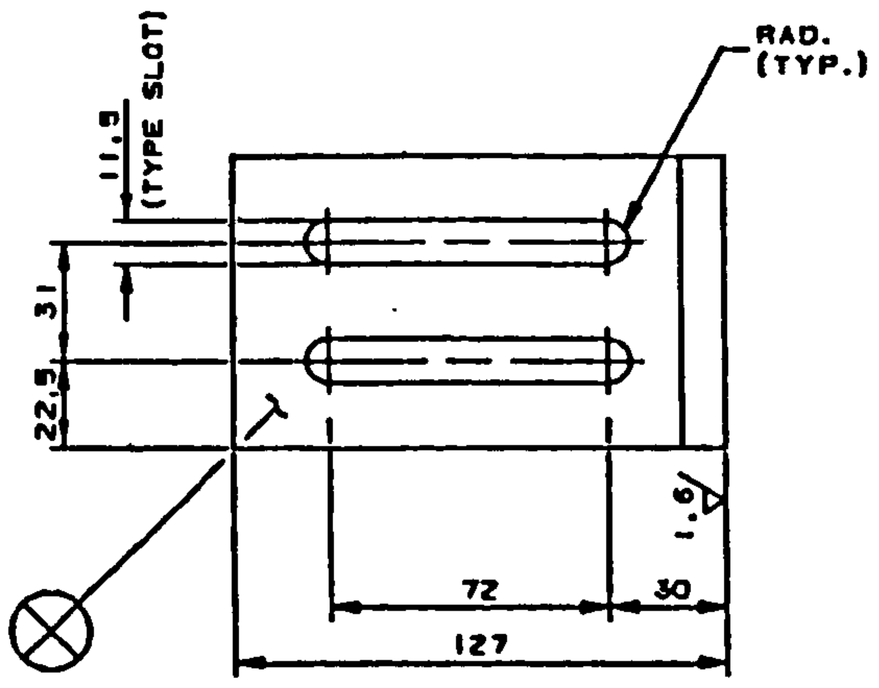

NOTES.

1. THIS DRAWING IS RETROSPECTIVE, TO RECORD EXISTING ITEM.
2. MATERIAL :- HTS.
3. LIGHTLY OIL AND PROTECT FROM DAMAGE.
4. USED ON Z04-9844. COMPRESSION TEST FRAME FOR FIBRE REINFORCED IMPACT SPECIMENS.

x2 CN24T

MODIFICATIONS		
A	INITIAL ISSUE	
DRN	R.AMES	APPROVAL DATE
CHK	I.P.COOK	
APP	P.J.SPILLER	15-07-96

		01E05	1	-201	A	ANGLE SUPPORT	SEE NOTE 2	HTS.		
		01E05	0	-200	A	ANGLE SUPPORT	SEE NOTE 2	HTS.		
10° OFF	2° OFF	MAP REF	LINE REF	PART NUMBER	ITEM QTY	KEYWORD - DESCRIPTION MAX 27 CHARACTERS - ADM LIMIT	MATERIAL	SPECIFICATION (or SUPPLY)	RUL.OIS	PROT. TREATMENT / GENERAL CODES
	ADV	HERO								
		181								

PART NUMBER

PROTECTIVE TREATMENT CHART ABP 0-1013

GENERAL MANUFACTURING PROCESSES LISTED IN ABP 0-0008 APPLY

PICTURE SHT.No 1 ISSUE A

PICTURE SHT.No ISSUE

THIS SCHEDULE CARRIES THE ISSUE OF PICTURE SHEET 1

COMPUTER PRODUCED DRAWING USING ANVIL 4000

NO MANUAL ALTERATION

DIMENSIONS IN ITALICS MAY NOT BE TO SCALE. PART (S) SHOULD BE SCREEN VERIFIED PRIOR TO USE.

THIS DRAWING IS SIMILAR TO :-

PART No.	INITIALLY USED ON

UNLESS NOT STATED ∅ 0,50 SURFACE FINISH 3.2 UOS.

IDENTIFICATION MARKINGS ENGRAVE INTERCHANGEABLE PART UNLESS NO. DRAWING NO.

SCALE VALID FOR MASTER DRAWING ONLY 1 : 1

BRITISH AEROSPACE AIRBUS LIMITED

DRN. R.AMES. CHKD. I.P. COOK. APPD. P.J. SPILLER.

STRESS STRT. FTG. PROCESS

D.O.DRTG.

TITLE AIRBUS ANGLE SUPPORT

FIRST ANGLE PROJECTION A1

SHEET OF SHEETS

Z04 9837 A ISSUE

MILLIMETRES 0 10 20 30 40 50 60 70 80

INCHES 0 1 2

ALL DIMENSIONS IN MILLIMETRES UNLESS OTHERWISE STATED

MODIFICATIONS		
A	INITIAL ISSUE	
DRN	R.AMES.	APPROVAL DATE
CHK	I.P.COOK.	
APP	P.J.SPILLER.	16-07-86
B		

DRN		APPROVAL DATE
CHK		
APP		

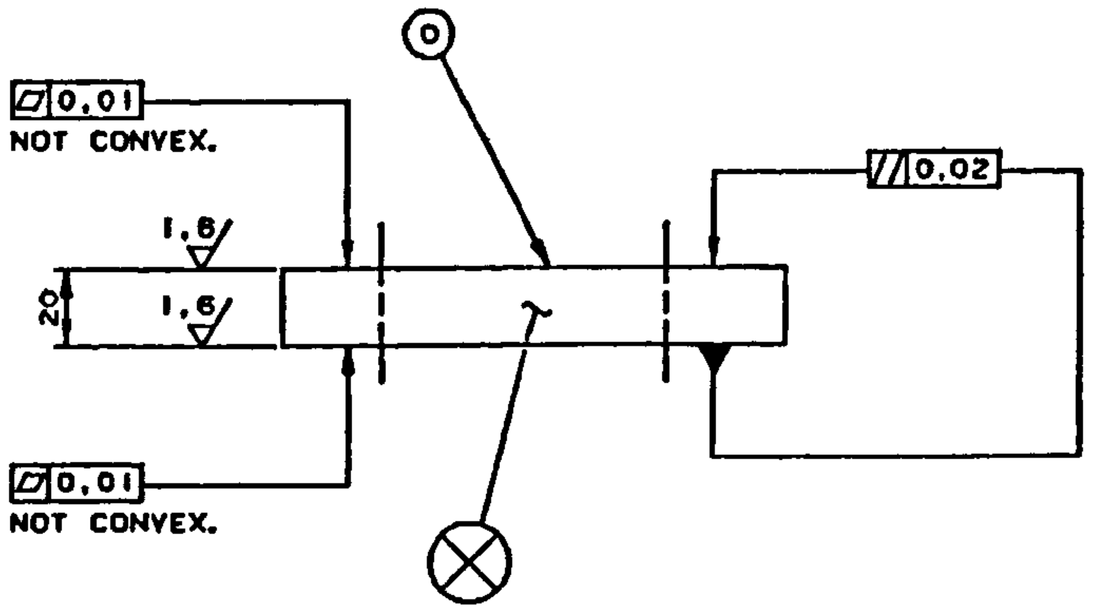

H.T.S EN24T

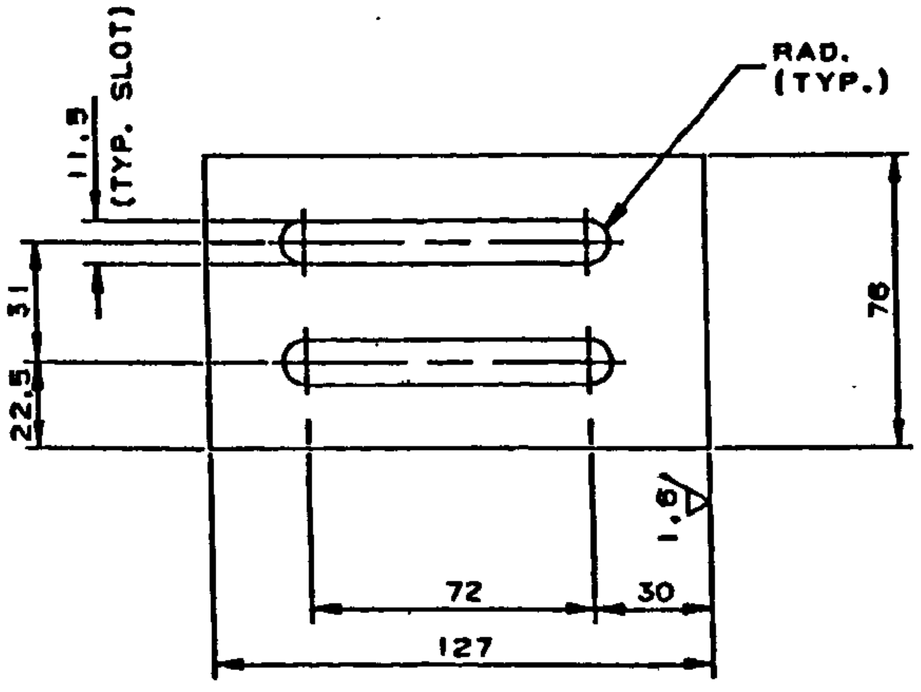

NOTES.

1. DEBURR.
2. LIGHTLY OIL AND PROTECT FROM DAMAGE.
3. USED ON Z04-9844. COMPRESSION TEST FRAME FOR FIBRE REINFORCED IMPACT SPECIMENS.

X2.

		01E05	0	-200	A	PACKER	HTS.	EN 24T.		SEE NOTE 2.
N° OFF	N° OFF	MAP REF	LINE REF	PART NUMBER	ITEM NO	KEYWORD - DESCRIPTION MAX 27 CHARACTERS - ADM LIMIT	MATERIAL	SPECIFICATION OR REMARKS	MUL.DIM	PROT. TREATMENT	GENERAL CODES
	A/D	HARD									
		198									

PART NUMBER

PROTECTIVE TREATMENT CHART ASP 0-1013

GENERAL MANUFACTURING PROCESSES LISTED IN ASP 0-0005 APPLY

PICTURE SHT.No 1 ISSUE A

PICTURE SHT.No ISSUE

THIS SCHEDULE CARRIES THE ISSUE OF PICTURE SHEET 1

COMPUTER PRODUCED DRAWING USING ANVIL 4000

NO MANUAL ALTERATION

DIMENSIONS IN *ITALICS* MAY NOT BE TO SCALE. PART FILE GEOMETRY SHOULD BE SCREEN VERIFIED PRIOR TO USE.

THIS DRAWING IS SIMILAR TO :-

PART No.	INITIALLY USED ON

MILLIMETRES 0 10 20 30 40 50 60 70 80

INCHES 0 1 2 3

ALL DIMENSIONS IN MILLIMETRES UNLESS OTHERWISE STATED

UNLESS NOT STATED ± 0,50

SURFACE FINISH 3,2 ▽ OUS.

SPECIFICATION MARKINGS ENGRAVE

INTERCHANGEABLE PART YES / NO

DRAWING NO.

BRITISH AEROSPACE AIRBORNE LIMITED

SCALE VALID FOR MASTER DRAWING ONLY 1 : 1

DRN.	CHKD.	STRESS	SYST.
R.AMES.	I.P.COOK.		
D.O.CHG.	APPD. P.J.SPILLER.	STS.	PROCESS

TITLE AIRBORNE

PACKER.

FIRST ANGLE PROJECTION A1

SHEET OF SHEETS

Z04 9843 A

ISSUE

D.A.L.

N° OFF	N° OFF	MAP REF	LINE REF	PART NUMBER	ITEM 155	KEYWORD - DESCRIPTION MAX 27 CHARACTERS - ADM LIMIT	MATERIAL	SPECIFICATION	RUL.DIM	PROT. TREATMENT	GENERAL CODES
		01804	0	-200	A	LOWER REACTION	HTS.	EN 24T.		SEE NOTE 2.	
	A/0	HAND					OR REMARKS				
		155									
		PART NUMBER									

PROTECTIVE TREATMENT CHART ABP 0-1013

GENERAL MANUFACTURING PROCESSES LISTED IN ABP 0-0003 APPLY

PICTURE SHT.No 1 ISSUE A

PICTURE SHT.No ISSUE

THIS SCHEDULE CARRIES THE ISSUE OF PICTURE SHEET 1

COMPUTER PRODUCED DRAWING USING ANVIL 4000

NO MANUAL ALTERATION

DIMENSIONS IN *ITALICS* MAY NOT BE TO SCALE- PART FILE GEOMETRY SHOULD BE SCREEN VERIFIED PRIOR TO USE.

THIS DRAWING IS SIMILAR TO :-

PART No.	INITIALLY USED ON

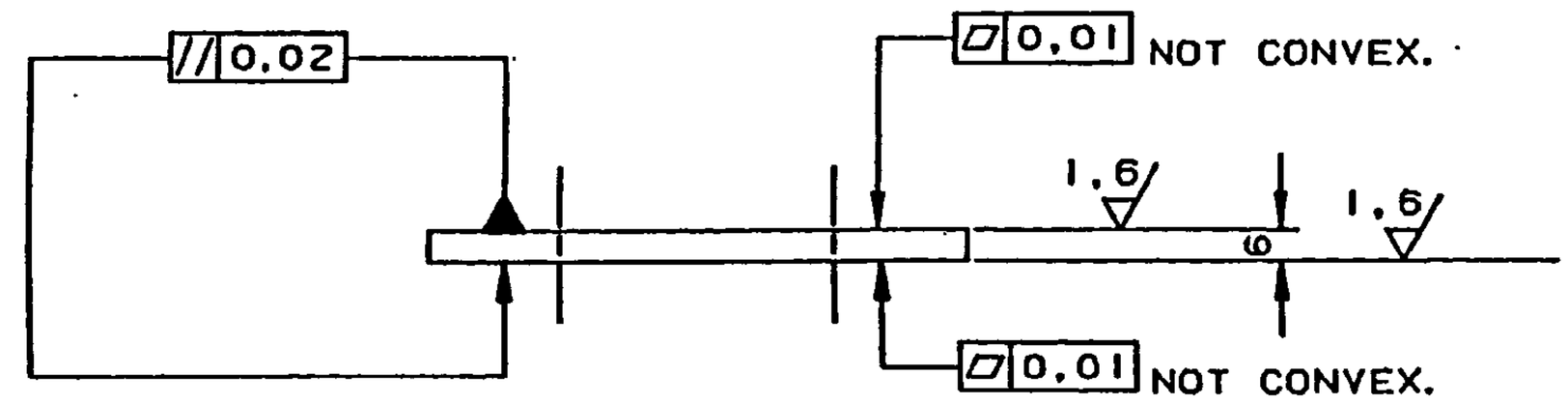

EN 24T

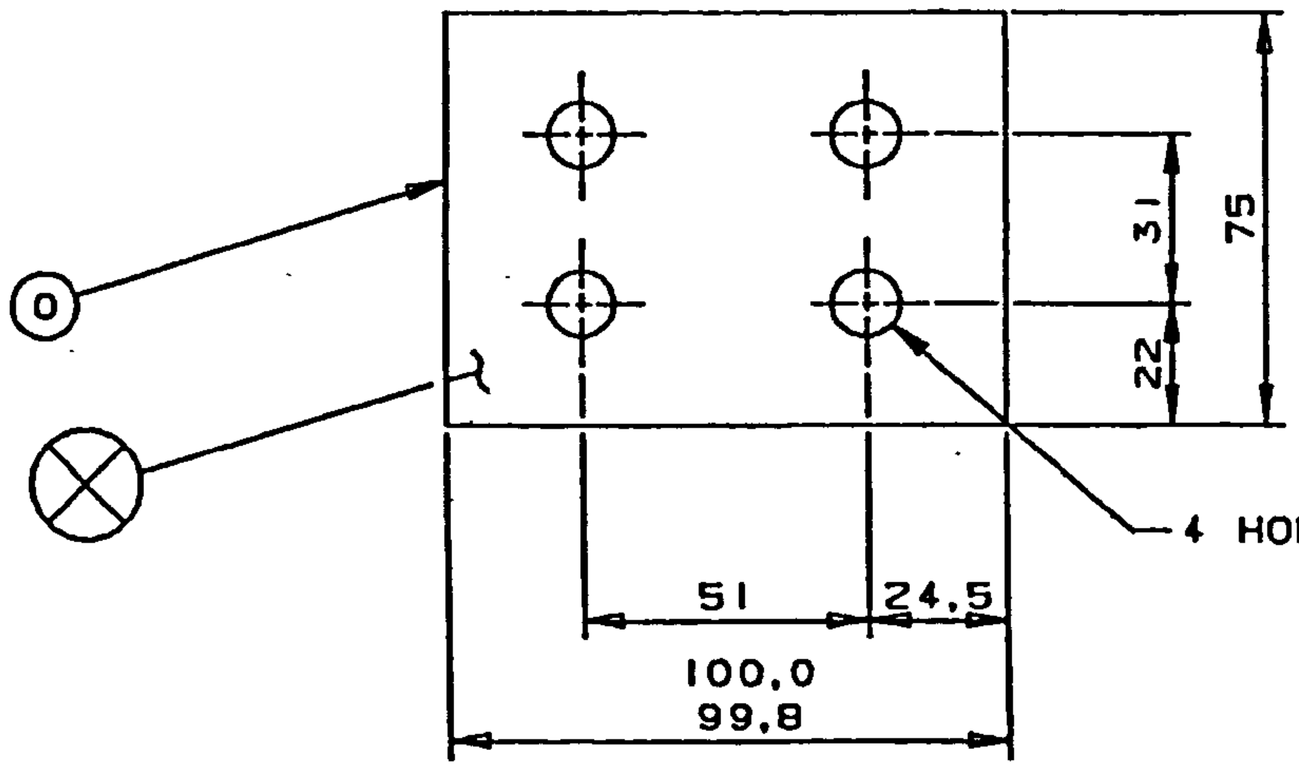

×1

ALL DIMENSIONS IN MILLIMETRES UNLESS OTHERWISE STATED

NOTES.

1. DEBURR.
2. LIGHTLY OIL AND PROTECT FROM DAMAGE.
3. USED ON Z04-9844. COMPRESSION TEST FRAME FOR FIBRE REINFORCED IMPACT SPECIMENS.

MODIFICATIONS

A	INITIAL ISSUE	
DRN	R.AMES.	APPROVAL DATE
CHK	I.P.COOK.	
APP	P.J.SPILLER.	16-07-96

MILLIMETRES 0 10 20 30 40 50 60 70 80

INCHES 0 1 2 3

LIMITS NOT STATED ~~ABP-0001-3~~ ± 0,50

SURFACE FINISH ~~ABP-0002~~ 3.2 UOS.

IDENTIFICATION MARKINGS ~~ABP-0003~~ ENGRAVE

INTERCHANGEABLE PART DRAWING NO. YES NO

SCALE VALID FOR MASTER DRAWING ONLY 1:1

BRITISH AEROSPACE AIRBUS LIMITED

DRN.	CHKD.	STRESS	SYST.
R.AMES	I.P.COOK.		
D.O.ORIG.	APPD. P.J.SPILLER.	WTS.	PROCESS

TITLE AIRBUS

LOWER REACTION

FIRST ANGLE PROJECTION A2

SHEET OF SHEETS

Z04 9847 A ISSUE

D.O.L

BAS6945

N° OFF	N° OFF	MAP REF	LINE REF	PART NUMBER	ITEM ISS	KEYWORD - DESCRIPTION MAX 27 CHARACTERS - ADM LIMIT	MATERIAL	SPECIFICATION OR REMARKS	RUL.DIM	PROT. TREATMENT	GENERAL CODES
		01B04	0	-200	A	BOTTOM GUIDE	HTS.	EN 24T.		SEE NOTE 2.	
	A/D	HAND									
		155									
		PART NUMBER									

PROTECTIVE TREATMENT CHART ABP 0-1013

PICTURE SHT.No 1 ISSUE A

PICTURE SHT.No ISSUE

COMPUTER PRODUCED DRAWING USING ANVIL 4000

NO MANUAL ALTERATION

THIS DRAWING IS SIMILAR TO :-

PART No.	INITIALLY USED ON

GENERAL MANUFACTURING PROCESSES LISTED IN ABP 0-0003 APPLY

THIS SCHEDULE CARRIES THE ISSUE OF PICTURE SHEET 1

DIMENSIONS IN *ITALICS* MAY NOT BE TO SCALE- PART FILE GEOMETRY SHOULD BE SCREEN VERIFIED PRIOR TO USE.

MODIFICATIONS

A	INITIAL ISSUE	
DRN	R.AMES.	APPROVAL DATE
CHK	I.P.COOK.	
APP	P.J.SPILLER.	16-07-96

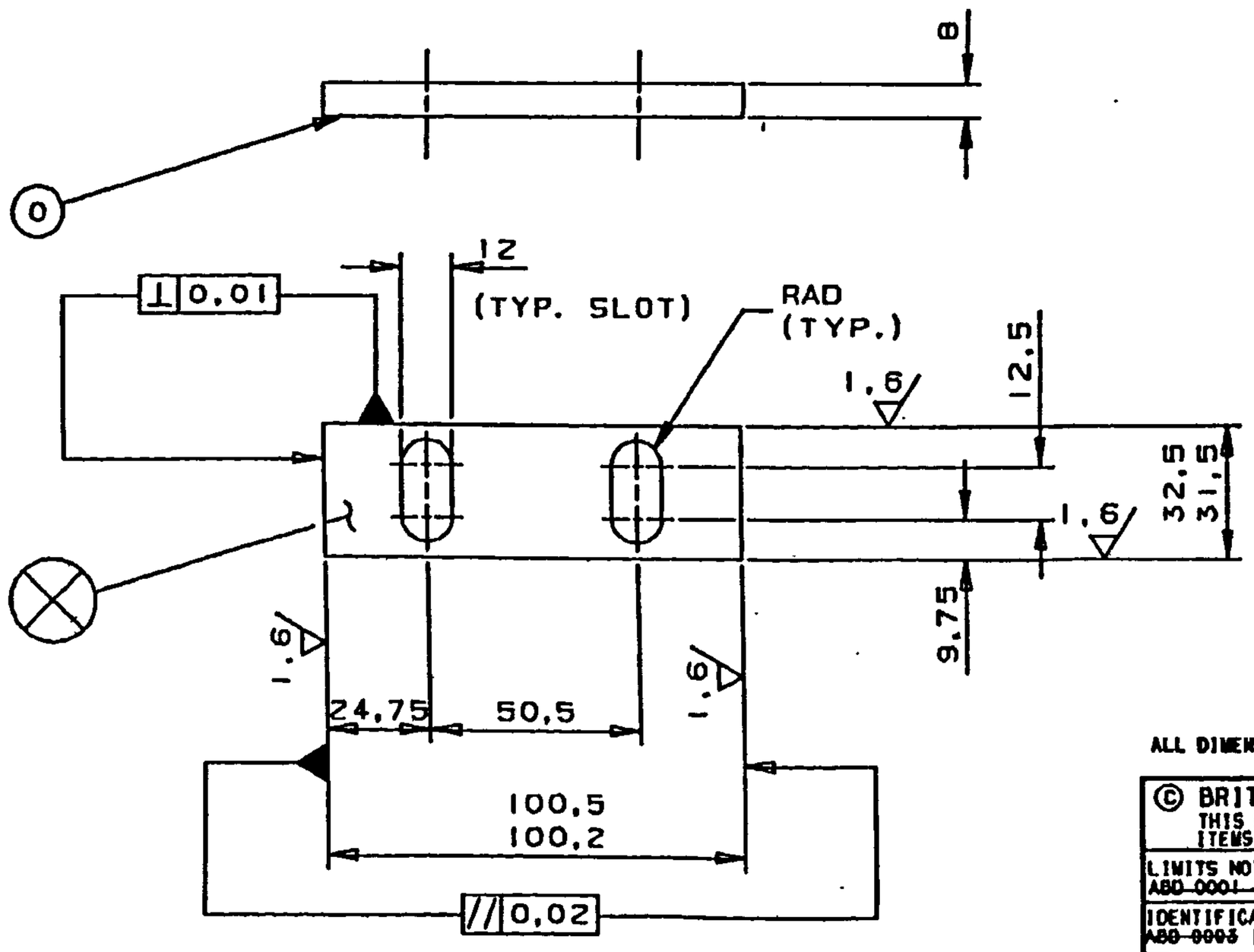

×2. EN24T

MILLIMETRES 0 10 20 30 40 50 60 70 80

INCHES 0 1 2 3

ALL DIMENSIONS IN MILLIMETRES UNLESS OTHERWISE STATED

LIMITS NOT STATED ~~ABO-0001-3~~ ± 0,50

SURFACE FINISH ~~ABO-0002~~ 3.2 UOS.

BRITISH AEROSPACE AIRBUS LIMITED

IDENTIFICATION MARKINGS ~~ABO-0003~~ ENGRAVE

INTERCHANGEABLE PART DRAWING NO. YES NO

SCALE VALID FOR MASTER DRAWING ONLY 1:1

DRN.	CHKD.	STRESS	SYST.
R.AMES	I.P.COOK.		
D.O.ORIG.	APPD. P.J.SPILLER.	WTS.	PROCESS

TITLE AIRBUS

BOTTOM GUIDE

FIRST ANGLE PROJECTION A2

SHEET 1 OF 1 SHEETS

Z04 9839 A ISSUE

NOTES.

1. DEBURR.
2. LIGHTLY OIL AND PROTECT FROM DAMAGE.
3. USED ON Z04-9844. COMPRESSION TEST FRAME FOR FIBRE REINFORCED IMPACT SPECIMENS.

D.D.L

BAS6945

		01A03	2	-202	A	WASHER	HTS.	EN 24T.		SEE NOTE 3.	
		01A04	0	-200	A	WASHER	HTS.	EN 24T.		SEE NOTE 3.	
N° OFF	N° OFF	MAP REF	LINE REF	PART NUMBER	ITEM ISS	KEYWORD - DESCRIPTION MAX 27 CHARACTERS - ADM LIMIT	MATERIAL	SPECIFICATION OR REMARKS	RUL.DIM	PROT. TREATMENT	GENERAL CODES
	A/D	HAND									
		ISS									

PART NUMBER

PROTECTIVE TREATMENT CHART ABP 0-1013

GENERAL MANUFACTURING PROCESSES LISTED IN ABP 0-0003 APPLY

PICTURE SHT.No 1 ISSUE A

PICTURE SHT.No ISSUE

THIS SCHEDULE CARRIES THE ISSUE OF PICTURE SHEET 1

COMPUTER PRODUCED DRAWING
USING ANVIL 4000
NO MANUAL ALTERATION

DIMENSIONS IN *ITALICS* MAY NOT BE TO SCALE- PART FILE GEOMETRY SHOULD BE SCREEN VERIFIED PRIOR TO USE.

THIS DRAWING IS SIMILAR TO :-

PART No.	INITIALLY USED ON

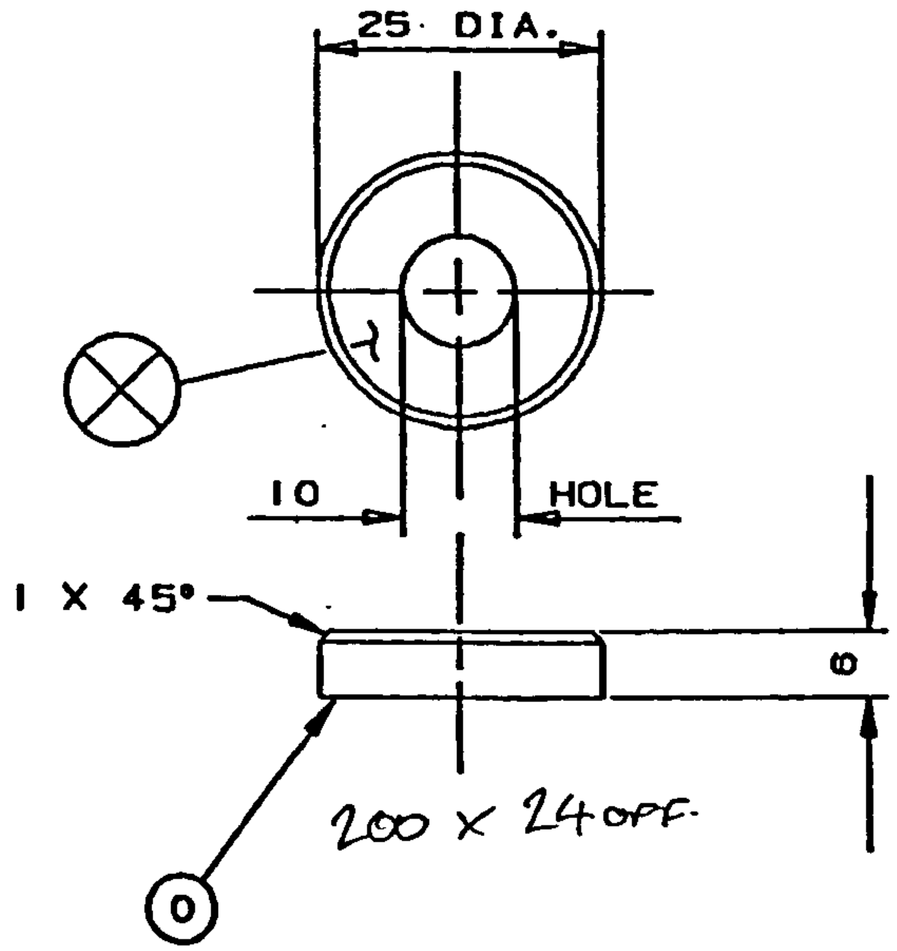

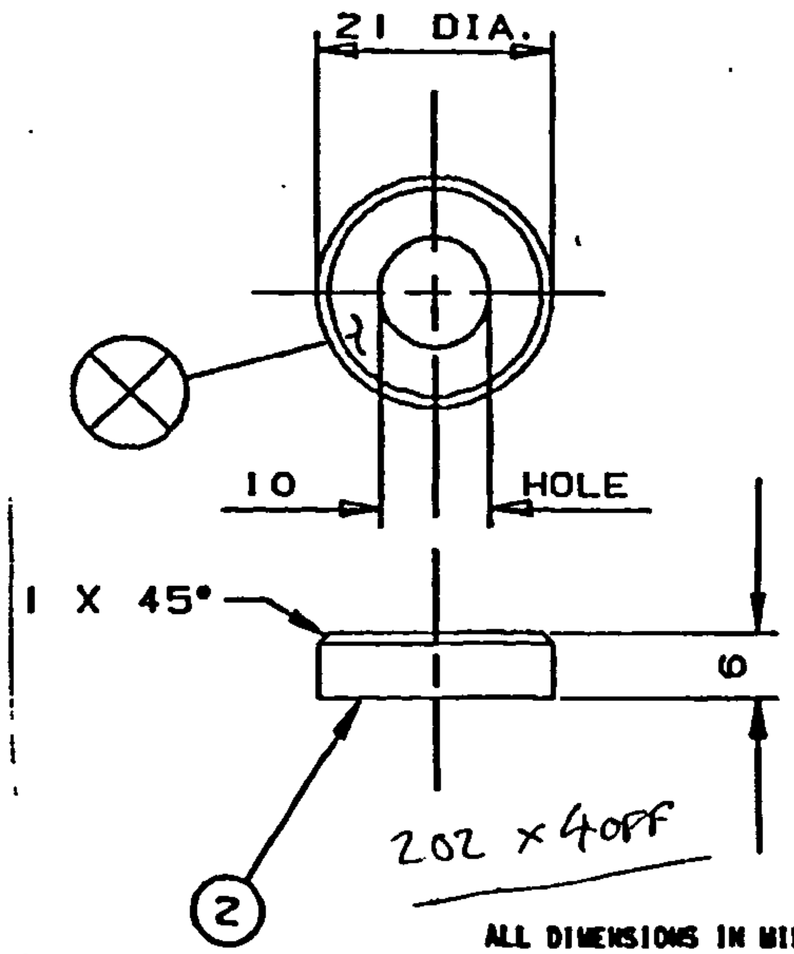

NOTES.

1. THIS DRAWING IS RETROSPECTIVE, TO RECORD EXISTING ITEMS.
2. MATERIAL :- HTS.
3. LIGHTLY OIL AND PROTECT FROM DAMAGE.
4. USED ON Z04-9844. COMPRESSION TEST FRAME FOR FIBRE REINFORCED IMPACT SPECIMENS.

MODIFICATIONS

A	INITIAL ISSUE

DRN	R.AMES.	APPROVAL DATE
CHK	I.P.COOK.	
APP	P.J.SPILLER.	16-07-96
B		

ALL DIMENSIONS IN MILLIMETRES UNLESS OTHERWISE STATED

MILLIMETRES 0 10 20 30 40 50 60 70 80
INCHES 0 1 2 3

LIMITS NOT STATED ABO-0001-3 ± 0,50	SURFACE FINISH ABO-0002 3.2 UOS.	BRITISH AEROSPACE AIRBUS LIMITED	
IDENTIFICATION MARKINGS ABO-0003 ENGRAVE	INTERCHANGEABLE PART DRAWING NO. YES NO	SCALE VALID FOR MASTER DRAWING ONLY 2:1	
DRN. R.AMES	CHKD. I.P.COOK.	STRESS	SYST.
D.O.ORIG.	APPD. P.J.SPILLER.	WTS.	PROCESS

TITLE AIRBUS
WASHERS

FIRST ANGLE PROJECTION A2

SHEET 1 OF 1 SHEETS

Z04 9848 A ISSUE

D.D.L

BA56045

N° OFF	N° OFF	MAP REF	LINE REF	PART NUMBER	ITEM ISS	KEYWORD - DESCRIPTION MAX 27 CHARACTERS - ADM LIMIT	MATERIAL	SPECIFICATION OR REMARKS	RUL.DIM	PROT. TREATMENT	GENERAL CODES
		01804	0	-200	A	TOP GUIDE	HTS.	EN 24T.		SEE NOTE 2.	
	A/D	HAND									
		155									

PART NUMBER

PROTECTIVE TREATMENT CHART ABP 0-1013

PICTURE SHT.No 1 ISSUE A

PICTURE SHT.No ISSUE

GENERAL MANUFACTURING PROCESSES LISTED IN ABP 0-0003 APPLY

THIS SCHEDULE CARRIES THE ISSUE OF PICTURE SHEET 1

COMPUTER PRODUCED DRAWING USING ANVIL 4000

NO MANUAL ALTERATION

DIMENSIONS IN *ITALICS* MAY NOT BE TO SCALE- PART FILE GEOMETRY SHOULD BE SCREEN VERIFIED PRIOR TO USE.

THIS DRAWING IS SIMILAR TO :-

PART No.	INITIALLY USED ON

MODIFICATIONS

A	INITIAL ISSUE
DRN	R.AMES.
CHK	I.P.COOK.
APP	P.J.SPILLER.

APPROVAL DATE 16-07-96

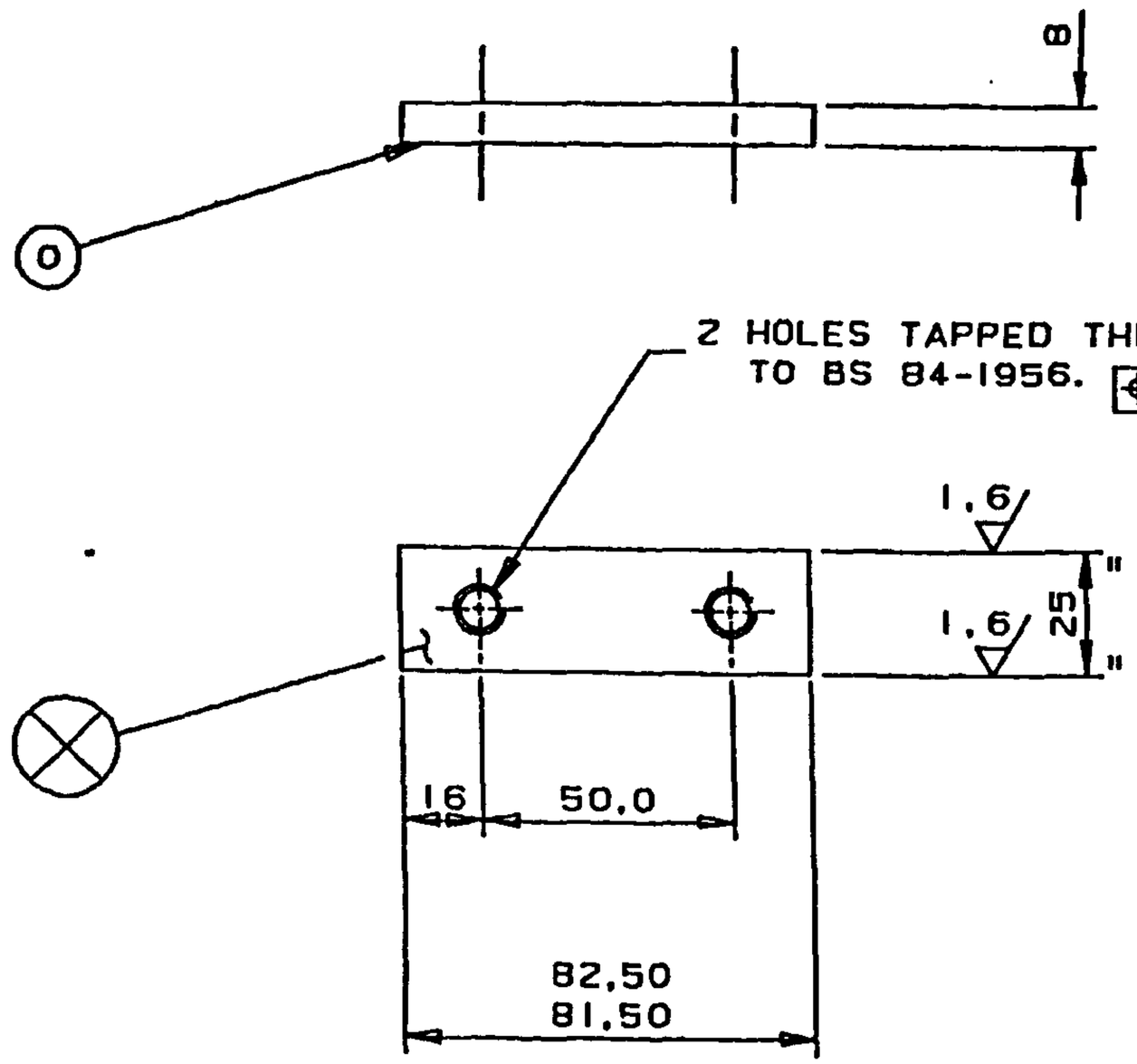

x2. EN 24T

NOTES.

1. DEBURR.
2. LIGHTLY OIL AND PROTECT FROM DAMAGE.
3. USED ON Z04-9844. COMPRESSION TEST FRAME FOR FIBRE REINFORCED IMPACT SPECIMENS.

ALL DIMENSIONS IN MILLIMETRES UNLESS OTHERWISE STATED

MILLIMETRES 0 10 20 30 40 50 60 70 80

INCHES 0 1 2 3

LIMITS NOT STATED ~~ABQ-0001-3~~ ± 0,50	SURFACE FINISH ~~ABQ-0002~~ 3,2 UOS.	BRITISH AEROSPACE AIRBUS LIMITED	
IDENTIFICATION MARKINGS ~~ABQ-0003~~ ENGRAVE	INTERCHANGEABLE PART YES NO DRAWING NO.	SCALE VALID FOR MASTER DRAWING ONLY 1:1	
DRN. R.AMES	CHKD. I.P.COOK.	STRESS	SYST.
D.O.ORIG.	APPD. P.J.SPILLER.	WTS.	PROCESS

TITLE AIRBUS

TOP GUIDE

FIRST ANGLE PROJECTION A2

SHEET 1 OF 1 SHEETS

Z04 9841 A ISSUE

D.O.L

BA56945

134 - 6 = 128 = 48/80

MODIFICATIONS		
A	INITIAL ISSUE	
DRN	R.AMES.	APPROVAL DATE
CHK	I.P.COOK.	
APP	P.J.SPILLER.	16-07-86
CO		

DRN		APPROVAL DATE
CHK		
APP		

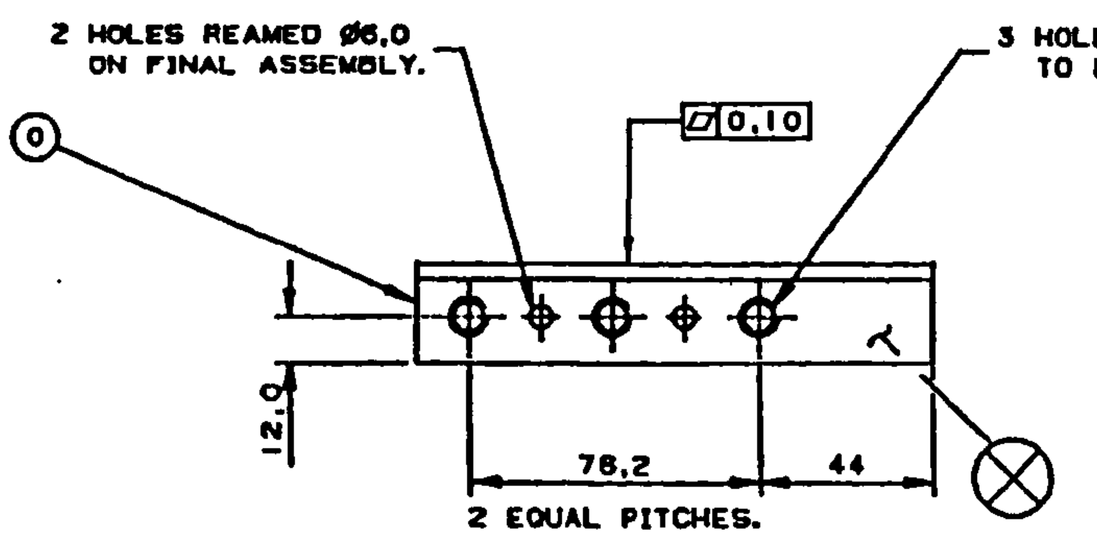

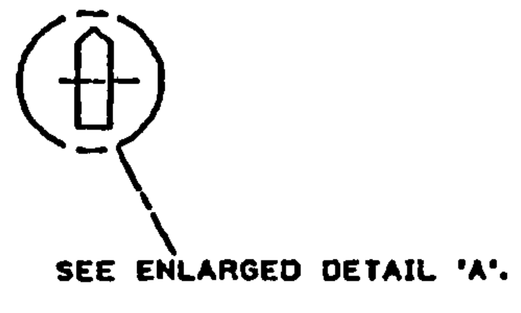

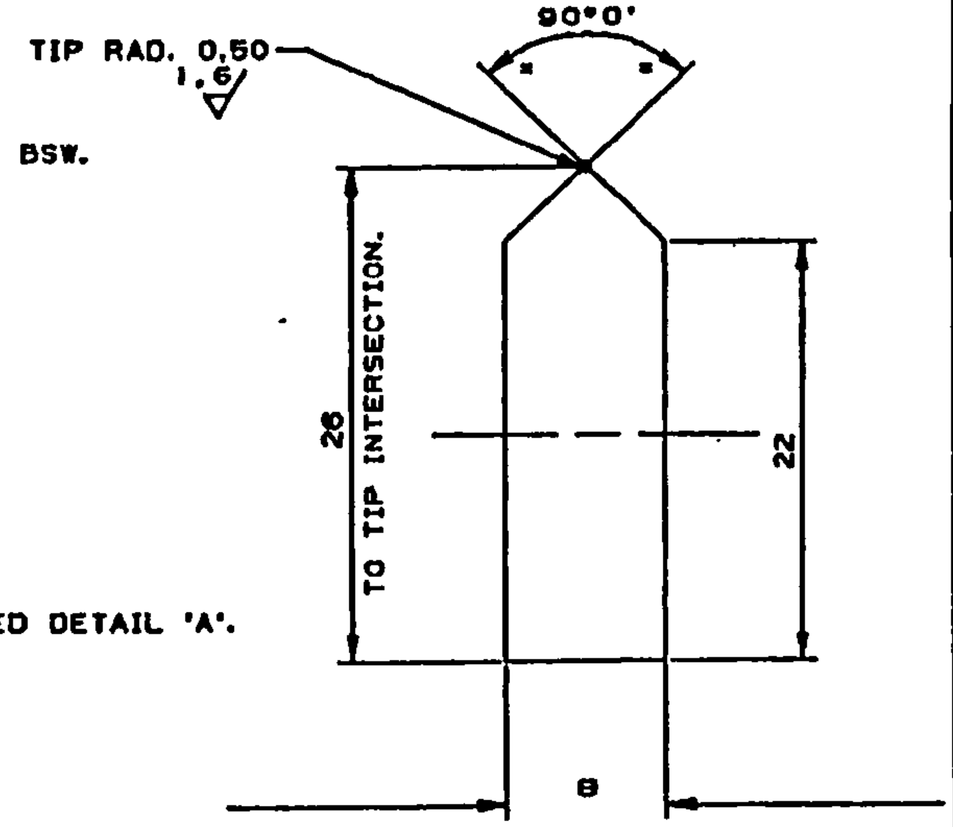

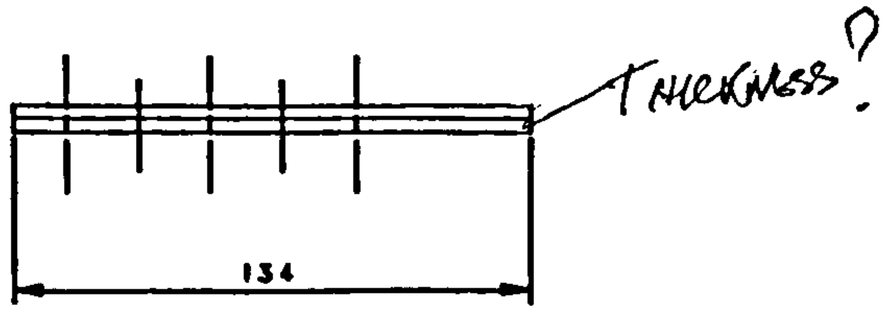

DETAIL 'A'.
SCALE:- 5.XF/SIZE.

×4.

NOTES.

1. DEBURR.
2. LIGHTLY OIL AND PROTECT FROM DAMAGE.
3. USED ON Z04-9844. COMPRESSION TEST FRAME FOR FIBRE REINFORCED IMPACT SPECIMENS.

M° O'Y	M° O'Y A/U	MAP REF	LINE REF	PART NUMBER	ISSN	KEYWORD - DESCRIPTION MAX 27 CHARACTERS - ADM LIMIT	MATERIAL	SPECIFICATION OR REMARKS	RUL.DIA	PROT. TREATMENT	GENERAL CODES
		01005	0	-200	A	SIDE GUIDE	HTS.	EN 24T.		SEE NOTE 2.	

PROTECTIVE TREATMENT CHART ABP 0-1013

GENERAL MANUFACTURING PROCESSES LISTED IN ABP 0-0005 APPLY

PICTURE SHT.No. 1 ISSUE A

PICTURE SHT.No. ISSUE

THIS SCHEDULE CARRIES THE ISSUE OF PICTURE SHEET 1

COMPUTER PRODUCED DRAWING USING ANVIL 4000

NO MANUAL ALTERATION

DIMENSIONS IN ITALICS MAY NOT BE TO SCALE. PART FULL DIMENSIONALLY BEFORE USE.

THIS DRAWING IS SIMILAR TO -

PART No.	INITIALLY USED ON

ALL DIMENSIONS IN MILLIMETRES UNLESS OTHERWISE STATED

MILLIMETRES 0 10 20 30 40 50 60 70 80

INCHES 0 1 2

UNITS NOT STATED ABP-0001 ± 0,50

SURFACE FINISH ABP-0008 3,2 ✓ OVS.

IDENTIFICATION MARKING ABP-0008 ENGRAVE

INTERCHANGEABLE PART DRAWING NO. UNSIG

BRITISH AEROSPACE AIRBUS LIMITED

SCALE VALID FOR MASTER DRAWING ONLY 1 : 1

DRN.	CHKD.	STRESS	STAT.
R.AMES.	I.P.COOK.		
D.O.M16.	APPD. P.J.SPILLER.	TYD.	PROCESS

TITLE AIRBUS
SIDE GUIDE

FIRST ANGLE PROJECTION A1

SHEET OF SHEETS

Z04 9840 A

		01B04	0	-200	A	BOTTOM GUIDE	HTS.	EN 24T.		SEE NOTE 2.	
N° OFF	N° OFF	MAP REF	LINE REF	PART NUMBER	ITEM ISS	KEYWORD - DESCRIPTION MAX 27 CHARACTERS - ADM LIMIT	MATERIAL	SPECIFICATION OR REMARKS	RUL.DIM	PROT. TREATMENT	GENERAL CODES
	A/D	HAND									
		ISS									
		PART NUMBER									

PROTECTIVE TREATMENT CHART ABP 0-1013

PICTURE SHT.No 1 / ISSUE A

PICTURE SHT.No / ISSUE

COMPUTER PRODUCED DRAWING USING ANVIL 4000

NO MANUAL ALTERATION

THIS DRAWING IS SIMILAR TO :-

PART No.	INITIALLY USED ON

GENERAL MANUFACTURING PROCESSES LISTED IN ABP 0-0003 APPLY

THIS SCHEDULE CARRIES THE ISSUE OF PICTURE SHEET 1

DIMENSIONS IN *ITALICS* MAY NOT BE TO SCALE- PART FILE GEOMETRY SHOULD BE SCREEN VERIFIED PRIOR TO USE.

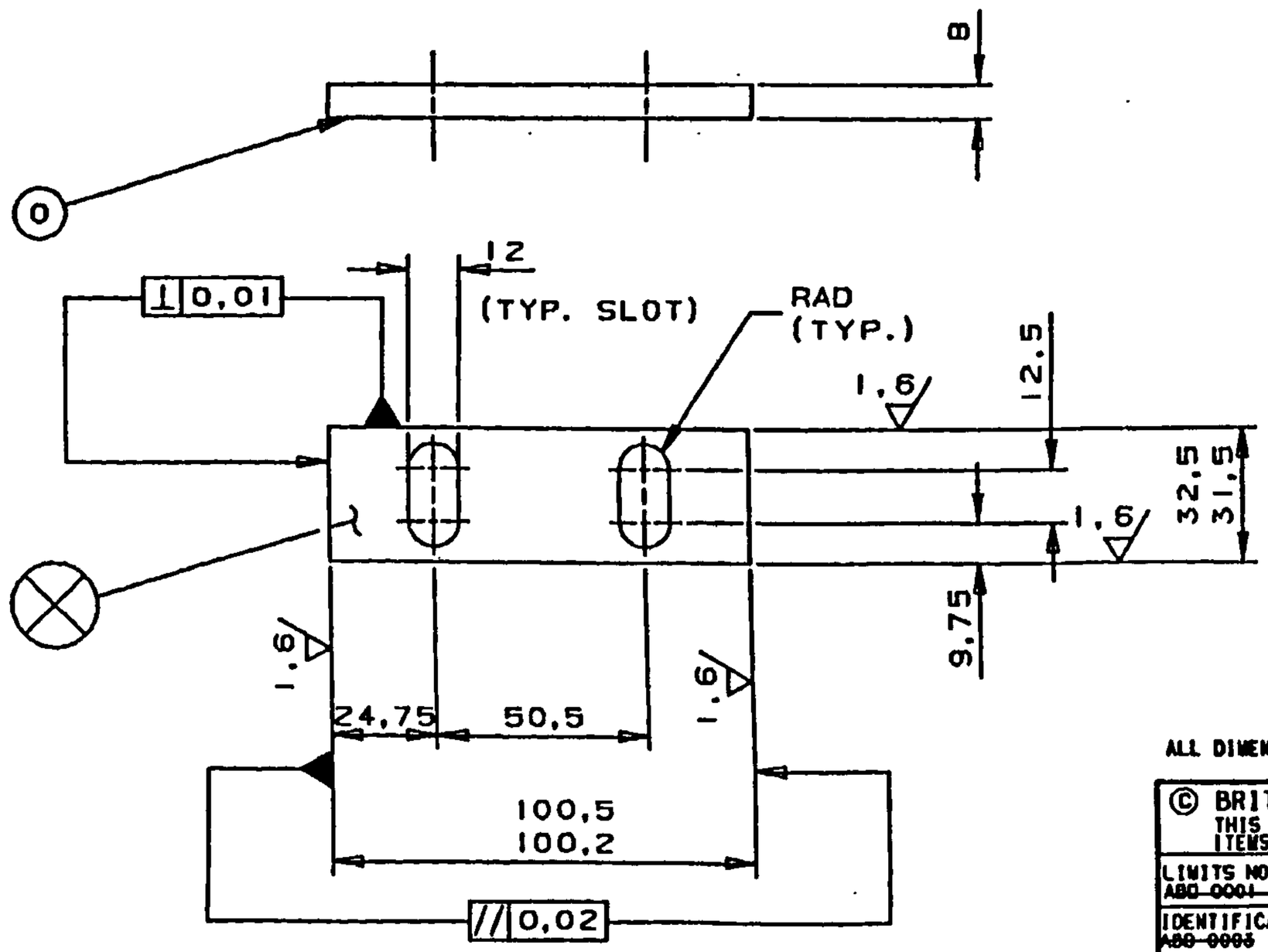

NOTES.

1. DEBURR.
2. LIGHTLY OIL AND PROTECT FROM DAMAGE.
3. USED ON Z04-9844. COMPRESSION TEST FRAME FOR FIBRE REINFORCED IMPACT SPECIMENS.

× 2. EN24T

MODIFICATIONS

A	INITIAL ISSUE
DRN	R.AMES.
CHK	I.P.COOK.
APP	P.J.SPILLER.
B	

APPROVAL DATE 16-07-96

MILLIMETRES 0 10 20 30 40 50 60 70 80
INCHES 0 1 2 3

ALL DIMENSIONS IN MILLIMETRES UNLESS OTHERWISE STATED

LIMITS NOT STATED ~~ABG-0001-3~~ ± 0,50	SURFACE FINISH ~~ABG-0002~~ 3.2 UOS.	BRITISH AEROSPACE AIRBUS LIMITED	
IDENTIFICATION MARKINGS ~~ABG-0003~~ ENGRAVE	INTERCHANGEABLE PART DRAWING NO. YES / NO	SCALE VALID FOR MASTER DRAWING ONLY 1:1	
DRN. R.AMES	CHKD. I.P.COOK.	STRESS	SYST.
D.O.ORIG.	APPD. P.J.SPILLER.	WTS.	PROCESS

TITLE AIRBUS
BOTTOM GUIDE

FIRST ANGLE PROJECTION A2

SHEET | OF | SHEETS

Z04 9839 A ISSUE

D.D.L.

BAS6945

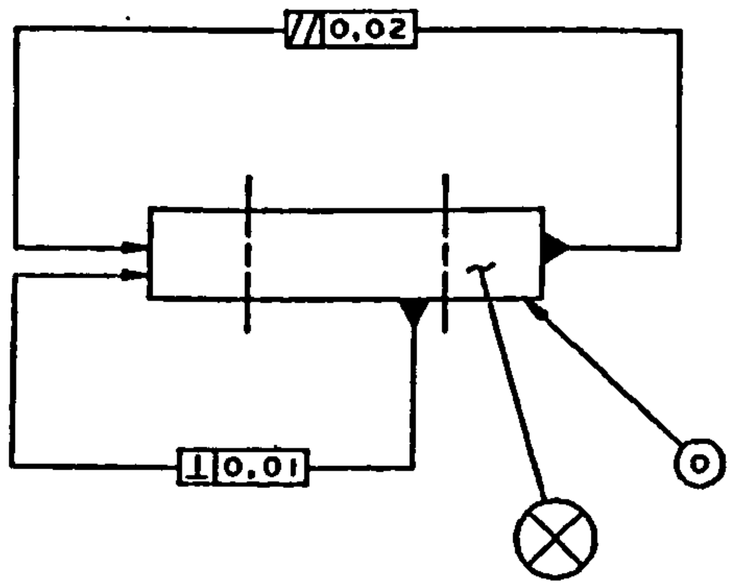

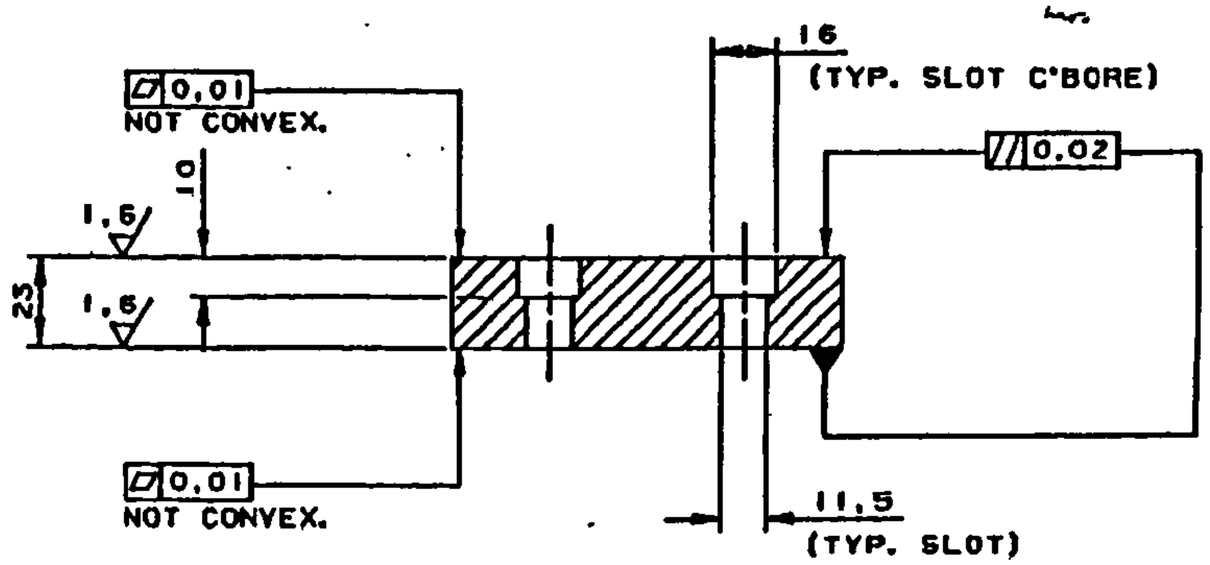

SECTION "A-A"

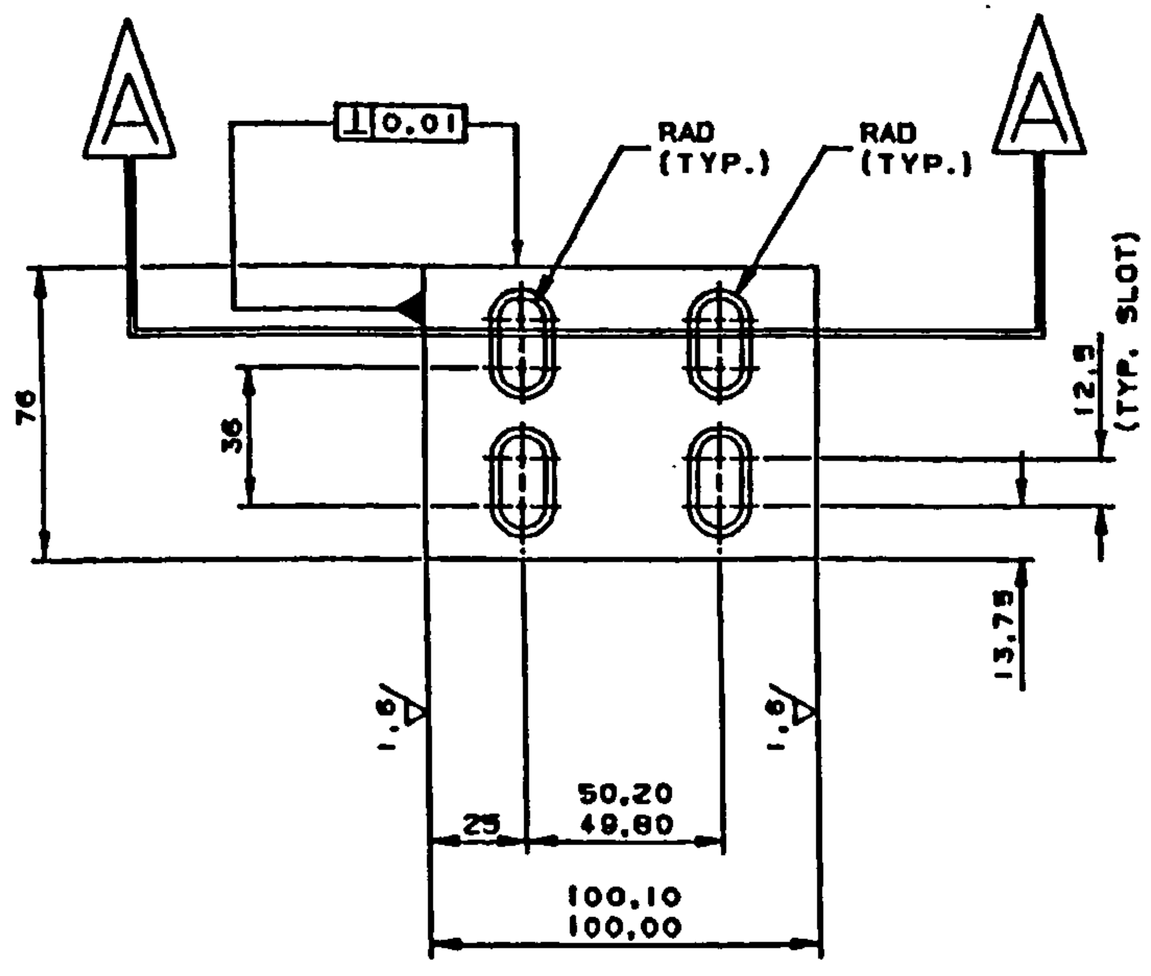

NOTES.

1. DEBURR.
2. LIGHTLY OIL AND PROTECT FROM DAMAGE.
3. USED ON Z04-9844. COMPRESSION TEST FRAME FOR FIBRE REINFORCED IMPACT SPECIMENS.

x1 EN24T

MODIFICATIONS		
A	INITIAL ISSUE	
DRN	R.AMES.	APPROVAL DATE
CHK	I.P.COOK.	
APP	P.J.SPILLER.	16-07-98
☐		

		01004	0	-200	A	LOAD PLATEN	HTS.	EN 24T.		SEE NOTE 2.
		PART NUMBER	LINE REF	PART NUMBER	TYPE NO.	KEYWORD - DESCRIPTION MAX 27 CHARACTERS - ADM LIMIT	MATERIAL	SPECIFICATION	MUL.DIM	PROT. TREATMENT / GENERAL CODES

PROTECTIVE TREATMENT CHART ASP 0-1015

PICTURE SHT.No 1 ISSUE A

PICTURE SHT.No ISSUE

GENERAL MANUFACTURING PROCESSES LISTED IN ASP 0-0005 APPLY

THIS SCHEDULE CARRIES THE ISSUE OF PICTURE SHEET 1

COMPUTER PRODUCED DRAWING USING ANVIL 4000

NO MANUAL ALTERATION

THIS DRAWING IS SIMILAR TO :-

PART No.	MATERIALLY USED ON

DIMENSIONS IN *ITALICS* MAY NOT BE TO SCALE. PART (S) ACCURACY SHOULD BE BORNE IN MIND PRIOR TO USE.

MILLIMETRES 0 10 20 30 40 50 60 70 80

INCHES 0 1 2

ALL DIMENSIONS IN MILLIMETRES UNLESS OTHERWISE STATED

LIMITS NOT STATED ± 0.50 | SURFACE FINISH 3.2 ∇ DUS. | BRITISH AEROSPACE AIRBUS LIMITED

IDENTIFICATION MARKING ENGRAVE | INTERCHANGEABLE PART YES/NO | SCALE VALID FOR MASTER DRAWING ONLY 1 : 1

DRN. R.AMES. | CHD. I.P.COOK. | STRESS | STYLE | SHEET | O.D.SRIS. | APPD. P.J.SPILLER. | STG. | PROCESS

TITLE AIRBUS
LOAD PLATEN

FIRST ANGLE PROJECTION | SHEET | OF | SHEETS

Z04 9842 | A ISSUE

D.C.L.

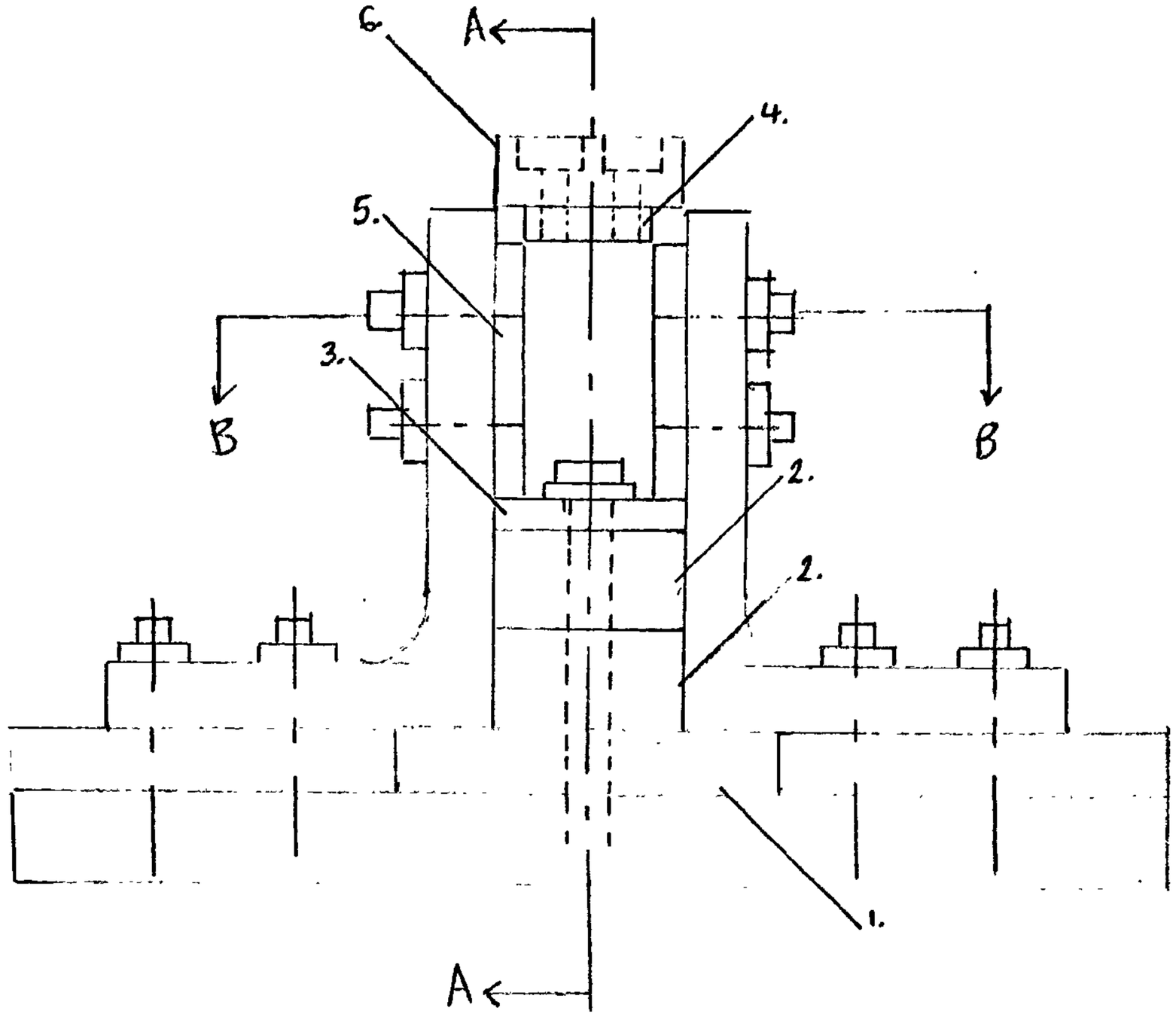
6.
A
4.
5.
3.
B
B
2.
2.
1.
A

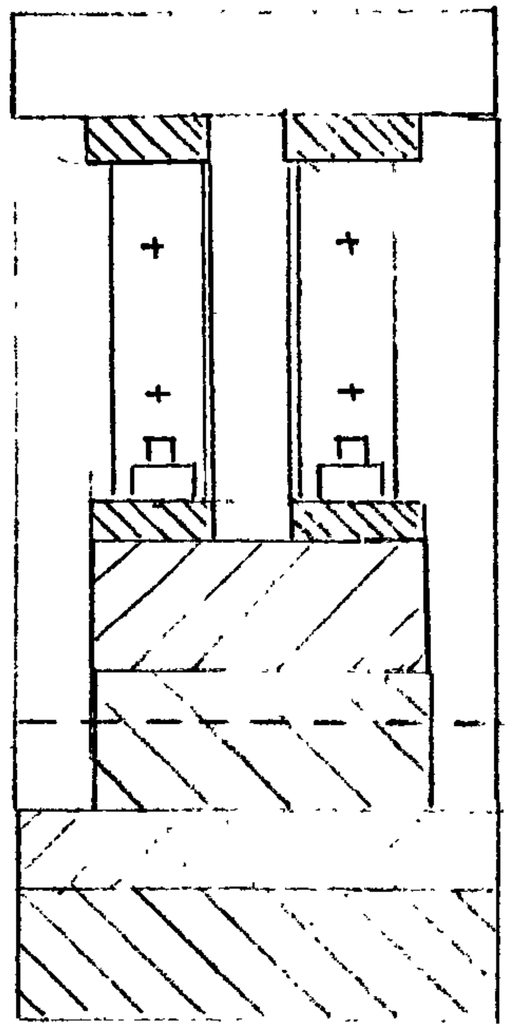

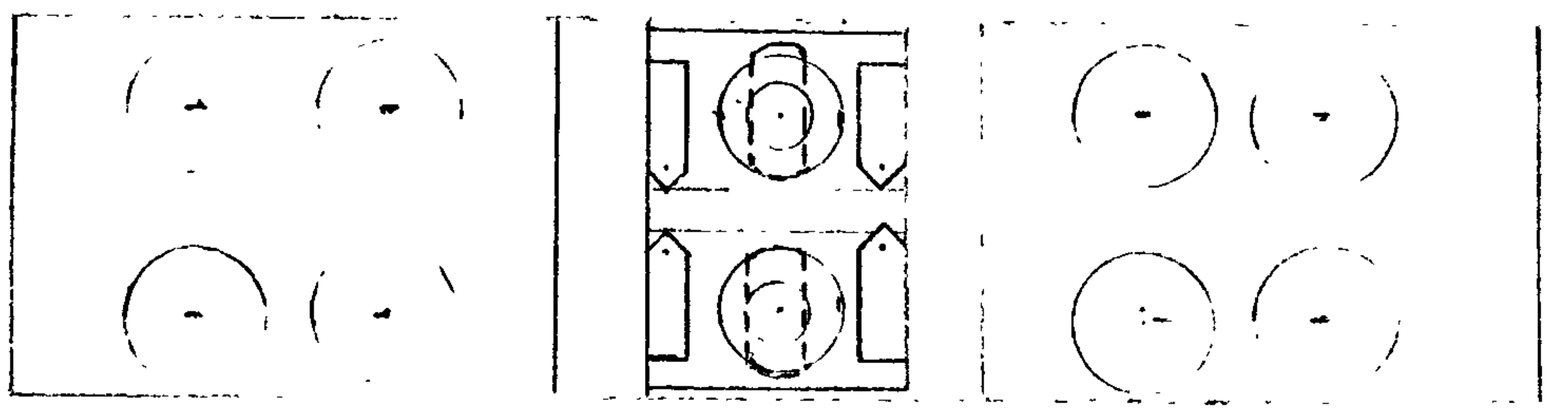

1. Lower Reaction.
EN 24T

2. Support Plates x2
EN24T

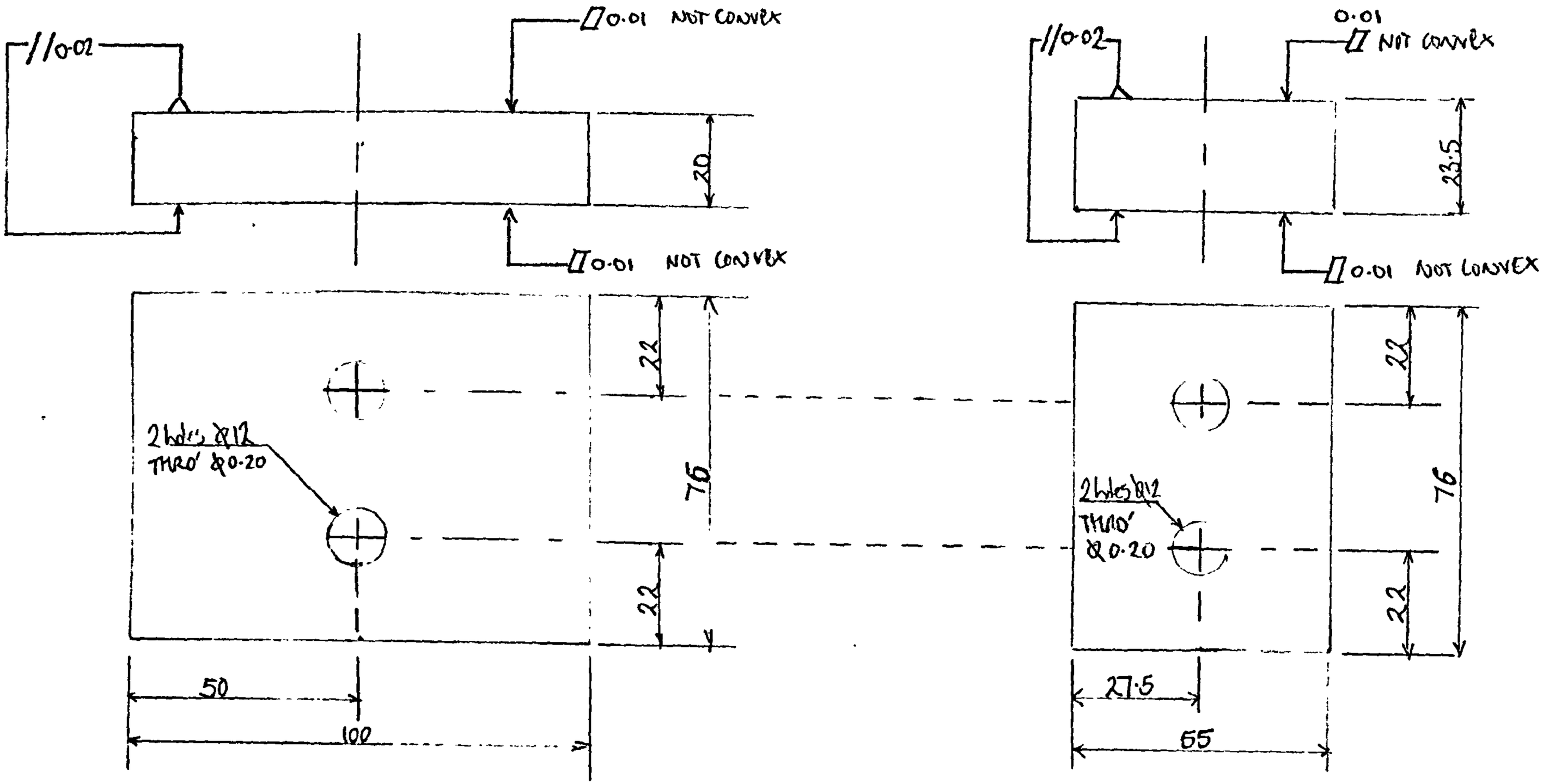

1. DEBURR
2. LIGHTLY OIL AND
PROTECT FROM DAMAGE

3. Bottom Guide x2
EN 24T

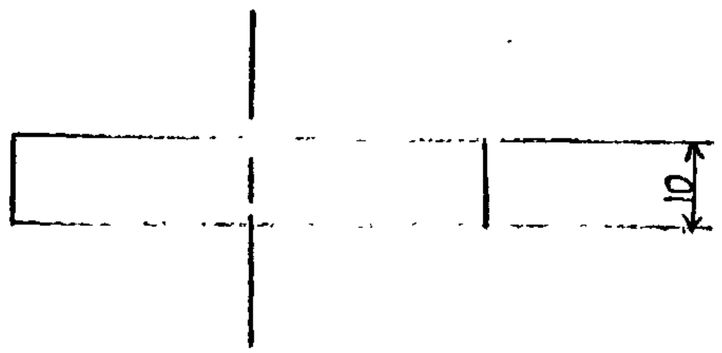

4. Top Guide x2
EN 24T

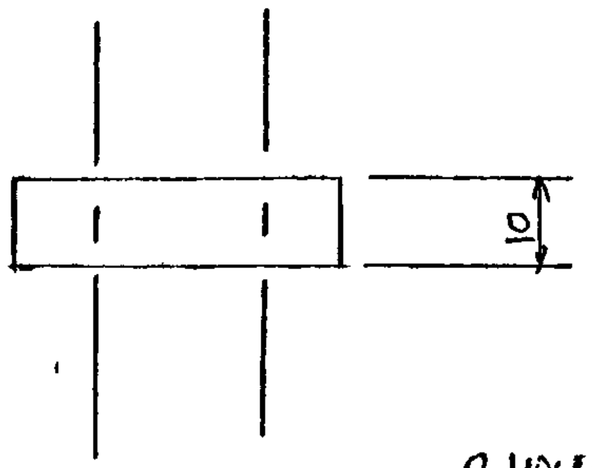

5. Side Guide x4
Gauge Plate

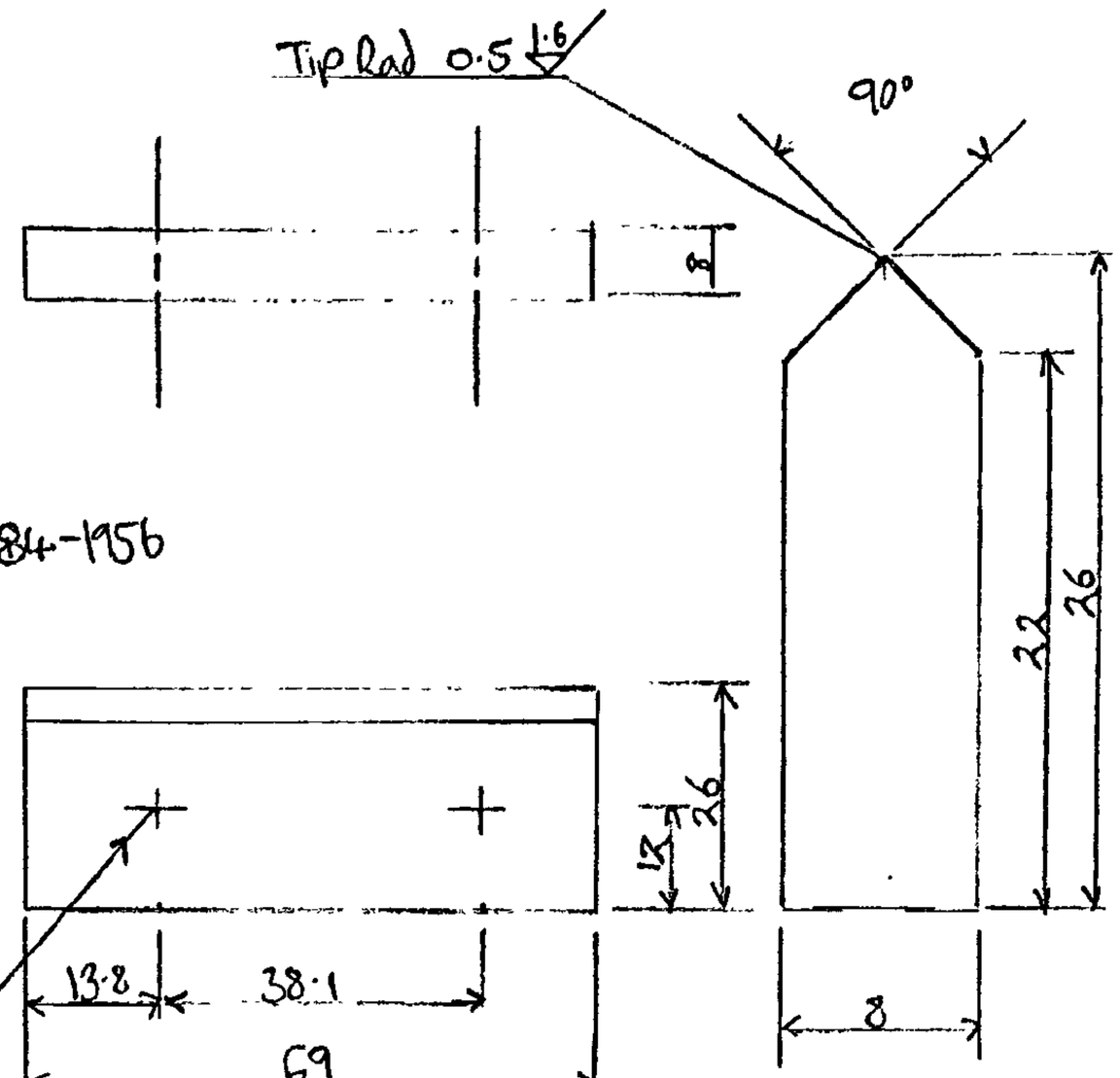

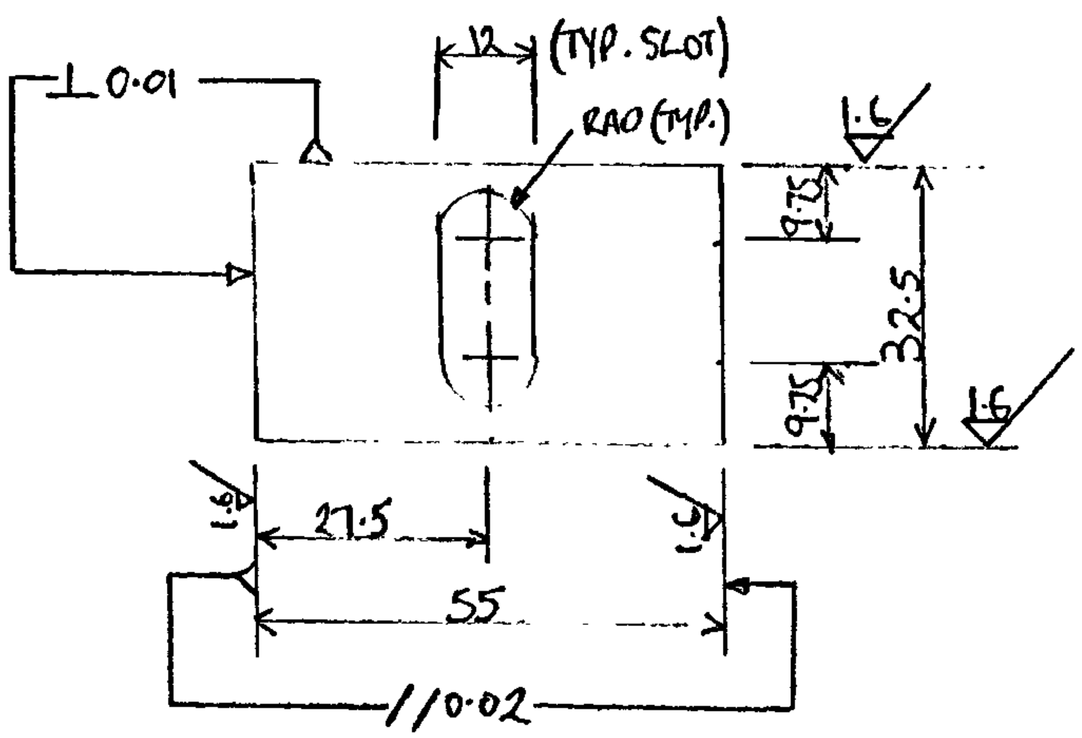

1. DEBURR
2. HIGHLY OIL AND PROTECT FROM DAMAGE

6. Load Platen

EN 24T

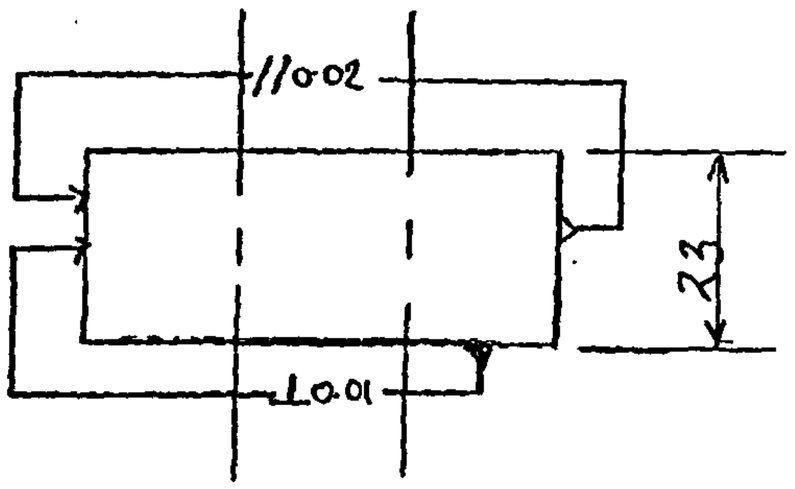

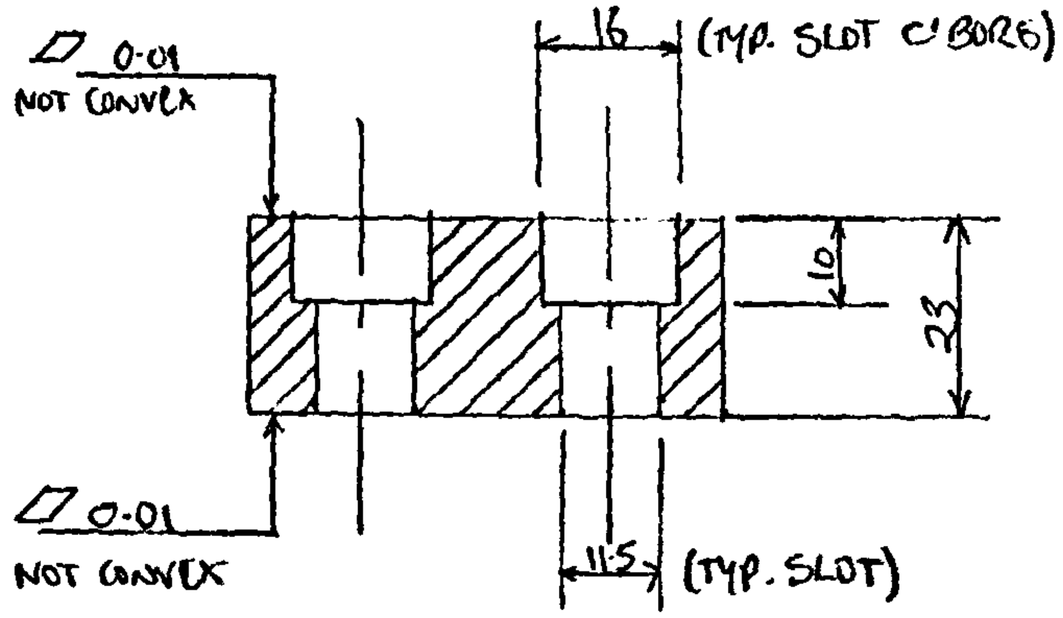

Section "A-A"

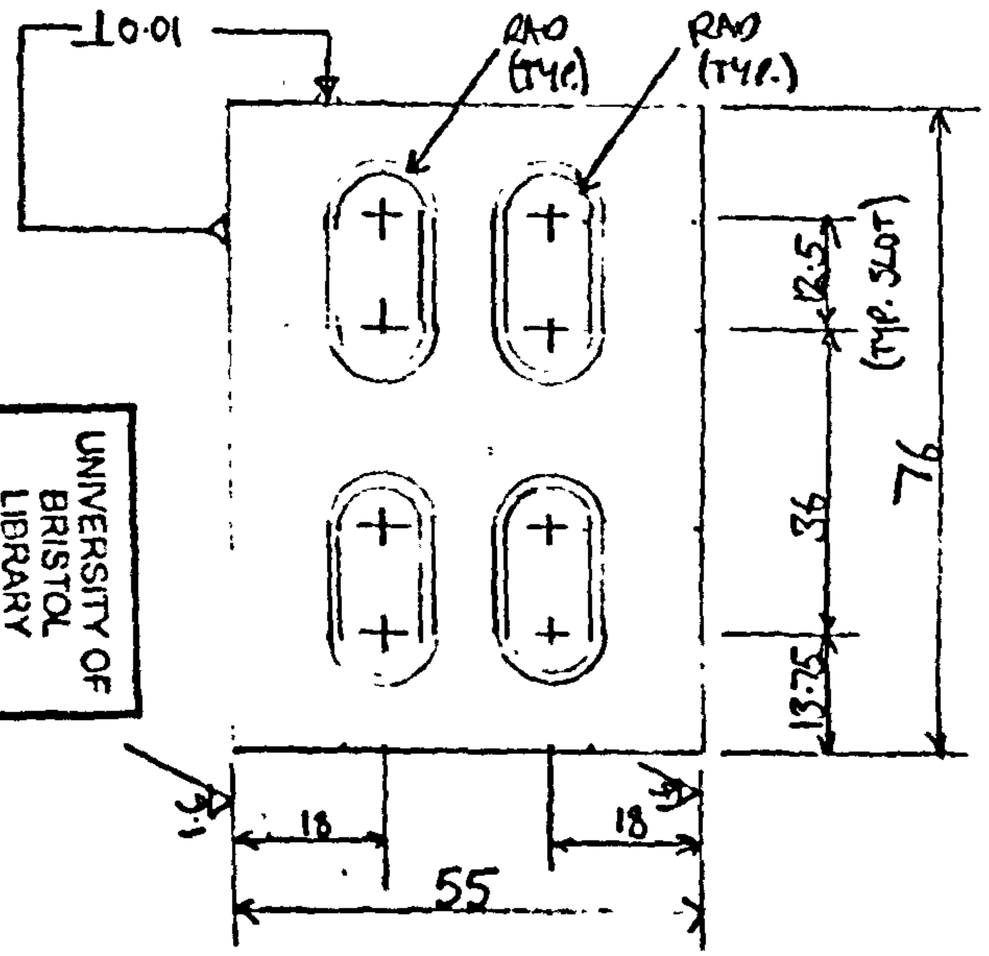

1. DEBURR
2. LIGHTLY OIL AND PROTECT FROM DAMAGE